University of Alberta

Rocky Mountain Carbonate Spring Deposit Development

by

Dustin Kyle Rainey

A thesis submitted to the Faculty of Graduate Studies and Research
in partial fulfillment of the requirements for the degree of

Doctor of Philosophy

Earth and Atmospheric Sciences

Fall 2009
Edmonton, Alberta

Examining Committee

Brian Jones, Earth & Atmospheric Sciences

Martin Sharp, Earth & Atmospheric Sciences

Karlis Muehlenbachs, Earth & Atmospheric Sciences

Robert Luth, Earth & Atmospheric Sciences

Douglas Schmitt, Physics

Henry Chafetz, Earth & Atmospheric Sciences Department, University of Houston

Abstract

Relict Holocene carbonate spring deposits containing diverse biotic and abiotic depositional textures are present at Fall Creek cold sulphur springs, Alberta, Fairmont Hot Springs, British Columbia, and Hot Creek cold springs, British Columbia. The relict deposits are formed mainly of low-magnesium crystalline calcite contained in laterally continuous strata. Paleo-flow regimes were characterized by extensive sheet flow that increased the surface area of spring water exposed to the atmosphere. Calcite precipitated inorganically from spring water that attained $CaCO_3$ supersaturation through agitation-induced CO_2 degassing that was facilitated by elevated flow rates and a large surface area as spring water flowed down-slope. Thus, the deposits contain only minor amounts of detrital, mechanically deposited, and biogenic carbonate. Evaporation was only a minor contributor to $CaCO_3$ supersaturation, mainly in quiescent environments. Photosynthetic CO_2 removal did not measurably contribute to $CaCO_3$ supersaturation. Calcite crystals precipitated in biotic facies formed from low to moderately supersaturated spring water, whereas abiotic dendrite crystals formed rapidly from highly supersaturated spring water. Calcite passively nucleated on cyanobacteria, bryophytes and macrophytes, and was probably facilitated by cyanobacterial extracellular polymeric substances. Cyanobacterial filaments and stromatolites are integral parts of all three deposits, whereas bryophytes were restricted to the Fall Creek and Hot Creek deposits. Diagenetic microbial degradation of crystalline calcite was common to all three deposits, but recrystallization was limited to the Fall Creek deposit. The amount and location of calcite precipitation relative to the vents was controlled by the concentrations of Ca^{2+} and HCO_3^- in solution, and discharge volume fluctuations. Spring water with high $[Ca^{2+}]$ and $[HCO_3^-]$ precipitated large amounts of calcite proximal to the vents (e.g. Fairmont), whereas spring water with low $[Ca^{2+}]$ and $[HCO_3^-]$

precipitated smaller quantities of calcite and required longer flow distances to achieve $CaCO_3$ supersaturation (e.g. Hot Creek). Spring water discharge volumes were controlled mainly by seasonal to millennial fluctuations in meteoric precipitation. Modern spring systems are characterized by reduced discharge volumes, channeled flow, and minimal calcite precipitation. Currently, spring water does not precipitate calcite where it flows into streams prior to achieving critical $CaCO_3$ supersaturation (e.g. Fall Creek).

Preface

Motivation can come from the strangest of places. I have spent hours observing the actions of my pet turtle, Popeye, in the closed system of her freshwater aquarium. Her shell, cold blood, and predatory nature speak to the efficiency of evolution, adaptation, and the expansiveness of geological time, even as she mistakes my fingers for goldfish and tries for a quick meal. The water that she swims in is very similar to many of the springs that I have had the pleasure of visiting – cyanobacteria rapidly colonize any surface exposed to light; microbes decompose organic matter; calcite precipitates on exposed glass and rocks where evaporation occurs – but impressive spring deposits do not develop. The reasons why are contained in this thesis, and without the aquarium, I probably would have missed a few conclusions.

Acknowledgements

I was lucky enough to receive the expertise and support of many people during my 14 year tenure at the University of Alberta. I must first thank my parents, for telling me to always stay in school (though I do not think that they intended for it to go on for this long). Thank you to Brian Jones, for providing the opportunity to undertake this thesis, and for teaching me how to be a better scientist and writer. Thanks to Denine and Dori for letting me follow in their footsteps. Thanks to the Carbonate/Springs research group, especially Sandy Bonny, whom was responsible for introducing me to my wife, Jenny Bonny; my best friend, main support and fellow science geek. Thanks to George Braybrook, whose expertise with the scanning electron microscope showed me how to see deeper than I ever have before. A thank you is deserved by a wonderful Yukon geological ambassador, Charlie Roots, with the Geological Survey of Canada, who graciously reviewed a complete draft of this thesis and provided constructive feedback. I am grateful to Duane Froese and Alberto Reyes for their assistance in preparing samples for radiocarbon dating. I appreciate the help of my field assistants – Michael Schultz, Sandy Bonny, Jasen Robalo, Alex McNeil and Ray Wheeler. I am grateful to Karlis Muehlenbachs for the use of his stable isotope laboratory. Thanks are also due to Jack Farrell, who provided a high-resolution air photo of the Fairmont Hot Springs resort, and to Dale Vitt for his assistance in bryophyte identification

This research was supported by the Natural Science and Engineering Research Council of Canada through grants provided to Brian Jones. Funding for fieldwork was subsidized with grants from the Mineralogical Association of Canada and the Geological Society of America. Reviews of earlier versions of the Fairmont manuscript by Dr. M. Pedley, and the Fall Creek manuscript by Drs. J. Andrews, J. Baldini, and G. Dix were helpful for improving the manuscripts.

Table Of Contents

LIST OF TABLES

LIST OF FIGURES

Chapter 1

Introduction

Perhaps no feature on the surface of the Earth has instilled as much scientific, cultural, historical, economic, medicinal and recreational wonder as water that springs forth from the ground. Modern genetic analysis would not be possible without polymerase isolated from the thermophilic archeaebacteria *Thermus aquaticus* that inhabits a hot spring in Yellowstone National Park, USA (Brock 1997). Cold, Rocky Mountain spring water is a lucrative product for the bottled water industry (e.g. Mountain Lite Spring Water Co., O'Canada Premium Mountain Water, Canadian Springs), whereas hot spring water is marketed to tourists by resorts and spas. Volcanically active Japan, for example, has about 24,000 springs and 2,300 hot spring resorts, 90 containing hospitals (Agishi et al. 1995). These *onsen* garner over 140 million annual visits and highlight how springs are deeply engrained into Japanese culture (Agishi et al. 1995).

Though not as popular as in Japan, people have long sought out the curative properties of springs in western Canada, which offers about a dozen hot spring resorts and numerous undeveloped springs (Fig. 1-1; Woodsworth 1999). First Nations groups waged war over the healing properties of Halcyon Hot Springs in southern British Columbia, and national park status failed to prevent the healed from littering the area around Banff Hot Springs with crutches (Elworthy 1917; McDonald et al. 1978). British Columbia has gone so far as to post highway signs reading "British Columbia – Mountains, Wineries and Hot Springs". The lucrative nature of hot spring tourism is easily illustrated by looking at the pools at Fairmont Hot Springs resort in southeast British Columbia on a typical day in July or August – upwards of 3,000 people will each pay $10 for the privilege of soaking away their worries in the soothing waters.

Springs in western Canada are not only major tourist attractions, but are historically significant to the development of the country. Many of the commercial resorts in operation today were originally used by First Nations and subsequently staked near the end of the 19th century when the Canadian Pacific

Fig. 1-1 Hot spring tourism in western Canada. A) Fairmont Hot Springs set against the Stanford Range at the western edge of the Rocky Mountains in southeast British Columbia. B) Ram Creek springs south of Fairmont. C) Lussier Hot Springs south of Fairmont. D) Earth and atmospheric science graduate student field trip to Lussier Hot Springs. E, F) Liard Hot Springs along the Alaska highway in northeast British Columbia. The area is a year-round ecological oasis with biotic diversity that could not be supported without the springs.

Railway was built through the mountains (McDonald et al. 1978). One spring in particular – the Cave and Basin spring – had a reserve created around it in 1885. It eventually became Banff National Park, Canada's first national park, and the second in North America behind another geothermal wonderland, Yellowstone National Park, USA (Gadd 1995). Ironically, it is now a federal offence to swim in the Cave and Basin springs; it has been designated as a protected area because of *Physella johnsoni*, an endangered snail inhabiting the water (Grasby and Lepitzki 2002).

Unbeknownst to most hot springs visitors, chemical precipitates of calcium carbonate ($CaCO_3$) commonly form from the waters that provide their bliss. Water emitted by the Fairmont Hot Springs and the Cave and Basin springs formed sizeable calcium carbonate deposits over several millennia (Grasby et al. 2003; Rainey and Jones 2005, 2009). Modern deposits of bright white calcium carbonate forming at Pamukkale (literally "cotton castle"), Turkey, and at Mammoth Hot Springs in Yellowstone National Park are huge tourist draws (Figs. 1-2A,B). Parras (Spanish for *vine*), Mexico, uses its several springs, carbonate spring deposits, and the oldest winery in North America to build the town's image. Parras is ripe with vineyard related carvings made from local carbonate spring deposits, and the town also unwittingly turned a domed, relict carbonate spring deposit into a tourist attraction by building a church atop it, high above the town (Figs. 1-2C,D).

North of Parras in the desert town of Cuatro Cienegas is a church built entirely of stone quarried from a local carbonate spring deposit (Figs. 1-2E,F). This church represents the oldest and most widespread use of these deposits for building stone. The stone is aesthetically pleasing and durable, yet its relative softness makes it much easier to quarry than harder stone like granite (Figs. 1-3A,B). Its use as a load-bearing building stone has diminished compared to Roman times, but is still commonly used as a natural facing stone (tile). Indeed, nearly every tile supply store sells "travertine" tiles, usually imported from Italy, Turkey, Mexico or China (Figs. 1-3C to E). After being extracted from the quarries and processed, the finished product exports for between $300 and $600

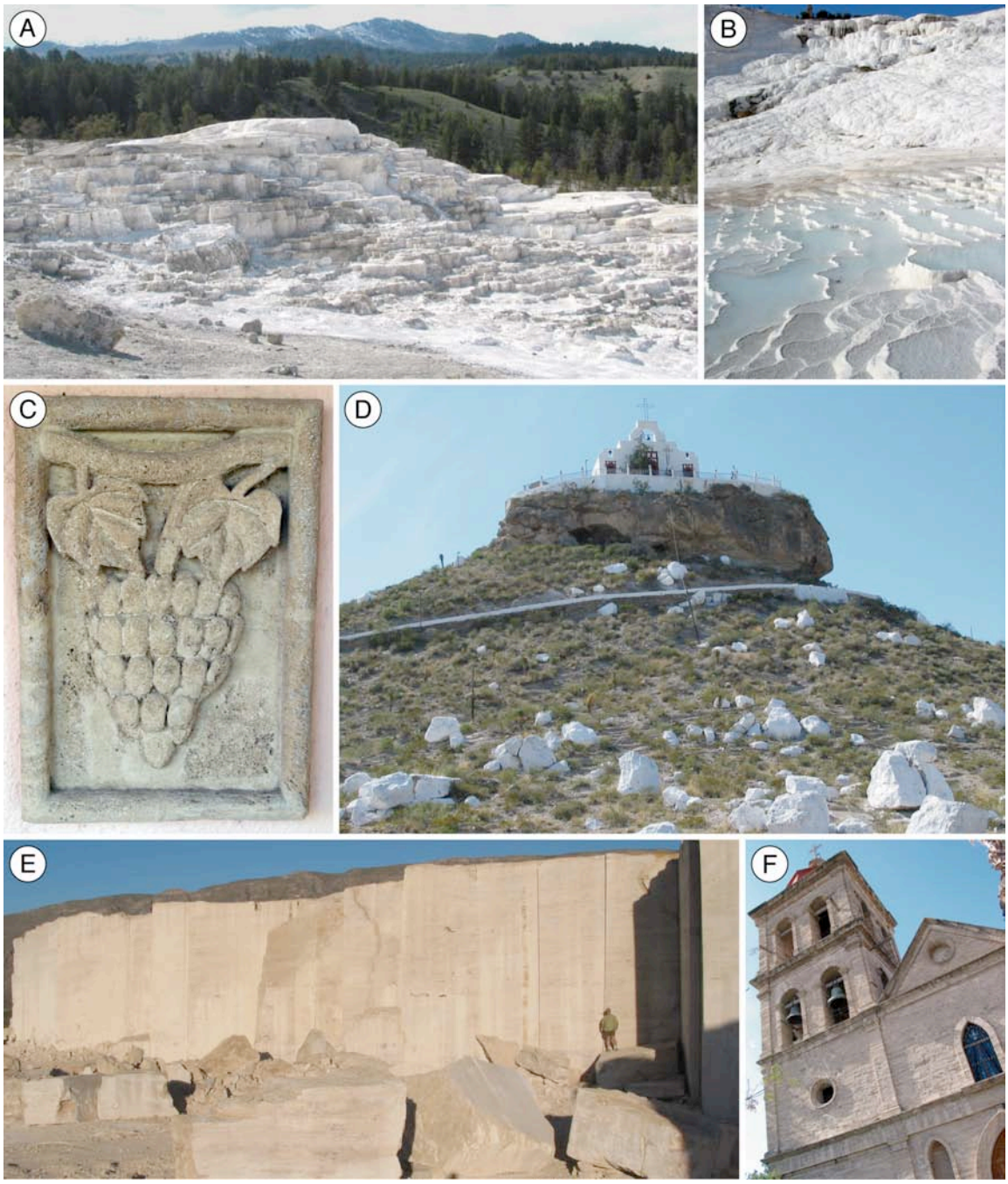

Fig. 1-2 Carbonate spring deposits worldwide. A) Modern deposit forming from 50-70°C water at Mammoth Hot Springs, Yellowstone National Park, Wyoming, USA. B) $CaCO_3$ actively precipitating from 30°C water at Pamukkale, Turkey. C) and D) Parras, Coahuila State, Mexico. C) Local carbonate spring deposits have been quarried and carved into designs celebrating the local winery industry. Parras, Spanish for "vine" has the oldest winery in Mexico (400 years old). D) El Santo Madero church set high above Parras built directly on top of relict carbonate spring deposit. Painted white blocks in foreground broke away from the main deposit above. Active springs used for a commercial pool located at a lower elevation than the church deposit. E) and F) Cuatrocienegas, Coahuila State, Mexico. E) Cuatrocienegas is located in a desert oasis with over 200 known springs, all of which emerge below the elevation of the quarried relict deposit. Note person for scale at right of image. F) Church in Cuatrocienegas town center built with blocks of stone quarried from the nearby relict carbonate spring deposit shown in E).

Fig. 1-3 Extraction and production of travertine to be used as facing stone. A) Three benches cut at the Ballik quarry near Denizli, Turkey. B) Each block weighs 20 to 30 tonnes and produces enough tile to cover an entire football field. C) Tile store in Edmonton on 170th street advertising travertine tile. D) Travertine tile samples. E) Travertine countertop.

per ton, making it an expensive building material worthy of upscale architecture (pers. comm. Yagiz 2005). It has proven to be popular in Edmonton and can be found on the University of Alberta campus in the Education building, the Rutherford North library, and on the outside of the Cameron Library (Fig. 1-4A). It has also been used in other prominent Edmonton buildings such as City Hall (Figs. 1-4C to E), West Edmonton Mall (Figs. 1-4B,G to I), the Muttart Conservatory (Fig. 1-4F) and the Crown Plaza Hotel.

Carbonate spring deposits in Canada however, have seen limited economic exploitation. An attempt was made during the 1930's to extract building stone from the Big Hill Springs deposit near Calgary, Alberta, but it lacked durability (Mussieux and Nelson 1998). The only deposit currently being exploited is the Wolfenden deposit in southeast British Columbia. Rocky Mountain Tufa Ltd. sells the quarried stone for landscaping purposes and exports it as far south as Arizona. The rock is buried beneath gardens where its abundant porosity facilitates water retention and reduces water consumption in arid climates.

Much of the scientific interest in carbonate spring deposits has focused on the ability of these deposits to react to and record past climatic conditions, and the biotic-abiotic interactions responsible for their development (e.g. Chafetz and Folk 1984; Pentecost 1985, 1995, 1998, 2003; Koban and Schweigert 1993; Folk 1994; Pedley 1994, 2000; Freytet and Plet 1996; Andrews et al. 1997; Das and Mohanti 1997; Pentecost et al. 1997; Chafetz and Guidry 1999; Andrews et al. 2000; Bonny and Jones 2003a,b; Fouke et al. 2003; Garnett et al. 2004; Andrews and Brasier 2005). Weed (1888) is one of the originators of scientific study of spring deposit development, but he acknowledged that studies of microbial growths in Icelandic spring waters by Sir William Hooker date back as far as 1809, and that in 1862, Dr. F. Cohn first discovered the relationship between algal growth and calcite precipitation in spring waters. From his investigations on Yellowstone springs, Weed (1888) concluded that calcium carbonate deposition was influenced by five major factors: 1) relief of pressure, 2) diffusion of carbonic acid by exposure to the atmosphere, 3) evaporation, 4) heating, and 5) influence of plant life. Though much of what Weed discovered is still relevant today, there

Fig. 1-4 Travertine tile used in Edmonton architecture. A) North side of Cameron Library on the University of Alberta campus. B) The brown banded tile in the foreground and the red Ferrari in West Edmonton Mall are two of Italy's luxury exports. C) Edmonton City Hall. The stairs leading to council chambers and the floor are made of travertine. D) Close-up of travertine tile used in the City Hall floor. E) Pillars on a building across from City Hall. F) Raw stone from a carbonate spring deposit was used to landscape the desert pyramid at the Muttart Conservatory. G) A statue saluting Alberta's oil and gas workers rests on travertine tile in West Edmonton Mall. H) Patterned floor design in West Edmonton Mall. I) Inlaid travertine, marble and serpentinite in West Edmonton Mall.

are at least sixty factors governing carbonate spring deposit development (Fig. 1-5). The importance of each factor varies between deposits, and their capacity to promote deposit formation or degradation lies in their ability to affect equation 1. The forward reaction controls calcium carbonate precipitation, whereas the reverse reaction controls dissolution.

[1] $$Ca^{2+}(aq) + 2HCO_3^-(aq) \leftrightarrow CaCO_3(s) + CO_2(g) + H_2O(l)$$

Carbonate minerals are incredibly reactive in nature, largely because they incorporate CO_2 into their crystal structures in the form of carbonate (CO_3^{2-}). In particular, $CaCO_3$ formation is highly exothermic and its constituent components, Ca^{2+} and CO_2, are readily available near Earth's surface. $CaCO_3$ solubility, being strongly controlled by the amount of CO_2 in solution, exhibits retrograde solubility akin to gases. This means that carbonates, unlike other minerals, are more soluble in cold solutions than hot solutions. Although Weed (1888) stated that heating promotes $CaCO_3$ formation, the faulty assumption that cooling promotes $CaCO_3$ precipitation is still perpetuated by some springs researchers (e.g. Pedley 2008, abstract).

The sixty factors that can influence the precipitation of $CaCO_3$ from spring water are broadly categorized as intrinsic or extrinsic (Fig. 1-5). Intrinsic factors control calcite precipitation within the spring system (e.g. flow conditions, biotic growth), whereas extrinsic factors control the setting where a spring system is active (e.g. geographical distribution, topography, spring water source). Most of these factors are interdependent, thus changing one property will affect the interactions of other factors. For example, the depth of subsurface meteoric water infiltration and its rate of ascent to the surface affect spring water temperature; the temperature impacts $CaCO_3$ solubility and the types of organisms capable of growing in the spring water, and the deposit textures are controlled by $CaCO_3$ supersaturation state and crystals precipitated in association with spring biota. Many of the factors vary temporally and spatially on daily to millennial scales, adding further complexity to these already complicated systems.

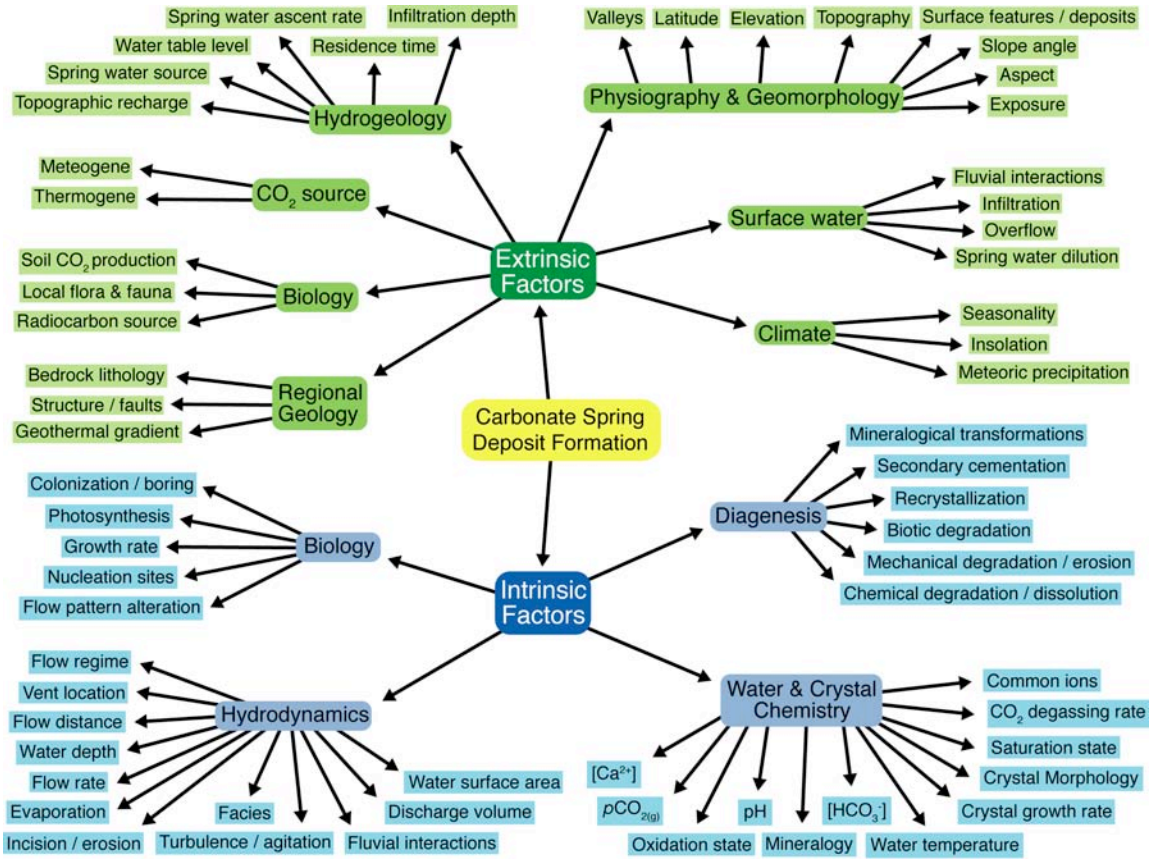

Fig. 1-5 Factors controlling carbonate spring deposit development.

The purpose of this thesis was to compare and contrast the development of several relict Holocene carbonate spring deposits present in the Rocky Mountains. This thesis focused mainly on the intrinsic and extrinsic factors that caused $CaCO_3$ to precipitate from spring water after it emerged from vents and became exposed to the atmosphere. Data pertaining to the regional geology, ecology, geothermal potential and water chemistry of western Canadian springs are in abundance, but have not been applied to a comprehensive assessment of carbonate spring deposit formation (e.g. Boyle and McIntosh 1914; Elworthy 1917, 1918, 1926; Satterly and Elworthy 1917; van Everdingen 1969, 1972, 1984; Souther and Halstead 1973; Crandall and Sadlier-Brown 1976; Lewis 1978; Borneuf 1983; Mazor et al. 1983; Souther and Dellechaie 1984; Souther 1992; Grasby et al. 2000; Grasby and Hutcheon 2001; Allen et al. 2006). Carbonate spring deposit studies are a more recent development, with all of the western Canadian investigations having been completed in the past decade. Besides the study of the carbonate deposit at the Cave and Basin spring in Banff National Park (Grasby et al. 2003), the Carbonate/Springs Research Group at the University of Alberta has been involved in all of them (Renaut and Jones 2000; Bonny 2002; Bonny and Jones 2003a,b; Rainey and Jones 2005, 2007, 2009; Turner and Jones 2005; Jones and Renaut 2008).

The Rocky Mountains were chosen as the research area because of a large number of springs with conditions that are favourable for the development of a variety of carbonate spring deposit types. The Rocky Mountains have ample meteoric precipitation for topographic recharge, Palaeozoic carbonate rocks as a calcium source, an elevated geothermal gradient to heat the water and groundwater circulation along major crustal-scale faults (Fig. 1-6; Souther and Halstead 1973; Borneuf 1983; Grasby and Hutcheon 2001; Allen et al. 2006). Rocky Mountain springs exhibit a wide range of temperatures and are a calcium-magnesium-bicarbonate type (ideal for $CaCO_3$ precipitation), as opposed to the calcium-magnesium-sulfate, sodium-sulfate and sodium-chloride type elsewhere in Alberta (Souther and Halstead 1973; Borneuf 1983). Springs are also abundant

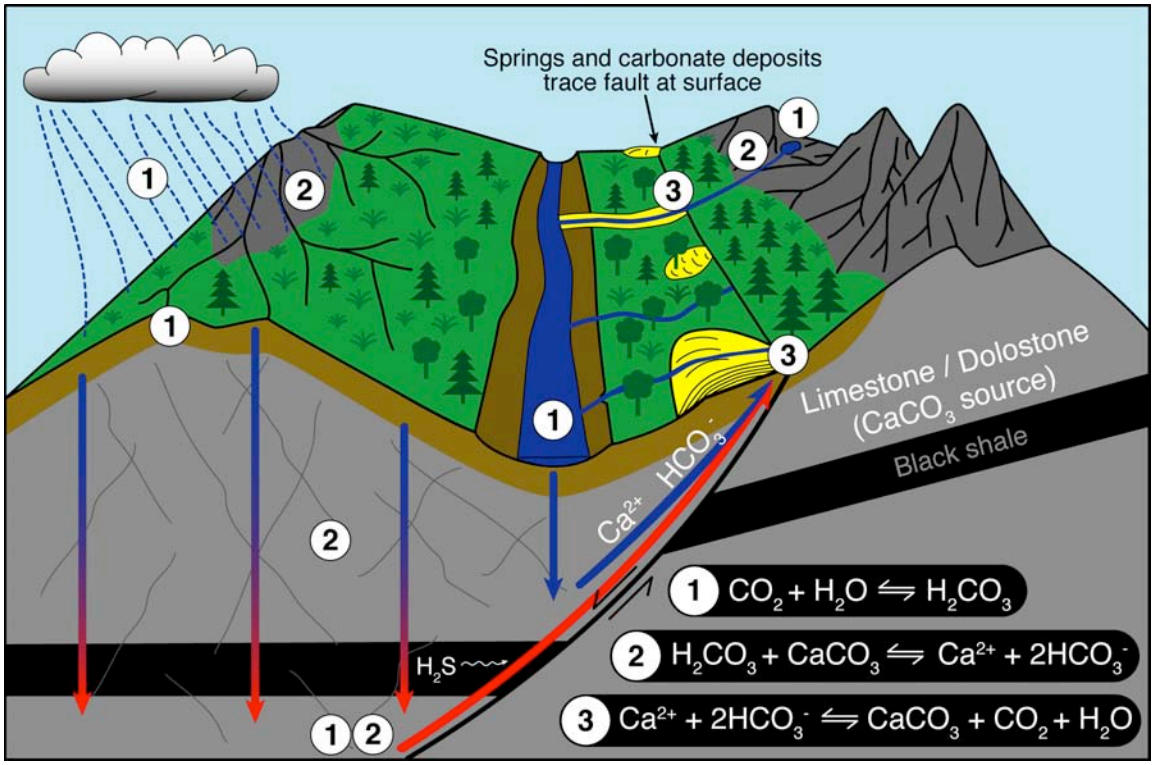

Fig. 1-6 Simplified schematic diagram illustrating regional controls on carbonate spring deposit development and distribution in western Canada. Numbers indicate locations where chemical reactions occur. Minimum infiltration depths for the hottest springs in the Rocky Mountains are estimated to be 0.9 to 2.2 km (Allen et al. 2006).

in southern British Columbia west of the Rocky Mountains, but lesser amounts of carbonate bedrock means fewer carbonate spring deposits.

The three Holocene carbonate spring deposits investigated for this thesis are at Fall Creek springs, Alberta, Fairmont Hot Springs, British Columbia, and Hot Creek springs, British Columbia (Fig. 1-7). They were chosen to complement and expand upon studies completed on deposits at Miette Hot Springs in Jasper National Park, Alberta (Bonny 2002; Bonny and Jones 2003a,b), Cave and Basin springs in Banff National Park, Alberta (Grasby et al. 2003), Big Hill Springs Provincial park, Alberta (Turner and Jones 2005), and Clinton, British Columbia (Renaut and Long 1986; Renaut and Jones 2000; Jones and Renaut 2008). Each chapter exposes a new facet of deposit formation and illustrates how slight changes in the controlling factors profoundly affected the development of each deposit. Each deposit is unique in regards to the physical and geomorphological characteristics that influenced their development. Fairmont Hot Springs are the only true hot springs studied (> 36.7°C, Pentecost et al. 2003), whereas the Fall Creek and Hot Creek springs are cold springs. Fairmont and Fall Creek formed directly from spring water with minimal influence from additional surface water, whereas the Hot Creek deposit formed in a fluvial setting with water derived from a spring and from surface runoff.

Conclusions regarding carbonate spring deposit development in western Canada were based mostly on observations and measurements of the relict deposits. Analyses were performed on 105 thin sections, 3350 scanning electron photomicrographs, 109 stable carbon and oxygen isotope samples, and 9 radiocarbon dated samples of organic material. Field observations revealed that the relict deposits contain large amounts of calcite compared to the volume of calcite that could potentially precipitate from the spring water volumes presently being discharged from the vents. Spring water presently flows in channels incised through the deposits, indicating that: 1) there has been a net loss of material from the deposits since the last period of carbonate accumulation, and 2) current calcite precipitation is not voluminous enough to replace the lost material.

Fig. 1-7 Locations of carbonate spring deposits in western Canada that have received detailed investigations (white labels). Springs with black labels were depicted in figure 1-1.

This thesis investigated the nature of the discrepancy between the paucity of modern carbonate precipitation and abundance of carbonate contained in the relict deposits. It tested the hypothesis that these spring deposits formed in response to a climate that was wetter than today. To do this, it was necessary to determine the dominant controls on carbonate spring deposit formation in western Canada, such as the role that microorganisms play in calcite precipitation. This was accomplished by establishing developmental controls for three different deposits in the Rocky Mountains, and then combining these results with previous research findings from western Canadian springs. Even though the modern springs are obviously not responsible for older deposits, they do provide a modern laboratory that can provide valuable insights into the processes involved. Furthermore, water sampled today (and hence its chemistry) is probably not exactly the same as that from which most of the older calcite was precipitated, but again can be used as a guide to understand paleo-flow conditions.

Chapter 2, titled "Rapid Cold Water Formation and Recrystallization of Relict Bryophyte Tufa at the Fall Creek Cold Springs, Alberta, Canada" deals with the development and diagenetic alteration of a carbonate spring deposit formed mainly of calcite-encrusted bryophytes (mosses). Bryophytes are common in spring systems, but at Fall Creek they are the primary components upon which a temporally and spatially variable, 4-stage developmental process acted. The Fall Creek deposit, unlike other deposits, was also subjected to extensive diagenesis whereby primary textures were masked, but not destroyed. The Fall Creek spring is also the only spring examined that currently emits $H_2S(g)$ and precipitates native sulphur. This chapter highlights the mutability of carbonate deposits in the natural environment and how post-depositional modifications can interfere with the discovery of primary depositional processes.

Chapter 3, titled "Abiotic versus biotic controls on the development of the Fairmont Hot Springs Carbonate Deposit, British Columbia, Canada" and chapter 4, titled "Radiating calcite dendrites – precursors for coated grain formation in the Fairmont Hot Springs carbonate deposit" explore the diverse facies present in the Fairmont deposit. The Fairmont deposit is probably the largest carbonate spring

deposit in Canada, and is formed of nearly equal parts biotic and abiotic facies. Chapter 3 illustrates how its development was regulated by the competition between biotic growth rates and calcite precipitation rates. Chapter 4 presents a novel, two-stage mechanism for coated grain formation whereby abiotic radiating calcite dendrite crystals formed nuclei, whereas cortical development was microbially mediated. These chapters illustrate the complexity of depositional environments in relict spring systems, and the lack of facies diversity in the modern systems.

Chapter 5, titled "Comparative Analysis of Soft-Tissue Preservation in the Hot Creek Carbonate Spring Deposit, British Columbia, Canada" examines how calcite precipitated in association with filamentous cyanobacteria led to the development of this deposit. Conditions in the Hot Creek spring system were unique because they favoured preservation of soft-tissue organisms like cyanobacteria, but excluded harder organisms like wood and diatoms. This study emphasizes the incomplete nature of the depositional history of carbonate spring deposits.

The final chapter compares deposit development at western Canadian springs, underscores factors common to their formation, and reveals site-specific differences responsible for unique characteristics of each deposit. The discussion also provides explanations for why springs like Lussier Hot Springs (Figs. 1-1C,D) that are capable of precipitating calcite (ie. have favourable water chemistry) lack modern and relict carbonate deposits. Ultimately, the factors that control carbonate spring deposit development in western Canada are characterized by temporal and spatial changes (rather than stasis) that act on microscopic to regional scales.

References

Agishi, Y., Ohtsuka, Y., Watanabe, I., Yabunaka, N., Noro, H., 1995. Present features of medical balneology in Japan. In: Y. Agishi and Y. Ohtsuka (Editors), Recent progress in medical balneology and climatology. Hokkaido University School of Medicine, Sapporo, Japan, pp. 1-10.

Allen, D.M., Grasby, S.E., Voormeij, D.A., 2006. Determining the circulation depth of thermal springs in the southern Rocky Mountain Trench, south-eastern British Columbia, Canada using geothermometry and borehole temperature logs. Hydrogeology Journal, 14: 159-172.

Andrews, J.E., Brasier, A.T., 2005. Seasonal records of climatic change in annually laminated tufas: short review and future prospects. Journal of Quaternary Science, 20(5): 411-421.

Andrews, J.E., Riding, R., Dennis, P.F., 1997. The stable isotope record of environmental and climatic signals in modern terrestrial microbial carbonates from Europe. Palaeogeography, Palaeoclimatology, Palaeoecology, 129: 171-189.

Andrews, J.E., Pedley, M., Dennis, P.F., 2000. Palaeoenvironmental records in Holocene Spanish tufas: a stable isotope approach in search of reliable climatic archives. Sedimentology, 47: 961-978.

Bonny, S., 2002. Relic tufa at Miette Hot Springs, Jasper National Park, Alberta. M.Sc. Thesis, University of Alberta, Edmonton.

Bonny, S., Jones, B., 2003a. Microbes and mineral precipitation, Miette Hot Springs, Jasper National Park, Alberta, Canada. Canadian Journal of Earth Sciences, 40: 1483-1500.

Bonny, S., Jones, B., 2003b. Relict tufa at Miette Hot Springs, Jasper National Park, Alberta, Canada. Canadian Journal of Earth Sciences, 40: 1459-1481.

Borneuf, D., 1983. Springs of Alberta. Earth Sciences Report 82-3. Alberta Research Council, Calgary, 95 pp.

Boyle, R.W., McIntosh, D., 1914. On the amount of radium and radium emanation present in the waters of several western springs. Royal Society of Canada Proceedings and Transactions, 3rd series, 7(Sec. 3): 163.

Brock, T.D., 1997. The value of basic research: discovery of *Thermus aquaticus* and other extreme thermophiles. Genetics, 146: 1207-1210.

Chafetz, H.S., Folk, R.L., 1984. Travertines: depositional morphology and the bacterially constructed constituents. Journal of Sedimentary Petrology, 54(1): 289-316.

Chafetz, H.S., Guidry, S.A., 1999. Bacterial shrubs, crystals shrubs, and ray-crystal shrubs: bacterial vs. abiotic precipitation. Sedimentary Geology, 126: 57-74.

Crandall, J.T., Sadlier-Brown, T.L., 1976. Data on geothermal areas Cordilleran Yukon, Northwest Territories, and adjacent British Columbia Canada. Contract Number 1SQ5-0136, Department of Supply Services, Earth Physics Branch Open File No. 78-1. Department of Energy, Mines and Resources Canada, Ottawa, Canada, 80 pp.

Das, S., Mohanti, M., 1997. Holocene microbial tufas: Orissa State, India. Carbonates and Evaporites, 12: 204-219.

Elworthy, R.T., 1917. Examination of the hot springs at Banff, Alberta. Royal Society of Canada Proceedings and Transactions, 3rd Series, 11(Sec. 3): 27-33.

Elworthy, R.T., 1918. Mineral springs of Canada; Part II, The chemical character of some Canadian mineral springs. Bulletin 20 (Mines Branch No. 472). Canada Department of Mines, 173 pp.

Elworthy, R.T., 1926. Hot springs in western Canada; their radioactive and chemical properties. Bulletin 699. Canada Department of Mines, Mines Branch, Investigations of mineral resources and the mining industry, 1925, 33 pp.

Folk, R.L., 1994. Interaction between bacteria, nannobacteria, and mineral precipitation in hot springs of central Italy. Géographie physique et Quaternaire, 48(3): 233-246.

Fouke, B.W., Bonheyo, G.T., Sanzenbacher, B., Frias-Lopez, J., 2003. Partitioning of bacterial communities between travertine depositional facies at

Mammoth Hot Springs, Yellowstone National Park, U.S.A. Canadian Journal of Earth Sciences, 40: 1531-1548.

Freytet, P., Plet, A., 1996. Modern freshwater microbial carbonates: the *Phormidium* stromatolites (tufa-travertine) of southeastern Burgundy (Paris Basin, France). Facies, 34: 219-238.

Gadd, B., 1995. Handbook of the Canadian Rockies. Corax Press, Jasper, 831 pp.

Garnett, E.R., Andrews, J.E., Preece, R.C., Dennis, P.F., 2004. Climatic change recorded by stable isotopes and trace elements in a British Holocene tufa. Journal of Quaternary Science, 19(3): 251-262.

Grasby, S.E., Hutcheon, I., 2001. Controls on the distribution of thermal springs in the southern Canadian Cordillera. Canadian Journal of Earth Sciences, 38: 427-440.

Grasby, S.E., Lepitzki, D.A.W., 2002. Physical and chemical properties of the Sulphur Mountain thermal springs, Banff National Park, and implications for endangered snails. Canadian Journal of Earth Sciences, 39: 1349-1361.

Grasby, S.E., Hutcheon, I., Krouse, H.R., 2000. The influence of water-rock interaction on the chemistry of thermal springs in western Canada. Applied Geochemistry, 15: 439-454.

Grasby, S.E., van Everdingen, R.O., Bednarski, J., Lepitzki, D.A.W., 2003. Travertine mounds of the Cave and Basin National Historic Site, Banff National Park. Canadian Journal of Earth Sciences, 40: 1501-1513.

Jones, B., Renaut, R.W., 2008. Cyclic development of large, complex, calcite dendrite crystals in the Clinton travertine, Interior British Columbia, Canada. Sedimentary Geology, 203: 17-35.

Koban, C.G., Schweigert, G., 1993. Microbial origin of travertine fabrics -- two examples from southern Germany (Pleistocene Stuttgart travertines and Miocene Riedöschingen travertine). Facies, 29: 251-264.

Lewis, T.J., 1978. Meager Mountain, B.C. - a possible geothermal energy source. Energy, Mines and Resources Canada, Ottawa, 17 pp.

Mazor, E., van Everdingen, R.O., Krouse, H.R., 1983. Noble-gas evidence for geothermal activity in a karstic terrain: Rocky Mountains, Canada. Geochimica et Cosmochimica Acta, 47: 1111-1115.

McDonald, J., Pollock, D., McDermot, B., 1978. Hotsprings of Western Canada. Labrador Tea Company, Vancouver, Canada, 162 pp.

Mussieux, R., Nelson, M., 1998. A Traveller's Guide to the Geological Wonders in Alberta. The Provincial Museum of Alberta, Edmonton, 254 pp.

Pedley, H.M., 1994. Prokaryote-microphyte biofilms and tufas: a sedimentological perspective. Kaupia, 4: 45-60.

Pedley, H.M., 2000. Ambient temperature freshwater microbial tufas. In: R.E. Riding and S.M. Awramik (Editors), Microbial Sediments. Springer-Verlag, Berlin, pp. 179-186.

Pedley, H.M., 2009. Tufas and travertines of the Mediterranean region: a testing ground for freshwater carbonate concepts and developments. Sedimentology, 56(1): 221-246.

Pentecost, A., 1985. Association of cyanobacteria with tufa deposits: identity, enumeration, and nature of the sheath material revealed by histochemistry. Geomicrobiology Journal, 4(3): 285-298.

Pentecost, A., 1995. Significance of the biomineralizing microniche in a *Lyngbya* (Cyanobacterium) travertine. Geomicrobiology Journal, 13: 213-222.

Pentecost, A., 1998. The significance of calcite (travertine) formation by algae in a moss-dominated travertine from Matlock Bath, England. Archiv fuer Hydrobiologie, 143(4): 487-509.

Pentecost, A., 2003. Cyanobacteria associated with hot spring travertines. Canadian Journal of Earth Sciences, 40: 1447-1457.

Pentecost, A., Bayari, S., Yesertener, C., 1997. Phototrophic microorganisms of the Pamukkale travertine, Turkey: their distribution and influence on travertine deposition. Geomicrobiology Journal, 14: 269-283.

Pentecost, A., Jones, B., Renaut, R.W., 2003. What is a hot spring? Canadian Journal of Earth Sciences, 40: 1443-1446.

Rainey, D.K., Jones, B., 2005. Radiating calcite dendrites -- precursors for coated grain formation in the Fairmont Hot Springs Travertine, Canada. In: M. Özkul, S. Yagiz and B. Jones (Editors), Proceedings of1st International Symposium on Travertine, Denizli, Turkey, pp. 25-32.

Rainey, D.K., Jones, B., 2007. Rapid cold water formation and recrystallization of relict bryophyte tufa at the Fall Creek cold springs, Alberta, Canada. Canadian Journal of Earth Sciences, 44: 889-909.

Rainey, D.K., Jones, B., 2009. Abiotic versus biotic controls on the development of the Fairmont Hot Springs carbonate spring deposit, British Columbia, Canada. Sedimentology, doi: 10.1111/j.1365-3091.2009.01059.x..

Renaut, R.W., Long, P.R., 1986. Post-glacial travertine deposits of the Clinton area, interior British Columbia, GAC, MAC, CGU Joint Annual Meeting Program With Abstracts. Carleton University, Ottawa, Canada, pp. 117.

Renaut, R.W., Jones, B., 2000. Microbial precipitates around continental hot springs and geysers. In: R.E. Riding and S.M. Awramik (Editors), Microbial Sediments. Springer-Verlag, Berlin, pp. 187-195.

Satterly, J., Elworthy, R.T., 1917. Mineral springs of Canada; Part I, The radioactivity of some Canadian mineral springs. Mines Branch No. 435. Canada Department of Mines Bulletin 16, 55 pp.

Souther, J.G., 1992. Energy and groundwater resources of the Canadian Cordillera; geothermal energy. Geological Survey of Canada, Vancouver.

Souther, J.G., Halstead, E.C., 1973. Mineral and thermal waters of Canada, Geological Survey of Canada Paper 73-18. Department of Energy, Mines and Resources, Canada, Ottawa, 225-256 pp.

Souther, J.G., Dellechaie, F., 1984. Geothermal exploration at Mr. Cayley; a Quaternary volcano in southwestern British Columbia, Geothermal Resources Council, 1984 annual meeting, Reno, Nevada, United States.

Turner, E.C., Jones, B., 2005. Microscopic calcite dendrites in cold-water tufa; implications for nucleation of micrite and cement. Sedimentology, 52(5): 1043-1066.

van Everdingen, R.O., 1969. Degree of saturation with respect to $CaCO_3$, $CaMg(CO_3)_2$, and $CaSO_4$ for some thermal and mineral springs in the Southern Rocky Mountains, Alberta and British Columbia. Canadian Journal of Earth Sciences, 6: 1421-1430.

van Everdingen, R.O., 1972. Thermal and mineral springs in the southern Rocky Mountains of Canada. Water Management Service, Department of the Environment, Environment Canada.

van Everdingen, R.O., 1984. Dirty-water events at Rocky Mountain hot springs and their correlation with other short-lived phenomena. Canadian Journal of Earth Sciences, 21: 997-1007.

Weed, W.H., 1888. Formation of Travertine and siliceous sinter by the vegetation of Hot Springs. United States Geological Survey Annual Report, 9, 613-676 pp.

Woodsworth, G., 1999. Hot Springs of Western Canada. Gordon Soules Book Publisher's Ltd., West Vancouver, 288 pp.

Chapter 2

Rapid Cold Water Formation and Recrystallization of Relict Bryophyte Tufa at the Fall Creek Cold Springs, Alberta, Canada[1]

Introduction

Worldwide, cold, freshwater carbonate spring deposits are localized geological features (e.g., Pentecost 1995; Ford and Pedley 1996) that form where groundwaters, supersaturated with respect to $CaCO_3$, are discharged from spring vents (Guo and Riding 1999; Pentecost et al. 2000). These deposits, formed dominantly of calcite and/or aragonite are characterized by diverse arrays of crystal morphologies and macroscopic textures. The most extensively studied deposits are the hot water deposits (> 36.7°C, cf. Pentecost et al. 2003) at Mammoth Hot Springs in Yellowstone National Park, USA (e.g., Weed 1889; Pentecost 1990; Fouke et al. 2000, 2003), and Rapolano and Tivoli in Italy (e.g., Chafetz and Folk 1984; Folk et al. 1985; Guo and Riding 1992, 1994, 1998, 1999; Pentecost 1994). Other studies focused on cooler water deposits in Britain and Spain (e.g., Pedley 1987; Pentecost 1993, 1999; Pedley et al. 1996; Peña et al. 2000; Martín-Algarra et al. 2003; Pedley et al. 2003), which have textures that are microbially, macrophytically, and crystallographically controlled.

Carbonate spring deposits in Canada are restricted to the western provinces and territories. Although over 130 active freshwater springs are known in the mountainous regions of Alberta, British Columbia, the Yukon, and the Northwest Territories (Woodsworth 1999), few have associated carbonate spring deposits, and even fewer have been described. Guidebooks (e.g., Gadd 1995; Woodsworth 1999) and spring surveys (e.g., van Everdingen 1972) generally give spring locations without discussing the associated deposits. Thus, most studies of

[1] A version of this chapter has been published. Rainey, D.K., Jones, B., 2007. Rapid cold water formation and recrystallization of relict bryophyte tufa at the Fall Creek cold springs, Alberta, Canada. Canadian Journal of Earth Sciences, 44: 889-909.

Canadian springs have focused on water chemistry (e.g., Gulley 1993; Grasby et al. 2000; Grasby and Hutcheon 2001), associated structural geology and stratigraphy (e.g., van Everdingen 1972), and/or gross deposit morphology (e.g., Wright 1980; Gulley 1993; Renaut and Jones 2000; Grasby et al. 2003). Exceptions include the analyses of tufa and modern precipitates at Miette Hot Springs in Jasper National Park, Alberta (Bonny 2002; Bonny and Jones 2003a, b), tufa from Big Hill Springs Provincial Park, Alberta (Turner and Jones 2005), and relict coated grains from Fairmont Hot Springs, British Columbia (Rainey and Jones 2005). Although some Canadian carbonate spring deposits display depositional features similar to those in the Yellowstone and Italian deposits, many are akin to the cooler (< 20°C), macrophyte-dominated tufas found in England (e.g., Pedley 1987; Pedley et al. 1996; Pentecost 1999) and Spain (Pedley et al. 1996; Peña et al. 2000; Pedley et al. 2003).

The Holocene tufa deposit at Fall Creek (Figs. 2-1 and 2-2) which is a poorly known Canadian carbonate spring deposit, is formed almost exclusively of the moss *Cratoneuron commutatum* that has been encrusted with calcium carbonate precipitated from cool (~ 13°C) spring water. The importance of mosses as tufa frame-builders has long been known (e.g., Emig 1918) as several studies have demonstrated their role in tufa development (e.g., Weijermars et al. 1986; Pentecost 1987, 1996; Zhang and Pentecost 2000). Petrographic analysis of the relict calcite deposit at Fall Creek shows that it evolved through repeated four-stage development cycles that were temporally and spatially variable. The most striking feature of this young deposit is the pervasive aggrading recrystallization that has masked many of the original fabrics. This paper focuses on these fabrics, presents a diagenetic model for tufa recrystallization, and demonstrates that even young tufas can undergo significant diagenetic alteration.

Methods And Materials

The large-scale features of the tufa were described in the field and 32 representative samples were collected and carefully located on a base map (Fig. 2-1C). Water temperature and pH measurements were taken in the field in

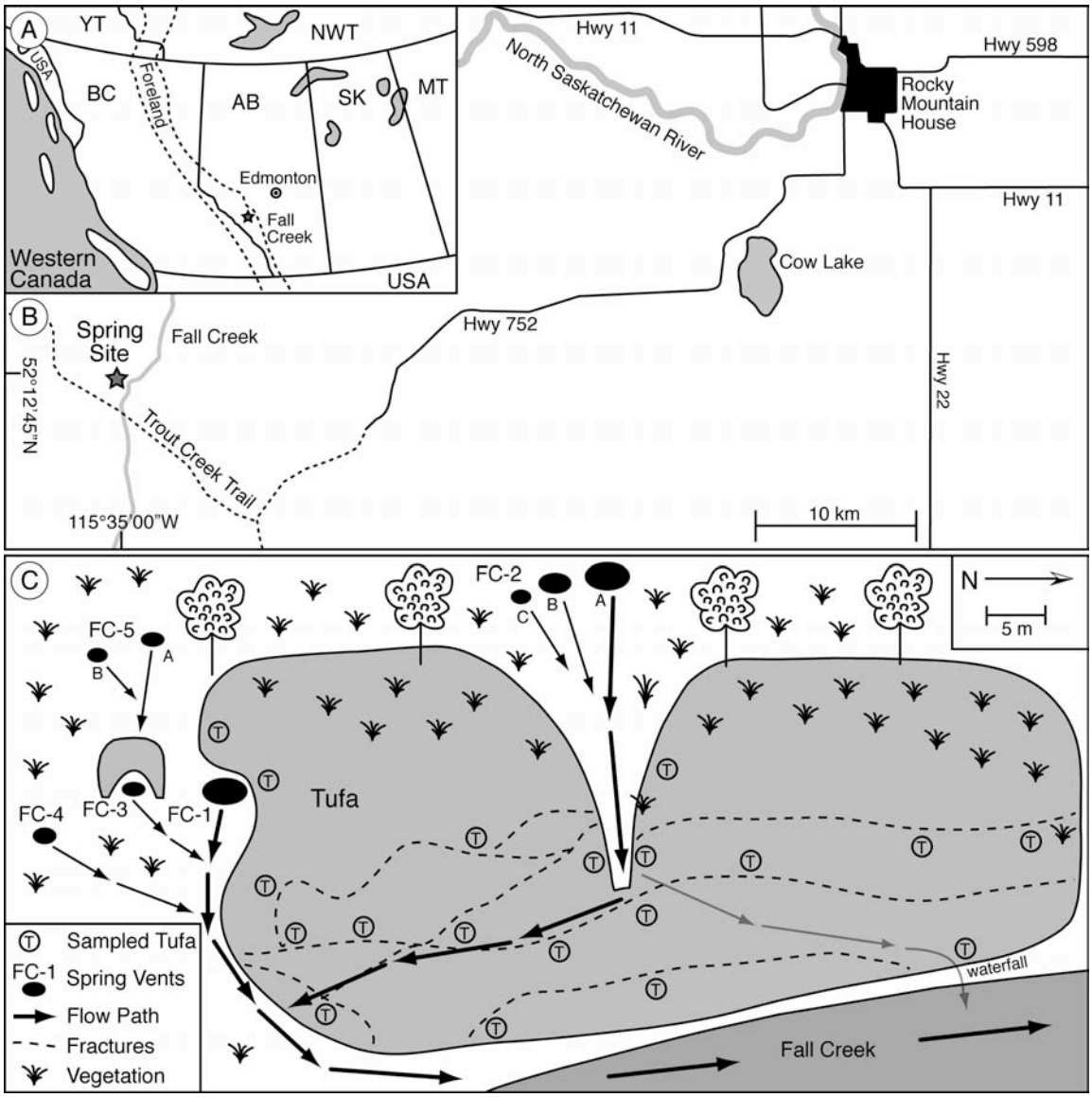

Fig. 2-1 Location of Fall Creek Tufa. A) Western Canada. B) Spring location in Rocky Mountains. C) Sketch map of main part of tufa deposit showing sample locations and spring vents (FC-1 to FC-5).

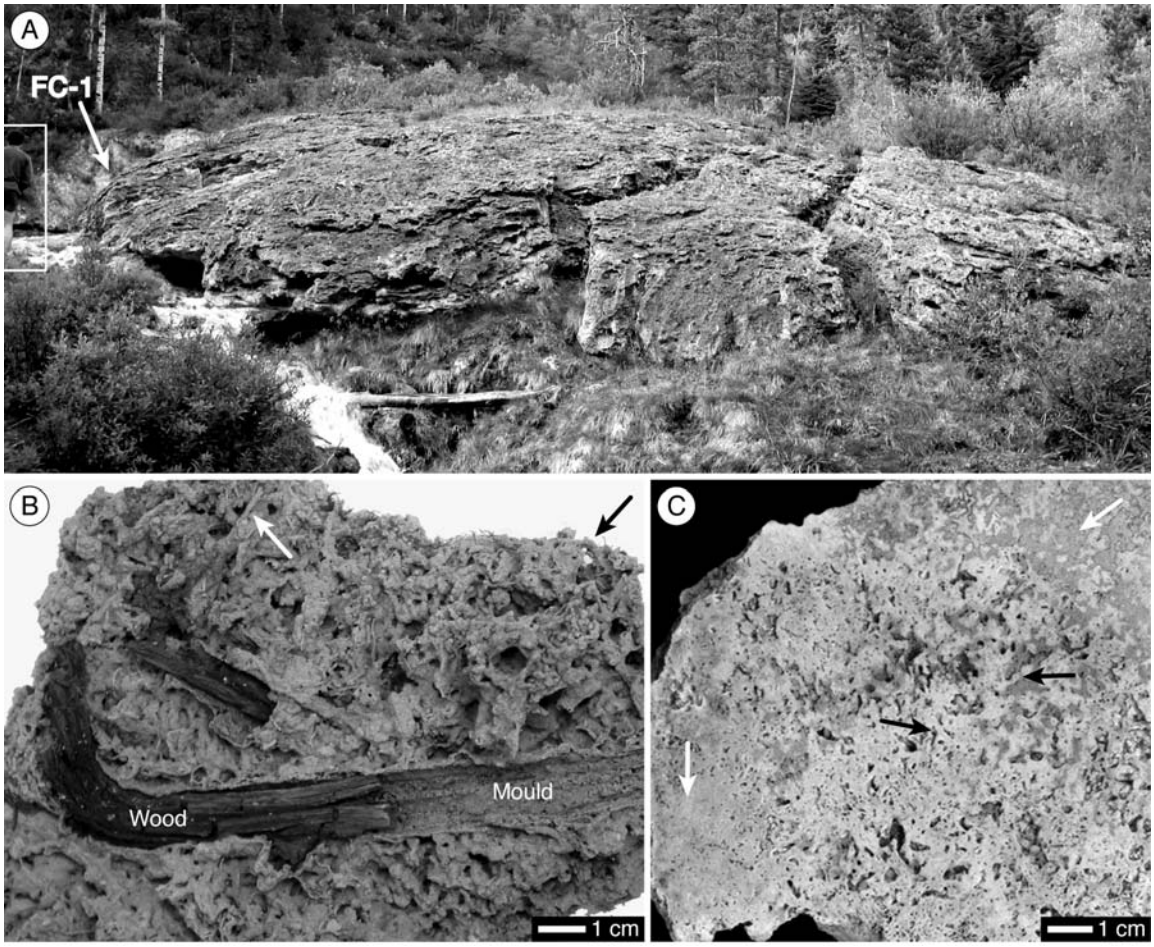

Fig. 2-2 Fall Creek Tufa. A) Looking west from Fall Creek to main part of tufa deposit. Main flow path from vent FC-1 visible on left. Person highlighted with white box for scale. B) Young, highly porous bryophyte tufa with minimal cavity occlusion. Arrows indicate bryophyte tubes. Wood embedded in tufa yielded an age of 310 +/- 50 ^{14}C years B.P.. C) Cut sample of older, highly cemented bryophyte tufa. Black arrows indicate bryophyte tubes with some surrounding porosity. White arrows indicate areas with porosity occluded by calcite cement and internal sediments. Darker colour due to higher concentration of organics.

September of 2001 and 2002 from vents numbered FC-1 to FC-6. Water samples were collected from FC-1 and FC-2, and a third sample was collected near the base of the slope at the convergence of several spring lines, just before the confluence with Fall Creek. Unfiltered water samples were collected in Nalgene plastic bottles. Filtered samples for isotope analysis, collected using a syringe and .22 micron filter, were stored in Teflon-capped 5 dram vials. Wood, which was embedded in the tufa, was collected in September 2002.

Thin sections were characterized using transmitted light and epifluorescence microscopy with an ultraviolet excitation filter. Fractured tufa samples and partially cemented bryophytes, sputter coated with gold, were examined on a JEOL 6301F field emission scanning electron microscope (SEM) at an accelerating voltage of 5-20 kV. A Rigaku Geigerflex Powder Diffractometer was used for X-ray analyses of powdered samples. Water analyses were undertaken in the Limnology Service Unit, University of Alberta, oxygen and carbon isotope analyses of the water were done by the Environmental Isotope Laboratory, University of Waterloo, and radiocarbon (^{14}C) dating of wood samples was completed at Isotrace Laboratories at the University of Toronto. Conventional radiocarbon ages were converted to calendar years using the CALIB radiocarbon calibration program and the IntCal04 terrestrial radiocarbon age calibration for 26 to 0 ka BP, and calibrated ages are reported as 2 sigma ranges (Stuiver and Reimer 1993; Reimer et al. 2004). Stable carbon and oxygen isotopic analyses of the calcite were completed in the stable isotope laboratory in the Department of Earth and Atmospheric Sciences, University of Alberta. Under vacuum, 4.5-5.5 mg of crushed limestone was reacted for 3 hours with 5 ml of phosphoric acid in a 25°C water bath, following the procedure of McCrea (1950). The carbon and oxygen isotopic composition of the liberated $CO_2(g)$ was measured with a Finnegan MAT 252 mass spectrometer.

The contrast and brightness of the digital field images and SEM photomicrographs used in this paper were adjusted using Adobe Photoshop©.

SEM photomicrographs, black backgrounds were introduced in order to highlight the features being shown.

Terminology

Modified after Pedley (1990) and Ford and Pedley (1996), tufa is herein treated as a carbonate deposit that formed from fresh waters and contains numerous micro- and macrophytic fossils, and fewer invertebrate fossils. This term is used regardless of sample porosity levels (cf. Emeis et al. 1987; Pedley 1990, 2000; Ford and Pedley 1996).

The biota associated with Fall Creek Spring is dominated by macrophytes, mainly bryophytes (mosses), along with fewer charophytes (branching green algae lacking a true vascular system), grasses, and woody plants. The photosynthetic microphyte biota is dominated by filamentous cyanobacteria.

Some of the calcite in the Fall Creek Tufa is formed of composite crystals (cf. Given and Wilkinson 1985; Sandberg 1985) that are formed of numerous subcrystals (cf. Sandberg 1985; Jones 1989b). Calcite grains < 4 μm long are termed micrite, with no genetic implications (cf. Kahle 1977; Jones 1989a).

Many of the primary cements in the Fall Creek Tufa have been diagenetically altered. Aggrading recrystallization refers to transformations that involved an increase in crystal size and change in crystal shape, but no change in mineralogy (cf. Folk 1965; Bathhurst 1975; Tucker and Bathhurst 1990; Tucker and Wright 1990). During aggrading recrystallization, the process of "diagenetic suturing" merged several smaller crystals into fewer, larger crystals, without destroying the primary cements.

Geological Setting

Fall Creek lies in a roughly north-south trending valley in the front ranges of the Alberta Rocky Mountains, ~ 75 km southwest of Rocky Mountain House (Figs. 2-1A,B). The springs and lobate tufa deposit (Fig. 2-1C) are on the west side of the valley, 5 km from the bridge where Trout Creek Trail crosses Fall Creek. There is a noticeable odour of H_2S around the springs. The spring waters

emerge from a slope composed of Devonian dolomitic limestone bedrock and flow down slope for ~ 50 m before entering the northward flowing Fall Creek. The main discharge vents are FC-1 (Fig. 2-2A) and FC-2, whereas FC-3, FC-4, FC-5, and FC-6 are small vents. Best described by the perched springline model of Pedley (1990), the Fall Creek Tufa also has elements of the cascade model where small caves formed around vents and around small waterfalls on the northeastern distal part of the fan. On a macroscopic scale, the Fall Creek Tufa is an autochthonous phytoherm framestone (cf. Pedley 1990), or a plant dominated freshwater reef structure.

The bryophyte tufa deposit, which formed directly below several cool water vents that emerge from a moderately steep slope, is composed of two fans contained in a ~ 250 m by 50 m area. This may be an underestimate of the true areal extent because of vegetation cover and the loss of some parts of the fan to erosion. Spring water flow beneath the southern part of the main fan promoted extensive erosion, which caused the tufa to fracture and slump. Today, spring waters flow around, through and under these blocks. The main part of the fan, which is up to 5 m thick (Fig. 2-2A), extends ~ 80 meters in a north-south direction, and up to 40 m down-slope towards Fall Creek. The toe of the fan terminates near Fall Creek in convex rollovers and in steep-sided, lipped edges. A smaller tufa fan, located ~ 60 m south of the main fan, is spread across the slope for ~ 60 m, extends down-slope for ~ 10 m and is up to 2 m thick. Unlike the main fan, the smaller fan does not reach the valley floor. The total volume of tufa is estimated to be between 4000 and 5000 m^3.

Deposit Age

Wood embedded in the youngest part of the deposit yielded a radiocarbon date of 310 +/- 50 ^{14}C years BP (Fig. 2-2B). This corresponds to a calendar age of 495-285 years BP, and most probably indicates the time when the tree died. The embedded wood is associated with minute, detrital charcoal fragments, indicating that the twig was washed into the spring flow path and encrusted by calcite after it had died.

The tufa in which the twig was embedded is therefore no older than 1455-1665 AD, and may have formed as late as the first half of the 18th century. Formation of the youngest part of the Fall Creek Tufa was concurrent with the Little Ice Age (LIA) event that occurred ca. 1700 AD in the Canadian Rocky Mountains (Luckman 1986, 2000). Evidence for the 1700 AD LIA event comes from localities 50-100 km west of Fall Creek. Tree-ring studies near Banff glaciers indicated increased precipitation from 1660-1720 AD (Luckman 2000; Watson and Luckman 2004), and glacial advance from 1700-1725 AD (Luckman 2000; Watson and Luckman 2004) was slightly preceded by a major cold interval that began in 1690 AD (Luckman et al. 1997; Luckman 2000).

Previous studies of Albertan spring deposits (Bonny 2002; Bonny and Jones 2003b; Grasby et al. 2003) suggested that large-scale calcite deposition from springs had ceased by 2500 years BP after being active for 2000-3000 years. Discovering wood embedded in Fall Creek Tufa that dates to the LIA indicates that the springs precipitated calcite 2000 years after calcite precipitation was thought to have stopped at other western Canadian springs. Late Holocene LIA glacier advances occurred during fluctuating climatic conditions, rather than during a sustained cold and wet period (Luckman et al. 1997). If carbonate spring deposit formation in western Canada responded to fluctuating climatic conditions during the latter half of the Holocene in a similar manner to glaciers, then carbonate precipitation from springs probably did not occur continuously for thousands of years. It is possible that the springs only actively precipitated calcite for 2000-3000 years in total, but the deposit formation was probably intermittent and protracted over 5000 years. Recent climate change may thus be responsible for the cessation of calcite precipitation during the past ~ 300 years.

Despite extensive searching, no organic matter was found in the oldest part of the Fall Creek Tufa. Although moulds of logs and twigs are present throughout the tufa, all of the organic material has been lost through decay. Thus, the oldest part of the tufa deposit could not be dated by radiocarbon methods. U-series dating of tufa is possible, but is commonly unreliable because of detrital

contamination, low initial U concentrations, and limited time for radiogenic Th production (e.g., Garnett et al. 2004). In addition, the high porosity of the Fall Creek tufa points to an open system that would have allowed leaching and/or addition of isotopes long after its deposition. Thus, accurate U/Th dating of this deposit was deemed unlikely. Comparison with other relict carbonate spring deposits in the Alberta Rocky Mountains suggests that the Fall Creek Tufa might be ~ 5000 years old. A date of 3770 +/- 60 ^{14}C years BP from a bison bone, coupled with tufa growth rate estimates, suggests that tufa formation at Miette Hot Springs in Jasper, Alberta, began 4500 years BP and continued until at least 2500 years BP (Bonny and Jones 2003b). Tentative radiocarbon dates from the Cave and Basin travertine in Banff National Park, Alberta, suggest peak deposition between 3200-5300 BP (Grasby et al. 2003). Both studies suggest that the deposits formed in response to cooler, wetter conditions at the onset of the Neoglacial. Given the proximity of Fall Creek to Banff and Jasper, it is possible that the Fall Creek Tufa began to form ~ 5000 years ago, when carbonate deposits began forming at the other Albertan springs.

Modern Spring Activity

Based on samples collected at FC-1, FC-2, FC-3, and FC-4, the spring waters have an average temperature of 13.1ºC, a pH of 7.6, and contain, on average, 463 mg·L^{-1} Ca, and 105 mg·L^{-1} Mg (Tables 2-1 and 2-2). Electrical conductivity averaged 2.39 μS·cm^{-1} (S = siemens), dissolved oxygen averaged 8.65 mg·L^{-1}, and salinity averaged 1.1. The δ^{18}O (VSMOW) values of the spring water average -19.3‰ (Table 2-1), which is similar to δ^{18}O values of water from other Rocky Mountain springs, indicating that the waters are meteorically derived (Grasby and Hutcheon 2001).

Spring water issues from several vents spread across the hillside. Water from each vent follows a particular flow path before the confluence with Fall Creek. Some spring water flows directly into Fall Creek, whereas other spring

Table 2-1 Fall Creek unfiltered spring water properties and stable oxygen isotope compositions.

Sample	pH	Temp. (°C)	Electrical Conductivity ($\mu S \cdot cm^{-1}$)	Salinity	Dissolved Oxygen ($mg \cdot L^{-1}$)	$\delta^{18}O$ (‰VSMOW)	
						#1	#2
FC-1	7.48	13.0	2.34	1.1	8.65	-19.4	-19.2
FC-1B	8.03	13.0	2.40	1.1	8.65		
FC-2	7.41	13.4	2.40	1.1	8.65	-19.5	-19.5
FC-3	7.42	13.1	2.41	1.1		-19.2	-19.0

Notes: All pH measurements were taken in the field, and units are the negative log of $[H^+]$. S = siemens.

Table 2-2 Fall Creek filtered spring water chemistry.

Sample	T (°C)	pH	DOC	DIC	Cl	Na	K	Ca	Mg	Fe	Si	EC
FC-1	13.0	7.5	0.82	2.4	2.5	6.6	2.0	471	107	0.07	4.3	2.22
FC-1B	13.0	8.0	0.56	3.1	2.6	6.6	1.9	460	105	0.04	4.3	2.26
FC2	13.4	7.4	0.52	4.8	2.6	6.6	1.9	457	104	0.03	4.3	2.24

Notes: All pH measurements were taken in the field, and units are the negative log of $[H^+]$. DOC = dissolved organic carbon. DIC = dissolved inorganic carbon. EC = electrical conductivity (measured in $\mu S \cdot cm^{-1}$, where S = siemens). Unless stated, all other units are in $mg \cdot L^{-1}$.

water flows through conduits in the relict tufa before entering Fall Creek. The only modern tufa formation at the Fall Creek spring is from water that has flowed through relict tufa, dissolved it, and re-precipitated the calcite down-stream. Most modern calcite precipitation occurs on moss drapes growing in the waterfall at the north end of the deposit, beneath large, fractured blocks of tufa. Spring water that flows directly into Fall Creek without passing through the tufa only precipitates gypsum and native sulphur. Gypsum crystals, up to 1 cm long, are visible under overhangs and slump blocks. White gypsum coats the outer surface of the fan and commonly lines cavities in the tufa. Native sulphur forms a surficial coating on all rocks and biota in the flow-path of the modern spring effluent.

Cratoneuron commutatum, common in western Canada where there are calcium-rich substrates (Vitt 1988), grows in isolated patches on the deposit. Most of the moss grows from overhangs at the northeastern end of the fan. Some moss tussocks with grasses growing out of their centers also grow on the upper slopes of the deposit where there is little spring water. These tussocks are not being calcified, but are analogous to the moss hummocks that blanketed the slope during peak deposit formation.

Tufa Components and Petrography

The tufa is formed of calcite cements, cavities, and internal sediments with calcite cements dominating. Initial development involved calcite cement precipitation around living bryophytes, charophytes, grasses, and cyanobacteria that grew on surfaces around the spring, and dead vegetation (e.g., twigs) caught in the spring flow path. Calcite-encrusted biota created a highly porous framework that served as a substrate for further tufa formation (Figs. 2-2B,C). The cavities, up to 10 cm long, with most being 0.5-5.0 mm long, formed where calcite-encrusted plant material decayed, and where spaces between encrusted plants were not occluded by cements. Many cavities were subsequently lined or filled with late stage cements and internal sediments. Fluorescence microscopy shows that most of the deposit has been recrystallized.

Calcite cements

The cements that coated the macrophytes and cavities include composite crystals, trigonal crystals, mosaic crystals, and isopachous banded cement/micrite couplets.

Composite calcite crystals

The composite euhedral calcite crystals (Fig. 2-3) are divided into blocky crystals (up to 50 μm long and 50 μm thick) with multi-stepped faces, and flat, platy crystals (up to 30 μm long and 10 μm thick). The former are more common than the latter. The composite calcite crystals, which are the least common cements in the deposit, are found only on the leaves and stems of *Cratoneuron commutatum*. They grew perpendicular to the irregular moss surfaces, and on pre-existing composite crystals. Accordingly, the crystals grew at variable angles to each other and commonly grew into one another.

The blocky multi-stepped crystals (Figs. 2-3A,C,G to I) preferred to grow directly on the moss leaves, rather than on moss stems or pre-existing crystals. Their subcrystals are rhombohedral, with the *c* axes aligned perpendicular to the moss surface. Adjacent subcrystals used each other as growth templates and therefore appear as parallel, overlapping trigonal crystals (Figs. 2-3C,G,H). The sides of the blocky crystal faces are flat near the base, with steps developing towards the tops of the crystals. The composite crystal faces have up to 30 steps, with approximately ~ 1 μm separating the steps (Fig. 2-3C). The spikes on top of the composite crystals form the rhombohedral terminations of the subcrystals (Fig. 2-3I).

Viewed down the *c* axis, the flat, platy composite crystals (Figs. 2-3D to F) have triangular to hexagonal outlines. The platy crystals formed primarily on pre-existing multi-stepped cements, and to a lesser extent on moss surfaces. The trigonal subcrystals, 0.5-2 μm wide, are blunted terminations of rhombohedral crystals that are aligned parallel to one another, and have their *c* axes perpendicular to the substrate. Adjacent subcrystals merged to form a composite crystal, but the subcrystals did not overlap and develop stepped faces.

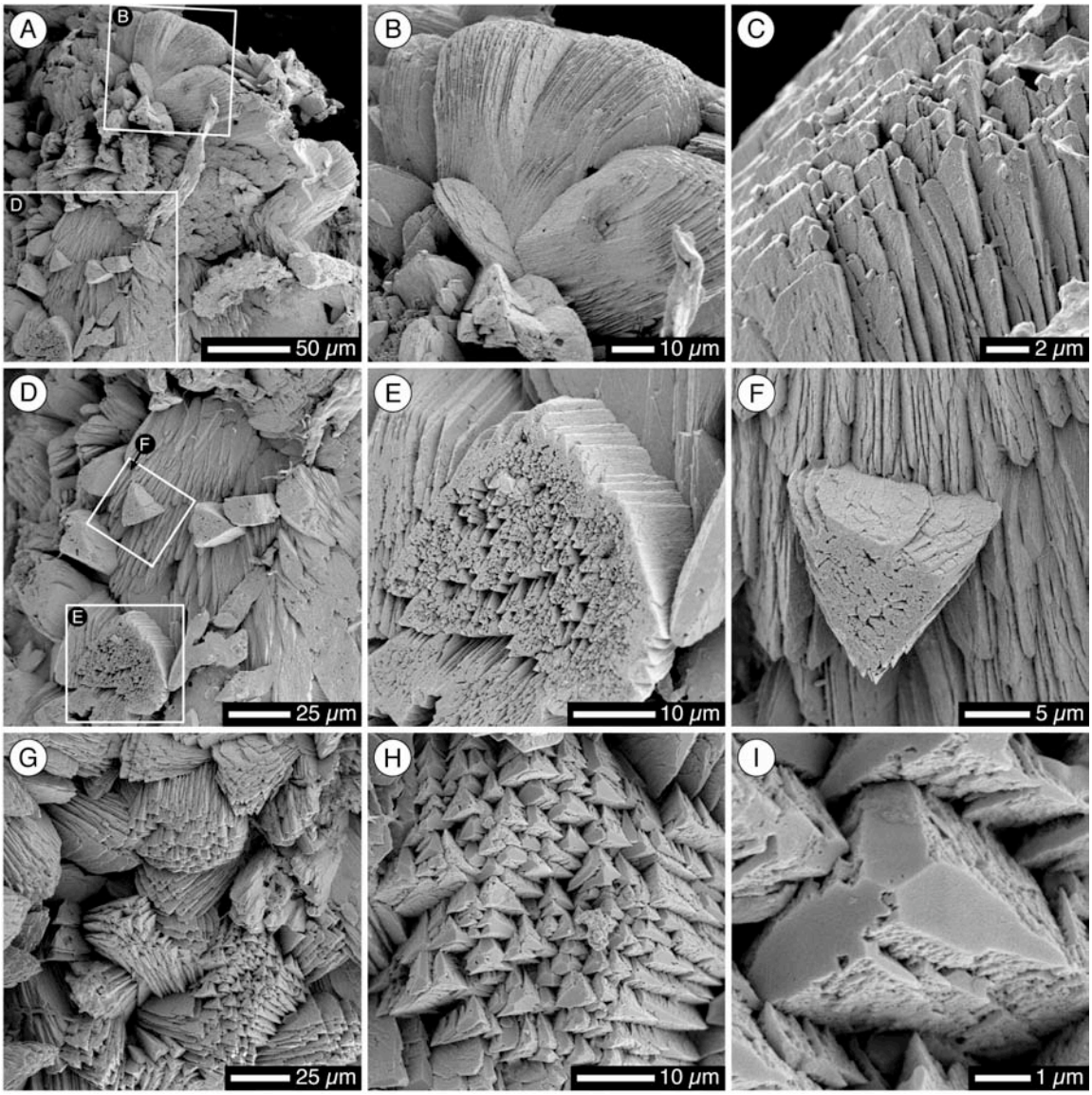

Fig. 2-3 SEM photomicrographs of composite calcite crystals. A) Overview of moss leaf tip encrusted with blocky and platy composite crystals. White boxes indicates crystals shown in figures 2-3B and D. B) Blocky composite crystals. C) Close-up of stepped crystal faces on blocky composite crystal. D) Flat, platy composite crystals formed on blocky composite crystal. White boxes indicate crystals shown in figures 2-3E and F. E) Flat-topped, platy composite crystal with high porosity between subcrystals. F) Flat-topped, triangular platy composite crystal with low porosity between subcrystals. G) Cluster of blocky composite crystals. H) Close-up of blocky composite crystal composed of aligned trigonal subcrystals. I) Close-up of individual subcrystal with tapered termination.

Trigonal calcite crystals

The trigonal calcite crystals (Fig. 2-4) are terminations of rhombohedral crystals, and thus appear similar to the composite crystals' subcrystals (Fig. 2-3I). The trigonal crystals, however, do not form aggregates of aligned crystals (Figs. 2-4A,B), and are present only as solitary, euhedral crystals (Fig. 2-4C) that line cavity surfaces (Fig. 2-4D), occlude cavities (Fig. 2-4E), and coat internal sediments. The crystals, which have their *c* axes perpendicular to the substrate, are 10-20 μm wide and 20-300 μm long. Ideally formed trigonal crystals have equilateral basal edges and side edges that narrow towards the pyramidal, blunted, or tapered crystal terminations. Pyramidal terminations formed when the three side edges meet in a point. Blunted terminations appear as though the top of the crystal was cut off parallel to the base, creating flat-topped crystals. The tapered terminations formed when each of the three side edges symmetrically bifurcated, to create 3 more visible crystal faces than the pyramidal crystals. Elongate trigonal crystals can appear tabular when viewed parallel to the *c* axis.

Mosaic calcite crystals

The mosaic calcite crystals (20-400 μm long) are dominantly anhedral with irregular, non-planar boundaries (Fig. 2-5). The mosaic crystals formed around the bryophytes (Figs. 2-5A to C), in the bryophyte tubes left behind after the encased bryophytes decayed, and around cyanophyte bushes. The mosaic crystals that formed around the bryophytes are clean and clear in thin section (Figs. 2-5D,E). Seen on the SEM, subhedral to euhedral terminations of blocky composite crystals are locally visible. Moulds of bryophyte leaves and stems (Figs. 2-5F to H), which are sparse in the tufa, are usually preserved in mosaic crystals that encased the bryophytes. The mosaic crystals filling the bryophyte tubes are cloudier than the encasing crystals, possibly due to staining by organic matter. The crystals filling the tubes do not display well-formed crystal habits.

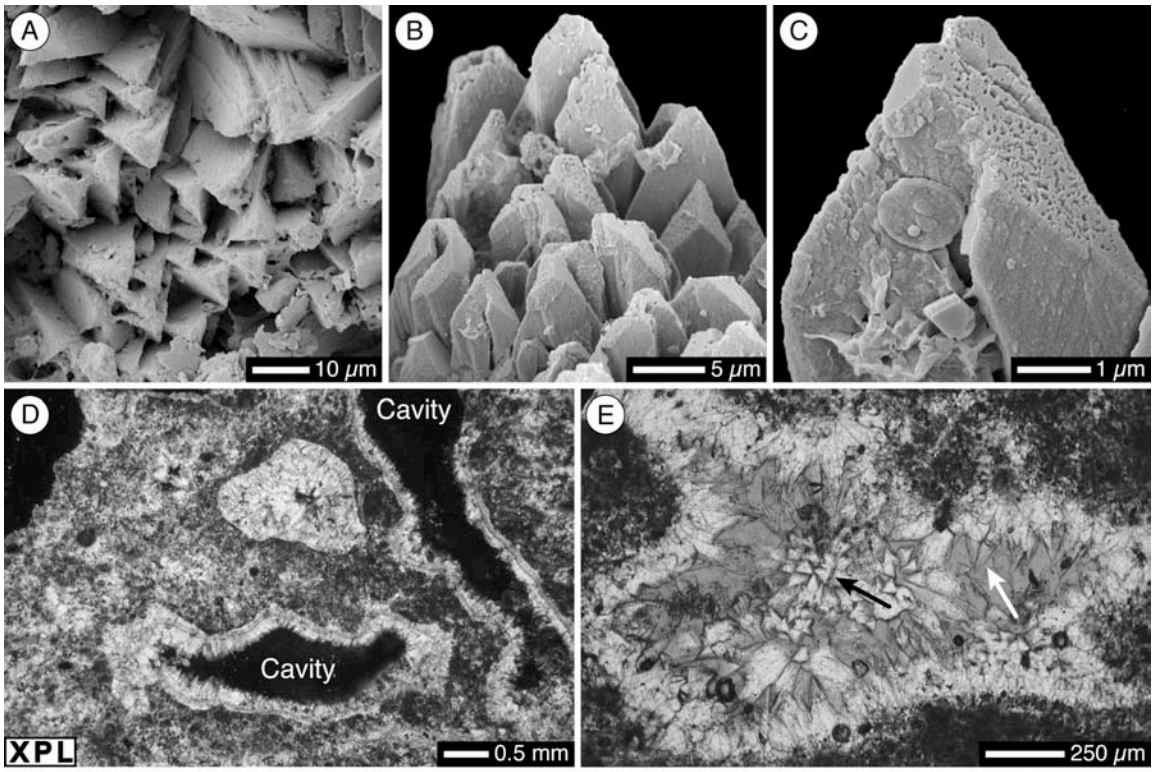

Fig. 2-4 Trigonal calcite crystals. (A-C) SEM photomicrographs; (D-E) Thin section photomicrographs. A) Surface coated with trigonal crystals. Note lack of crystal alignment. B) Cluster of trigonal calcite crystals. C) Enlarged view of trigonal calcite crystal from figure 2-4B showing tapered termination. D) Bryophyte tufa with cavity occluded by trigonal crystals (top) and open cavities lined with trigonal crystals (right and bottom). Crossed-polars. E) Cavity occluded by trigonal crystals that grew from cavity wall (white arrow). Trigonal crystals viewed down *c*-axis are in center of cavity (black arrow).

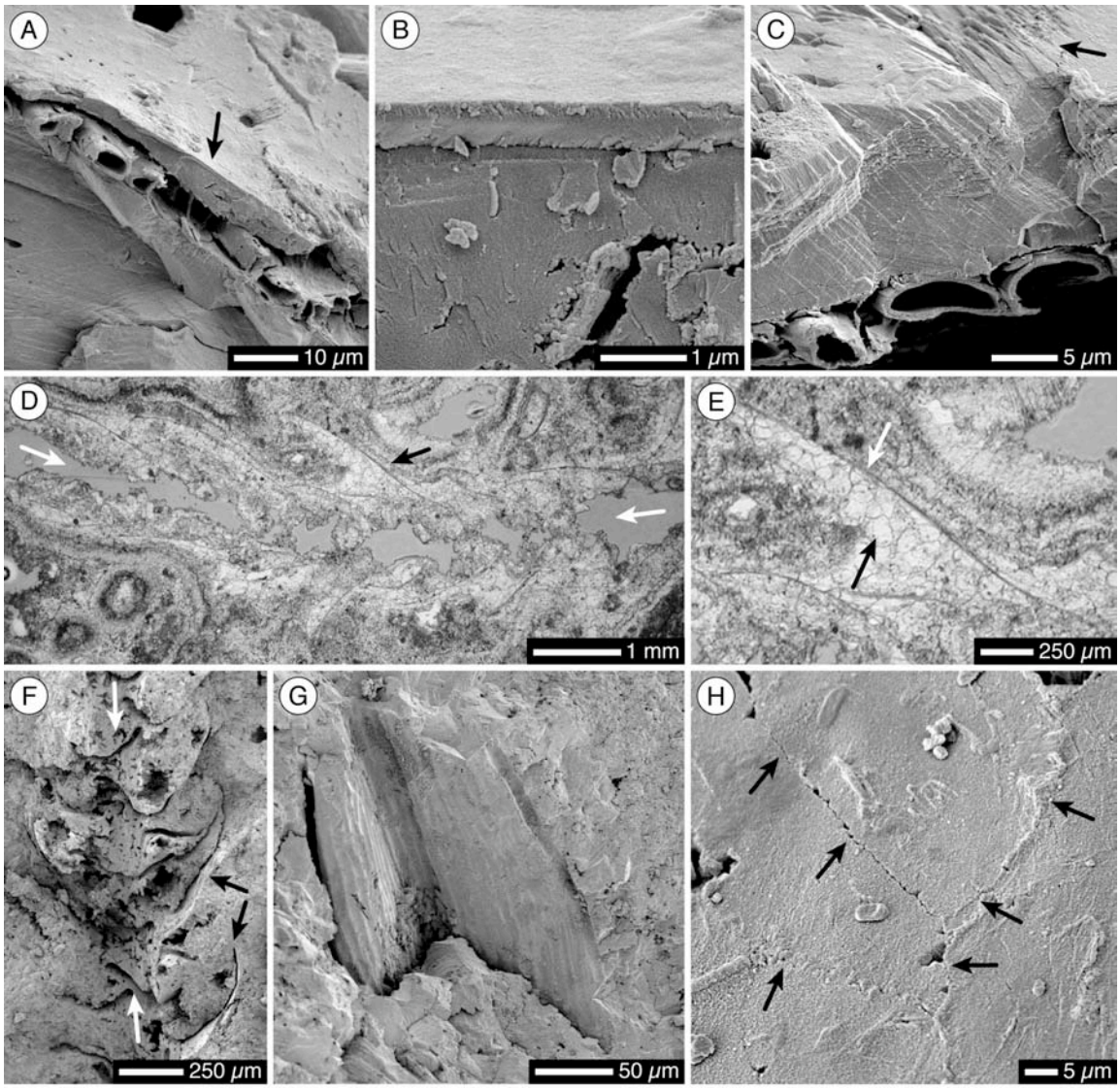

Fig. 2-5 Mosaic calcite crystals. (A-C, F-H) SEM photomicrographs; (D-E) Thin section photomicrographs. A) Moss leaf cells encased in featureless mosaic calcite. Area indicated by black arrow shown in figure 2-5B. B) Smooth, featureless mosaic calcite with no indication of original crystal morphology. C) Mosaic calcite coating moss leaf cells. Note remnant composite crystal features indicated by black arrow. D) Bryophyte mould in mosaic calcite crystals. White arrows indicate moss stem. Black arrow indicates moss leaf mould shown in figure 2-3E. E) Close-up of mosaic calcite crystals (black arrow) surrounding bryophyte leaf mould (white arrow). F) Bryophyte mould preserved in mosaic calcite crystals. White arrows indicate main tube created by bryophyte stem. Black arrows indicate moss leaf moulds. G) Bryophyte leaf mould preserved in featureless mosaic calcite. H) Surface of moss leaf mould showing mosaic calcite crystal boundaries (black arrows).

Isopachous banded crystal-micrite couplets

The isopachous banded cement is 250 μm to 5 mm thick, with most being 1-2 mm thick (Fig. 2-6). This cement, present in most samples, is formed of alternating layers (10-250 μm thick) of light coloured crystals and dark coloured micrite (Figs. 2-6A to C). Up to 25 crystal-micrite couplets are present with the calcite crystal layers usually being thicker than the micrite laminations (Figs. 2-6D,E). The number of couplets can be difficult to determine because successive layers of cement may mask previous layers. The crystalline layers are well cemented and composed of anhedral calcite crystals, 10-20 μm wide. The micrite laminations, which have high micro-porosity (Figs. 2-6D to G), are composed of degraded calcite crystals that are < 4 μm wide. Cavities in the tufa are commonly lined by isopachous banded crystal-micrite couplets (Figs. 2-6A to C). The roofs of some cavities have isopachous banded couplets as brightly fluorescent pendant cements, formed when calcite precipitated from water percolating down through the deposit (Figs. 2-6H,I).

Aggraded Recrystallized Calcite Crystals

The recrystallized mosaic calcite crystals (20 μm to1 mm long), which are anhedral with irregular, non-planar boundaries, are similar to the primary mosaic crystals (Fig. 2-7). The crystals can be clean and clear (Figs. 2-7B,C), or cloudy from entrained micrite (Figs. 2-7A,D). Thus, primary and recrystallized mosaic crystals cannot be differentiated using transmitted light and scanning electron microscopy. Epifluorescence microscopy, however, reveals ghost structures in the recrystallized calcite, including relict textures of primary mosaic crystals (Fig. 2-7A), isopachous banded crystal-micrite couplets (Figs. 2-7B to D), and trigonal crystals (Figs. 2-7A,C,D). Individual recrystallized mosaic crystals may contain several types of primary calcite cement crystals. Other features that become evident include bryophyte tubes (Fig. 2-7A) delineated by isopachous banded cements, and filled with primary mosaic crystals, and interstitial spaces filled with trigonal crystals.

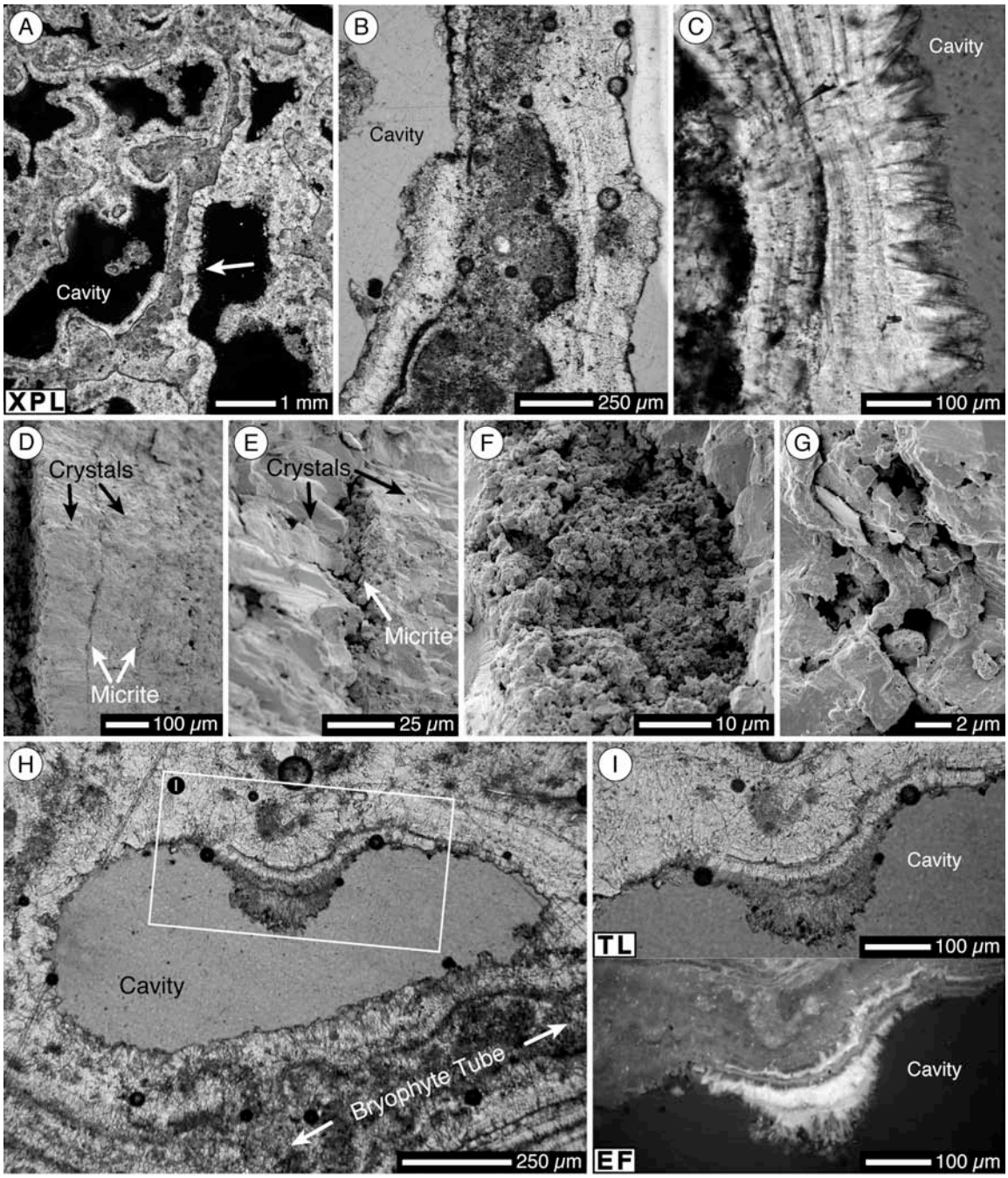

Fig. 2-6 Isopachous banded crystal-micrite couplets. (A-C, H-I) Thin section photomicrographs; (D-G) SEM photomicrographs. A) Highly porous framework of filled bryophyte tubes encased by isopachous banded cements. White arrow indicates area shown in figure 2-6B. Crossed-polars. B) Enlarged view of bryophyte tube occluded by cemented micrite and encased by isopachous banded crystal-micrite couplets. C) Fine laminations preserved in isopachous banded couplets. Cavity-facing band is formed of trigonal calcite crystals. D) Repeating thick crystal and thin micrite couplets. E) Micrite band between two crystal bands. F, G) Fine texture of micrite bands. H) Open cavity lined with isopachous banded cements, and isopachous banded pendant cement hanging from top of cavity (white box). I) Top, transmitted light image of pendant cement. Bottom, epifluorescence image of same target showing highly fluorescent pendant cement formed later than weakly fluorescent isopachous banded cements.

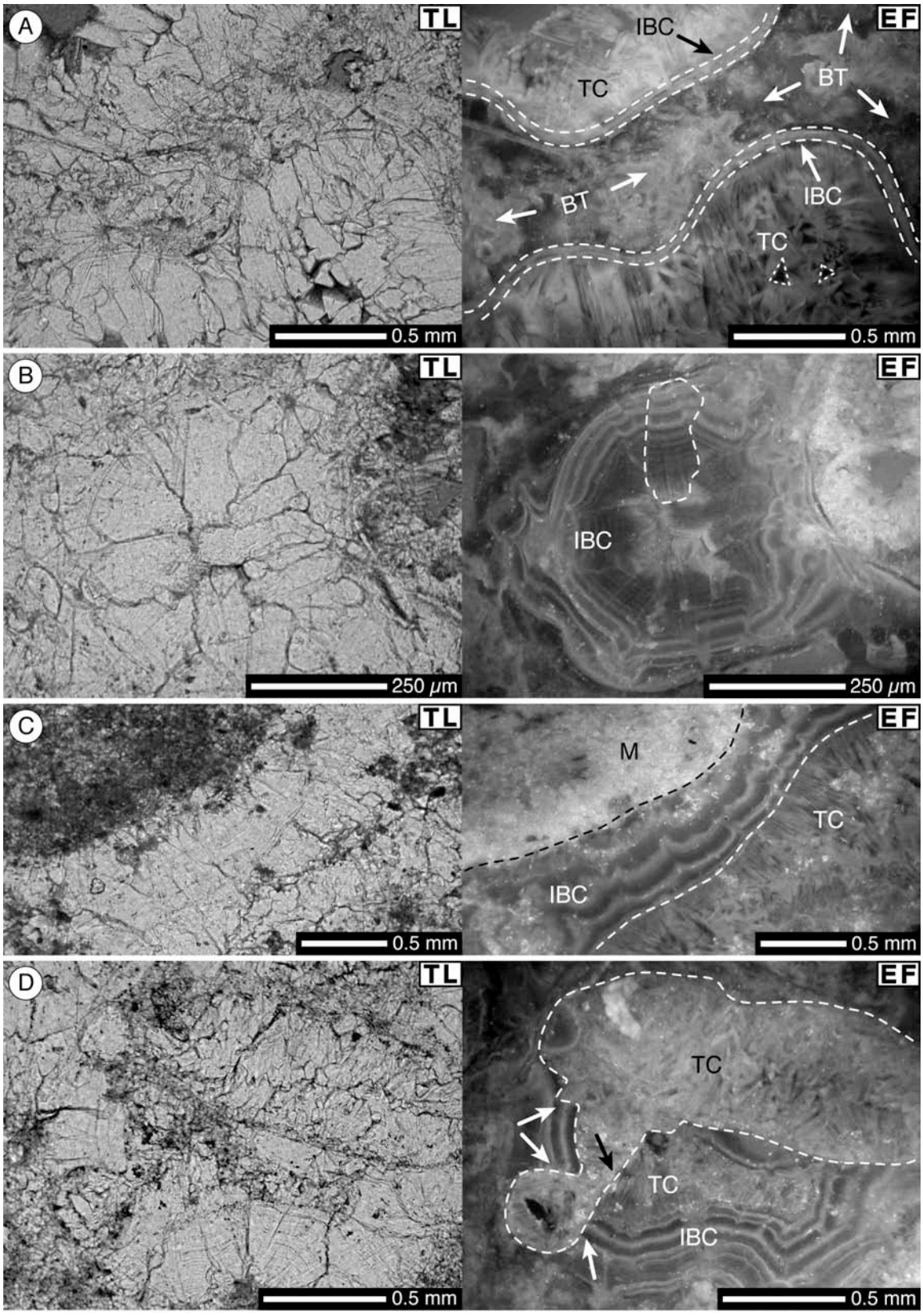
A
TL
EF
IBC
TC
BT
BT
IBC
TC
0.5 mm
0.5 mm
B
TL
EF
IBC
250 μm
250 μm
C
TL
EF
M
TC
IBC
0.5 mm
0.5 mm
D
TL
EF
TC
TC
IBC
0.5 mm
0.5 mm

Fig. 2-7 Thin section photomicrographs of diagenetic mosaic calcite crystals. Images on left illuminated with transmitted light (TL). Images on right match views on left, but illuminated with epifluorescent light (EF). A) Left, sample composed almost entirely of mosaic calcite crystals. Right, EF shows a recrystallized bryophyte tube ("BT") filled with micritic primary mosaic calcite crystals, and encapsulated by isopachous banded cements ("IBC"). Cavities all lined with trigonal calcite crystals ("TC"). Note trigonal crystal outlines in occluded cavity at lower right. B) Left, mosaic calcite crystals. Right, mosaic calcite crystals were originally isopachous banded cements ("IBC") that occluded a cavity, and were later recrystallized. White dashed line outlines a single mosaic calcite crystal. C) Left, tufa composed of mosaic calcite crystals and micrite (upper left). Right, micrite ("M") fluoresces brightly, whereas weakly fluorescent mosaic crystals are composed of recrystallized isopachous banded cements ("IBC") and trigonal calcite crystals ("TC"). D) Left, mosaic calcite crystals of various sizes. Right, EF reveals a complex paragenesis. Cavity in bryophyte tufa lined by isopachous banded cements ("IBC"), then occluded by trigonal calcite crystals (white "TC"). Later, dissolution and/or boring created new cavity. Dashed line outlines dissolution surface. White arrows indicate truncation of isopachous banded cements; black arrow indicates truncation of trigonal crystals. Following dissolution, trigonal calcite crystals (black "TC") filled the cavity. Finally, cements were recrystallized to form diagenetic mosaic calcite crystals.

Internal Sediments

Many cavities in the tufa contain internal sediments (Fig. 2-8) that are formed of various combinations of micrite, peloids, tufa intraclasts, bioclasts, dolomitic extraclasts, quartz lithoclasts, and clay.

Micrite

The micrite (Fig. 2-8D), which is mostly sparmicrite formed by degradation of calcite cement (cf. Kahle 1977), is variably compacted and cemented by calcite. The porosity of the micrite is controlled by the amounts of compaction and cement. Dense, dark brown micrite has minimal calcite crystal cement, whereas areas with little micrite are light brown and well cemented.

Bryophytes formed most of the sparmicrite as their rhizoids mechanically degraded the calcite. Residual micrite was a dissolution byproduct of calcite cement being chemically degraded by weakly acidic organic compounds. Endolithic microbes (fungi and cyanobacteria) produced minor amounts of sparmicrite by boring into the tufa.

Peloids

The spherical to ellipsoid peloids (50-200 μm long), which are brown to grey in colour and lack internal structure, occur in loosely or densely clustered

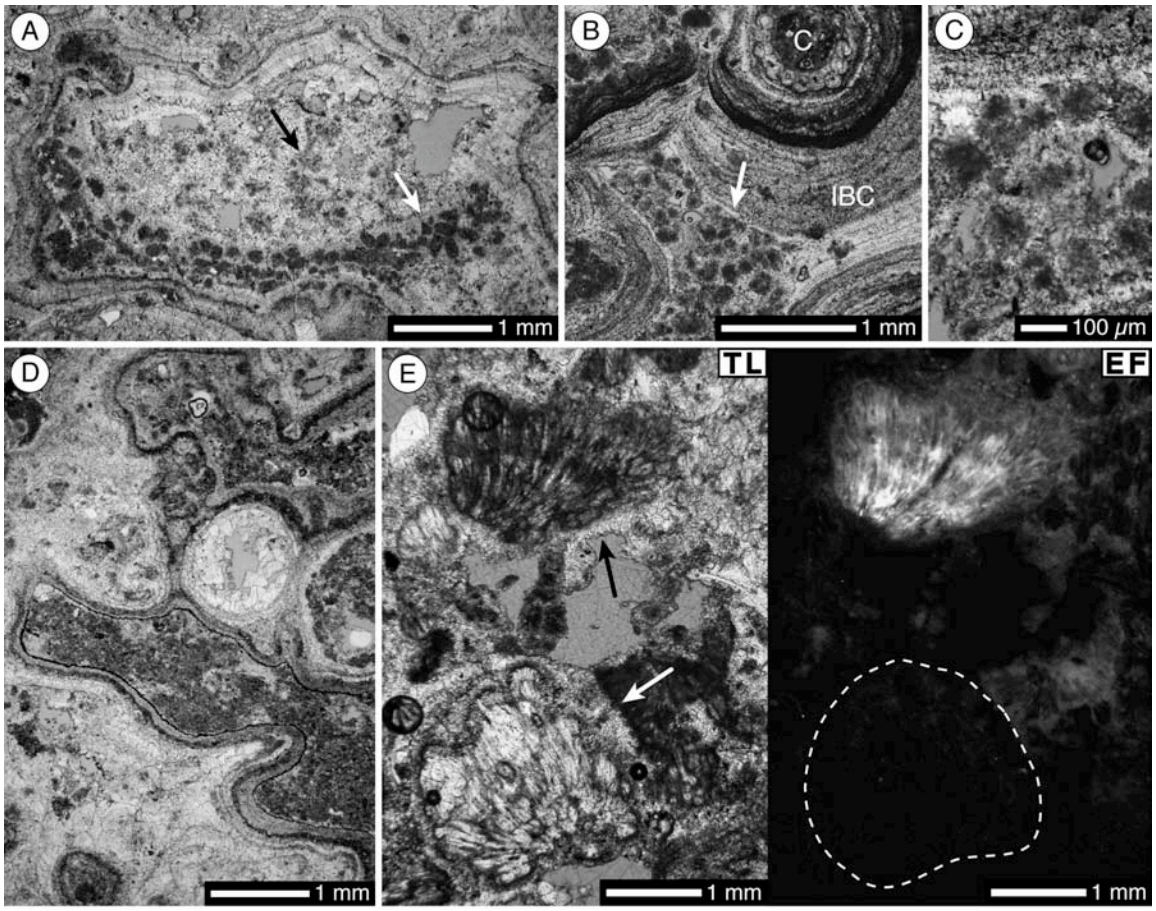

Fig. 2-8 Thin section photomicrographs of internal sediments. A) Loosely (black arrow) and densely (white arrow) clustered peloid aggregates cemented by trigonal calcite crystals. B) Densely clustered peloids (white arrow) occluding cavity in tufa formed of charophyte moulds ("C") preserved by isopachous banded cements ("IBC"). C) Enlarged view of peloids rimmed with trigonal crystals. D) Cavities in cemented bryophyte tufa occluded by dark coloured micrite. E) Left, transmitted light image of cyanophyte bush intraclasts. Upper, dark-coloured clast (black arrow) contains abundant micrite, whereas lower, light-coloured clast (white arrow) contains abundant mosaic calcite. Right, epifluorescence shows that upper, micrite-rich clast fluoresces brightly, whereas lower mosaic-rich clast (outlined by white dashed line) does not fluoresce.

aggregates (Figs. 2-8A to C). Though less abundant than micrite, peloids are common throughout the tufa. Cementation by calcite created a clotted, or grumose texture (e.g., Pedley 1992). Although the peloids may be fecal pellets that were produced by the gastropods and ostracodes that are found in the tufa, the possibility that they formed through abiogenic processes (cf., Macintyre 1985; Jones 1989b) or by precipitation around bacteria (Chafetz 1986) cannot be ignored.

Other sediments

Tufa intraclasts (Fig. 2-8E), bioclasts, dolomitic extraclasts, quartz lithoclasts, and clays are minor components of the tufa. Most of these components are embedded in a micrite matrix, with the exception of angular dolomitic extraclasts (up to 10 cm long), which were derived from the surrounding country rock and then cemented together to form clast-supported breccias. Tufa intraclasts, up to 2 mm long, are formed largely of cemented cyanophyte bushes that have been ripped up and redeposited (Fig. 2-8E). Bioclasts include gastropod shells (up to 5 mm in diameter), and articulated or disarticulated ostracodes (up to 1 mm long). Most of the shells are whole. The angular quartz lithoclasts, 1-5 mm long, are rare. These sediments were probably deposited during periods of high precipitation and runoff.

Tufa Fluorescence

Epifluorescence microscopy (EF) reveals many textures in the Fall Creek Tufa that were masked by aggrading recrystallization. Such fluorescence reflects the presence of organic acids that were assimilated into the calcite crystals during their growth (e.g., Isdale 1984; Fang and Chou 1992; Isdale et al. 1998; McGarry and Baker 2000). In the Fall Creek Tufa, bright fluorescent calcite is restricted to the younger, isopachous banded pendant cements (Fig. 2-6I) and micrite-rich areas (Figs. 2-7C and 2-8E). Recrystallized tufa fluoresces with lower intensity than the pendant cement or micrite because the organic acids were further degraded or removed during diagenesis. Dead moss fragments embedded in the

tufa do not fluoresce, indicating that they were not the source of the fluorescence inducing compounds. In contrast, cyanobacterial filaments preserved in the tufa do fluoresce, suggesting that they may have been one source of the organic acids.

Bryophyte Tufa Development

The bryophyte tufa at the Fall Creek cold springs evolved through four stages: (I) encrustation, (II) encapsulation, (III) cavity occlusion, and (IV) diagenetic alteration (Figs. 2-9 to 2-11). The stages are spatially and temporally variable, so the tufa did not necessarily pass through each stage successively, nor did all of the tufa progress through each developmental stage. Likewise, at any time during tufa development, different parts of the deposit were simultaneously progressing through different stages. Thus, some parts of the tufa have experienced all four stages, whereas other parts have exhibited only Stages I, I and II, or I, II, and III. After passing through Stage IV, the tufa could even have repeated Stage III. The resultant textures are a product of tufa development being process dependent, not temporally dependent.

Fig. 2-9 SEM photomicrographs of bryophyte tufa formation from Stage I (encrustation) to Stage III (cavity occlusion). A) Moss leaf in Stage I development. White arrows indicate surface of exposed moss leaf. Between arrows, isolated composite calcite crystals encrusting leaf. Lower portion of leaf covered with a crust of composite calcite crystals. B) Moss that has entered Stage II development. Leaves completely encapsulated by composite calcite crystals. White arrow indicates area shown in figure 2-9C. C) Enlarged view of encapsulated moss leaves. White arrow indicates area shown in figure 2-9E. D) Coalescence of adjacent calcite crystals leading to a rigid bryophyte tufa framework. Calcite crystals from adjacent moss leaves that have coalesced (top), and calcite crystals about to coalesce (bottom). E) Flat, platy composite calcite crystals (top), and blocky composite calcite crystals (bottom) that have coalesced and encapsulated a moss leaf. F) Cross-section through bryophyte tube encased in thin crust with irregular boundaries following contours of gametophyte. Arrows indicate bryophyte leaf mould and bryophyte tube ("B"). G) Bryophyte tufa that has entered Stage III. Bryophyte stem (white arrows and "B") and leaf moulds preserved by coalesced composite calcite crystals. Black arrows indicate cements shown in figure 2-9H. H) Enlarged view of edge of bryophyte tube. Moss gametophyte moulds preserved in composite calcite crystals ("C") and encased by mosaic calcite crystals ("M"). Trigonal calcite crystals ("T") have partially occluded cavity at top of image. I) Mat of fungi and sediment (white arrows) in cavity between two bryophyte tubes encased in thick crusts with regular boundaries. Bryophyte tube on left (white "B") has not been fractured, whereas tube on right (black "B") has been fractured. Fractured bryophyte tube is composed of mosaic and composite calcite crystals. Bryophyte moulds visible at center of tube (black arrow).

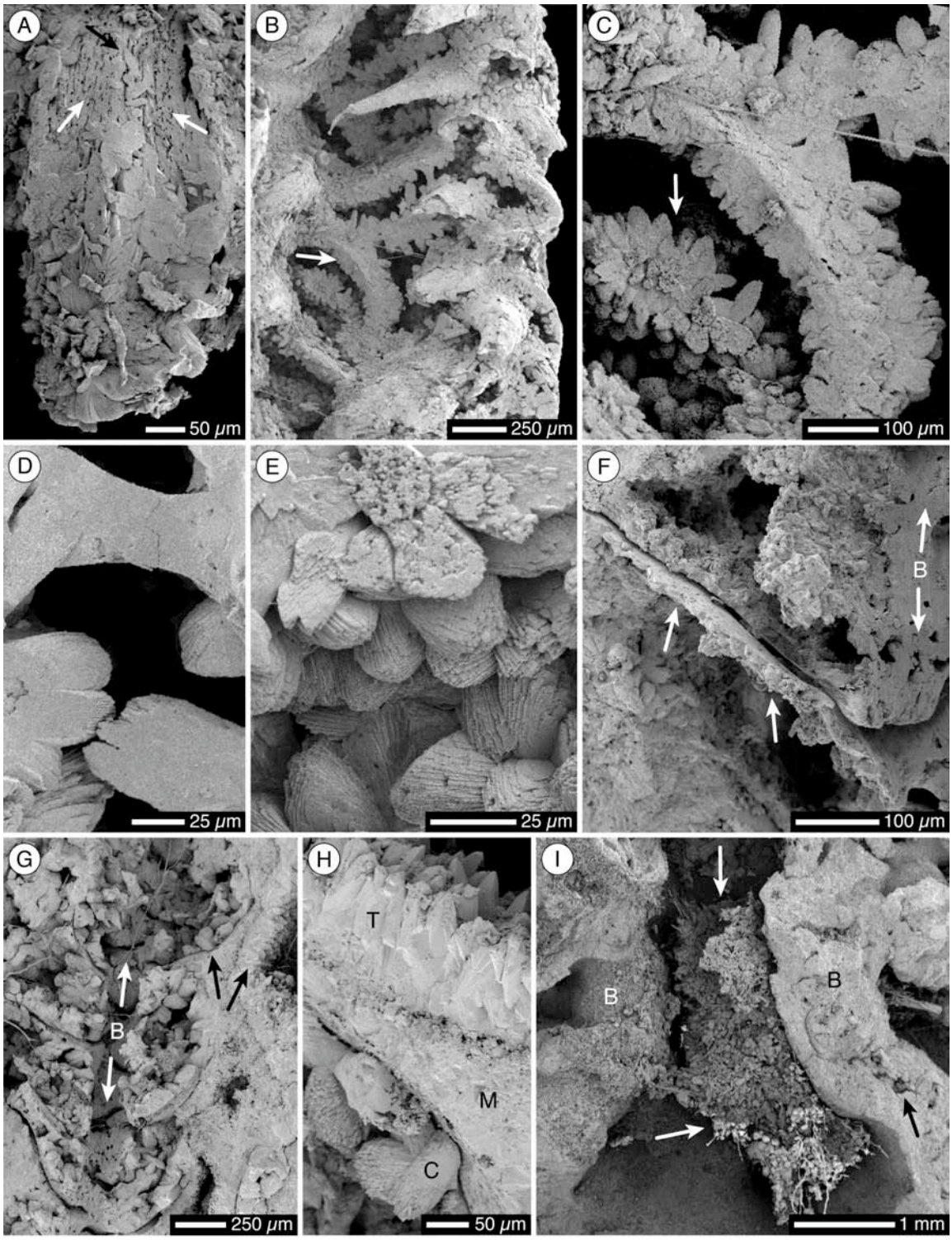
A
50 μm
B
250 μm
C
100 μm
D
25 μm
E
25 μm
F
B
100 μm
G
B
250 μm
H
T
M
C
50 μm
I
B
B
1 mm

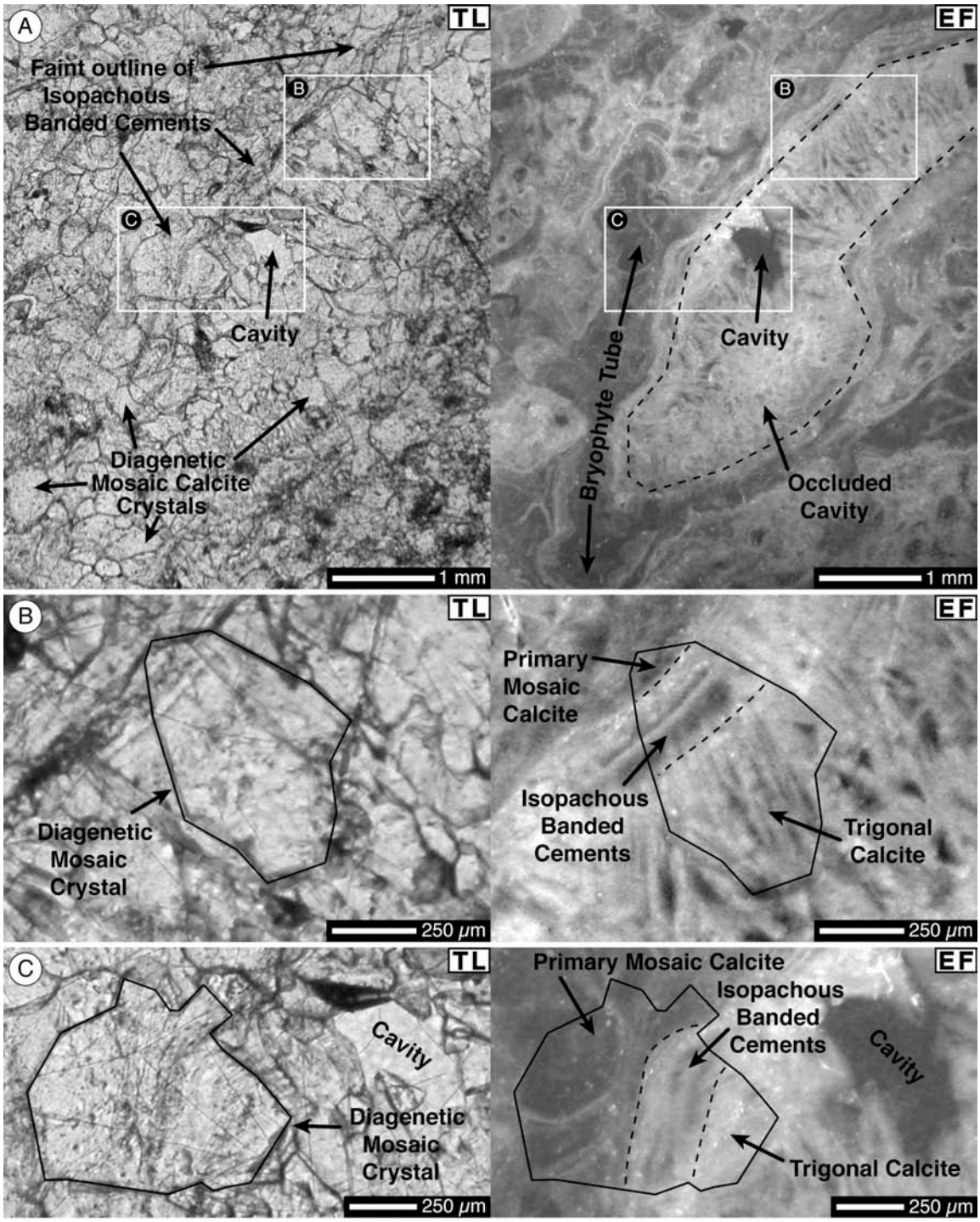

Fig. 2-10 Thin section photomicrographs of recrystallized mosaic calcite crystals from Stage IV diagenesis. Images on left illuminated with transmitted light (TL). Images on right same as those on left, but illuminated with epifluorescent light (EF). A) Left, sample composed almost entirely of recrystallized mosaic calcite crystals. Right, fluorescence highlights primary depositional textures masked by recrystallization. Boxes labeled "B" and "C" indicate positions of figures 2-10B and C. Boxes show fabrics from bryophyte tube and occluded cavity. B) Left, single diagenetic mosaic calcite crystal. Right, crystal composed of three different types of primary cement that were sutured together. C) Shows similar relationships as figure 2-10B, but with different proportions of primary cements forming diagenetic mosaic calcite crystal.

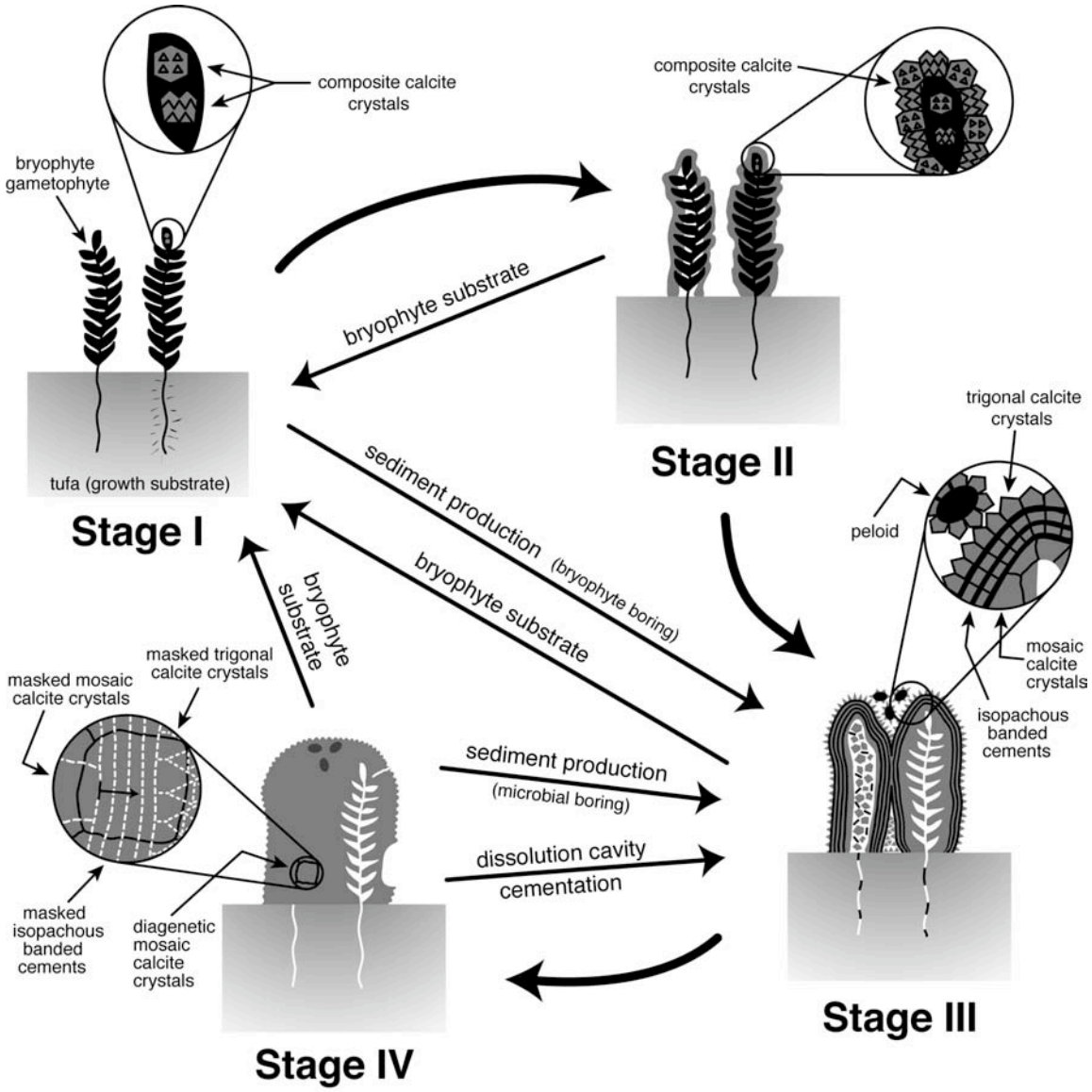

Fig. 2-11 Flow diagram illustrating stepwise development through Stages I to IV of bryophyte tufa at Fall Creek.

The difficulty in distinguishing between formational and diagenetic processes in freshwater spring carbonates is mainly due to the fact that virtually all of the calcium carbonate is chemically precipitated from spring water. Deposition, cementation, and lithification thus occur contemporaneously (Pedley et al. 2003). For the purpose of this study, all calcite precipitated directly from spring water is considered formational, whereas alteration (biogenic or abiogenic) is considered diagenetic. Thus, Stages I, II, and III, are formational stages, whereas Stage IV is a diagenetic stage.

Stage 1 – Encrustation

Stage I began with precipitation of isolated composite calcite crystals on *Cratoneuron commutatum* gametophytes (Fig. 2-9A). Blocky crystals with stepped faces commonly developed first. Platy crystals formed directly on some of the moss, but more commonly precipitated on the blocky crystals. The cements that formed during Stage I produced a diverse array of crystal morphologies. Stage I crystals formed euhedral terminations during precipitation, but these terminations are rarely evident due to subsequent burial by mosaic calcite crystals, dissolution by fluids undersaturated with respect to calcium carbonate, or sparmicritization. The merging and suturing of adjacent crystals on the moss marked the end of Stage I.

Stage II – Encapsulation

Stage II began when the composite calcite crystals grew into each other and formed a crust around the gametophytes (Figs. 2-9B to F). This is the most important stage in terms of deposit lithification, because encapsulation led to the development of a rigid framework. Although friable at the beginning of Stage II, continued crust thickening progressively increased the strength of the tufa.

Most bryophytes are preserved as cylindrical “tubes”. The thickness of the cement crust around the tubes and the regularity of the outer crust surface was a function of the duration of uninterrupted composite and mosaic crystal growth. Little continuous cementation left more open space between the leaves and stems,

resulting in thinner crusts with outer surfaces that followed the irregular contours of the leaves and stems (Fig. 2-9F). Abundant continuous cementation filled more space between the moss leaves and stems, generating thicker cement crusts with smooth, regular outer surfaces (Fig. 2-9I).

Once encased by calcite cements, open stem tubes and leaf moulds formed as the bryophytes died and decomposed. These moulds remained open and were best preserved in tufa that did not progress past Stage II. Generally, moulds in tufa that progressed beyond Stage II were filled with Stage III cements and sediments, or degraded during Stage IV. Stage II continued until chemical precipitation of composite and mosaic crystals ceased, or was disrupted by mechanical sedimentation.

Stage III – Cavity Occlusion

Stage III involved cement precipitation and/or mechanical sedimentation in cavities in the tufa (Figs. 2-9G to I). Cementation was dominated by the formation of isopachous banded crystal-micrite couplets and trigonal calcite crystals, with lesser amounts of mosaic crystals.

Cement precipitation during Stage III commonly began when trigonal calcite crystals lined cavities created by the formation of bryophyte tubes during Stage II. Intermittent disruption and sparmicritization of the trigonal crystals, followed by renewed precipitation of trigonal calcite crystals produced isopachous banded cements. These banded couplets, which formed over short time spans, reflect seasonal variations in the water chemistry, with one couplet representing the passage of one year.

Mechanical sedimentation during Stage III involved the deposition of endogenic (micrite, peloids, tufa intraclasts, bioclasts) and exogenic (quartz lithoclasts, clays, dolomitic extraclasts) sediments in tufa cavities. The bryophyte tubes typically contain a higher proportion of mosaic cement and small particles than the interstitial pores in the surrounding framework. Trigonal calcite crystals, which cemented sediment grains in the interstitial pore, merged locally to form

mosaic calcite crystals. Smaller cavities (< 2 mm wide) were commonly occluded by such cement, whereas larger cavities (> 2 mm wide) remained partly open.

Of the four developmental stages, the cavity occlusion stage caused the largest reduction in porosity. The end of Stage III was marked by the cessation of chemical and mechanical deposition, or by any of the tufa components being diagenetically altered.

Stage IV – Diagenetic Modification

Stage IV involved diagenetic modification of the tufa components that formed during Stages I, II, or III (Fig. 2-9). Aggrading recrystallization, the most important aspect of this stage, involved diagenetic suturing that led to the formation of secondary mosaic calcite crystals (Fig. 2-10). Biogenic diagenesis involved destructive processes mediated by bryophytes and endolithic microbes (fungi and cyanobacteria) that bored into the tufa, and bacteria that colonized and dissolved some of the calcite.

Cements were transformed into coarser-grained, secondary mosaic calcite crystals through aggrading recrystallization. Although only visible with epifluorescence microscopy, the primary depositional textures were preserved (Fig. 2-10). Thus, recrystallization merely masked the primary calcite crystals that merged to form the secondary mosaic calcite crystals. During recrystallization, adjacent calcite crystals were sutured together along crystal boundaries, with little to no change to the crystal cores. As a result, individual mosaic crystals commonly contain ghost structures of several types of primary cement, such as mosaic calcite, trigonal calcite, and isopachous banded cements (Figs. 2-10B,C). Coalescive recrystallization (cf. Folk 1965) or Ostwald Ripening, whereby primary crystals are consumed during recrystallization, do not seem to have been involved in the formation of these mosaics.

Recrystallization took place in the vadose environment. Thus, the volume of surface runoff and precipitation that flowed through the deposit probably controlled the degree of recrystallization. This also suggests that recrystallization is currently an active process. In general, tufa samples composed of diagenetic

mosaic crystals lack other cements or contain only minor amounts of cement. As recrystallization proceeded, organic acids were removed from the calcite, decreasing the fluorescence intensity.

Stable Isotope Results

Stable carbon and oxygen isotope compositions were determined for 21 samples of modern, recent, and relict tufa and one sample of soil carbonate embedded in the tufa (Table 2-3, Fig. 2-12). It must be stressed, however, that the division of the tufa into modern, recent, and relict does not directly correspond to the four stages of tufa development. Modern tufa was collected from moss drapes actively growing in the spring flow path, whereas recent tufa was collected from dead bryophytes on an abandoned part of the fan. The modern and recent tufa progressed through Stage II, whereas the relict tufa, collected from parts of the deposit lacking bryophyte material, had progressed through Stages III and/or IV.

The Fall Creek Tufa is characterized by narrow ranges in $\delta^{18}O$ (VPDB) values (-18.4 to -17.7‰) and $\delta^{13}C$ (VPDB) values (-1.2 to 0.5‰). When placed in a global context, the ^{18}O-poor, and ^{13}C-rich nature of the tufa indicates that the parent waters were strongly continental, and derived from a deep limestone aquifer (cf., Andrews 2006). The spring water may thus be hydrothermal in origin, even though it is cool and meteorically derived. Paleo-spring water temperatures were determined using equation 1 (Kim and O'Neil 1997), and yielded temperatures between 11.2°C and 14.4°C (Table 2-3), which is comparable to average modern spring water temperatures of 13°C (Table 2-1). This similarity in temperatures suggests that the calcite was in isotopic equilibrium with the spring water from which it was precipitated.

[1] $$1000 \ln \alpha \text{ (calcite-}H_2O) = 18.03 (10^3 T^{-1}) - 32.42$$

where α is the fractionation factor and T is in kelvins.

Table 2-3 Fall Creek Tufa stable oxygen and carbon isotopic compositions.

Samples		$\delta^{18}O$ (‰ VPDB)		$\delta^{13}C$ (‰ VPDB)		Calculated T Values (°C)	
Type	N	Min	Max	Min	Max	Min	Max
Modern Tufa	2	-18.3	-17.8	-0.1	-0.3	11.8	13.5
Recent Tufa	3	-18.4	-18.1	0.0	0.5	13.1	14.0
Relict Tufa	16	-18.4	-17.7	-1.2	0.2	11.2	14.4
Soil Carbonate	1	-17.3		-0.4		9.2	

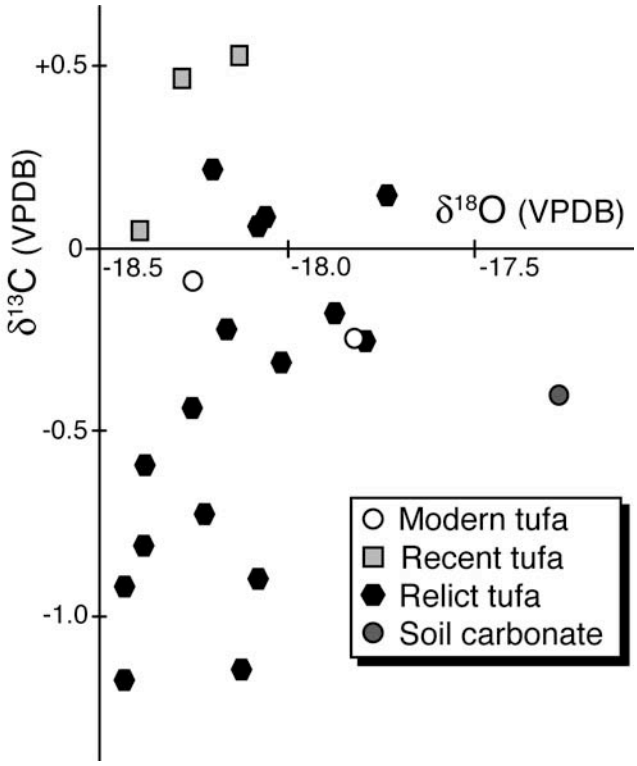

Fig. 2-12 Stable isotopes for tufa and soil carbonate from Fall Creek.

The maximum and minimum $\delta^{13}C$ values vary by only 0.2‰ for modern tufa, 0.5‰ for recent tufa, 1.4‰ for relict tufa, and 1.7‰ overall. The limited number of modern and recent tufa samples makes it difficult to determine if the larger variation in relict tufa values is related to sample bias, primary formation, or diagenetic ^{13}C depletion. Belgian tufa deposits yielded $\delta^{13}C$ values with 4‰ differences, and within that range had a 2‰ enrichment in ^{13}C that was attributed

to diagenesis (Janssen et al. 1999). Data pertaining to the effects of tufa diagenesis on stable isotopes is limited, and as of yet, no stable isotope signatures that are diagnostic of recrystallization have been discovered (Andrews and Brasier 2005; Andrews 2006).

Carbonate spring deposits typically exhibit wide ranges in $\delta^{13}C$ values even in precipitates that formed within centimeters of each other (Chafetz and Lawrence 1994) because spring water composition, temperature, pH, saturation, and flow conditions are spatially variable. Hot water deposits at Mammoth Hot Springs in Yellowstone National Park and at Rapolano Terme, Italy, for example, have $\delta^{13}C$ values with ranges between 4 and 8‰ (e.g., Guo et al. 1996; Fouke et al. 2000; Chafetz and Guidry 2003). Downstream enrichments in ^{13}C were attributed to inorganic and microbially-mediated CO_2 degassing. Similarly, a 500 m long section of a stream-deposited travertine in the United Kingdom had downstream ^{13}C enrichments of 2.6‰ due to the activity of photosynthetic microbes (Pentecost and Spiro 1990). These isotopic variations, however, were due to primary formational processes, not diagenesis.

The narrow range in $\delta^{13}C$ values for the Fall Creek Tufa $\delta^{13}C$ is similar to those in the moss-dominated travertines precipitated from 20°C water at Matlock Bath, Derbyshire. The $\delta^{13}C$ values of all tufa at Matlock Bath (recent and relict) differed by only 1.2‰, and were at or close to isotopic equilibrium with the spring water during formation (Pentecost 1999). The small range in $\delta^{13}C$ values from the Fall Creek Tufa may be due to the relatively short spring water flow path (~ 50 m) before the confluence with Fall Creek.

Discussion

The Fall Creek Tufa is a young (mid- to late-Holocene) freshwater carbonate spring deposit that is composed largely of calcite cements precipitated around a framework of *Cratoneuron commutatum* gametophytes that followed a four-stage developmental process (Fig. 2-11). Despite its geological youth, much of the calcite has been recrystallized with suturing of adjacent crystals producing

large, anhedral crystals that contain ghost structures of as many as three different types of primary cement (Fig. 2-10). Recrystallization and aggrading neomorphism have also been reported from other travertine and tufa deposits (e.g., Heimann and Sass 1989; Freytet and Verrecchia 1999; Arp et al. 2001). Pentecost (2005, p. 20), for example, noted that while "…a primary micrite is being precipitated around the surface of an algal colony it may be recrystallizing into a sparite only a few mm below the surface…". Similarly, by staining tufa from the Arbuckle Mountains in Oklahoma with methylene blue, Love and Chafetz (1988, 1990) revealed traces of algal shrubs that had been masked by aggrading neomorphism. Likewise, Janssen et al. (1999) suggested that calcite crystals in some Belgian tufa deposits had formed through recrystallization of micrite. These changes are important because they transform the tufa fabrics and commonly mask the features that are critical to the interpretation of original depositional setting.

Recrystallization of any limestone takes place as primary minerals equilibrate with their surroundings (cf. Sunagawa 1990). Such changes may be driven by the polymorphic transformation of aragonite to calcite (e.g., Purdy 1968; Bathurst 1975; James and Choquette 1984; Tucker and Wright 1990) and/or the exposure of marine carbonates to meteoric water (e.g., Bathurst 1975; Tucker and Wright 1990). Such factors, however, cannot be invoked to explain the recrystallization of the calcite in the Fall Creek Tufa because there is no indication that aragonite was ever part of the deposit and there is no evidence that the environmental setting of the deposit has changed. Thus, the diagenesis of the calcite in the Fall Creek Tufa must be related to crystal size, crystal shape, porosity, and/or permeability (cf. James and Choquette 1984).

Throughout the development of the Fall Creek Tufa, spring water, rainwater, and/or snowmelt water have percolated through the tufa. Fluid transmission was enabled by the high porosity and permeability of the tufa. Cavities throughout the deposit, irrespective of size, were commonly filled with water and thereby created phreatic conditions in spite of the vadose setting. This

is reflected by the dominance of isopachous or blocky mosaic cements found in the tufa. Stable isotope results did not show if spring water, rainwater, or snowmelt water was responsible for recrystallization, probably because the diagenetic waters were similar to those from which the calcite originally formed (cf. Andrews and Brasier 2005; Andrews 2006). Rainwater, however, is mildly acidic, slightly undersaturated with respect to calcium carbonate (James and Choquette 1984; Tucker and Wright 1990), and when derived from snowmelt, is much colder than spring water. Combined, these factors give atmospheric precipitation a greater capacity than the spring water for dissolving the calcite and/or mediating calcite recrystallization.

Much of the calcite in the Fall Creek Tufa was precipitated as composite crystals that have commonly been attributed to rapid precipitation caused by rapid CO_2 degassing (e.g., Jones et al. 2005). These complex crystals are formed of numerous small subcrystals that are characterized by numerous vertices, edges, and high surface roughness. Such intricate crystal arrangements have a high number of unsatisfied bonds (e.g., Saratovkin 1959) and are therefore prone to recrystallization as crystals reduce their surface free energies by forming less complex shapes, increasing crystal size, and reducing the number of crystals (Bathurst 1975). The presence of ghost structures in the large calcite crystals shows that diagenesis involved crystal growth but little or no dissolution of the original calcite. Many of the large calcite crystals were probably produced by suturing of adjacent crystals via a thin film of water that once existed between neighbouring crystals (cf. Bathurst 1975). That water film may have provided the Ca and CO_3 for precipitation of calcite that filled the spaces between adjacent crystals or mediated a dissolution-precipitation process whereby Ca and CO_3 obtained by dissolution of one or both neighbouring crystal faces was immediately reprecipitated as a cement that united adjacent crystals.

Diagenetic fabrics in Holocene and Pleistocene spring tufa and travertine (Guo and Riding 1994; Pedley et al. 2003), which formed over the course of millennia, involved recrystallization of cyanobacterial shrubs (e.g., Love and

Chafetz 1988; Freytet and Verrecchia 1999), micritization (e.g., Chafetz et al. 1994; Guo and Riding 1994), and speleothem precipitation (e.g., Pedley et al. 2003). The aggrading neomorphism found in the Fall Creek Tufa incorporated all types of primary tufa components as part of a continuous formational process. This suggests that the recrystallization is driven by environmental conditions and is not a time-dependent process.

Conclusions

Morphological, petrographic and stable isotopic analyses of the Fall Creek Tufa have yielded the following conclusions.

- Although the spring is currently active, there is no calcite presently being precipitated from the cold (~ 13°C) meteorically derived spring water.
- Tufa formation probably began during the mid-Holocene (~ 5000 years BP) and ended no earlier than 390 +/- 105 calendar years BP.
- The tufa is largely formed of calcite-encased *Cratoneuron commutatum* gametophytes that were subjected to a cyclical, four-stage developmental process that involved encrustation, encapsulation, cavity occlusion and diagenetic alteration. The developmental process was temporally and spatially variable.
- Many of the primary depositional fabrics were masked by aggrading recrystallization as adjacent calcite crystals were diagenetically sutured to produce larger, less complex crystals that are more energetically favourable.
- The original mineralogy and stable carbon and oxygen isotopic compositions of the tufa have been preserved because the formational and diagenetic processes took place in the same environment and were mediated by fresh waters with similar compositions.

References

Andrews, J.E. 2006. Palaeoclimatic records from stable isotopes in riverine tufas: Synthesis and review. Earth-Science Reviews, **75**: 85-104.

Andrews, J.E., and Brasier, A.T. 2005. Seasonal records of climatic change in annually laminated tufas: short review and future prospects. Journal of Quaternary Science, **20**: 411-421.

Arp, G., Wedemeyer, N., and Reitner, J. 2001. Fluvial tufa formation in a hard-water creek (Deinschwanger Bach, Franconian Alb, Germany). Facies, **44**: 1-22.

Bathurst, R.G.C. 1975. Carbonate Sediments and their Diagenesis. Amsterdam, Elsevier Scientific Publishing Company.

Bonny, S. 2002. Recent and fossil spring deposits at Miette Hot Springs, Jasper National Park, Alberta, Canada. M.Sc. thesis, University of Alberta, Edmonton, Alberta.

Bonny, S., and Jones, B. 2003a. Microbes and mineral precipitation, Miette Hot Springs, Jasper National Park, Alberta, Canada. Canadian Journal of Earth Sciences, **40**: 1483-1500.

Bonny, S., and Jones, B. 2003b. Relict tufa at Miette Hot Springs, Jasper National Park, Alberta, Canada. Canadian Journal of Earth Sciences, **40**: 1459-1481.

Chafetz, H.S. 1986. Marine peloids: a product of bacterially induced precipitation of calcite. Journal of Sedimentary Petrology, **56**: 812-817.

Chafetz, H.S., and Folk, R.L. 1984. Travertines: depositional morphology and the bacterially constructed constituents. Journal of Sedimentary Petrology, **54**: 289-316.

Chafetz, H.S., and Guidry, S.A. 2003. Deposition and diagenesis of Mammoth Hot Springs travertine, Yellowstone National Park, Wyoming, U.S.A. Canadian Journal of Earth Sciences, **40**: 1515-1529.

Chafetz, H.S., and Lawrence, J.R. 1994. Stable isotopic variability within modern travertines. Géographie physique et Quaternaire, **48**: 257-273.

Chafetz, H.S., Srdoc, D., and Horvatincic, N. 1994. Early Diagenesis of Plitvice Lakes Waterfall and Barrier Travertine Deposits. Géographie Physique et Quaternaire, **48**: 247-255.

Emeis, K.C., Richnow H.H., and Kempe, S. 1987. Travertine formation in Plitvice National Park, Yugoslavia: chemical versus biological control. Sedimentology, **34**: 595-609.

Emig, W.H. 1918. Mosses as rock builders. Bryologist, **21**: 55-59.

Fang, L.S. and Chou, Y.C. 1992. Concentration of fulvic-acid in the growth bands of hermatypic corals in relation to local precipitation. Coral Reefs **11**: 187-191.

Folk, R.L. 1965. Some aspects of recrystallization in ancient limestones. SEPM (Society of Economic Paleontologists and Mineralogists), Special Publication 13, pp. 14-48.

Folk, R.L., Chafetz, H.S., and Tiezzi, P. 1985. Bizarre forms of depositional and diagenetic calcite in hot-spring travertines, central Italy. *In* Carbonate cements. *Edited by* N. Schneidermann and P.M. Harris. SEPM (Society of Economic Paleontologists and Mineralogists), Special Publication 36, pp. 349-369.

Ford, T.D., and Pedley, H.M. 1996. A review of tufa and travertine deposits of the world. Earth-Science Reviews, **41**: 117-175.

Fouke, B.W., Farmer, J.D., Des Marais, D.J., Prat, L., Sturchio, N.C., Burns, P.C., and Discipulo, M.K. 2000. Depositional facies and aqueous-solid geochemistry of travertine-depositing hot springs Angel Terrace, Mammoth Hot Springs, Yellowstone National Park, U.S.A.. Journal of Sedimentary Research, **70**: 565-585.

Fouke, B.W., Bonheyo, G.T., Sanzenbacher, B., and Frias-Lopez, J. 2003. Partitioning of bacterial communities between travertine depositional facies at Mammoth Hot Springs, Yellowstone National Park, U.S.A. Canadian Journal of Earth Sciences, **40**: 1531-1548.

Freytet, P., and Verrecchia, E.P. 1999. Calcitic radial palisadic fabric in freshwater stromatolites; diagenetic and recrystallized feature or physicochemical sinter crust? Sedimentary Geology, **126**: 97-102.

Gadd, B. 1995. Handbook of the Canadian Rockies. Jasper, Corax Press.

Garnett, E.R., Gilmour, M.A., Rowe, P.J., Andrews, J.E., and Preece, R.C. 2004. Th-230/U-234 dating of Holocene tufas: possibilities and problems. Quaternary Science Reviews **23**, 947-958.

Given, R.K., and Wilkinson, B.H. 1985. Kinetic control of morphology, composition, and mineralogy of abiotic sedimentary carbonates. Journal of Sedimentary Petrology, **55**: 109-119.

Grasby, S.E., and Hutcheon, I. 2001. Controls on the distribution of thermal springs in the southern Canadian Cordillera. Canadian Journal of Earth Sciences, **38**: 427-440.

Grasby, S.E., Hutcheon, I., and Krouse, H.R. 2000. The influence of water-rock interaction on the chemistry of thermal springs in western Canada. Applied Geochemistry, **15**: 439-454.

Grasby, S.E., van Everdingen, R.O., Bednarski, J., and Lepitzki, D.A.W. 2003. Travertine mounds of the Cave and Basin National Historic Site, Banff National Park. Canadian Journal of Earth Sciences, **40**: 1501-1513.

Gulley, A.L. 1993. Rabbitkettle Hotsprings, Nahanni National Park Reserve, Northwest Territories: a hydrogeological study. M.Sc. thesis, Carleton University, Ottawa, Ont.

Guo, L., and Riding, R.E. 1992. Aragonite laminae in hot water travertine crusts, Rapolano Terme, Italy. Sedimentology, **39**: 1067-1079.

Guo, L., and Riding, R. 1994. Origin and diagenesis of Quaternary travertine shrub fabrics, Rapolano Terme, central Italy. Sedimentology, **41**: 499-520.

Guo, L., and Riding, R.E. 1998. Hot-spring travertine facies and sequences, Late Pleistocene, Rapolano Terme, Italy. Sedimentology, **45**: 163-180.

Guo, L., and Riding, R.E. 1999. Rapid facies changes in Holocene fissure ridge hot spring travertines, Rapolano Terme, Italy. Sedimentology, **46**: 1145-1158.

Guo, L., Andrews, J., Riding, R., Dennis, P., and Dresser, Q. 1996. Possible microbial effects on stable carbon isotopes in hot-spring travertines. Journal of Sedimentary Research, **66**: 468-473.

Heimann, A., and Sass, E. 1989. Travertines in the northern Hula Valley, Israel. Sedimentology, **36**: 95-108.

Isdale, P. 1984. Fluorescent bands in massive corals records centuries of coastal rainfall. Nature, **310**: 578-579.

Isdale, P.J., Stewart, B.J., Tickle, K.S., and Lough, J.M. 1998. Palaeohydrological variation in a tropical river catchment: a reconstruction using fluorescent bands in corals of the Great Barrier Reef, Australia. Holocene, **8**: 1-8.

James, N.P., and Choquette, P.W. 1984. Chapter 9: Limestones - the meteoric diagenetic environment. Geoscience Canada, **11**: 161-194.

Janssen, A., Swennen, R., Podoor, N., and Keppens, E. 1999. Biological and diagenetic influence in recent and fossil tufa deposits from Belgium. Sedimentary Geology, **126**: 75-95.

Jones, B. 1989a. Calcite rafts, peloids and micrite in cave deposits from Cayman Brac, British West Indies. Canadian Journal of Earth Sciences, **26**: 654-664.

Jones, B. 1989b. Syntaxial overgrowths on dolomite crystals in the Bluff Formation, Grand Cayman, British West Indies. Journal of Sedimentary Petrology, **59**: 839-847.

Jones, B., Renaut, R.W., Owen, R.B., and Torfason, H. 2005. Growth patterns and implications of complex dendrites in calcite travertines from Lysuhóll, Snæfellsnes, Iceland. Sedimentology, **52**: 1277-1301.

Kahle, C.F. 1977. Origin of Sub-Aerial Holocene Calcareous Crusts - Role of Algae, Fungi and Sparmicritization. Sedimentology, **24**: 413-435.

Kim, S.-T., and O'Neil, J.R. 1997. Equilibrium and nonequilibrium oxygen isotope effects in synthetic carbonates. Geochimica et Cosmochimica Acta, **61**: 3461-3475.

Love, K.M., and Chafetz, H.S. 1988. Diagenesis of laminated travertine crusts, Arbuckle Mountains, Oklahoma. Journal of Sedimentary Petrology, **58**: 441-445.

Love, K.M., and Chafetz, H.S. 1990. Petrology of Quaternary travertine deposits, Arbuckle Mountains, Oklahoma. *In* Travertine-marl: stream deposits in Virginia. *Edited by* S. Herman and D.A. Hubbard. Virginia Division of Mineral Resources, Publication 101, pp. 65-78.

Luckman, B. H. 1986. Reconstruction of the Little Ice Age events in the Canadian Rocky Mountains. Géographie physique et Quaternaire **40**: 17-28.

Luckman, B.H. 2000. The Little Ice Age in the Canadian Rockies. Geomorphology, **32**: 357-384.

Luckman, B.H., Briffa, K.R., Jones, P.D., and Schweingruber, F.H. 1997. Tree-ring based reconstruction of summer temperatures at the Columbia Icefield, Alberta, Canada, AD 1073-1983. The Holocene, **74**: 375-389.

Macintyre, I.G. 1985. Submarine cements – the peloidal question. *In* Carbonate cements. *Edited by* N. Schneidermann and P.M. Harris**.** SEPM (Society of Economic Paleontologists and Mineralogists), Special Publication 36, pp. 109-116.

Martín-Algarra, A., Martín-Martín, M., and Andreo, B. 2003. Sedimentary patterns in perched spring travertines near Granada Spain as indicators of the paleohydrological and paleoclimatological evolution of a karst massif. Sedimentary Geology, **161**: 217-228.

McCrea, J.M. 1950. On the isotope chemistry of carbonates and paleotemperature scale. Journal of Chemical Physics, **18**: 849-857.

McGarry, S.F., and Baker, A. 2000. Organic acid fluorescence: applications to speleothem palaeoenvironmental reconstruction. Quaternary Science Reviews, **19**: 1087-1101.

Pedley, H.M. 1987. The Flandrian Quaternary Caerwys tufa, North Wales: an ancient barrage tufa deposit. Proceedings of the Yorkshire Geological Society, **46**: 141-152.

Pedley, H.M. 1990. Classification and environmental models of cool freshwater tufas. Sedimentary Geology, **68**: 143-154.

Pedley, H.M. 1992. Freshwater (phytoherm) reefs: the role of biofilms and their bearing on marine reef cementation. Sedimentary Geology, **79**: 255-274.

Pedley, H.M. 2000. Ambient temperature freshwater microbial tufas. *In* Microbial Sediments. *Edited by* R.E. Riding and S.M. Awramik. Springer, Berlin, pp. 179-186.

Pedley, H.M., Andrews, J.E., Ordonez, S., Garcia del Cura, M.A., González Martín, J.-A., and Taylor, D. 1996. Does climate control the morphological fabric of freshwater carbonates? A comparative study of Holocene barrage tufas from Spain and Britain. Palaeogeography, Palaeoclimatology, Palaeoecology, **121**: 239-257.

Pedley, H.M., González Martín, J.-A., Delgado, S.O., and Del Cura, Á.G. 2003. Sedimentology of Quaternary Perched Springline and Paludal Tufas: Criteria for Recognition, With Examples from Guadalajara Province, Spain. Sedimentology, **50**: 23-44.

Peña, J.L., Sancho, C., and Lozano, M.V. 2000. Climatic and Tectonic Significance of Late Pleistocene and Holocene Tufa Deposits in the Mijares River Canyon, Eastern Iberian Range, Northeast Spain. Earth Surface Processes and Landforms, **25**: 1403-1417.

Pentecost, A. 1987. Some observations on the growth rates of mosses associated with tufa and the interpretation of some postglacial bryoliths. Journal of Bryology, **14**: 543-550.

Pentecost, A. 1990. The formation of travertine shrubs: Mammoth Hot Springs, Wyoming. Geological Magazine, **127**: 159-168.

Pentecost, A. 1993. British travertines: a review. Proceedings of the Geologists' Association, **104**: 23-39.

Pentecost, A. 1994. Formation of laminate travertines at Bagno Vignone, Italy. Geomicrobiology Journal, **12**: 239-251.

Pentecost, A. 1995. The Quaternary travertine deposits of Europe and Asia Minor. Quaternary Science Reviews, **14**: 1005-1028.

Pentecost, A. 1996. Moss Growth and Travertine Deposition: The Significance of Photosynthesis, Evaporation and Degassing of Carbon Dioxide. Journal of Bryology, **19**: 229-234.

Pentecost, A. 1999. The origin and development of the travertines and associated thermal waters at Matlock Bath, Derbyshire. Proceedings of the Geologists' Association, **110**: 217-232.

Pentecost, A. 2005. Travertine. Berlin, Springer-Verlag.

Pentecost, A., and Spiro, B. 1990. Stable carbon and oxygen isotope composition of calcites associated with modern freshwater cyanobacteria and algae. Geomicrobiology Journal, **8**: 17-26.

Pentecost, A., Peterken, G.F., and Viles, H.C. 2000. The travertine dams of Slade Brook, Gloucestershire: their formation and conservation. Geology Today, **16**: 22-25.

Pentecost, A., Jones, B., and Renaut, R.W. 2003. What is a hot spring? Canadian Journal of Earth Sciences, **40**: 1443-1446.

Purdy, E.G. 1968. Carbonate diagenesis; an environmental survey. Geologica Romana, **7**: 183-227.

Rainey, D.K., and Jones, B. 2005. Radiating calcite dendrites -- precursors for coated grain formation in the Fairmont Hot Springs Travertine, Canada. *In* Proceedings of the 1st international symposium on travertine, Denizli, Turkey, September 21-25, 2005, pp. 25-32.

Reimer, P., Baillie, M., Bard, E., Bayliss, A., Beck, J., Bertrand, C., Blackwell, P., Buck, C., Burr, G., Cutler, K., Damon, P., Edwards, R., Fairbanks, R., Friedrich, M., Guilderson, T., Hughen, K., Southon, J., Stuiver, M., Talamo, S., Taylor, F., van der Plicht, J., and Weyhenmeyer, C. 2004. IntCal04 Terrestrial radiocarbon age calibration, 26-0 ka BP. Radiocarbon, **46**: 1029-1058.

Renaut, R.W., and Jones, B. 2000. Microbial precipitates around continental hot springs and geysers. *In* Microbial Sediments. *Edited by* R.E. Riding and S.M. Awramik. Springer, Berlin, pp. 187-195.

Sandberg, P. 1985. Aragonite cements and their occurrence in ancient limestones. *In* Carbonate cements. *Edited by* N. Schneidermann and P.M. Harris**.** SEPM (Society of Economic Paleontologists and Mineralogists), Special Publication 36, pp. 33-57.

Saratovkin, D.D. 1959. Dendritic Crystallization. New York, Consultants Bureau.

Stuiver, M., and Reimer, P. 1993. Extended 14C database and revised CALIB radiocarbon calibration program. Radiocarbon, **35**: 215-230.

Sunagawa, I. 1990. In situ observation of nucleation, growth and dissolution of crystals in ordinary temperature aqueous solutions and high temperature silicate solutions. *In* Dynamic processes of material transport and transformation in the Earth's Interior. *Edited by* F. Marumo. Terra Scientific Publishing Company, Tokyo, pp. 139-168.

Tucker, M.E., and Bathurst, R.G.C. 1990. Carbonate Diagenesis. London, Blackwell Scientific Publications.

Tucker, M.E., and Wright, V.P. 1990. Carbonate Sedimentology. London, Blackwell Scientific Publications.

Turner, E.C., and Jones, B. 2005. Microscopic calcite dendrites in cold-water tufa: implications for nucleation of micrite and cement. Sedimentology, **52**: 1043-1066.

van Everdingen, R.O. 1972. Thermal and mineral springs in the southern Rocky Mountains of Canada, Water Management Service, Department of the Environment, Environment Canada.

Vitt, D.H., Marsh, J.E., and Bovey, R.B. 1988. Mosses, Lichens & Ferns of Northwest North America. Edmonton, Lone Pine Publishing.

Watson, E., and Luckman, B.H. 2004. Tree-ring-based mass-balance estimates for the past 300 years at Peyto Glacier, Alberta, Canada. Quaternary Research, **62**: 9-18.

Weed, W.H. 1889. Formation of Travertine and siliceous sinter by the vegetation of Hot Springs. United States Geological Survey, 9th Annual Report (1887-1888), pp. 613-676.

Weijermars, R., Mulder-Blanken, C.W., and Wiegers, J. 1986. Growth rate observation from the moss-built Checa travertine terrace, central Spain. Geological Magazine, **123**: 279-286.

Woodsworth, G. 1999. Hot Springs of Western Canada. West Vancouver, Gordon Soules Book Publisher's Ltd.

Wright, D.J. 1980. The physical geography of the Rabbitkettle Hot Springs, Nahanni National Park, N.W.T. M.Sc. thesis, University of Alberta, Edmonton, Alta.

Zhang, Z., and Pentecost, A. 2000. New and noteworthy bryophytes from the travertines of Guizhou and Sichuan, SW China. Journal of Bryology, **22**: 66-68.

Chapter 3

Abiotic versus biotic controls on the development of the Fairmont Hot Springs Carbonate Deposit, British Columbia, Canada[1]

Introduction

Carbonate spring deposits form through the interplay of biotic and abiotic processes (Chafetz & Folk, 1984; Folk *et al.*, 1985; Chafetz & Guidry, 1999; Janssen *et al.*, 1999; Fouke *et al.*, 2000; Renaut & Jones, 2000; Andrews & Brasier, 2005). Much of the focus on spring deposits has, however, been on biotic processes, such as the effect of microbes and other biota (mainly photosynthesizers) on $CaCO_3$ precipitation (Pentecost, 1990; Guo *et al.*, 1996; Chafetz & Guidry, 1999; Fouke *et al.*, 2000; Andrews & Riding, 2001; Pedley, 2000; Fouke, 2001; Pentecost & Coletta, 2007; Pedley *et al.*, 2008). During pioneering work at Mammoth Hot Springs in Yellowstone National Park, USA, Weed (1888) noted the importance of vegetation growing in the spring water on deposit formation, but also understood the significance of physicochemical processes, "…since we have seen that the water will deposit a coating of carbonate of lime without the influence of plant life." Biotic growth concurrent with $CaCO_3$ precipitation undoubtedly creates fabrics that could not form abiotically, however, biota being present during crystal growth does not automatically imply that they affect crystal growth (cf. Folk *et al.*, 1985; Pentecost & Coletta, 2007). Despite their crucial role in carbonate spring deposit formation, much remains unknown about biotic-abiotic interactions in spring settings.

When compared with other fossil-dominated carbonate spring deposits in the Canadian Rocky Mountains, the Fairmont Hot Springs carbonate deposit (Fig. 3-1A) is unusual because of its abundance of abiotic facies (Bonny & Jones, 2003a, b; Turner & Jones, 2005; Rainey & Jones, 2007). The combination of biotic and

[1] A version of this chapter has been published. Rainey, D.K., Jones, B., 2009. Abiotic versus biotic controls on the development of the Fairmont Hot Springs carbonate spring deposit, British Columbia, Canada. Sedimentology, doi: 10.1111/j.1365-3091.2009.01059.x.

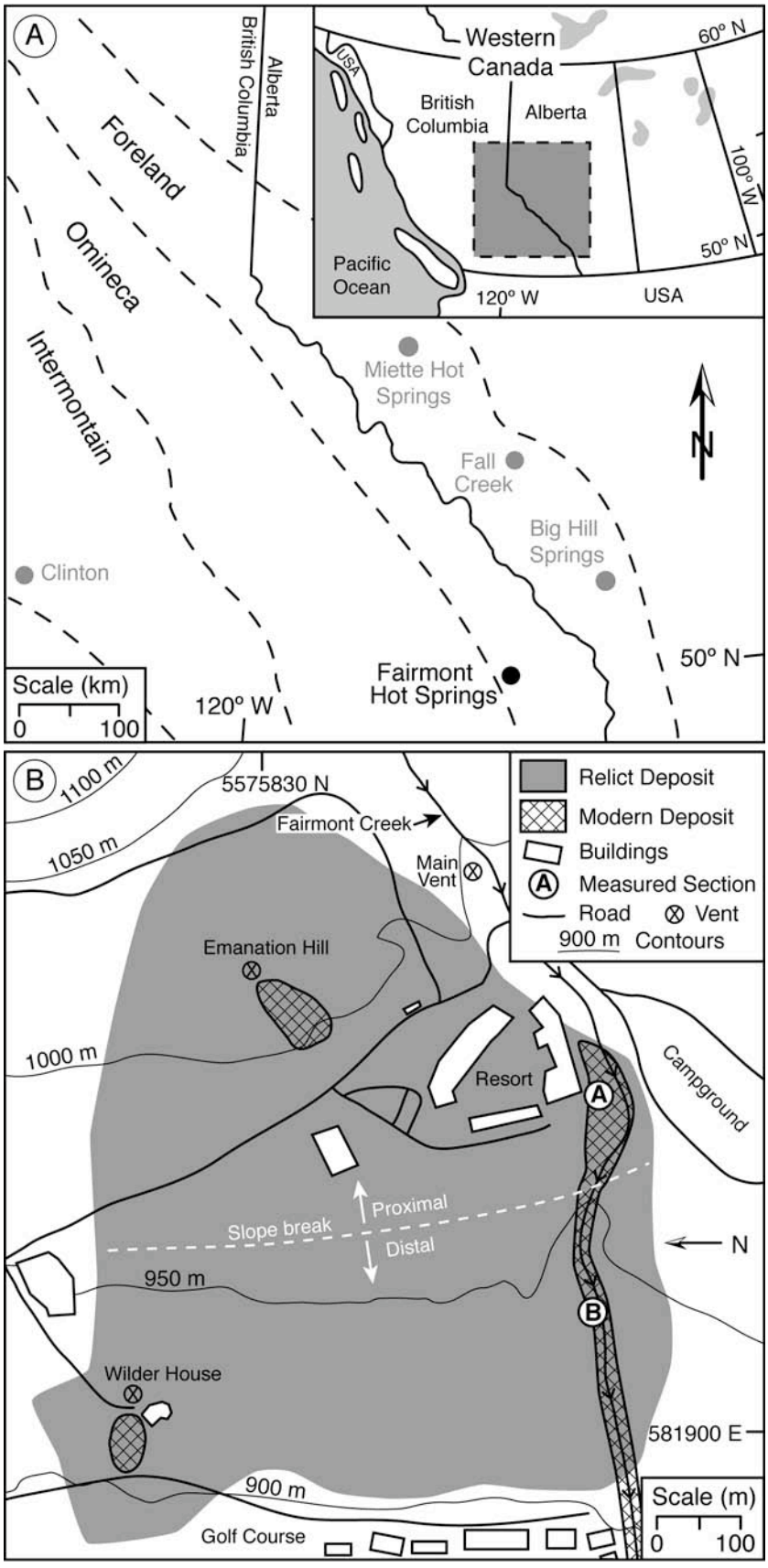

Fig. 3-1 A) Fairmont Hot Springs location near western margin of Rocky Mountains (Foreland). Carbonate spring deposits in Alberta and British Columbia with completed petrographic analyses have also been indicated. B) Areal extent of Fairmont deposit. Modern calcite precipitation extremely limited compared to area covered by relict deposit. Best exposure through deposit in Fairmont Creek valley at right of image.

abiotic fabrics preserved in the Fairmont deposit make it morphologically and petrographically similar to the extensive deposits at Mammoth Hot Springs in Yellowstone (Weed, 1888; Allen & Day, 1935; Chafetz & Folk, 1984; Pentecost, 1990; Fouke *et al*., 2000; Chafetz & Guidry, 2003; Fouke *et al*., 2003), Rapolano Terme and Bagni di Tivoli in Italy (Folk & Chafetz, 1983; Folk *et al*., 1985; Guo & Riding, 1992, 1994, 1998, 1999; Pentecost, 1994; Guo *et al*., 1996), and Pamukkale, Turkey (Altunel & Hancock, 1993; Ekmecki *et al*., 1995; Pentecost *et al*., 1997; Özkul *et al*., 2002; Alçiçek *et al*., 2005). Fabrics common to all of these deposits include dendrite crystals, stromatolites, microbes, coated grains, coated bubbles and macrophytes.

This paper describes the spatial and temporal distributions of biotic and abiotic facies in the Fairmont deposit, infers the paleo-hydrodynamic conditions necessary for their formation, and demonstrates how competition between calcite precipitation rates and biotic growth rates controlled facies distribution. By so doing, it demonstrates clearly the delicate balance that exists between biotic and abiotic processes and the impact that this balance has on the development of facies within a spring system.

Materials and Methods

Fieldwork during the summer of 2002 examined the large-scale features of the deposit with 38 samples being collected from seven sections. Water temperature and pH measurements were taken in the field at the source for the resort hot spring water (herein called the Main Vent), at Emanation Hill, and at Fairmont Creek, below the confluence with the hot spring water (Fig. 3-1B). Filtered samples, for isotope analysis, were collected using a syringe and 0.22 micron filter, and stored in Teflon-capped 5 dram vials. In the summer of 2003, climbing gear was utilized to examine 13 sections and collect 76 samples from the vertical to sub-vertical walled Fairmont Creek valley. In the summer of 2004, the deposit was mapped and two charcoal samples embedded in the deposit were collected for ^{14}C dating. In autumn 2005, climbing gear was once again utilized in order to create two measured sections (Fig. 3-1B).

Of the 114 samples collected, large (5 X 7 cm) thin sections were produced from 45 samples that represented the various fabrics. The thin sections were characterized using transmitted light and epifluorescence microscopy with an ultraviolet excitation filter. Fractured carbonate samples, sputter coated with a thin layer of gold, were examined on a JEOL 6301F field emission scanning electron microscope (SEM) at accelerating voltages of 5 to 20 kV. Carbonate samples were confirmed to be calcite by powdering and analyzing them using X-ray diffraction (XRD) with a Rigaku Geigerflex Powder Diffractometer. The oxygen isotopic compositions of the spring water were determined by the Environmental Isotope Laboratory at the University of Waterloo.

Stable carbon and oxygen isotopic compositions were measured for 81 carbonate samples collected from 10 vertical sections across a 350 m long exposure. Stable carbon and oxygen isotopic analyses were completed in the stable isotope laboratory in the Department of Earth and Atmospheric Sciences at the University of Alberta. Under vacuum, 4.5 to 5.5 mg of crushed limestone was reacted for 3 hours with 5 ml of phosphoric acid in a 25°C water bath, following the procedure of McCrea (1950). The carbon and oxygen isotopic composition of the liberated CO_2(g) was measured with a Finnegan MAT 252 mass spectrometer.

Pre-treatment of the charcoal samples for ^{14}C dating was completed at the University of Alberta. Samples were washed with 10% HCl for 1 hour to remove calcium carbonate, then washed with 1M NaOH hourly until the wash was colourless. This was followed by a final 10% HCl wash and rinsing with ultra-pure H_2O until neutral. Accelerator mass spectrometry dating of the washed samples was completed at the Keck Carbon Cycle AMS facility, Earth System Science Department, University of California, Irvine. Conventional radiocarbon ages were converted to calendar years using the CALIB radiocarbon calibration program and the IntCal04 terrestrial radiocarbon age calibration for 26-0 ka BP, and calibrated ages are reported as 2 sigma ranges (Stuiver and Reimer 1993; Reimer et al. 2004).

The contrast and brightness of the digital field images and SEM photomicrographs used in this paper were adjusted using Adobe Photoshop©.

SEM photomicrographs, black backgrounds were introduced in order to highlight the features being shown.

Terminology

Tufa and travertine are lithological terms used commonly to describe carbonate spring deposits. Nevertheless, standardized definitions of these terms are still lacking (Viles & Goudie, 1990; Ford & Pedley, 1996; Pentecost, 2005), and many researchers have abandoned the term tufa (Pentecost, 1981, 1985, 1987; Pentecost *et al.*, 1990; Viles & Goudie, 1990) in favour of travertine (Julia, 1983; Pentecost, 1993, 1995a, b, 2005; Pentecost & Viles, 1994). Despite this debate, deposits labeled as tufa contain abundant fossils (Irion & Müller, 1968; Pentecost, 1985, 1987; Pedley, 1987; Rands *et al.*, 1995; Das & Mohanti, 1997; Bonny & Jones, 2003b; Turner & Jones, 2005; Rainey & Jones, 2007). Some tufa and travertine definitions were based on genetic factors (e.g. water temperature), hardness, porosity and contained fossils, but no definitions were based solely on fossil content (Pedley, 1990; Koban & Schweigert, 1993; Ford & Pedley, 1996). Ford & Pedley (1996) stated that, "…macro- and micro-vegetation invariably are major components of many tufa systems and serve to distinguish tufa deposits from travertines…" but failed to utilize this as the defining characteristic. For the purpose of this paper, tufa is a carbonate spring deposit (or part of a deposit) with fabrics that are controlled by the contained fossils (such as macrophytes, microphytes, stromatolites, microbes, invertebrates, and/or vertebrates), whereas travertine is formed of inorganic crystal fabrics. Travertine is not precluded from containing fossils, but the gross textures and morphologies did not result from the presence of biota during formation.

A dendrite is a single crystal with multiple levels of branching (Strickland-Constable, 1968; Jones & Kahle, 1986, 1993; Jones & Renaut, 1995). Non-crystallographic dendrites are those in which branching is not governed by the crystallographic properties of the mineral (cf. Keith & Padden, 1964; Jones & Renaut, 1995; Chafetz & Guidry, 1999). Feather dendrites have thin wispy branches extending from a main stem (cf. Jones & Renaut, 1995). Radiating

dendrites are spherical to sub-spherical crystals composed of branching calcite that spreads out from a central point (cf. Rainey & Jones, 2005).

Geological Setting

The Fairmont Hot Springs are located in the town of Fairmont Hot Springs along Highway 93/95 at the western limit of the Rocky Mountains in south-east British Columbia (Fig. 3-1). The springs are situated on the eastern slopes of the Rocky Mountain Trench at the base of the N-S trending Stanford Range on a forested terrace overlooking the Columbia River to the west. The Fairmont Hot Springs are sandwiched between two major NW-SE trending thrust faults 20 km apart, the Redwall to the east and Purcell to the west (Grasby & Hutcheon, 2001). The spring water emerges from dolostones of the Cambrian Jubilee Formation at the intersection of two smaller unnamed faults (van Everdingen, 1972, figs 55 and 56). To reach the surface, the spring water passes through an unknown thickness of diamictite, upon which the carbonate deposit rests unconformably (Fig. 3-2). The diamictite was deposited in a glaciofluvial kame terrace along the margins of valley formed along the Rocky Mountain Trench (Clague, 1975).

Dawson (1886) first noted the relict deposit at Fairmont and described it as a "…calcareous tufa, which in superimposed flaggy layers, forms a thick deposit." Most of the deposit is covered by fluvial deposits, soil, vegetation, and the Fairmont Hot Springs resort. The best exposure (and the locale where Dawson made his observations) is in the E-W trending Fairmont Creek valley, which incises the deposit near its southern margin (Figs. 3-1B and 3-2). The valley provides a 0.5 km long, continuously exposed cross-section of the deposit that is parallel to the east to west paleo-flow direction. Most of the deposit is on the north side of Fairmont Creek, as is the thickest exposure (Figs. 3-2A,B). On the north side of the valley, the basal unconformity with the kame terrace is only exposed down-slope of the thickest accumulation (Fig. 3-2D). The kame terrace deposit on the south side of the creek is up to 15 m thick and capped by carbonate accumulations up to 5 m thick (Fig. 3-2E). The higher basal unconformity on the south side of the creek prevented thick accumulations of calcium carbonate from

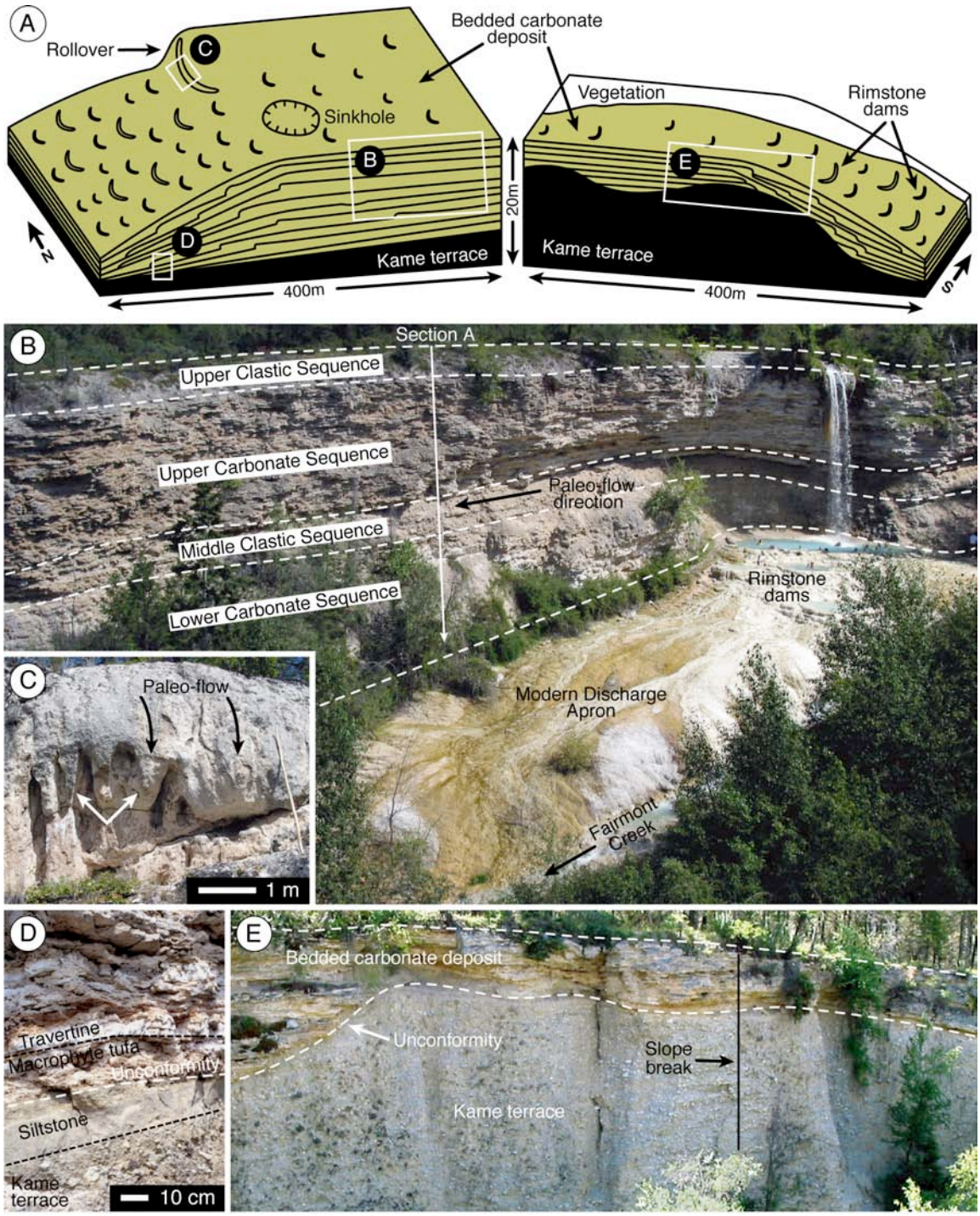

Fig. 3-2 Fairmont deposit overview. A) Block diagram of deposit exposures north (left) and south (right) of Fairmont Creek. B) North side of valley with relict Holocene carbonate deposit extending E-W. Exposure through 16 m thick section with four sequences outlined by white dashed lines. Anthropogenic waterfall at right drains resort swimming pool *ca* 100 m north-east. C) Part of a 100 m long ridge formed of rollover and waterfall structures with stalagtite development (white arrows). D) Lower unconformity (white dashed line) *ca* 100 m down-slope of Section B, which could not be photographed. Basal unit is gravel to cobble conglomerate overlain by glacio-lacustrine silts. Above unconformity macrophyte tufa overlain by feather dendrite travertine. E) South side of valley showing irregular unconformity (white dashed line) between 12 to 15 m of glaciofluvial clastics and 2 to 5 m of overlying bedded carbonate.

forming on the kame terrace. Only a fraction of the deposit is thus present on the south side of the creek. Fairmont Creek is 1 to 4 m wide and several centimetres to 1 m deep, yet the valley width varies from 30 to 50 m and is up to 20 m deep.

Deposit Morphology

The Fairmont deposit is a relict, fan-shaped accumulation of calcium carbonate that may be the largest of its kind in Canada. It extends laterally for *ca* 700 m, extends down-slope for *ca* 700 m (with a 150 m loss in elevation), covers an area of 0.5 km^2 and is at least 16 m thick (Fig. 3-1B). The mound-like deposit at Rabbitkettle Hot Springs in Nahanni National Park, NWT, was reported as the largest carbonate spring deposit in Canada (Wright, 1980; Gulley, 1993), but with a thickness of 18.5 m and a diameter of 79 m, is considerably smaller than the Fairmont deposit.

The west-dipping Fairmont deposit has a discharge apron with well-defined proximal and distal parts. The proximal part formed on the upper flat terrace, whereas the distal part formed on a lower, dipping hillside (Fig. 3-2A). The proximal and distal parts are each 300 to 400 m long. The deposit is thickest proximally, and thins distally. The beds forming the proximal part dip < 10°, whereas the beds forming the distal part dip at 10 to 15°. The change in dip is readily observable in outcrop, and the transition is even visible on the surface as a marked break in slope. Some rollover structures (convex structures formed by a rapid change from sub-horizontal to steeply dipping beds) and rimstone dams have beds that locally dip up to 90°, but the overall tendency is towards shallow (< 15°) dipping beds.

The deposit is well bedded, with individual laminations and beds 1 mm to 10 cm thick. Beds commonly formed over laterally continuous surfaces indicating that entire surfaces were inundated by sheet flow during formation, with little evidence of channeled flow. Shallow, patchy, ephemeral pools and depressions (< 10 cm deep) are common on the proximal part of the apron, but nowhere are there extensive lake-fill deposits like those in the Italian quarries (Chafetz & Folk, 1984; Guo & Riding, 1998) and in the relict Mammoth Hot

Springs deposit (Chafetz & Folk, 1984; Chafetz & Guidry, 2003). On steeper, distal slopes at Fairmont, scattered rimstone dams and/or rollover structures formed in response to elevation loss, but pools or depressions are rare (cf. Ekmekci *et al.*, 1995; Goldenfeld *et al.*, 2006; Jettestuen *et al.*, 2006; Hammer *et al.*, 2007). Although rimstone dams and rollovers are present, extensive step-like terraces with steep-walled rimstone dams like those presently forming at Mammoth Hot Springs and Pamukkale are poorly developed in the Fairmont deposit.

At Fairmont, the vents responsible for most of the paleo-spring water efflux are not exposed. At least some of the paleo-vents existed above the modern vents, as evidenced by relict carbonate extending upslope to a cliff face behind (east of) the deposit.

The Fairmont Creek valley bottom is composed of glaciofluvial and fluvial clastics and contains none of the *in situ* relict deposit. Truncated, flat-lying carbonate beds are exposed on the north and south valley walls. Coupled with the lack of evidence of paleo-vents on the south side of the valley, it is likely that the deposits on the north and south sides of the valley were connected and part of the same continuous strata. The abundance of fluvial siliciclastics interbedded with the carbonate spring deposit indicates that Fairmont Creek was active during peak deposit formation, even though the Fairmont Creek valley did not exist in its present form.

It is impossible to determine if Fairmont Creek always flowed over the actively growing deposit, only flowed over it during high flow events (e.g. floods and snowmelt), or if the deposit formed a bridge over the creek (cf. Bayari, 2002). Regardless of the nature of the past interactions between Fairmont Creek and the spring water, when carbonate deposition ceased, the limestone that once filled the Fairmont Creek valley was eroded away.

Modern Spring Activity

There are three active vents at Fairmont Hot Springs: the Main Vent, Emanation Hill/Indian Baths, and the Wilder House (Fig. 3-1B). At one time

development diverted the creek and tapped the hottest uphill vent as an intake for swimming pool water. Although some of the minor vents are cold springs, most of the spring water is emitted by the Main Vent, which consistently registers temperatures above 36.7°C and is thus considered to be a true hot spring (cf. Pentecost *et al*., 2003).

From historical data, vent temperatures range from 30 to 48.9°C. The lowest temperature measured for this study was 27.8°C from Emanation Hill, and a high of 43.6°C from the Main Vent (Table 3-1). Water chemistry data show little variability during nearly a century of sampling (Table 3-2). The spring water is slightly saturated with respect to calcite (Allen *et al*., 2006, his table 3); however, there is little modern calcite precipitation when compared to the volume of calcite in the relict deposit.

Table 3-1 Fairmont unfiltered spring water properties and stable oxygen isotope compositions.

Sample	Temp. (°C)	pH	EC ($mS \cdot cm^{-1}$)	Salinity	$\delta^{18}O$ VSMOW (‰)	
					#1	#2
Pool Intake	43.6	6.2	2.25	1.0	-18.1	-17.9
Emanation Hill	27.8	7.3	2.48	1.1	-17.8	-17.7
Creek	25.1	8.3	1.55	0.6	-16.9	-16.6

Notes: Creek samples were collected ~ 50 m downstream of where the chlorinated spring water from the pool enters the creek. Grasby et al. 2000 measured a $\delta^{18}O$ VSMOW of –18.8‰. EC = electrical conductivity where S = siemens.

Spring water currently inundates only a small fraction of the surface area covered by the relict deposit (Fig. 3-1B). This is probably due to modern spring water discharge being much lower than during peak deposit formation. Most of the modern calcite precipitation, though limited in extent, occurs on two discharge aprons below the pool drainage pipes, and in Fairmont Creek downstream of the pool drainage (Fig. 3-2B). Discharge from the Emanation Hill and Wilder House

Table 3-2 Fairmont spring water chemistry.

Spring	T (°C)	pH	Ca^{2+}	Mg^{2+}	Na^{+}	K^{+}	HCO_3^{-}	SO_4^{2-}	Cl^{-}	EC
Swimming Bath[1]	38.9		348	84.0	30.1	5.0	574	740	32.5	
Hot Bath[1]	44.4		485	100	37.3	5.5	770	980	43.5	
Emanation Hill[2]	45.7	6.8	484	105	31.2	6.2	709	1009	40.5	2480
Emanation Hill[2]	35.7 - 48.9	7.0	472	112	31.0	5.6	699	990	41.9	2430
Emanation Hill[2]	45.9	6.1	430	113	32.0	5.9	713	984	33.0	2360
Emanation Hill[3]	47.0	6.3	451	107	29.0	5.5	685	929	34.0	2277
Wilder House[2]	31.6	6.8	480	110	31.6	6.8	708	1013	44.0	2530
Wilder House[2]	32.0 - 39.0	6.3	413	115	32.9	6.1	703	896	34.5	2450
Main Vent[2]	34.6 - 42.2	6.8	372	87.6	23.7	4.4	627	774	33.0	2050
Main Vent[2]	41.8	6.8	314	83.0	19.9	3.6	559	628	27.0	1800
Main Vent[2]	31.5 - 38.1	6.1	330	88.0	22.5	4.3	585	682	25.0	1950
Fairmont Creek[2]	4.8	8.3	31.4	17.4	0.6	0.4	165	11.2	0.2	271
Fairmont Creek[2]	8.5	8.3	23.4	14.2	0.8	0.4	134	10.0	<0.1	220

Notes: All pH measurements were taken in the field, and unless stated, all units are in $mg \cdot L^{-1}$, with the exception of pH, which is the negative log of $[H^+]$, and electrical conductivity (EC), which is $\mu S \cdot cm^{-1}$.

[1]Elworthy 1926

[2]van Everdingen 1972

[3]Grasby et al. 2000

vents is so low that the water soaks into the ground within 50 m of the vent. The calcite precipitated around these vents forms small fan-like accumulations of limited thickness.

Large amounts of gas bubble up from the Main Vent, and one analysis claimed 54.16% CO_2, 11.6% O_2 and 34.24% N_2 (Elworthy, 1926). The oxidized nature of the spring water, coupled with a lack of CH_4 and H_2S indicates appreciable atmospheric contact, or mixing of deeply derived waters with surface waters (van Everdingen, 1972). The spring water, with an average $\delta^{18}O$ Vienna Standard Mean Ocean Water (VSMOW) of –18.0‰ (Table 3-1; compared to –18.8‰ as determined by Grasby *et al.*, 2000), is meteoric in origin, but noble gas contents indicate a strong geothermal component (Mazor *et al.*, 1983). Meteoric surface waters were circulated to depths of 0.9 to 2.2 km where they were heated by an elevated geothermal gradient, and then reached the surface by way of brittle, deep-seated faults (Grasby & Hutcheon, 2001; Allen *et al.*, 2006).

Modern Climate

The present climate around Fairmont is semi-arid with strong seasonal temperature fluctuations (Atmospheric Environment Service, 1982a, b). Due to its aspect and location on an elevated terrace, Fairmont Hot Springs receives abundant solar exposure during the hot summers (July mean: 18.6°C, up to 38°C). Winters are generally cold, with a January mean air temperature of -9.4°C, and lows down to -41.7°C. Current climatic conditions at Fairmont, however, are different than the climatic conditions that existed when carbonate spring deposit formation was most active. Given that the deposit did not form under modern climatic conditions, the influence of the present climate on spring deposit formation can only be used as a general guide.

Facies

Three lithologies comprise the Fairmont deposit: 1) travertine, 2) tufa, and 3) conglomerate. Travertine is formed of abiotic feather dendrite, radiating dendrite and intraclast facies, but is not precluded from containing biotic

components, such as microbes, and/or macrophyte moulds. Tufa contains abundant fossils such as those formed in the stromatolite, microbe, bubble, macrophyte, and oncoid facies. The fossils were preserved as moulds with no evidence of replacement or permineralization. Conglomerate is formed of fluvial clastic facies that were deposited by Fairmont Creek.

Feather dendrite facies

This facies forms nearly half of the Fairmont deposit. The three-dimensional feather dendrites, 1 mm to 10 cm long and 1 mm to 5 cm wide, have variable morphologies, but all grew perpendicular to the bedding plane as evenly spaced columns, fanning arrays, or isolated crystals (Fig. 3-3). Smaller dendrites have fewer levels of branching and more tightly packed branches than large dendrites. Branches extend in all directions, but most are aligned parallel to flow. Many dendrites are curved, but lack preference for curving towards or away from the flow direction. Feather dendrites are most abundant on sloping surfaces, rimstone dams, and rollovers. Some beds can be traced continuously for several hundred metres.

Individual branches, 20 to 250 μm wide and up to 5 cm long, are formed mainly of overlapping rhombohedral sub-crystals with multi-stepped faces, and fewer chevron-shaped sub-crystals (Figs. 3-3D to G, J to L). The steps, 1 to 5 μm apart, continue for the entire length of the branch. Adjacent sub-crystals used each other as growth templates and therefore have their *c*-axes aligned parallel to each other and to the branch. Branching is dominantly non-crystallographic, with minor development of crystallographic branches. In thin section, pristine dendrites are composed of clean and clear crystalline calcite, whereas micritized dendrites are brown.

Some of the dendrites contain micritic laminations (20 μm to 2 mm thick, most < 200 μm) that formed parallel to bedding and hence, perpendicular to the dendrites. The laminations are spaced 20 μm to 5 cm apart and contain abundant micro-porosity. Most dendrite crystals are continuous across the micrite laminae. Evidently, the micrite disrupted but did not prevent continued dendrite crystal

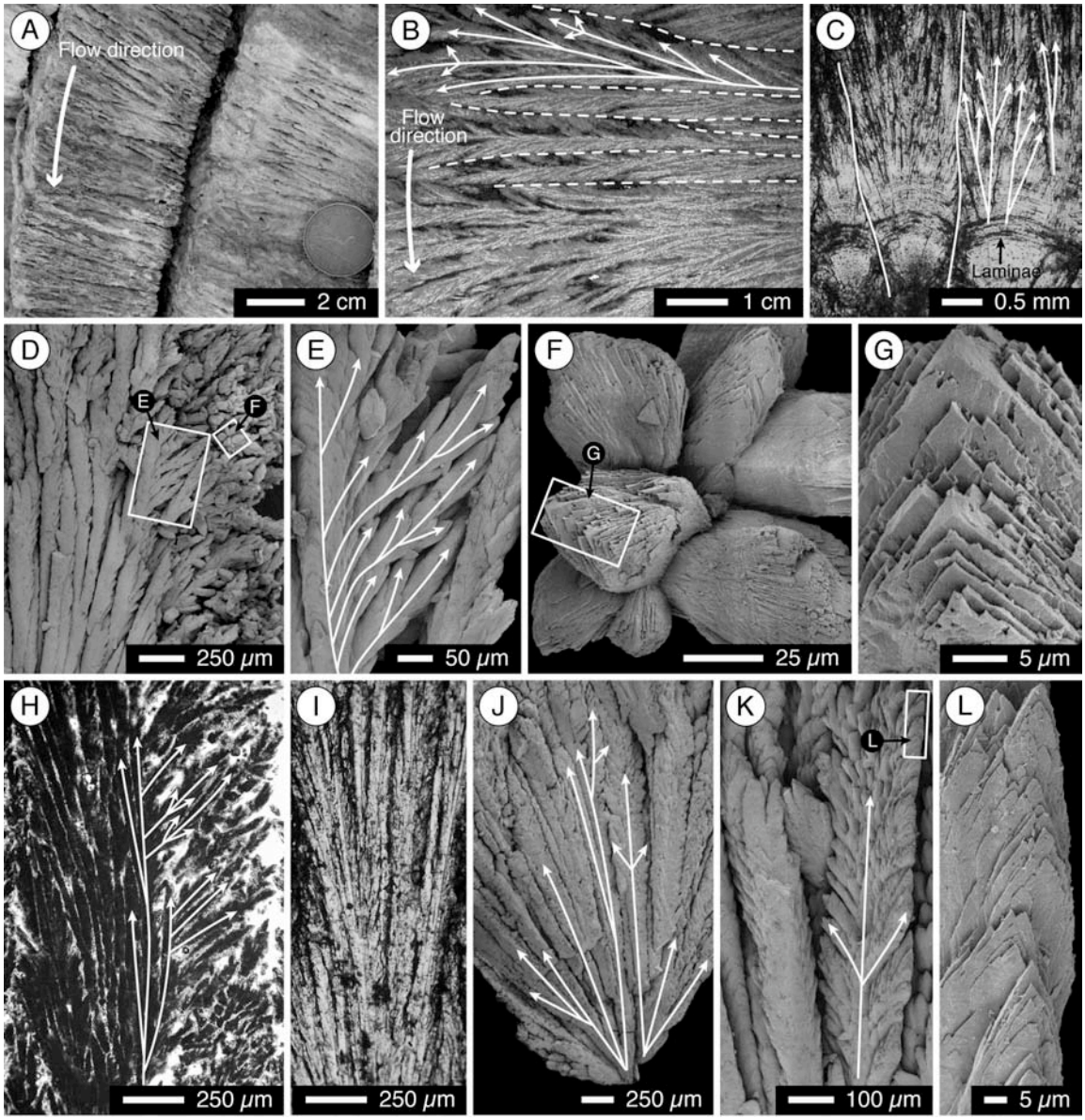

Fig. 3-3 Feather dendrite travertine. (A-B) Photographs; (C, H-I) Thin section photomicrographs; (D-G, J-L) SEM photomicrographs. A) Two distinct dendrite beds on rollover. B) Thin section of feather dendrites from Fig. 3A. Dashed white lines delineate individual crystals. White arrows show branching patterns. C) Tightly packed fanning dendrite crystals. Dark daily growth bands visible near the crystal bases (black arrow) but lacking in the branches. White lines delineate individual crystals. White arrows show branching patterns. D) Tightly packed branches on left. Asymmetrical branching growing into space on right. E) Asymmetrical branching. No branching to the left, whereas branches splay towards right. F) Tips of crystal splays viewed down *c*-axis. G) Dendrite branch terminus formed of overlapping trigonal crystals. H) Altered dendrite crystal. Non-crystallographic branching on left. Crystallographic branching on right. I) Unaltered, tightly packed fanning dendrites. J) Tightly packed fanning array of branches. K) Narrow branch on left. Symmetrical "wheat-sheaf" branch on right made of stacked rhombs. L) Close-up of branch edge showing stacked rhombs.

growth. The laminations probably formed as result of diurnal variations, seasonal variations, and random changes in local flow conditions on the apron in response to channels being blocked by precipitates.

Radiating dendrite facies

The spherical to sub-spherical dendrites, up to 4 mm in diameter, are composed of branching crystalline calcite that radiates from a nucleus (Fig. 3-4). Primary branches are up to 1.5 mm long and 30 to 200 μm wide, with most *ca* 0.5 mm long (Figs. 3-4C,E to G). Crystals forming secondary and tertiary branches are 30 to 50 μm long, and 30 to 50 μm wide. The irregular branching is non-crystallographic. The sub-crystals forming the branches, with their kite-shaped stepped faces, have the appearance of stacked rhombs (Fig. 3-4H). Since formation, many of the crystal edges have been rounded (Fig. 3-4G). As with the feather dendrites, pristine crystals are composed of clean and clear crystalline calcite (Figs. 3-4B,C), whereas micritized dendrites are brown (Fig. 3-4D).

The radiating structure is most clearly visible in spheres that have been broken in half (Figs. 3-4C,F). Under crossed polars, the branches become extinct at 90° intervals, creating a '+' shaped extinction pattern oriented NS-EW. The branches are in optical continuity with each other, as evidenced by sweeping extinction upon rotation of the stage. Efforts to determine the nature of the dendrite nuclei were unsuccessful. Possible agents include colloidal calcium carbonate and bacteria suspended in solution (Rainey & Jones, 2005).

The radiating dendrites are found in laminations (1 to 4 mm thick) or in semi-continuous beds that are < 2 m long and up to 10 cm thick (Fig. 3-4A). The dendrites formed in shallow pools or depressions that were probably < 10 cm deep, and possibly much shallower. Sub-spherical dendrites developed when adjacent crystals grew into each other, causing concaved depressions to form on the outsides of the spheres. Dendrite size remains consistent in individual beds, but varies from one bed to another. Some of the radiating dendrite beds grade into feather dendrites at the lips of rimstone dams and rollovers. Moulds of encrusted

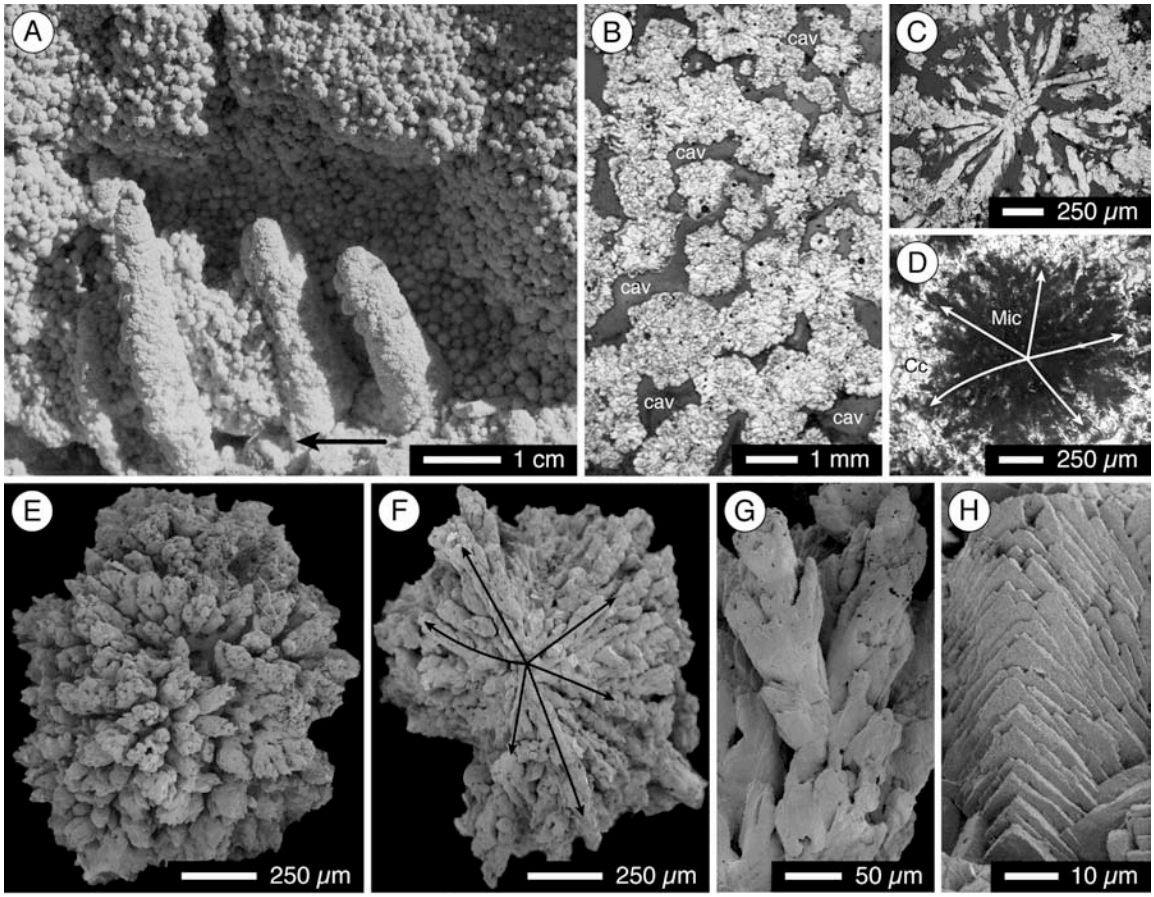

Fig. 3-4 Radiating dendrite travertine. (B-D) Transmitted light photomicrographs. (E-H) SEM photomicrographs. A) Outcrop of pool containing radiating calcite dendrites. Pinnacles are calcite-encrusted plant stems. Arrow points down-slope. B) Crystalline radiating calcite dendrites with cavities (cav). C) Radiating branches of crystalline calcite. Darker regions are pores filled with blue epoxy. D) Dark and clouded dendrite altered to micrite (Mic) then later encased in crystalline calcite (Cc). White arrows highlight radiating fabric. E) Spherical dendrite with radiating branches. F) Cross section through fractured sphere shows solid nucleus and radiating branch structure. G) Smoothed branches. H) Pristine branch with stepped crystal faces formed of stacked calcite rhombs.

grasses, moulds of filamentous microbes, and/or terrigenous clastics are found in some of the radiating dendrite beds.

Stromatolite facies

This facies forms about one third of the Fairmont deposit and is present in accumulations that are up to 2 m thick and laterally continuous for tens of metres. Stromatolite facies formed on horizontal and dipping surfaces, commonly with microbe tufa and bubble tufa.

The stromatolite facies is composed of thin sheets (100 μm to 2 mm) of calcite crystals separated by fenestral cavities that are 1 mm to 5 cm long, and 1 mm to 1 cm thick (Fig. 3-5). The cavities, forming 20 to 70% of the tufa, are moulds of microbial mats that were encrusted by the calcite sheets (Figs. 3-5A,B). The undulatory nature of the calcite sheets makes it difficult to determine the true thickness of individual beds. The calcite sheets formed sub-parallel to each other, and contoured the irregular surfaces of the mats. Most of the sheets are formed of calcite crystals that have their *c*-axis mainly perpendicular to the plane of the sheet (Figs. 3-5C to E,H,I). The bottom of the sheet is formed of flat crystal bases, whereas the top is formed of euhedral rhombohedral crystal terminations. Double-sided sheets (joined back to back) are more common than single sheets. Although rare, some sheets are formed of biterminal calcite crystals that have their *c*-axis mainly parallel to the plane of the sheet, but randomly oriented within that plane (Fig. 3-5F). Most sheets are formed of either gothic arch or trigonal calcite crystals, but each sheet is formed of only one type of crystal. Gothic arch crystals (cf. Folk *et al.*, 1985) with multistepped faces are most common. The crystals, 50 to 100 μm wide, have < 10 steps separated by 5 to 10 μm (Figs. 3-5D,E). Some trigonal calcite crystals (10 to 20 μm long, 5 to 20 μm wide, Fig. 3-5I) form simple points, whereas others are tapered (cf. gutter-edge calcite; Folk *et al.*, 1985). Pitting on some crystals (Fig. 3-5E) suggests that biofilms may have influenced crystal growth (Pedley, 2000; Pedley *et al.*, 2008).

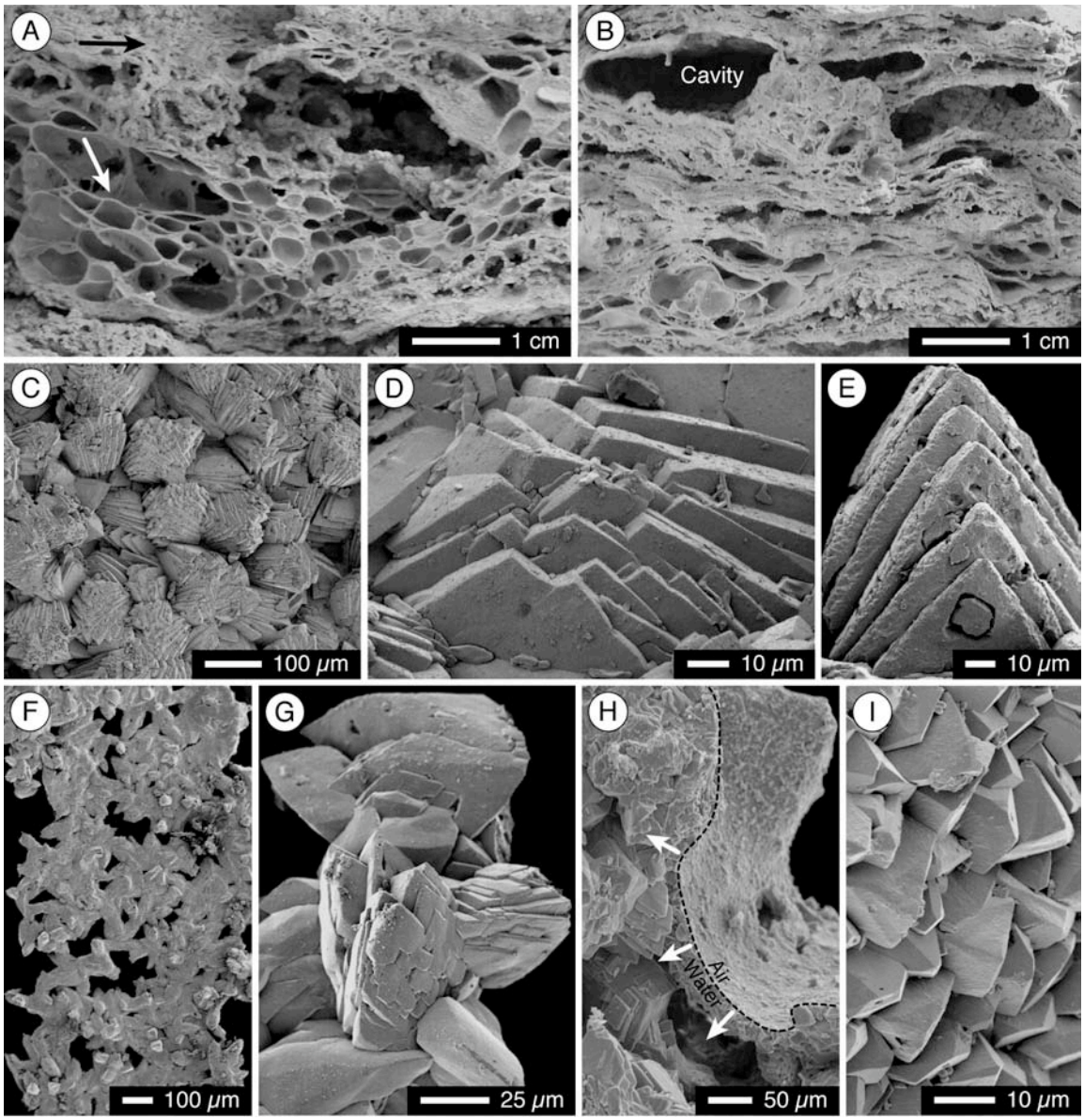

Fig. 3-5 Stromatolite Tufa. (C-I) SEM photomicrographs. A) Porous stromatolite tufa in outcrop overlain by thin bed of dense stromatolite tufa (black arrow). Porous stromatolites are preserved as an open network of interconnected thin calcite sheets (white arrow). B) Outcrop of dense stromatolite tufa with tightly packed calcite sheets. C) Calcite sheet composed of gothic arch calcite crystals oriented normal to plane of sheet. D) Gothic arch crystal. E) Gothic arch crystal with natural etch pits. F) Thin calcite sheet composed of calcite crystal latticework with *c*-axes mainly parallel to plane of sheet. G) Close-up of crystals with random growth directions. H) Calcite precipitation at the air-water interface. Calcite grew perpendicularly (white arrows) away from the interface (black dashed line) into water-filled pore. I) Close-up of trigonal crystals from water side of interface.

Microbe facies

This facies, formed of filamentous microbes encrusted by crystalline calcite, is widely distributed, but not abundant (Figs. 3-6A to F). The calcite coatings, 50 to 150 μm thick, are formed of trigonal, gothic arch, and biterminal calcite crystals that are 20 to 50 μm long (Figs. 3-6A,D,E). Cross sections through encrusted filaments show that they are composed of solid calcite, with the 5 to 10 μm wide filaments or their moulds rarely preserved (Figs. 3-6B to C,F). Microbes that grew as streamer colonies were preserved as sub-parallel wavy bundles. Solitary microbes were preserved as randomly oriented filaments in a mass of calcite crystals (Figs. 3-6A to C). Bacterial shrubs (cf. Folk & Chafetz, 1983; Chafetz & Folk, 1984; Guo & Riding, 1994; Chafetz & Guidry, 1999) are rare in the Fairmont deposit, being present only in the proximal part of the deposit as a single isolated bed < 10 cm thick.

Bubble facies

The bubble facies, widely distributed but not abundant, is formed of spherical, calcite-coated gas bubbles that are 1 to 5 mm in diameter (Fig. 3-6G). The coating is formed of trigonal, gothic arch, and biterminal calcite crystals, similar in size and shape to the crystals in the stromatolite and microbe facies. Bubble facies are poorly bedded and commonly associated with stromatolite and microbe facies.

Macrophyte facies

This facies is formed of the moulds of detrital and *in situ* non-aquatic plants (leaves, tree branches and stumps, grasses, and scattered pine cones) that were coated with crystalline calcite (Figs. 3-6H,I). After encrustation, the organic matter decayed, leaving behind moulds. The plants were encrusted by trigonal, gothic arch, and biterminal calcite crystals, like those in the stromatolite, microbe and bubble facies. The macrophyte facies is most common at the base of the deposit where local vegetation was inundated by spring water and encrusted with calcite. Some small lenses and beds of detrital macrophyte facies (< 10 cm thick) are present throughout the deposit where leaves or trees fell, or were washed onto

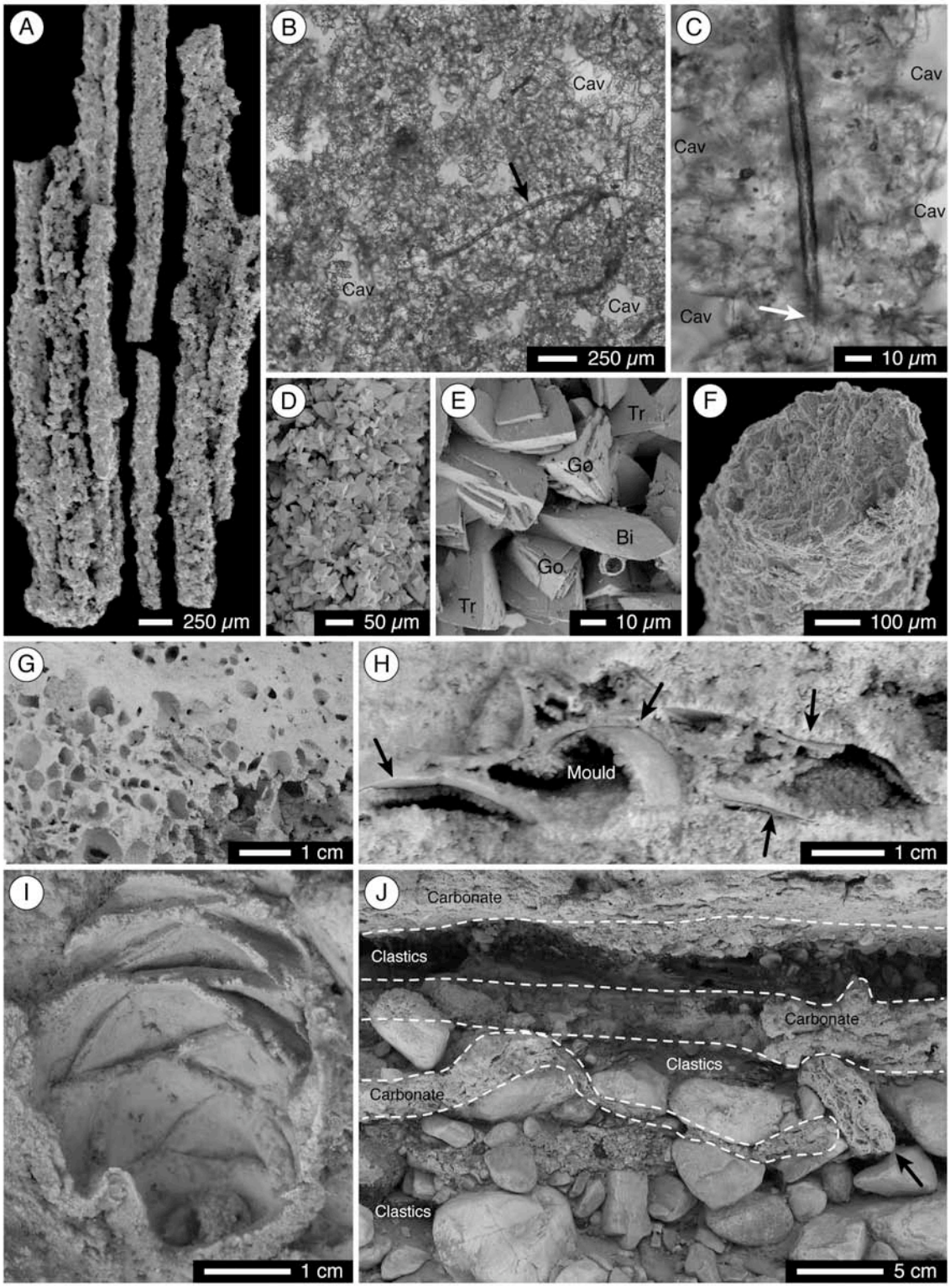
A
250 μm
B
Cav
Cav
Cav
250 μm
C
Cav
Cav
Cav
Cav
10 μm
D
50 μm
E
Tr
Gø
Bi
Go
Tr
10 μm
F
100 μm
G
1 cm
H
Mould
1 cm
I
1 cm
J
Carbonate
Clastics
Carbonate
Clastics
Carbonate
Clastics
5 cm

Fig. 3-6 Microbe tufa, bubble tufa, macrophyte tufa and fluvial clastics. (B,C) Transmitted light photomicrographs. (A,D-F) SEM photomicrographs. A) Calcite encrusted filamentous streamers. B) Homogeneous mass of crystals with few cavities (Cav) and some microbial filaments preserved (black arrow). C) Encrusted microbial filament with cavities (Cav) on either side. Filament only partially preserved. White arrow indicates truncation. D) Surface of calcite encrusted filament. E) Variety of calcite crystal morphologies from surface of encrusted filament. Trigonal (Tr), gothic arch (Go) and bi-terminal (Bi) crystals. F) Fractured end of encrusted filament reveals no evidence of microbe or other organic material. G) Bubble tufa in outcrop. H) Abundant mouldic porosity in macrophyte tufa formed of leaf moulds (black arrows). I) Pine cone mould from macrophyte tufa. J) Carbonate material interbedded with fluvial siliclastics. High energy environment indicated by carbonate intraclast (black arrow).

the bedding surface. Detrital macrophyte accumulations on bedding surfaces commonly developed into rimstone dams, creating spring water pools.

Intraclast facies

The intraclast facies is rare. Angular to sub-angular intraclasts (1 to 10 cm long) form lenses 2 to 10 cm thick and 0.3 to 1.0 m long, and may contain a sandy siliciclastic matrix. Intraclasts formed from beds of travertine or tufa that were brecciated and re-deposited (Fig. 3-6J). The angular and blocky nature of the clasts is due to fracture along bedding planes.

Oncoid facies

This facies, formed of rounded to ellipsoid oncoids (2 to 15 mm diameter) is the least abundant being found only in small catchment pools (< 20 cm wide, < 10 cm deep) in the distal part of the deposit. The nuclei, 0.5 to 3.0 mm in diameter, are hollow or formed of radiating calcite dendrites. The cortices (1 to 10 mm thick) are formed of concentric laminations 5 to 300 μm thick, which are composed of spar and micrite. Cortical development resulted from contemporaneous calcite precipitation and microbial growth, and began when radiating calcite dendrites were washed out of their pools and transported down-slope (Rainey & Jones, 2005).

Fluvial clastic facies

Fluvial siliciclastic sediments, which form 5 to 10% of the deposit, are commonly interbedded with other facies (Fig. 3-6J). The clastics, found in thin lenses, pods, and beds that are < 1 cm to 1 m thick, are poorly sorted. Some beds are dominated by coarse sand with scattered larger grains, whereas other beds

have grain sizes ranging from mud to 1 m long boulders. The clasts are formed largely of quartzite, limestone, and dolostone, with lesser amounts of shale and mudstone. Scattered charcoal fragments are present locally.

Depositional Succession

Two measured sections (A, and B), located on the north side of Fairmont Creek (Figs. 3-1B and 3-2B and 3-7) include five sequences (I-V) that reflect the temporal and spatial development of the spring system. Section A (units A1 to A6), with beds that dip at 0 to 10° to the west, represents the proximal part of the deposit. Section B (units B1 to B5), with beds dipping at 10 to 15° to the west, represents the distal part of the deposit. This succession is formed of the 1) Basal Macrophyte, 2) Lower Carbonate, 3) Middle Clastic, 4) Upper Carbonate, and 5) Upper Clastic Sequences.

1) Basal Macrophyte Sequence

This basal sequence (0.3 to 2.0 m thick), which rests unconformably on a glaciofluvial kame deposit, is only exposed in the Fairmont Creek valley. It is continually exposed along the south valley wall and along the distal part of the deposit on the north valley wall (unit B1). Proximally, this sequence is not exposed on the north valley wall (Fig. 3-7).

The basal macrophyte sequence is formed of interbedded non-aquatic macrophyte tufa and fluvial conglomerate. Detrital leaves, twigs, pine cones, and grasses are the dominant fossil moulds, with fewer *in situ* grasses and tree stump moulds. The fossilized macrophytes are part of the indigenous vegetation that colonized the area following glacial retreat, but before the Fairmont Hot Springs became active during the early Holocene. Once active, spring water flowed down the hillside, drowned the non-aquatic vegetation and encased it in calcite. Recurring hiatuses in calcite precipitation (possibly due to spring inactivity or flow redirection) allowed local vegetation to repeatedly encroach on the deposit before being fossilized when spring activity resumed. Fluvial conglomerate interbedded with the tufa indicates that periodic high flow events led to fluvial conglomerate deposition on the recently formed tufa beds.

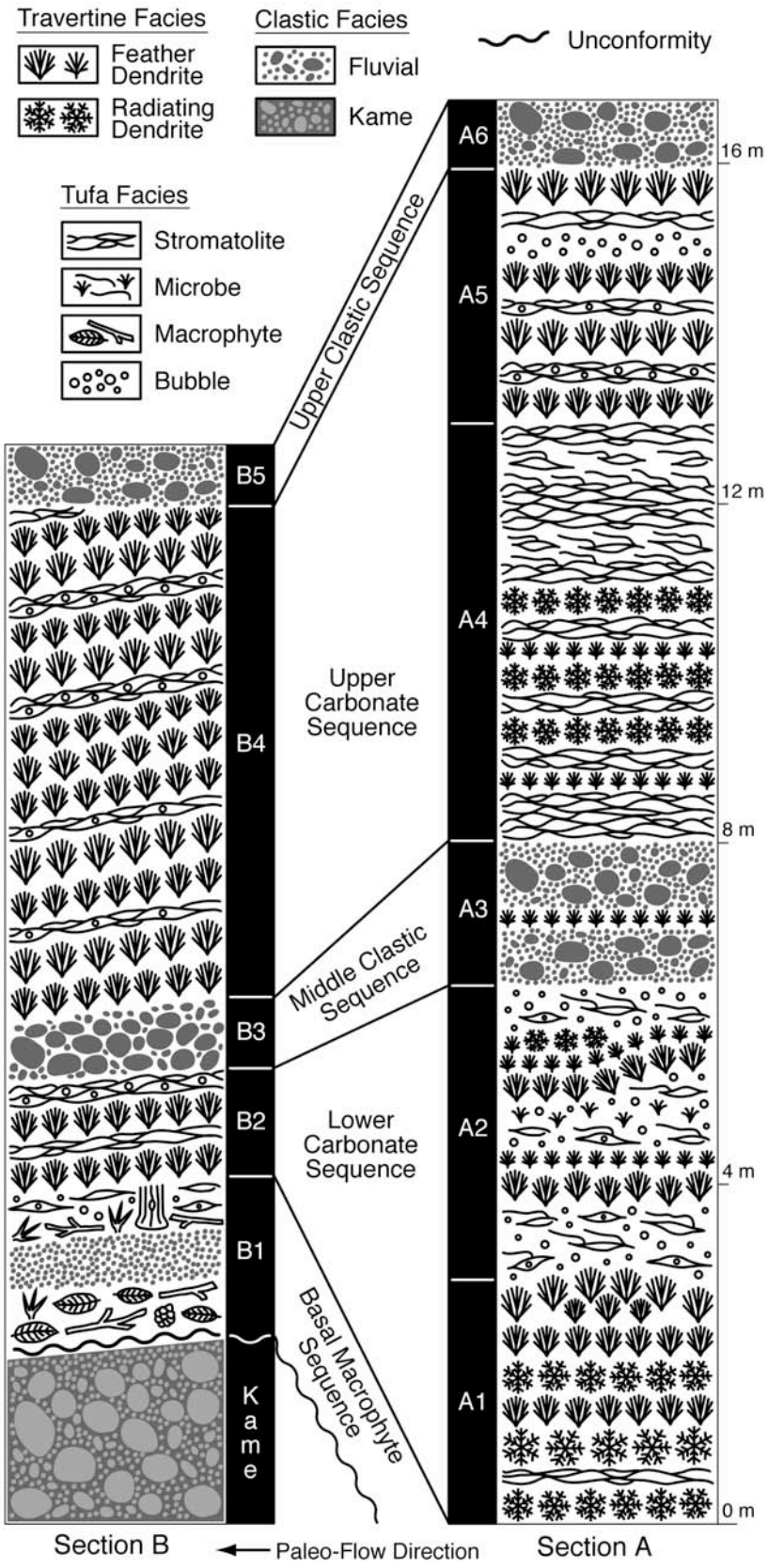

Fig. 3-7 Measured sections A and B from north exposure of Fairmont Creek valley. Sections convey gross morphological changes on a *ca* 0.5 m scale. Individual beds are 1 mm to 10 cm thick, and could not be individually represented on the sections.

2) Lower Carbonate Sequence

Units A1 and A2 are mostly flat lying with a dip of < 10° to the west, whereas unit B2 dips at 10 to 15° to the west. Rare, steeply dipping beds (10 to 90°) form lips of rollovers, mounds and rimstone dams. This sequence is 6 m thick in Section A (Fig. 3-2B), but only 1 m thick in Section B.

The Lower Carbonate Sequence formed with little influence from local vegetation or from Fairmont Creek (Fig. 3-7). Unit A1 is composed largely of abiotic radiating dendrite and feather dendrite travertine, with only minor amounts of stromatolite tufa. Radiating dendrite travertine is most abundant in the lower half of A1, whereas feather dendrite travertine dominates in the upper half. A2 is dominated by stromatolite tufa, bubble tufa, and microbe tufa with some radiating dendrite travertine and finely laminated, poorly developed feather dendrite travertine. B2 is formed of interbedded feather dendrite travertine and stromatolite tufa, with lesser amounts of bubble tufa.

3) Middle Clastic Sequence

This fluvial conglomerate (units A3, B3), 0.75 to 1.75 m thick, separates the Lower and Upper Carbonate Sequences (Figs. 3-2B and 3-7). This sequence is thickest and coarsest in the proximal area where the sediments range from sand-size to boulder-size. The sequence thins distally where it is formed of cobble-size clasts held in a sandy matrix. The sequence includes some thin feather dendrite beds, indicating that it was not the product of a single event.

4) Upper Carbonate Sequence

The Upper Carbonate Sequence (units A4, A5, B6) is 6 to 8 m thick (Figs. 3-2A,B and 3-7). Units A4 and A5 dip at < 10° to the west, whereas the beds in unit B4 dip at 10 to 15° to the west. The steepest beds (15 to 90°) are the lips of rollovers, mounds, and rimstone dams.

Unit A4 (5 m thick) is formed largely of stromatolite tufa with lesser amounts of microbe tufa and radiating dendrite travertine. Some thin beds of feather dendrite travertine are present. Unit A5 (3 m thick) is composed of feather dendrite travertine, stromatolite tufa, and microbe tufa, whereas unit B4 (6 m

thick) is formed mainly of feather dendrite travertine with lesser amounts of stromatolite and bubble tufa. Rimstone dams are more common in B4 than A4 and A5.

5) Upper Clastic Sequence

This sequence (0.5 to 1.0 m thick), which includes units A6 and B5, is capped by a modern soil layer that has been colonized by local vegetation (Fig. 3-2B). This sequence is formed of fluvial conglomerate with grains ranging from sand to boulders (Fig. 3-7). It does not contain any interbedded carbonate, so it is unknown if this unit is an event deposit or if it formed during a time when Fairmont Creek continually flowed over the surface of the deposit.

Stable Isotopes

Calcite forming travertine has $\delta^{18}O$ Vienna Pee Dee Belemnite (VPDB) values from –16.8 to –21.5‰, and $\delta^{13}C$ VPDB values from 1.3 to 5.3‰. Calcite forming tufa has $\delta^{18}O$ VPDB values from –17.5 to –20.5‰, and $\delta^{13}C$ VPDB values from 1.0 to 5.1‰ (Fig. 3-8, Table 3-3). Isotope values do not correlate with specific facies or with distance down-slope.

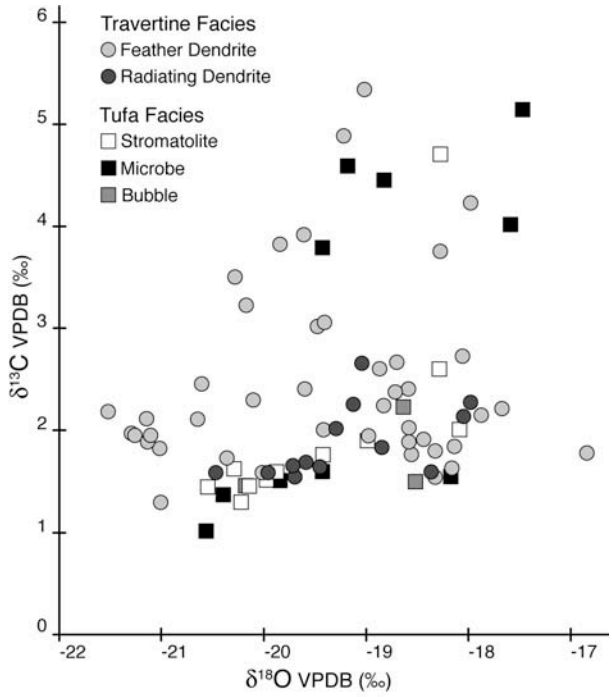

Fig. 3-8 Stable carbon and oxygen isotopes of calcite formed in travertine and tufa facies.

Table 3-3 Calcite stable oxygen and carbon isotopic compositions.

Samples		$\delta^{18}O$ VPDB (‰)			$\delta^{13}C$ VPDB (‰)			Calculated T Values (°C)	
Facies	N	Min	Max	Ave	Min	Max	Ave	Min	Max
Travertine									
Feather Dendrite	43	-21.5	-16.8	-19.4	1.3	5.3	2.5	12.6	35.6
Radiating Dendrite	14	-20.5	-18.0	-19.2	1.5	2.7	1.9	17.8	30.0
Tufa									
Stromatolite	10	-20.5	-18.1	-19.5	1.3	2.6	2.0	18.3	30.4
Microbe	10	-20.5	-17.5	-19.1	1.0	5.1	2.9	15.5	30.5
Bubble	3	-20.2	-18.5	-19.1	1.4	2.2	1.7	20.4	28.5

Notes: Temperatures were calculated using the revised temperature equation of Kim and O'Neil (1997), $1000 \ln \alpha$ (calcite-H_2O) = $18.03 (10^3 T^{-1}) - 32.42$, where α is the fractionation factor and T is in kelvins. The main vent spring water average $\delta^{18}O$ VSMOW of –18.0‰ was used in the calculations.

Deposit Age and Paleoenvironmental Implications

The Fairmont Hot Springs deposit is post-glacial in age. During the last major glaciation, the Rocky Mountain Trench (RMT) was completely covered in ice. The glacier that filled the RMT retreated northwards, exposing Fairmont at the end of the Pleistocene by *ca* 10,500 years ago (Fulton, 1971; Clague, 1982). Within a few thousand years following deglaciation, Fairmont Creek incised the glaciofluvial kame deposit underlying the Fairmont deposit (cf. Clague, 1975). It is unknown if spring water was being emitted while the kame was being incised, or if the springs became active some time later.

Two samples of charcoal embedded in the Lower Carbonate Sequence yielded dates of 7905 +/- 25 ^{14}C years B.P. and 7455 +/- 20 ^{14}C years B.P., which correspond to calendar ages of 8600 to 8780 years B.P. and 8200 to 8340 years B.P., respectively. One sample was embedded in macrophyte tufa whereas the other sample came from a fluvial conglomerate sand lens. Modern sediment transport studies indicated that most coarse sediment generated by a forest fire is delivered to streams by rain and snowmelt within 5 years (Reneau *et al.*, 2007). Nevertheless, the age of *ca* 8800 years B.P. must be considered a maximum age for the deposit because the charcoal may have resided elsewhere prior to being incorporated into the Lower Carbonate Sequence.

The charcoal dates suggest that much of the Fairmont deposit formed 3000 to 4000 years before other spring deposits in western Canada. Carbonate spring deposit formation in Jasper and Banff National Parks was most active *ca* 5000 to 2000 years B.P. (Bonny, 2002; Bonny & Jones, 2003b; Grasby *et al.*, 2003). The Clinton deposit in south-central British Columbia is overlain by the 2440 year-old Bridge River tephra, which provides a minimum age for that deposit (Renaut & Long, 1986; Jones & Renaut, 2008), and the youngest part of the Fall Creek deposit in west-central Alberta formed as recently as 350 years ago (Rainey & Jones, 2007). All of these carbonate deposits formed during the Neoglacial in the latter half of the Holocene. The deposits probably formed in response to cooler and wetter conditions in western Canada as indicated by glacial advances, speleothem growth, vegetation shifts, and sedimentation changes (Porter & Denton, 1967; Luckman & Osborn, 1979; Hennig *et al.*, 1983; Osborn & Luckman, 1988; Luckman, 1993, 2000; Luckman *et al.*, 1993). Increased meteoric precipitation during the Neoglacial allowed greater volumes of water to penetrate the sub-surface, which in turn caused greater spring activity and carbonate deposit formation.

The time of formation of the Fairmont deposit is anomalous because the first half of the Holocene was characterized by relatively warm and dry conditions (Porter & Denton, 1967; Kearney & Luckman, 1983a, b; Ritchie *et al.*, 1983; Luckman & Kearney 1986; MacDonald, 1989; Beaudoin & King, 1990; Luckman

et al., 1993). Reduced meteoric precipitation seems incompatible with the large volumes of spring water that were required for the Fairmont deposit to form. Glacial advances are known to have occurred in western Canada after Late Pleistocene deglaciation (*ca* 12 ka B.P.) and before Mazama ash deposition (*ca* 6.8 ka B.P.), but no definitive evidence for an extended early Holocene cool and moist climatic interval has been found in western Canada (Luckman & Osborn, 1979; Osborn, 1985; Luckman, 1988; Osborn & Luckman, 1988; Luckman *et al.*, 1993). On the eastern slopes of the Rocky Mountains in Alberta, MacDonald (1989) found evidence for a hiatus in aridity between *ca* 9.4 to 8.4 ka B.P., when moist climatic conditions coincided with increased fire activity (possibly due to increased lightning strikes from storms). Increased spring activity could also be related to a 400-year long Northern Hemispheric cold event, which lasted from 8.4 to 8.0 ka B.P. (Alley *et al.*, 1997; Barber *et al.*, 1999; Alley & Ágústsdóttir, 2005). Regardless of exact timing, millenial-scale changes in climate and moisture availability in British Columbia probably controlled stratigraphic development of the Fairmont deposit (cf. Cumming *et al.*, 2002).

The valley through which Fairmont Creek flows truncates all of the sequences in the Fairmont deposit, indicating that deposit formation had ceased before the valley formed. Although the exact time of formation is unknown, the lack of detrital carbonate in the valley and downstream of the deposit indicates that it must have formed some time ago. Today, Fairmont Creek appears too small to have carved the large valley through which it flows. However, the valley may have formed through catastrophic flooding caused by a low frequency high magnitude storm event, from meteoric precipitation events associated with a wetter Neoglacial, or from glacial lakes that were common in western Canadian mountain ranges during the first half of the Holocene (cf. Miller, 1991; Clague & Evans, 2000). Down-cutting of the valley may also have caused significant changes in vent locations and spring flow dynamics, such as the diversion of spring water into the valley instead of over the deposit.

Discussion

The lithological terms tufa and travertine are most functional when used to differentiate limestone spring deposits with fabrics that are controlled by the contained fossils, from those with fabrics that are not. All too often, tufa has been used to describe carbonate spring deposits that formed from cold water, whereas travertine has been used to describe hot water deposits (Pedley, 1990; Ford & Pedley, 1996; Andrews *et al.*, 2000; Torres *et al.*, 2005; Arenas *et al.*, 2007). Temperature classifications are of limited use, however, when studying relict carbonate deposits, or deposits that formed from spring water with temperatures that regularly fluctuated. In the Fairmont Hot Springs deposit, there is little evidence indicating that water temperature exerted any control over facies development and architecture. Rather, it seems that the tufa and travertine formed from the same parent spring water (i.e., same initial spring water chemistry and temperature at point of discharge) as a result of the interactions between hydrodynamics, calcite precipitation rates, and biotic growth rates. The Fairmont deposit is composed of almost equal proportions of tufa and travertine (Figs. 3-9A,B) and their fabrics commonly grade into one another (Fig. 3-10). The precipitated calcite and the fabrics that it formed were probably controlled by supersaturation levels with respect to calcite, biotic activity and ion availability (e.g. flowing or replenishing solutions versus still solutions).

The trigonal, stepped and biterminal crystals found in the stromatolite, microbe, bubble and macrophyte tufa formed from spring water with low to moderate $CaCO_3$ supersaturation, whereas the feather dendrites and radiating dendrites formed from highly supersaturated spring water (cf. Rimstidt, 1997). Biotic activity at Fairmont was thus not responsible for generating the high levels of supersaturation necessary for dendrite formation. Rapid development of calcite dendrites from spring water has been attributed to high supersaturation states generated when CO_2 rapidly degassed from water with elevated pCO_2 (Jones & Renaut, 1995; Jones *et al.*, 2000; Jones *et al.*, 2005; Jones & Renaut, 2008). In the Fairmont deposit, feather dendrites formed mainly on sloping surfaces (10 to 15°) that caused water to flow quickly. Turbulence-induced CO_2 degassing may

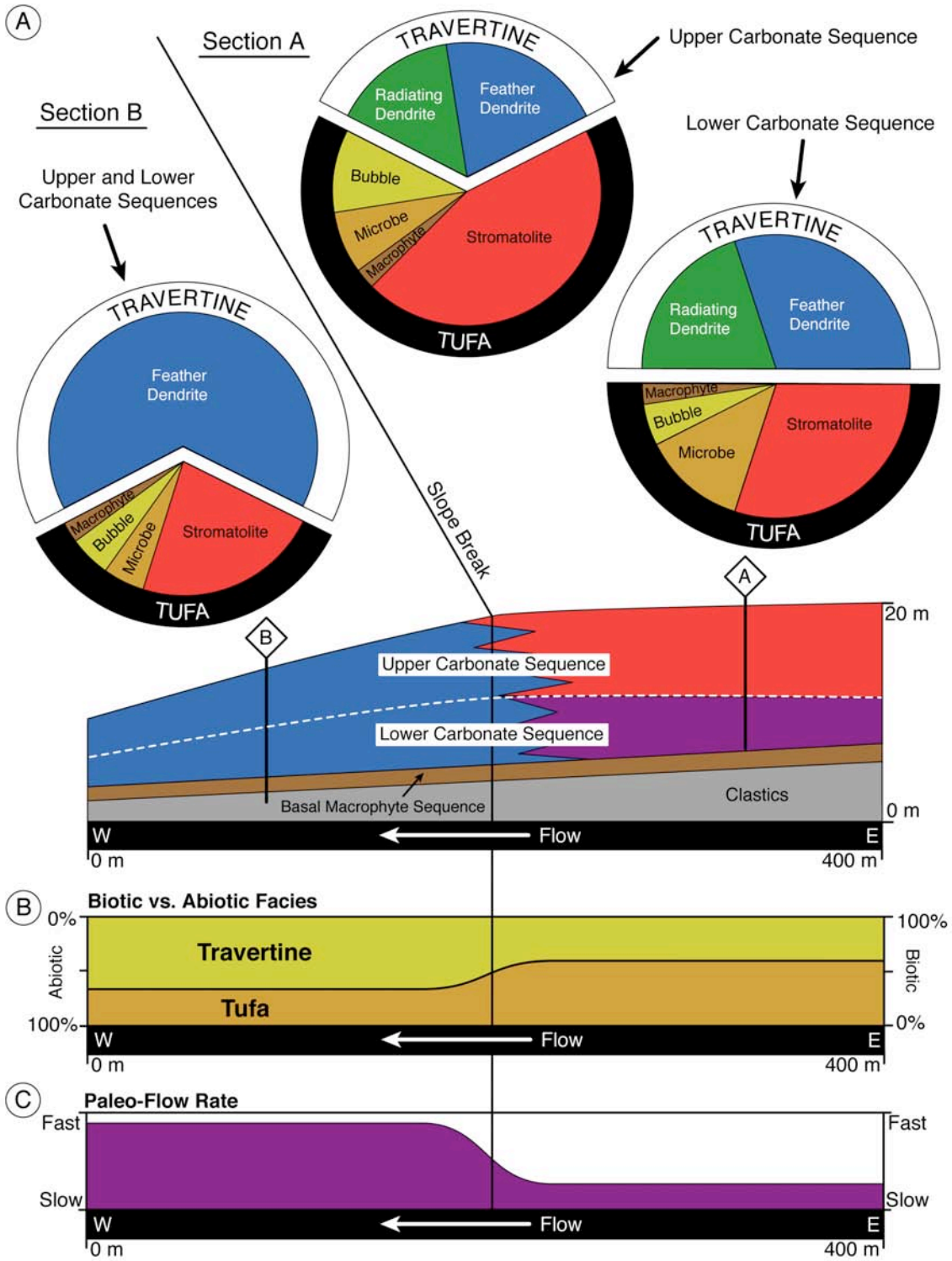

Fig. 3-9 Distribution of biotic and abiotic facies in the main carbonate-bearing sequences forming the Fairmont deposit. A) Pie charts based on measured sections show percentage of tufa and travertine forming Lower and Upper Carbonate Sequences proximally and distally. B) Above slope break, biotic tufa facies more abundant than abiotic travertine facies. Below slope break, travertine more abundant than tufa. C) Interpreted paleo-flow rate. Horizontal to sub-horizontal topography above slope break kept flow rates slow. Sloping topography below slope break increased flow rates.

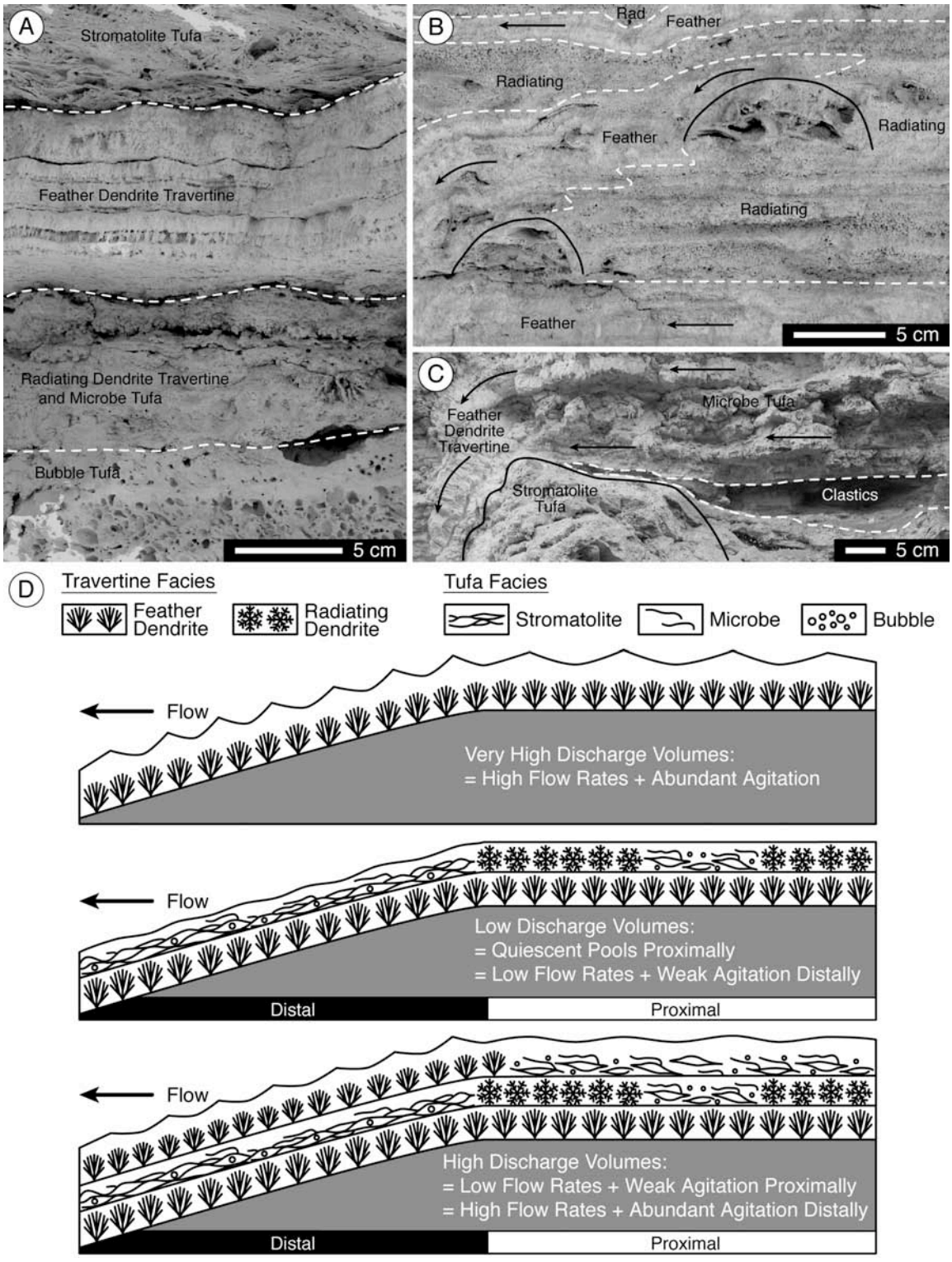
A
Stromatolite Tufa
Feather Dendrite Travertine
Radiating Dendrite Travertine and Microbe Tufa
Bubble Tufa
5 cm
B
Rad
Feather
Radiating
Feather
Radiating
Radiating
Feather
5 cm
C
Feather Dendrite Travertine
Microbe Tufa
Stromatolite Tufa
Clastics
5 cm
D
Travertine Facies
Feather Dendrite
Radiating Dendrite
Tufa Facies
Stromatolite
Microbe
Bubble
Flow
Very High Discharge Volumes:
= High Flow Rates + Abundant Agitation
Flow
Low Discharge Volumes:
= Quiescent Pools Proximally
= Low Flow Rates + Weak Agitation Distally
Distal
Proximal
Flow
High Discharge Volumes:
= Low Flow Rates + Weak Agitation Proximally
= High Flow Rates + Abundant Agitation Distally
Distal
Proximal

Fig. 3-10 Spatial and temporal changes in facies distribution. A) Sharp vertical facies contacts in outcrop. B) Outcrop formed mainly of feather dendrite and radiating dendrite travertine. Beds with unobstructed flow paths (black arrow) formed of feather dendrites. Leaf mounds on bedding surface (black domed lines) obstructed flow and formed shallow pools where radiating dendrites precipitated. C) Rimstone dam (solid black line) formed a pool that filled with coarse fluvial sand (white dashed line). Above clastic bed, microbe tufa formed as spring water slowly flowed through a small rimstone pool (straight black arrows). Feather dendrite travertine developed as the water flowed over the dam (curved black arrows). D) Examples of facies that developed as a result of topography-induced flow rate changes and fluctuations in discharge volumes.

therefore account for the high supersaturation states responsible for rapid feather dendrite growth (cf. Jones & Renaut, 1995; Renaut & Jones, 1997; Jones *et al.*, 2000; Jones & Renaut, 2008). In contrast, radiating dendrites formed on flat-lying surfaces from quiescent spring water and thus, could not have formed as a result of turbulence-induced CO_2 degassing. High supersaturation states could, however, have been generated by rapid evaporation and/or by CO_2 degassing driven by solar heating. In order for solar-induced evaporation and/or CO_2 degassing to have occurred rapidly enough for the dendrites to grow and preclude microbial colonization, a restricted pool environment was required. These pools would have been very shallow (< 5 mm deep, slightly deeper than the largest radiating dendrites) with little to no influx of fresh spring water. A lack of microbial evidence makes it unlikely that photosynthetic CO_2 uptake contributed to supersaturation.

It is difficult to qualify the effects of biota on calcite crystal growth because of the myriad ways in which microbes may affect deposit formation. Photosynthesizers may actively contribute to calcite precipitation by removing CO_2 from solution (cf. Pedley, 1992; Guo *et al.*, 1996), or passively provide surfaces for calcite nucleation (cf. Fouke *et al.*, 2000; Pentecost & Coletta, 2007). Organic compounds in solution can induce precipitation of spherical calcite at lower saturation states than would otherwise be required (Braissant *et al.*, 2003; Bosak & Newman, 2005). Alternatively, microbes colonizing crystal surfaces may reduce the number of sites available for ion adsorption, and disrupt the regular addition of Ca^{2+} and CO_3^{2-} ions onto a growing surface (cf. Hillner *et al.*, 1992).

Stromatolite, microbe and bubble tufa are all spatially related and formed of similar crystal morphologies, suggesting that they all had similar formational conditions. The lack of well-preserved microbes in the Fairmont tufa prevented identification of species that formed mats and filaments, but their general morphology, the oxidized nature of the water, and a lack of H_2S suggest that they were cyanobacteria. If photosynthetic CO_2 removal contributed to tufa formation, the calcite should be enriched in ^{13}C relative to travertine (cf. Guo *et al.*, 1996). Stable carbon isotope results from the Fairmont Hot Springs deposit, however, show no correlations between tufa facies and elevated $\delta^{13}C$ values (Table 3-3, Fig. 3-8). Indeed, the highest $\delta^{13}C$ value (5.3‰) came from the feather dendrite travertine. The similarity in $\delta^{13}C$ averages for all facies indicates that inorganic CO_2 degassing was more important than photosynthetic CO_2 removal for driving calcite precipitation, and that the microbes passively served as substrates upon which calcite precipitated.

Facies in the Fairmont deposit formed under conditions where calcite formation rates were much higher than microbial growth rates (e.g. dendrite travertine), or where microbial growth rates were higher than calcite precipitation rates (e.g. stromatolite tufa). It was the competition between calcite crystal growth rates and biotic growth rates that ultimately determined if a facies was biotic or abiotic. Increased calcite precipitation rates associated with higher supersaturation states (cf. Given & Wilkinson, 1985; Gonzalez *et al.*, 1992) probably accounted for the lack of biotic growth in dendrite facies. Dendrites grew extremely rapidly, which allowed them to outpace biotic growth rates and preclude colonization of crystal surfaces. Environments that were conducive to abiotic dendrite crystal formation may also have been amenable to microbial growth, but slow biotic growth rates probably prevented colonization of the rapidly growing dendrites.

The balance between microbial growth rates and calcite precipitation rates was affected by flow conditions that changed in response to topography and discharge (cf. Pentecost & Viles, 1994). Topographically controlled flow rate changes account for gradational lateral facies transitions, whereby one facies

grades into another as slope angle changes (Figs. 3-10B,C). Vertical facies transitions, however, are very sharp (Fig. 3-10A) suggesting that spring water flow rates varied greatly and fluctuated often in response to factors other than topography, such as flow re-direction on the discharge apron, or changes in the volume of water discharged from the vent. Flow re-direction may account for localized facies changes, but only discharge volume changes could have affected widespread facies development concurrently on the proximal and distal parts of the discharge apron.

Discharge volumes from active western Canadian springs fluctuate daily in response to meteoric precipitation (van Everdingen, 1984), yearly in response to drought conditions (Grasby & Hutcheon, 2001), and seasonally, such as the late summer flow cessation of the Emanation Hill vent at Fairmont. At Fairmont, flow rates were always higher on the steep distal part of the discharge apron than on the flatter proximal part (Fig. 3-9C). Regular and continual fluctuation of spring water discharge volumes, however, controlled the distribution of biotic and abiotic facies across the discharge apron. During periods of elevated spring water discharge, the proximal part of the apron was covered with mildly turbulent, slow flowing sheets of water and continually fed spring water pools ideal for stromatolite, microbe, and bubble tufa formation. Meanwhile, the distal part of the apron was inundated with highly turbulent, fast-flowing water conducive to rapid calcite precipitation and the formation of feather dendrite travertine. Reduced spring water discharge caused the proximal part of the apron to be covered with restricted, shallow depressions conducive to the formation of radiating dendrite travertine, whereas decreased flow volume on the distal part of the apron was amenable to microbial mat growth. Despite the sloping surface, microbial mat growth further retarded spring flow velocities and created an environment with slowly flowing, weakly agitated spring water conducive to stromatolite, microbe and bubble tufa formation. Elevated spring water discharge volumes thus caused biotic facies to form proximally and abiotic facies to form distally, whereas reduced spring water discharge volumes caused abiotic facies to form proximally and biotic facies to form distally (Fig. 3-10D). Consequently,

biota was only capable of growing and influencing depositional fabrics in environments where physicochemical-induced supersaturation did not cause rapid calcite crystal growth.

In comparison to other western Canadian carbonate spring deposits, the Fairmont deposit is unusual with regards to its time of formation and constituent facies. Much of the Fairmont deposit formed in the early to mid Holocene, whereas the other spring deposits in western Canada were known to have formed during the mid to late Holocene (Renaut & Long, 1986; Bonny, 2002; Bonny & Jones, 2003b; Grasby *et al.*, 2003; Rainey & Jones, 2007). It must be noted, however, that known timing of formation of western Canada spring deposits is poorly constrained, largely due to the complete decay of organic matter in older parts of the deposits that has prevented radiocarbon dating of the earliest phases of carbonate spring deposit formation.

Facies-wise, most of the other western Canadian carbonate spring deposits are dominated by macrophyte, bryophyte, and stromatolite tufa, with little evidence for abiotic crystal fabrics (Bonny, 2002; Bonny & Jones, 2003b; Turner & Jones, 2005; Rainey & Jones, 2007). The only exception is the Clinton deposit, which contains abundant dendrite crystals that resemble, but are still morphologically distinct from, the Fairmont feather dendrites (Jones & Renaut, 2008). Specifically, the Clinton dendrites are crystallographic and formed on rimstone dams, whereas the Fairmont dendrites are non-crystallographic and formed on smooth, sloping surfaces.

Fairmont differs from other carbonate spring deposits worldwide in regards to the distribution and types of biotic facies. In Yellowstone and Italian deposits, the formation of travertine proximally and tufa distally has been attributed to cooling of spring water as it flowed away from the vent (Chafetz & Folk, 1984; Ford & Pedley, 1996; Guo & Riding, 1998; Chafetz & Guidry, 2003). This implies that biotic facies should be associated with cooler water, but Fairmont facies lack such a relationship. Calculated Fairmont paleo-spring water temperatures range from 12.6 to 35.6°C, and these minimum and maximum temperatures are from feather dendrite travertine (Table 3-3). Stable oxygen

isotope values for Fairmont calcite do not correlate with specific facies or with distance flowed down-slope, suggesting that temperature did not control facies distribution. Distal tufa formation at other spring sites, in addition to spring water cooling, may have been related to decreased calcite precipitation rates associated with lower CO_2 degassing rates caused by topographic leveling.

Although spring water temperature did not control the distribution of tufa and travertine on the Fairmont discharge apron, it probably had an effect on the types of biota that were capable of growing in the spring water. There is a general paucity of macrophyte and bryophyte tufa in the Lower and Upper Carbonate Sequences, despite the abundance of stromatolite and microbe tufa. Fairmont spring water cooled adequately (down to 12.6°C) to favour macrophyte and bryophyte growth, but the cooler temperatures were probably not maintained for long enough periods of time to promote the growth of mosses and higher plants.

Compared to the other deposits worldwide, one of Fairmont's biggest differences is a lack of extensive paludal environments conducive to bacterial shrub formation. Bacterial shrubs are common in the Mammoth deposit and form up to 90% of some Italian deposits, but are present in only one small isolated bed at Fairmont (Chafetz & Folk, 1984; Folk *et al.*, 1985; Guo & Riding, 1994, 1998; Chafetz & Guidry, 1999, 2003; Fouke *et al.*, 2000; Riding 2000). High water temperatures (*ca* 70°C) at Mammoth and abundant H_2S at Italian sites (Chafetz & Folk, 1984; Folk *et al.*, 1985) favoured bacterial over cyanobacterial growth, and may account for shrub formation. A more likely explanation is that bacterial shrub formation resulted from concurrent microbial growth and calcite precipitation. All of the Fairmont facies formed under conditions where microbial growth rates outpaced calcite precipitation rates, or where calcite precipitation rates outpaced microbial growth rates. These findings from Fairmont highlight the fact that microbial growth rates and calcite crystal growth rates can exert greater control over facies distribution and architecture in carbonate spring deposits than other factors such as water temperature and chemistry.

Calcite precipitation from spring water is not a simple, continuous process, but a series of event deposits that are commonly cyclic in nature. The most easily

recognizable events are those that are diurnal or seasonal in nature, such as daily growth bands, and growth lines caused by yearly hiatuses in calcite deposition (Jones *et al*., 2005; Jones & Renaut, 2008). Distinct and regular seasonal signals were difficult to resolve in the Fairmont deposit, being only occasionally visible in stacked beds of feather dendrite travertine. Strong seasonal temperature fluctuations at Fairmont (Atmospheric Environment Service, 1982a, b) suggest that the semi-cyclic proximal to distal, abiotic-biotic facies reversals at Fairmont probably had some seasonal influence. The lack of distinct yearly indicators in the Fairmont deposit, however, indicates that facies development responded to climatic changes that operated on a decadal, and possibly a centennial scale. The irregular, semi-cyclical nature of the stratigraphic facies ordering at Fairmont highlights the complex interactions involved in the development of carbonate spring deposits, and such interactions have probably manifest themselves at other carbonate-depositing spring systems.

Conclusions

The small size and relative inactivity of the modern spring at Fairmont has rendered it incapable of having produced the large amount of calcite and the varied facies that characterize the relict deposit. Detailed analyses of the calcite in the relict deposit have yielded the following conclusions:

- The relict deposit rapidly aggraded from extensive sheet flow during the early to mid Holocene before incision of the Fairmont Creek valley.
- Biotic facies formed from low to moderately saturated spring water, whereas abiotic facies formed from highly supersaturated solutions.
- Microbes did not contribute to generating elevated supersaturation states, and passively served as substrates upon which calcite precipitated.
- Rapid formation of calcite dendrites from highly supersaturated solutions precluded colonization of calcite crystal surfaces by biota.

- Feather dendrites formed as a result of turbulence-induced CO_2 degassing from flowing water, whereas radiating dendrites formed as a result of solar-induced CO_2 degassing and/or evaporation from quiescent water.
- The balance between biotic growth rates and calcite crystal growth rates was controlled by flow rate. Flow rate changed in response to steeper topography with increased distance from the vents, and to discharge volume fluctuations.
- High discharge volumes caused biotic tufa facies to develop on the flat-lying proximal part of the deposit, wherease abiotic travertine facies developed on the dipping, distal part of the deposit. Low discharge volumes caused a proximal-to-distal reversal between travertine and tufa.
- Spring water temperature did not control the distribution of tufa and travertine across the discharge apron.

References

Alçiçek, H., Varol, B. and **Özkul, M.** (2005) Pisolith formation in self-built channel travertine, Pamukkale, Denizli, Western Turkey. In: *1st International Symposium on Travertine* (Eds M. Özkul, S. Yagiz and B. Jones), pp. 62-69, Denizli, Turkey.

Allen, D.M., Grasby, S.E. and **Voormeij, D.A.** (2006) Determining the circulation depth of thermal springs in the southern Rocky Mountain Trench, south-eastern British Columbia, Canada using geothermometry and borehole temperature logs. *Hydrogeology Journal*, **14**, 159-172.

Allen, E.T. and **Day, A.L.** (1935) *Hot Springs of the Yellowstone National Park*: *Publication No. 466*. Carnegie Institution of Washington, Washington, 525 pp.

Alley, R.B. and **Ágústsdóttir, A.M.** (2005) The 8k event: cause and consequence of a major Holocene abrupt climate change. *Quatern. Sci. Rev.*, **24**, 1123-1149.

Alley, R.B., Mayewski, P.A., Sowers, T., Stuiver, M., Taylor, K.C. and **Clark, P.U.** (1997) Holocene climatic instability: A prominent, widespread even 8200 yr ago. *Geology*, **25**, 483-486.

Altunel, E. and **Hancock, P.L.** (1993) Morphology and structural setting of Quaternary travertines at Pamukkale, Turkey. *Geological Journal*, **28**, 335-346.

Andrews, J.E. and **Brasier, A.T.** (2005) Seasonal records of climatic change in annually laminated tufas: short review and future prospects. *J. Quatern. Sci.*, **20**, 411-421.

Andrews, J.E. and **Riding, R.** (2001) Depositional facies and aqueous-solid geochemistry of travertine-depositing hot springs (Angel Terrace, Mammoth Hot Springs, Yellowstone National Park, U.S.A.) – Discussion. *J. Sed. Res.*, **71**, 496-497.

Andrews, J.E., Pedley, M. and **Dennis, P.F.** (2000) Palaeoenvironmental records in Holocene Spanish tufas: a stable isotope approach in search of reliable climatic archives. *Sedimentology*, **47**, 961-978.

Arenas, C., Cabrera, L. and **Ramos, E.** (2007) Sedimentology of tufa facies and continental microbialites from the Palaeogene of Mallorca Island (Spain). *Sedimentary Geology*, **197**, 1-27.

Atmospheric Environment Service (1982a) Canadian Climate Normals 1951-1980: Volume 3, Precipitation. Environment Canada, Toronto, 602 pp.

Atmospheric Environment Service (1982b) Canadian Climate Normals 1951-1980: Volume 2, Temperature. Environment Canada, Toronto, 306 pp.

Barber, D.C., Dyke, A., Hillaire-Marcel, C., Jennings, A.E., Andrews, J.T., Kerwin, M.W., Bilodeau, G., McNeely, R., Southon, J., Morehead, M.D. and **Gagnon, J.-M.** (1999) Forcing of the cold event of 8,200 years ago by catastrophic drainage of Laurentide lakes. *Nature*, **400**, 344-348.

Bayari, S. (2002) A rare landform: Yerköprü travertine bridges in the Taurids Karst Range, Turkey. *Earth Surf. Proc. Land.*, **27**, 577-590.

Beaudoin, A.B. and **King, R.H.** (1990) Late Quaternary vegetation history of Wilcox Pass, Jasper National Park, Alberta. *Palaeogeogr. Palaeoclimatol. Palaeoecol.*, **80**, 129-144.

Bonny, S. (2002) *Recent and fossil spring deposits at Miette Hot Springs, Jasper National Park, Alberta, Canada*. M.Sc., University of Alberta, Edmonton, 180 pp.

Bonny, S. and **Jones, B.** (2003a) Microbes and mineral precipitation, Miette Hot Springs, Jasper National Park, Alberta, Canada. *Can. J. Earth Sci.*, **40**, 1483-1500.

Bonny, S. and **Jones, B.** (2003b) Relict tufa at Miette Hot Springs, Jasper National Park, Alberta, Canada. *Can. J. Earth Sci.*, **40**, 1459-1481.

Bosak, T. and **Newman, D.K.** (2005) Microbial kinetic controls on calcite morphology in supersaturated solutions. *J. Sed. Res.*, **75**, 190-199.

Braissant, O., Cailleau, G., Dupraz, C. and **Verrecchia, E.P.** (2003) Bacterially induced mineralization of calcium carbonate in terrestrial environments: the role of exopolysaccharides and amino acids. *J. Sed. Res.*, **73**, 485-490.

Chafetz, H.S. and **Folk, R.L.** (1984) Travertines: depositional morphology and the bacterially constructed constituents. *J. Sed. Petrol.*, **54**, 289-316.

Chafetz, H.S. and **Guidry, S.A.** (1999) Bacterial shrubs, crystals shrubs, and ray-crystal shrubs: bacterial vs. abiotic precipitation. *Sed. Geol.*, **126**, 57-74.

Chafetz, H.S. and **Guidry, S.A.** (2003) Deposition and diagenesis of Mammoth Hot Springs travertine, Yellowstone National Park, Wyoming, U.S.A. *Can. J. Earth Sci.*, **40**, 1515-1529.

Clague, J.J. (1975) Late Quaternary sediments and geomorphic history of the southern Rocky Mountain Trench, British Columbia. *Can. J. Earth Sci.*, **12**, 595-605.

Clague, J.J. (1982) Minimum age of deglaciation of upper Elk Valley, British Columbia: Discussion. *Canadian Journal of Earth Sciences*, **19**, 1099-1100.

Clague, J.J. and **Evans, S.G.** (2000) A review of catastrophic drainage of moraine-dammed lakes in British Columbia. *Quatern. Sci. Rev.*, **19**, 1763-1783.

Cumming, B.F., Laird, K.R., Bennett, J.R., Smol, J.P. and Salomon, A.K. (2002) Persistent millennial-scale shifts in moisture regimes in western Canada during the past six millennia. *PNAS*, **99**, 16117-16121.

Das, S. and **Mohanti, M.** (1997) Holocene microbial tufas: Orissa State, India. *Carbonates Evaporites*, **12**, 204-219.

Dawson, G.M. (1886) *Preliminary report on the physical and geological features of that portion of the Rocky Mountains between latitudes 49° and 51°30'*. Report B, Volume 1. Geological Survey of Canada, Montreal, 169 pp.

Ekmekci, M., Gunay, G. and **Simsek, S.** (1995) Morphology of rimstone pools at Pamukkale, western Turkey. *Cave and Karst Science*, **22**, 103-106.

Elworthy, R.T. (1926) *Hot springs in western Canada; their radioactive and chemical properties*. Bulletin 699. Canada Department of Mines, Mines Branch, Investigations of mineral resources and the mining industry, 1925, 33 pp.

Folk, R.L. and **Chafetz, H.S.** (1983) Pisoliths (pisoids) in Quaternary travertines of Tivoli, Italy. In: *Coated Grains* (Ed. T.M. Peryt), pp. 475-487. Springer-Verlag, Berlin Heidelberg.

Folk, R.L., Chafetz, H.S. and **Tiezzi, P.** (1985) Bizarre forms of depositional and diagenetic calcite in hot-spring travertines, central Italy. In: *Carbonate Cements* (Eds N. Schneidermann and P.M. Harris), *SEPM Spec. Publ.,* **36**, 349-369.

Ford, T.D. and **Pedley, H.M.** (1996) A review of tufa and travertine deposits of the world. *Earth-Sci. Rev.*, **41**, 117-175.

Fouke, B.W. (2001) Depositional facies and aqueous-solid geochemistry of travertine-depositing hot springs (Angel Terrace, Mammoth Hot Springs, Yellowstone National Park, U.S.A.) – Reply. *J. Sed. Res.*, **71**, 497-500.

Fouke, B.W., Farmer, J.D., Des Marais, D.J., Prat, L., Sturchio, N.C., Burns, P.C. and **Discipulo, M.K.** (2000) Depositional facies and aqueous-solid geochemistry of travertine-depositing hot springs (Angel Terrace, Mammoth Hot Springs, Yellowstone National Park, U.S.A.). *J. Sed. Res.*, **70**, 565-585.

Fouke, B.W., Bonheyo, G.T., Sanzenbacher, B. and **Frias-Lopez, J.** (2003) Partitioning of bacterial communities between travertine depositional facies at Mammoth Hot Springs, Yellowstone National Park, U.S.A. *Can. J. Earth Sci.*, **40**, 1531-1548.

Fulton, R.J. (1971) Radiocarbon geochronology of southern British Columbia. *Geol. Surv. Can. Pap. 71-37*28.

Given, R.K. and **Wilkinson, B.H.** (1985) Kinetic control of morphology, composition, and mineralogy of abiotic sedimentary carbonates. *J. Sed. Petrol.*, **55**, 109-119.

Goldenfeld, N., Chan, P.Y. and **Veysey, J.** (2006) Dynamics of precipitation pattern formation at geothermal hot springs. *Phys. Rev. Lett.*, **96**, 1-4.

Gonzalez, L.A., Carpenter, S.J. and **Lohmann, K.C.** (1992) Inorganic calcite morphology: roles of fluid chemistry and fluid flow. *J. Sed. Petrol.*, **62**, 382-399.

Grasby, S.E. and **Hutcheon, I.** (2001) Controls on the distribution of thermal springs in the southern Canadian Cordillera. *Can. J. Earth Sci.*, **38**, 427-440.

Grasby, S.E., Hutcheon, I. and **Krouse, H.R.** (2000) The influence of water-rock interaction on the chemistry of thermal springs in western Canada. *Appl. Geochem.*, **15**, 439-454.

Grasby, S.E., van Everdingen, R.O., Bednarski, J. and **Lepitzki, D.A.W.** (2003) Travertine mounds of the Cave and Basin National Historic Site, Banff National Park. *Can. J. Earth Sci.*, **40**, 1501-1513.

Gulley, A.L. (1993) *Rabbitkettle Hotsprings, Nahanni National Park Reserve, Northwest Territories: a hydrogeological study*. M.Sc., Carleton University, Ottawa, 109 pp.

Guo, L. and **Riding, R.E.** (1992) Aragonite laminae in hot water travertine crusts, Rapolano Terme, Italy. *Sedimentology*, **39**, 1067-1079.

Guo, L. and **Riding, R.E.** (1994) Origin and diagenesis of Quaternary travertine shrub fabrics, Rapolano Terme, central Italy. *Sedimentology*, **41**, 499-520.

Guo, L. and **Riding, R.E.** (1998) Hot-spring travertine facies and sequences, Late Pleistocene, Rapolano Terme, Italy. *Sedimentology*, **45**, 163-180.

Guo, L. and **Riding, R.E.** (1999) Rapid facies changes in Holocene fissure ridge hot spring travertines, Rapolano Terme, Italy. *Sedimentology*, **46**, 1145-1158.

Guo, L., Andrews, J., Riding, R., Dennis, P. and **Dresser, Q.** (1996) Possible microbial effects on stable carbon isotopes in hot-spring travertines. *J. Sed. Res.*, **66**, 468-473.

Hammer, Ø., Dysthe, D.K. and **Jamtveit, B.** (2007) The dynamics of travetine dams. *Earth Planet. Sci. Lett.*, **256**, 258-263.

Hennig, G.J., Grun, R. and **Brunnacker, K.** (1983) Speleothems, travertines, and paleoclimates. *Quatern. Res.*, **20**, 1-29.

Hillner, P.E., Gratz, A.J., Manne, S. and **Hansma, P.K.** (1992) Atomic-scale imaging of calcite growth and dissolution in real time. *Geology*, **20**, 359-362.

Irion, G. and **Müller, G.** (1968) Mineralogy, petrology and chemical composition of some calcareous tufa from the Schwäbische Alb, Germany. In: *Recent Developments in Carbonate Sedimentology in Central Europe* (Eds G. Müller and G.M. Friedman), pp. 157-171. Springer Verlag, New York.

Janssen, A., Swennen, R., Podoor, N. and **Keppens, E.** (1999) Biological and diagenetic influence in recent and fossil tufa deposits from Belgium. *Sed. Geol.*, **126**, 75-95.

Jettestuen, E., Jamtveit, B., Podladchikov, Y.Y., deVilliers, S., Amundsen, H.E.F. and **Meakin, P.** (2006) Growth and characterization of complex mineral surfaces. *Earth Planet. Sci. Lett.*, **249**, 108-118.

Jones, B. and **Kahle, C.F.** (1986) Dendritic calcite crystals formed by calcification of algal filaments in a vadose environment. *J. Sed. Petrol.*, **56**, 217-227.

Jones, B. and **Kahle, C.F.** (1993) Morphology, relationship, and origin of fiber and dendrite calcite crystals. *J. Sed. Petrol.*, **63**, 1018-1031.

Jones, B. and **Renaut, R.W.** (1995) Noncrystallographic calcite dendrites from hot-spring deposits at Lake Bogoria, Kenya. *J. Sed. Res.*, **A65**, 154-169.

Jones, B. and **Renaut, R.W.** (2008) Cyclic development of large, complex, calcite dendrite crystals in the Clinton travertine, Interior British Columbia, Canada. *Sed. Geol.*, **203**, 17-35.

Jones, B., Renaut, R.W. and **Rosen, M.R.** (2000) Trigonal dendritic calcite crystals forming from hot spring waters at Waikite, North Island, New Zealand. *J. Sed. Res.*, **70**, 586-603.

Jones, B., Renaut, R.W., Owen, R.B. and **Torfason, H.** (2005) Growth patterns and implications of complex dendrites in calcite travertines from Lysuhóll, Snæfellsnes, Iceland. *Sedimentology*, **52**, 1277-1301.

Julia, R. (1983) Travertines. In: *Carbonate Depositional Environments* (Eds P.A. Scholle, D.G. Bebout and C.H. Moore), pp. 64-72. American Association of Petroleum Geologists, Tulsa.

Kearney, M.S. and **Luckman, B.H.** (1983a) Holocene timberline fluctuations in Jasper National Park, Alberta. *Science*, **221**, 261-263.

Kearney, M.S. and **Luckman, B.H.** (1983b) Postglacial vegetational history of Tonquin Pass, British Columbia. *Can. J. Earth Sci.*, **20**, 776-786.

Keith, H.D. and **Padden, F.J.** (1964) Spherulitic crystallization from the melt, I: Fractionation and impurity segregation and their influence on crystalline morphology. *Journal of Applied Physics*, **35**, 1270-1285.

Kim, S.-T. and **O'Neil, J.R.** (1997) Equilibrium and nonequilibrium oxygen isotope effects in synthetic carbonates. *Geochim. Cosmochim. Acta*, **61**, 3461-3475.

Koban, C.G. and **Schweigert, G.** (1993) Microbial origin of travertine fabrics -- two examples from southern Germany (Pleistocene Stuttgart travertines and Miocene Riedöschingen travertine). *Facies*, **29**, 251-264.

Luckman, B.H. (1988) 8000 year old wood from the Athabasca Glacier, Alberta. *Can. J. Earth Sci.*, **25**, 148-151.

Luckman, B.H. (1993) Glacier fluctuation and tree-ring records for the last millennium in the Canadian Rockies. *Quatern. Sci. Rev.*, **12**, 441-450.

Luckman, B.H. (2000) The Little Ice Age in the Canadian Rockies. *Geomorphology*, **32**, 357-384.

Luckman, B.H. and **Kearney, M.S.** (1986) Reconstruction of Holocene changes in alpine vegetation and climate in the Maligne Range, Jasper National Park, Alberta. *Quatern. Res.*, **26**, 244-261.

Luckman, B.H. and **Osborn, G.D.** (1979) Holocene glacier fluctuations in the middle Canadian Rocky Mountains. *Quatern. Res.*, **11**, 52-77.

Luckman, B.H., Holdsworth, G. and **Osborn, G.D.** (1993) Neoglacial glacier fluctuations in the Canadian Rockies. *Quatern. Res.*, **39**, 144-153.

MacDonald, G.M. (1989) Postglacial palaeoecology of the subalpine forest - grassland ecotone of southwestern Alberta: new insights on vegetation and climate change in the Canadian Rocky Mountains and adjacent foothills. *Palaeogeogr. Palaeoclimatol. Palaeoecol.*, **73**, 155-173.

Mazor, E., van Everdingen, R.O. and **Krouse, H.R.** (1983) Noble-gas evidence for geothermal activity in a karstic terrain: Rocky Mountains, Canada. *Geochim. Cosmochim. Acta*, **47**, 1111-1115.

McCrea, J.M. (1950) On the isotope chemistry of carbonates and paleotemperature scale. *J. Chem. Phys.*, **18**, 849-857.

Miller, L.A. (1991) *A paleogeographic reconstruction of glacial lakes Elk and Wigwam, southeastern British Columbia*. M.Sc., University of Calgary, Calgary, 128 pp.

Osborn, G.D. (1985) Holocene tephrostratigraphy and glacial fluctuations in Waterton Lakes and Glacier national parks, Alberta and Montana. *Can. J. Earth Sci.*, **22**, 1093-1101.

Osborn, G.D. and **Luckman, B.H.** (1988) Holocene glacier fluctuations in the Canadian Cordillera (Alberta and British Columbia). *Quatern. Sci. Rev.*, **7**, 115-128.

Özkul, M., Varol, B. and **Alçiçek, M.C.** (2002) Depositional environments and petrography of Denizli travertines. *Bull. Mineral Res. Explor. Inst. Turk.*, **125**, 13-29.

Pedley, H.M. (1987) The Flandrian (Quaternary) Caerwys tufa, North Wales: an ancient barrage tufa deposit. *Proc. Yorks. Geol. Soc.*, **46**, 141-152.

Pedley, H.M. (1990) Classification and environmental models of cool freshwater tufas. *Sed. Geol.*, **68**, 143-154.

Pedley, H.M. (1992) Freshwater (phytoherm) reefs: the role of biofilms and their bearing on marine reef cementation. *Sed. Geol.*, **79**, 255-274.

Pedley, H.M. (2000) Ambient temperature freshwater microbial tufas. In: *Microbial Sediments* (Eds R.E. Riding and S.M. Awramik), pp. 179-186. Springer-Verlag, Berlin.

Pedley, M., Rogerson, M. and **Middleton, R.** (2008) Freshwater calcite precipitates from *in vitro* mesocosm flume experiments: a case for biomediation of tufas. *Sedimentology*. doi: 10.1111/j.1365-3091.2008.00983.x.

Pentecost, A. (1981) The tufa deposits of the Malham District, North Yorkshire. *Field Stud.*, **5**, 365-387.

Pentecost, A. (1985) Association of cyanobacteria with tufa deposits: identity, enumeration, and nature of the sheath material revealed by histochemistry. *Geomicrobiol J.*, **4**, 285-298.

Pentecost, A. (1987) Some observations on the growth rates of mosses associated with tufa and the interpretation of some postglacial bryoliths. *Journal of Bryology*, **14**, 543-550.

Pentecost, A. (1990) The formation of travertine shrubs: Mammoth Hot Springs, Wyoming. *Geol. Mag.*, **127**, 159-168.

Pentecost, A. (1993) British travertines: a review. *Proc. Geol. Assoc.*, **104**, 23-39.

Pentecost, A. (1994) Formation of laminate travertines at Bagno Vignone, Italy. *Geomicrobiol J.*, **12**, 239-251.

Pentecost, A. (1995a) The Quaternary travertine deposits of Europe and Asia Minor. *Quatern. Sci. Rev.*, **14**, 1005-1028.

Pentecost, A. (1995b) Geochemistry of carbon dioxide in six travertine-depositing waters of Italy. *J. Hydrol.*, **167**, 263-278.

Pentecost, A. (2005) *Travertine*. Springer-Verlag, Berlin, 445 pp.

Pentecost, A. and **Coletta, P.** (2007) The role of photosynthesis and CO_2 evasion in travertine formation: a quantitative investigation at an important travertine-depositing hot spring, Le Zitelle, Italy. *J. Geol. Soc. London*, **164**, 843-853.

Pentecost, A. and **Viles, H.** (1994) A review and reassessment of travertine classification. *Géog. Phys. Quatern.*, **48**, 305-314.

Pentecost, A., Thorpe, P., Harkness, D. and **Lord, T.** (1990) Some radiocarbon-dates for tufas of the Craven District of Yorkshire. *Radiocarbon*, **32**, 93-97.

Pentecost, A., Bayari, S. and **Yesertener, C.** (1997) Phototrophic microorganisms of the Pamukkale travertine, Turkey: their distribution and influence on travertine deposition. *Geomicrobiol J.*, **14**, 269-283.

Pentecost, A., Jones, B. and **Renaut, R.W.** (2003) What is a hot spring? *Can. J. Earth Sci.*, **40**, 1443-1446.

Porter, S.C. and **Denton, G.H.** (1967) Chronology of the Neoglaciation in the North American Cordillera. *Am. J. Sci.*, **265**, 177-210.

Rainey, D.K. and **Jones, B.** (2005) Radiating calcite dendrites -- precursors for coated grain formation in the Fairmont Hot Springs Travertine, Canada. In: *Proceedings of 1st International Symposium on Travertine* (Eds M. Özkul, S. Yagiz and B. Jones), pp. 25-32, Denizli, Turkey.

Rainey, D.K. and **Jones, B.** (2007) Rapid cold water formation and recrystallization of relict bryophyte tufa at the Fall Creek cold springs, Alberta, Canada. *Can. J. Earth Sci.*, **44**, 889-909.

Rands, D.G., Davis, J.S., Broadway, S.K. and **Keller, B.J.** (1995) Chemical processes in tufa formation. *Florida Scientist*, **58**, 366-372.

Reimer, P., Baillie, M., Bard, E., Bayliss, A., Beck, J., Bertrand, C., Blackwell, P., Buck, C., Burr, G., Cutler, K., Damon, P., Edwards, R., Fairbanks, R., Friedrich, M., Guilderson, T., Hughen, K., Southon, J., Stuiver, M., Talamo, S., Taylor, F., van der Plicht, J. and **Weyhenmeyer, C.** (2004) IntCal04 Terrestrial radiocarbon age calibration, 26-0 ka BP. *Radiocarbon*, **46**, 1029-1058.

Renaut, R.W. and **Jones, B.** (1997) Controls on aragonite and calcite precipitation in hot spring travertines at Chemurkeu, Lake Bogoria, Kenya. *Can. J. Earth Sci.*, **34**, 801-818.

Renaut, R.W. and **Jones, B.** (2000) Microbial precipitates around continental hot springs and geysers. In: *Microbial Sediments* (Eds R.E. Riding and S.M. Awramik), pp. 187-195. Springer-Verlag, Berlin.

Renaut, R.W. and **Long, P.R.** (1986) Post-glacial travertine deposits of the Clinton area, interior British Columbia. In: *GAC, MAC, CGU Joint Annual Meeting Program With Abstracts*, **11**, pp. 117. Carleton University, Ottawa, Canada.

Reneau, S.L., Katzman, D., Kuyumjian, G.A., Lavine, A. and **Malmon, D.V.** (2007) Sediment delivery after a wildfire. *Geology*, **35**, 151-154.

Riding, R. (2000) Microbial carbonates: the geological record of calcified bacterial-algal mats and biofilms. *Sedimentology*, **47**, 179-214.

Rimstidt, D.J. (1997) Gangue mineral transport and deposition. In: *Geochemistry of hydrothermal ore deposits* (Ed. H.L. Barnes), 3rd edn, pp. 488-515. John Wiley & Sons, New York.

Ritchie, J.C., Cwynar, L.C. and **Spear, R.W.** (1983) Evidence from north-west Canada for an early Holocene Milankovitch thermal maximum. *Nature*, **305**, 126-128.

Strickland-Constable, R.F. (1968) *Kinetics and mechanism of crystallization from the fluid phase and of the condensation and evaporation of liquids*. Academic Press, London, 347 pp.

Stuiver, M. and **Reimer, P.** (1993) Extended ^{14}C database and revised CALIB radiocarbon calibration program. *Radiocarbon*, **35**, 215-230.

Torres, T., Ortiz, J.E., García de la Morena, M.A., Llamas, F.J. and **Goodfriend, G.** (2005) Ostracode-based aminostratigraphy and aminochronology of a tufa system in central Spain. *Quaternary International*, **135**, 21-33.

Turner, E.C. and **Jones, B.** (2005) Microscopic calcite dendrites in cold-water tufa; implications for nucleation of micrite and cement. *Sedimentology*, **52**, 1043-1066.

van Everdingen, R.O. (1972) *Thermal and mineral springs in the southern Rocky Mountains of Canada.* Water Management Service, Department of the Environment, Environment Canada, 151 pp.

van Everdingen, R.O. (1984) Dirty-water events at Rocky Mountain hot springs and their correlation with other short-lived phenomena. *Can. J. Earth Sci.*, **21**, 997-1007.

Viles, H.A. and **Goudie, A.S.** (1990) Tufas, travertines and allied carbonate deposits. *Prog. Phys. Geogr.*, **14**, 19-41.

Weed, W.H. (1888) *Formation of travertine and siliceous sinter by the vegetation of hot springs.* United States Geological Survey Annual Report, **9**, pp. 613-676.

Wright, D.J. (1980) *The physical geography of the Rabbitkettle Hot Springs, Nahanni National Park, N.W.T.* M.Sc., University of Alberta, Edmonton, 164 pp.

Chapter 4

Radiating calcite dendrites – precursors for coated grain formation in the Fairmont Hot Springs carbonate deposit[1]

Introduction

Spherical grains are common components of carbonate spring deposits, including the relict Holocene deposit at Fairmont Hot Springs, British Columbia (Fig. 4-1). The morphology and internal structure of spherical grains from Fairmont are similar in appearance to spherical grains from Italian and American deposits (e.g. Chafetz and Meredith 1983; Folk and Chafetz 1983; Chafetz and Guidry 2003). The two most common spherical grain morphologies are those with 1) radiating crystal structures, and 2) concentric laminations. Radial structures have been attributed to calcite precipitation around bacteria (cf. Chafetz and Meredith 1983; Folk and Chafetz 1983; Chafetz and Guidry 2003), whereas the development of laminations has been attributed to inorganic calcite precipitation in agitated water (cf. Folk and Chafetz 1983). In contrast, this study shows that spherical grains from the Fairmont Hot Springs deposit are composed of radiating crystals that developed abiotically, and biologically mediated concentric laminations.

Radial and laminated spherical grains have been found together in other deposits, but those from the Fairmont deposit are the first to reveal a genetic relationship. Coated grains develop when a cortex forms around a nucleus. Nuclei from other deposits are composed of intraclasts (e.g. Chafetz and Meredith 1983), bacterial sediment (e.g. Folk and Chafetz 1983), and even gas bubbles (e.g. Eckel 1939). The Fairmont coated grains, however, have nuclei formed of radiating calcite dendrites and cortices formed of micrite laminae and crystalline calcite. The micrite was produced microbially, implying that the coated grains are oncoids. It is probable that radiating calcite dendrites are important components of other hot spring travertines, but poor preservation could have prevented

[1] A version of this chapter has been published. Rainey, D.K., Jones, B., 2005. Radiating calcite dendrites – precursors for coated grain formation in the Fairmont Hot Springs Travertine, Canada. In: M. Özkul, S. Yagiz and B. Jones (Editors), Proceedings of1st International Symposium on Travertine, Denizli, Turkey, pp. 25-32.

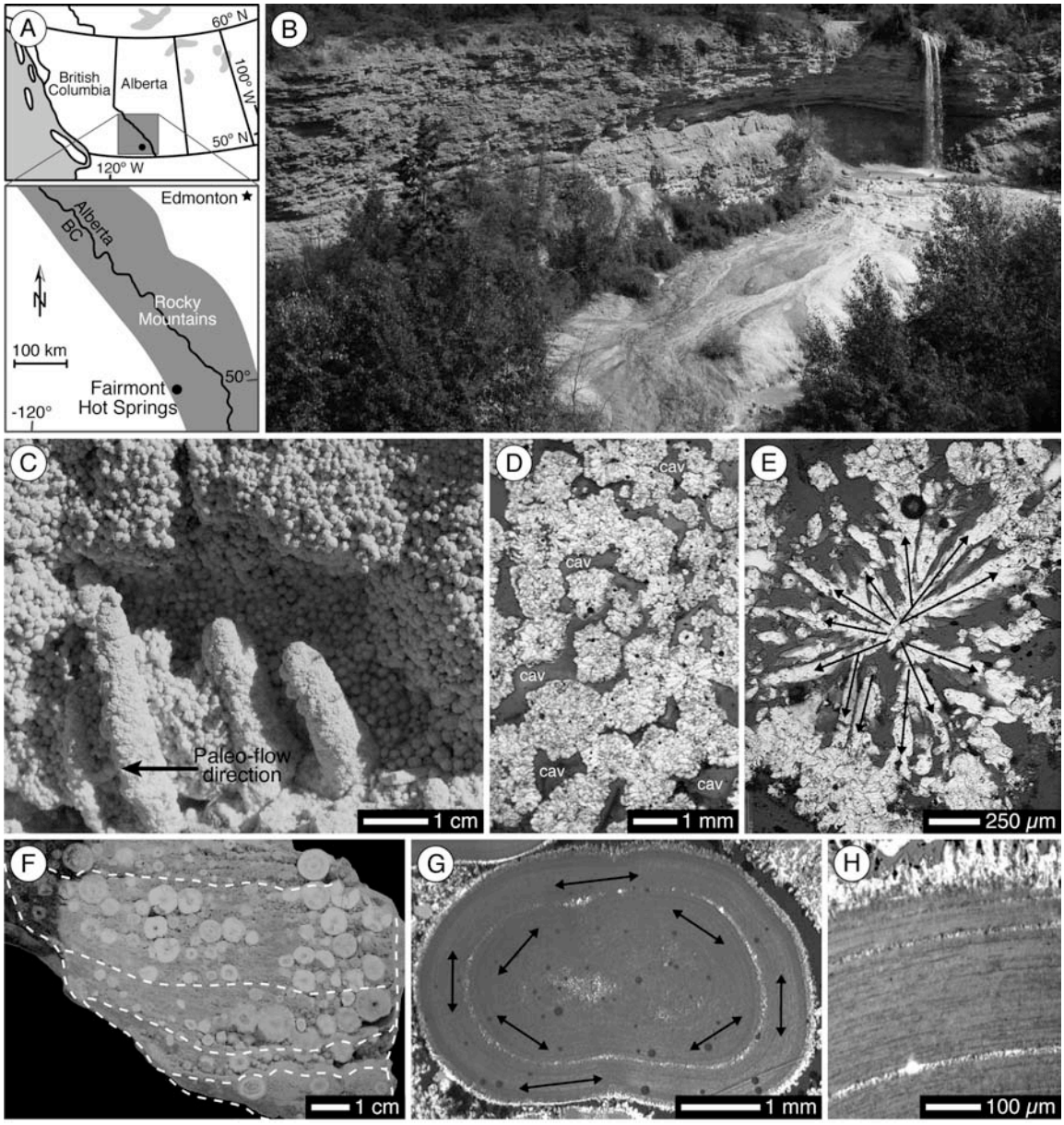

Fig. 4-1 Radiating calcite dendrites and coated grains from the relict Fairmont Hot Springs carbonate deposit. (B-C, F) Photographs; (D-E, G-H) Thin section photomicrographs. A) Fairmont Hot Springs is in southeast British Columbia at the western margin of the Rocky Mountains. B) Thickest exposure through the flat-lying proximal part of the relict deposit where most of the radiating dendrites formed. C) Thick accumulation of radiating calcite dendrites in down-slope pool. Upright structures are calcite-encrusted grass stems. D) Clean and clear crystalline radiating calcite dendrites separated by small cavities ("cav"). E) Close-up of dendrite with black arrows highlighting radial arrangement of branches. F) Cut sample of a rimstone pool filled with oncoids and radiating dendrites. Pool outline and some bedding demarcated by white dashed lines. G) Ellipsoid oncoid dominated by concentric micritic laminations. Black arrows highlight tangential fabric. A single crystalline lamination present in middle of cortex and covering outer surface of oncoid. H) Close-up of finely laminated micritic cortex.

their identification. This paper elucidates the genetic relationship between the radiating calcite dendrites and the oncoids, outlines their formation mechanisms, and provides new insight into the role of biotic and abiotic processes on the formation of spherical grains.

Geological Setting

Fairmont Hot Springs is located in the Rocky Mountain Trench in southeastern British Columbia, at the western limit of the Rocky Mountains (Fig. 4-1A). The spring water emerges at an average temperature of 44°C from the Cambrian Jubilee Formation along the intersection of two merging thrust faults (van Everdingen 1972). The Fairmont Hot Springs carbonate spring deposit is Holocene in age, and there is little modern calcite precipitation when compared to the volume of calcite forming the relict deposit. The deposit extends laterally for ~ 700 m, down-slope for ~ 700 m (with a 100 m loss in elevation), and is up to 16 m thick (Fig. 4-1B), which probably makes it the largest known carbonate spring deposit in Canada. Spherical grains form up to 1/5 of the deposit, with radiating calcite dendrites being the most abundant. Radiating calcite dendrites (Figs. 4-1C to E and 4-2) are common in shallow pools throughout the deposit, whereas oncoids (Figs. 4-1F to H and 4-3) are restricted to the lower elevation, down-slope pool facies. There are no modern environments where radiating calcite dendrites or oncoids are actively forming.

Materials and Methods

Thin sections were characterized using transmitted light microscopy. Fractured oncoids and radiating calcite dendrites, coated with a thin layer of gold, were examined on a JEOL 6301F field emission scanning electron microscope (SEM) at accelerating voltages of 5-20 kV.

Spherical Grain Components

Radiating Calcite Dendrites

The spherical to sub-spherical dendrite crystals are composed of multiple levels of branching crystalline calcite that radiates from a central point (Figs. 4-1E and 4-2). Primary branches are 30-200 μm wide and up to 1.5 mm long, with most being ~ 0.5 mm

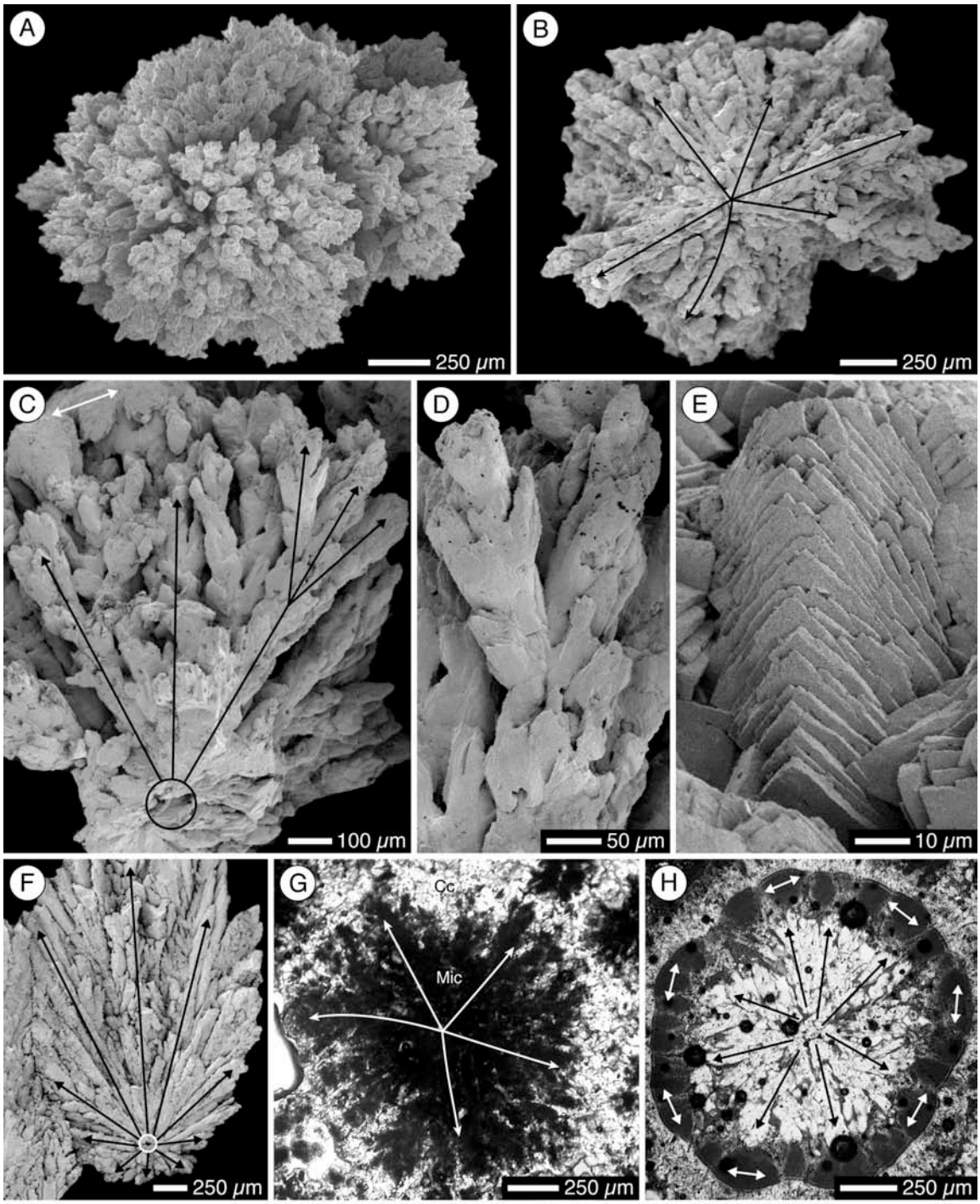

Fig. 4-2 Radiating calcite dendrites. (A-F) SEM photomicrographs; (G-H) Thin section photomicrographs. A) Elliptical dendrite formed of radiating calcite branches. B) Fractured dendrite showing a cross section through nucleus of solid calcite. Black arrows show radial arrangement of dendrite branches. C) Fractured dendrite showing a hollow nucleus (black circle), radiating branches, and a solid crust forming a tangential fabric (white arrow). D) Close up of smoothed branches. E) Euhedral stepped crystal faces formed of stacked calcite rhombs. F) Radiating calcite dendrite that developed into a feather dendrite. White circle around nucleus. G) Radiating calcite dendrite that appears dark and clouded because microbes colonized the branches and degraded the crystalline calcite into sparmicrite ("Mic"). The degraded dendrite was then encased in crystalline calcite ("Cc"). H) Beginning of oncoid formation. Highly cemented radiating dendrite (black arrows) that has a micritic, concentrically laminated crust (white arrows).

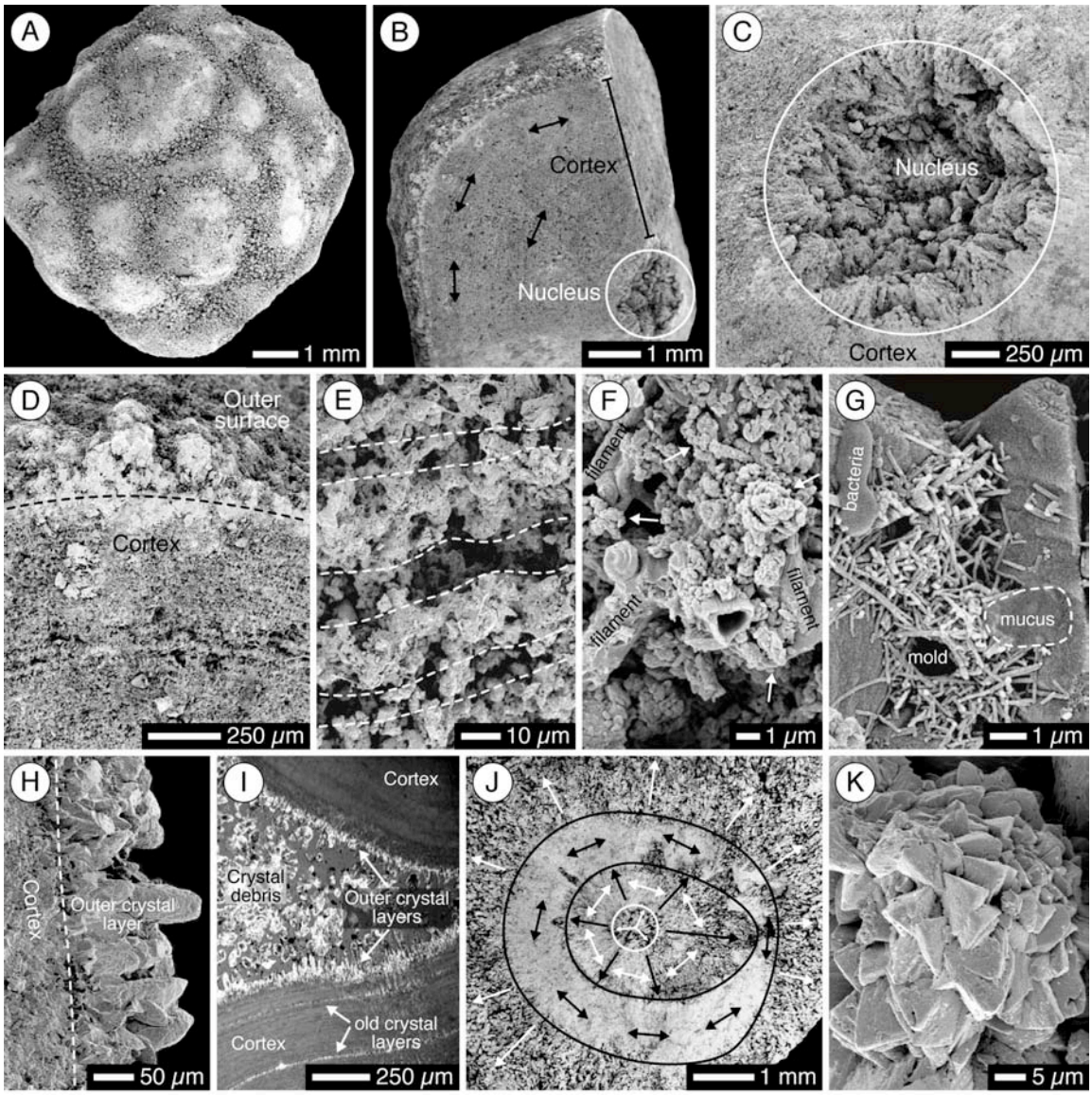

Fig. 4-3 Oncoids. (A-H, J-K) SEM photomicrographs; (I) Thin section photomicrograph. A) Irregular surface of sub-spherical oncoid. Darker regions are topographically lower, porous crystalline areas. Lighter regions are topographically higher, low porosity areas that experienced crystal degradation. B) Fractured oncoid with a well-defined, hollow nucleus lined with splaying dendrite branches, and a well-developed cortex formed of micritic concentric laminations. Black arrows highlight tangential cortical fabrics. C) Close-up of nucleus formed of a radiating calcite dendrite. D) Fractured oncoid showing concentric laminations and outer surface. E) Close-up of concentric laminations (white dashed lines) visible due to porosity differences. F) Anhedral micrite grains (white arrows) and microbial filaments are the main components of the concentric laminations. G) Needle fiber calcite common in cortices. H) Crystalline calcite forms radial fabric on outer surface of oncoid. These crystals were broken when oncoids rolled over terraces during transportation. I) Crystalline calcite debris generated during transport then deposited with oncoids. J) Oncoid formed by three phases of cortical development around radiating dendrite nucleus (white circle). First phase had radial and tangential fabrics formed by contemporaneous crystalline calcite and microbial growth (mixed black and white arrows). Second phase dominated by microbially mediated tangential fabric development (tangential black arrows). Third phase dominated by growth of elongate calcite crystals perpendicular to oncoid surface (white radiating arrows). K) Typical non-branching calcite crystal contained in cortices.

long (Figs. 4-2B,C). Crystals forming secondary and tertiary branches are 30-50 μm long, and 30-50 μm wide (Fig. 4-2D). The irregular branching is non-crystallographic. The subcrystals forming the branches, with their kite-shaped stepped faces, have the appearance of stacked rhombs (Fig. 4-2E). Most crystal faces, however, have been smoothed, obliterating the crystal edges (Fig. 4-2D). Thus, very few of the dendrites have stepped crystal faces preserved.

In thin section, well-preserved spherical dendrites are composed entirely of clean and clear crystalline calcite (Figs. 4-1D to E). Spherical dendrites that have been colonized by bacteria appear brown in thin section and thus appear as if their formation was microbially influenced (Fig. 4-2G). This appearance, however, is due to bacterial colonization of the dendrite branches after inorganic crystallization. The brown, micritic appearance was a result of sparmicritization (cf. Kahle 1977).

A well-formed radiating structure is most clearly visible in dendrite crystals that have been split in half (Figs. 4-1E and 4-2B to C). Under crossed polars, the branches become extinct at 90° intervals, creating a '+' shaped extinction pattern oriented in a north-south/east-west direction. Upon rotation of the stage, the '+' shaped extinction pattern remains stationary, giving the dendrites sweeping extinction. This indicates that the dendrite branches are in optical continuity with each other.

Efforts to determine the exact nature of the dendrite nuclei were unsuccessful. Some centers are hollow, some solid, and some contained minor amounts of mucus. The external morphologies of the dendrites are spherical to subspherical. The spherical dendrites formed where the crystals grew outward without being impeded by adjacent crystals. The subspherical dendrites formed when adjacent crystals grew into each other, forming concave depressions on the outsides of the crystals.

Oncoids

The oncoids, 2-15 mm in diameter, are rounded to ellipsoid and differ from the radiating dendrites in that their cortices have tangential fabrics (Figs. 4-1F to H and 4-3). The outer surfaces of the oncoids can be smooth or undulating. The degree of sphericity is controlled by the original morphology of the nucleus around which the oncoid formed.

Nuclei

The nuclei of the oncoids, which are 0.5-3 mm in diameter, are hollow or are composed of radiating calcite dendrites (Figs. 4-3B to C). Hollow nuclei may be lined with remnants of the dendrites. The boundaries between the nuclei and the cortices are characterized by reduced porosity and the presence of concentric laminations. The boundary can be sharp or transitional over 1-2 mm. Spherical nuclei are at the center of spherical oncoids, and irregular shaped nuclei are at the center of sub-rounded to ellipsoid oncoids.

Cortices

The cortices, 100 μm to 1 cm thick, are formed of micritic concentric laminations, 5-100 μm thick, and radial crystalline calcite laminations, 5 μm to 1 mm thick (Figs. 4-3D to K). Some cortices are formed entirely of micritic laminations with tangential fabrics (Fig. 4-3B), whereas other cortices exhibit alternating layers of tangential and/or radial fabrics (Fig. 4-3J). The micrite grains, 1-3 μm long and wide, are completely anhedral and ragged in appearance (Fig. 4-3F). The calcite crystals, up to 200 μm long (usually ~ 50 μm long) and 30-50 μm wide, grew perpendicular to the oncoid surface (Figs. 4-3H to K). Pristine calcite crystals are generally only preserved on the outer oncoid surfaces, indicating that transportation over the discharge apron caused mechanical crystal destruction (Fig. 4-3I). Secondary needle fiber calcite cements, up to 5 μm long and 30-60 nm wide, are commonly present with the micrite and coat surfaces of crystalline calcite (Fig. 4-3G). The micrite and needle fibers are associated with mucus, filaments, and bacteria, indicating that they are biological in origin. The micrite is sparmicrite (cf. Kahle 1977) formed by microbial crystalline calcite degradation. This microbial transformation of crystalline calcite to micrite in the cortex implies that the coated grains are oncoids.

Discussion

Two different processes led to the development of radial and tangential fabrics in the Fairmont Hot Springs spherical grains. The fabrics formed in different environments, each with specific physico-chemical and biotic conditions. The radial fabrics formed

abiotically in quiescent waters, whereas the tangential concentric laminations formed in flowing water with microbial mediation (Fig. 4-4).

Radial fabrics are present in nuclei and cortices and are defined by elongate calcite crystals that are oriented perpendicular to the spherical grains. Calcite crystals forming the nuclei are dendrites with multiple levels of branching, whereas cortical calcite crystals rarely exhibit branching. Cortical and nuclear calcite crystals however, formed in similar quiescent environments, with the main differences being the substrates upon which the crystals nucleated and the $CaCO_3$ supersaturation state of the spring water.

Dendrites are products of rapid crystallization from highly supersaturated solutions (e.g. Saratovkin 1959; Jackson 1977; Rimstidt 1997). Dendrites that nucleate on a surface grow and branch away from the surface. Radiating dendrites require a suspended nucleation point to allow branches to grow out in all directions from a central point. To allow for spherical dendritic growth, the initiation of crystallization may have taken place on colloidal calcite suspended in quiescent spring water pools supersaturated with respect to $CaCO_3$ (Fig. 4-4A). Once they grew too large to remain in suspension, the spherical seed dendrites settled to the pool bottoms. The delicate, radially branching nature of the dendrites, and indents where adjacent dendrites grew into one another indicate that the crystals were stationary during formation.

Agitation-induced CO_2 degassing from flowing water with elevated pCO_2 is the most common mechanism for driving $CaCO_3$ supersaturation in spring systems (Herman and Lorah 1988; Chafetz et al. 1991; Gonzalez et al. 1992; Jones and Renaut 1995, 2008; Pentecost 1994, 1995; Jones et al. 2000; Jones et al. 2005). The radiating dendrites however, formed in still spring water, indicating some mechanism other than agitation-induced CO_2 degassing was responsible for elevating $CaCO_3$ supersaturation states. The most probable cause of high supersaturation states was rapid evaporation and/or CO_2 degassing driven by solar input. Solar radiation could only have driven such rapid evaporation and/or CO_2 degassing in a very shallow, restricted pool environment. The pools were probably < 5 mm deep (slightly deeper than the largest radiating dendrites) and received little to no influx of fresh spring water. A lack of microbial evidence preserved with the radiating dendrites indicates that rapid crystal growth rates precluded

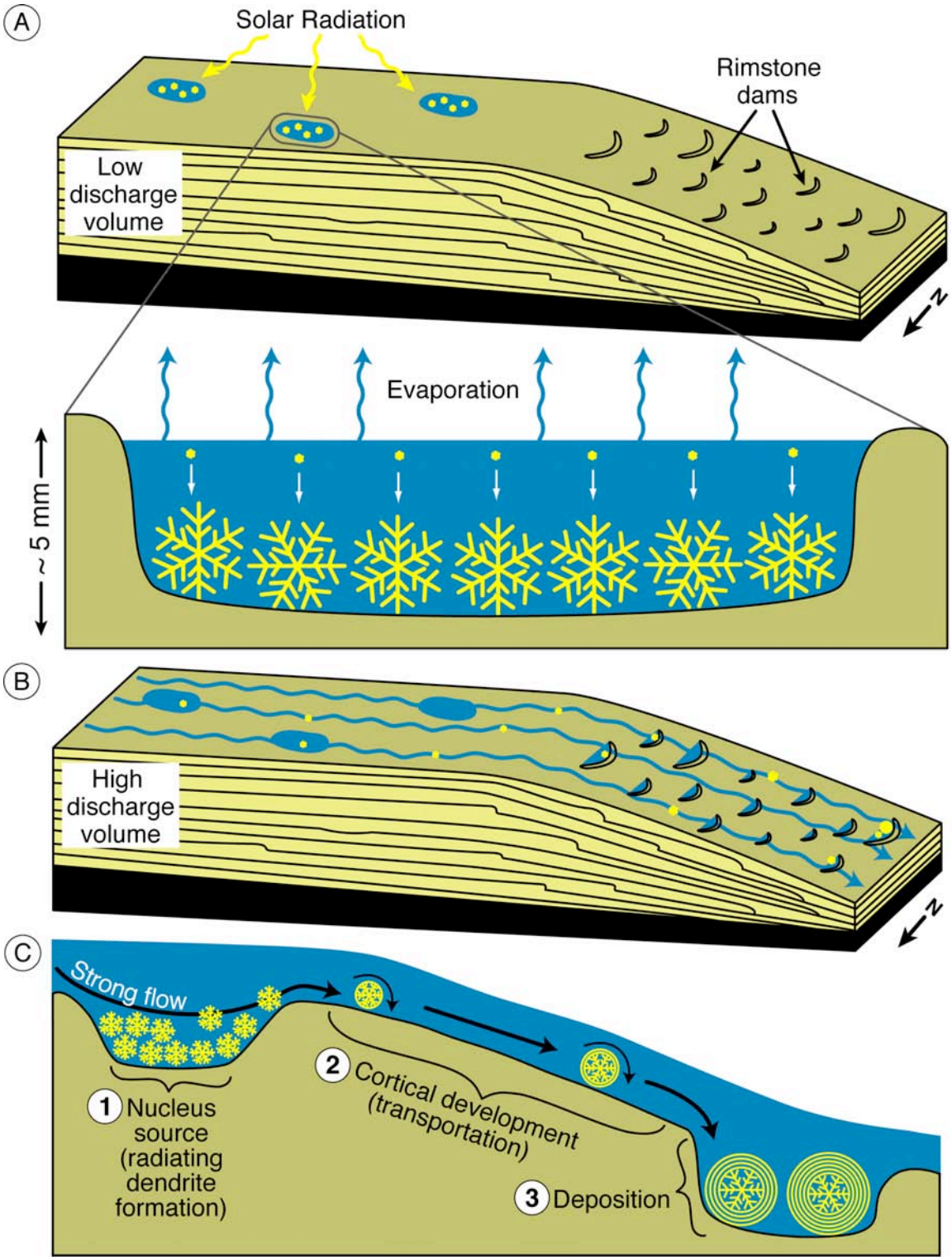

Fig. 4-4 Formation of radiating calcite dendrites and oncoids. A) $CaCO_3$ supersaturation achieved by abundant solar radiation causing evaporation and/or CO_2 degassing in shallow, restricted spring water pools. Radiating calcite dendrites nucleate in suspension and settle to bottom of pool where they enlarge under quiescent conditions. B) Dendrites episodically washed out of pools during periods of elevated spring water discharge and transported to sloping, distal part of discharge apron. C) Genetic relationship linking radiating calcite dendrites and oncoids.

biotic growth, and that microbial metabolism (e.g. photosynthesis) did not contribute to elevating $CaCO_3$ supersaturation states.

If left undisturbed in quiescent spring water pools, the dendrites grew until all available space was consumed by radiating branches. Periods or pulses of increased spring flow then washed the spherical dendrites out of the spring pools and onto the discharge apron, where they rolled down-slope (Figs. 4-4B,C). Rarely, radiating dendrites developed into feather dendrites when flowing water caused calcite crystal growth without dislodging them (Fig. 4-2F). Calcite was still precipitated during transportation, but conditions were too rough for elongate, delicate branched dendrite crystals to form. As a result, crystalline calcite precipitated in the spaces between the dendrite branches, which reduced porosity in the outer region of the dendrites, and a calcite 'crust' was formed around the dendrite (Figs. 4-2C,H). Microbial colonization of the inorganic calcite crust marked the completion of the first stage of oncoid growth. The crust formation prepared the radial dendrites to act as nuclei for cortical development, the second stage of oncoid growth.

Stage two of oncoid development involved the formation of cortices with tangential, concentrically laminated fabrics. The proportions and thicknesses of micritic versus crystalline laminations vary between oncoids, indicating varied multi-phase, yet semi-cyclical developmental histories. Micritic laminations formed from flowing water during transport of the grains on the discharge apron, whereas radial crystalline laminations formed when the grains were deposited in pools down-slope from where the radiating dendrites formed. Down-slope pools present on the sloping, distal part of the discharge apron were rimstone pools that were probably deeper than the shallow restricted pools from the flatter proximal part of the discharge apron. Thus, $CaCO_3$ supersaturation states in the distal pool were high enough to cause radial crystalline calcite fabrics to form, but not so high as to facilitate dendrite development. Furthermore, crystalline calcite that formed in the down-slope pools nucleated on the outer surface of the oncoids, rather than in suspension like the radiating calcite dendrites.

The simplest depositional history for an oncoid involved radiating calcite dendrite development in a proximal pool, followed by micritic concentric lamination development during transport, and final deposition in a down-slope pool (Figs. 4-2C and 4-4). More

complex depositional histories involved oncoids being deposited in down-slope pools and re-mobilized multiple times (Fig. 4-3J). Multi-phase cortical development also involved oncoids being only partly submerged in spring water, which explains the irregular nature of many cortical fabrics.

Four concurrent processes were involved in generating a cortex while the grains were being transported across the discharge apron: crystalline calcite precipitation, mechanical crystal destruction, microbial colonization of the crystals, and microbial degradation of the calcite crystals to sparmicrite. The microbes produced the sparmicrite, so the amount of sparmicrite produced was directly related to the amount of microbial growth. The proportion of crystalline calcite to sparmicrite forming each lamination was therefore controlled by the rate of calcite precipitation in relation to the rate of microbial colonization. If calcite precipitated faster than the rate of microbial growth, then laminations contained more crystalline calcite than sparmicrite, causing radial fabrics to be superimposed on the concentric tangential fabrics. If the microbes colonized the calcite crystals faster than it could precipitate, then the laminations contained abundant sparmicrite. The rates of crystal and microbial growth were not constant, so cyclic growth rate variations were responsible for the laminated fabrics. The nature of the fluctuations are not known, but may represent diurnal variations, or spring flow rate changes related to fluctuating discharge volumes.

Microbes are believed to actively influence carbonate deposition by acting as substrates upon which calcite can precipitate (e.g. Chafetz and Meredith 1983; Folk and Chafetz 1983; Chafetz and Guidry 2003). The role of microbes in forming the Fairmont oncoids is in stark contrast to this notion, as the microbes' main role was the degradation of large, well-formed calcite crystals to small, irregularly-shaped micrite grains. All of the micrite in the cortices is microbial sparmicrite. Thus, the formation of cortical concentric laminations was the direct result of microbial destruction of inorganically precipitated calcite crystals. In the absence of microbes, inorganic calcite precipitation would only have been impeded by mechanical degradation caused by rolling the grains over the discharge apron during transportation. Therefore, microbes were necessary to develop the tangential fabrics formed during the second stage of oncoid growth.

Conclusions

Analysis of spherical grains from the Fairmont Hot Springs carbonate deposit has led to the following important conclusions:

1) Radiating calcite dendrites can be an important component of carbonate spring deposits, and represent novel precursors to the development of oncoids in carbonate spring deposits.
2) Rapid abiotic crystal growth in quiescent water was responsible for the development of dendrites that radiate from a nucleus, whereas cyclic growth of crystals and microbes in flowing water was responsible for the development of tangential, concentrically laminated fabrics.
3) All of the micrite comprising the spherical grains is sparmicrite. All of the crystalline calcite was inorganically precipitated, whereas the sparmicrite formed as a result of microbes actively degrading the calcite crystals.

References

Chafetz, H.S., Meredith, J.C., 1983. Recent travertine pisoliths (pisoids) from southeastern Idaho, U.S.A. In: T.M. Peryt (Editor), Coated Grains. Springer-Verlag, Berlin Heidelberg, pp. 450-455.

Chafetz, H.S., Guidry, S.A., 2003. Deposition and diagenesis of Mammoth Hot Springs travertine, Yellowstone National Park, Wyoming, U.S.A. Canadian Journal of Earth Sciences, 40: 1515-1529.

Chafetz, H.S., Rush, P.F., Utech, N.M., 1991. Microenvironmental controls on mineralogy and habit of $CaCO_3$ precipitates: an example from an active travertine system. Sedimentology, 38: 107-126.

Eckel, E.B., 1939. Gas bubbles as nuclei for "oolites". Science, 89(2298): 37-38.

Folk, R.L., Chafetz, H.S., 1983. Pisoliths (pisoids) in Quaternary travertines of Tivoli, Italy. In: T.M. Peryt (Editor), Coated Grains. Springer-Verlag, Berlin Heidelberg, pp. 475-487.

Gonzalez, L.A., Carpenter, S.J., Lohmann, K.C., 1992. Inorganic calcite morphology: roles of fluid chemistry and fluid flow. Journal of Sedimentary Petrology, 62(3): 382-399.

Herman, J.S., Lorah, M.M., 1988. The chemical evolution of a travertine-depositing stream: geochemical processes and mass transfer reactions. Water Resources Research, 24(9): 1541-1552.

Jackson, K.A., 1977. Nucleation and atomic kinetics. In: W. Bardsley, D.T.J. Hurle and J.B. Mullin (Editors), Crystal growth: a tutorial approach: proceedings of the 3rd international summer school on crystal growth. North-Holland, Amsterdam, pp. 139-155.

Jones, B., Renaut, R.W., 1995. Noncrystallographic calcite dendrites from hot-spring deposits at Lake Bogoria, Kenya. Journal of Sedimentary Research, A65(1): 154-169.

Jones, B., Renaut, R.W., 2008. Cyclic development of large, complex, calcite dendrite crystals in the Clinton travertine, Interior British Columbia, Canada. Sedimentary Geology, 203: 17-35.

Jones, B., Renaut, R.W., Rosen, M.R., 2000. Trigonal dendritic calcite crystals forming from hot spring waters at Waikite, North Island, New Zealand. Journal of Sedimentary Research, 70(3): 586-603.

Jones, B., Renaut, R.W., Owen, R.B., Torfason, H., 2005. Growth patterns and implications of complex dendrites in calcite travertines from Lysuhóll, Snæfellsnes, Iceland. Sedimentology, 52: 1277-1301.

Kahle, C.F., 1977. Origin of Sub-Aerial Holocene Calcareous Crusts - Role of Algae, Fungi and Sparmicritization. Sedimentology, 24(3): 413-435.

Pentecost, A., 1994. Formation of laminate travertines at Bagno Vignone, Italy. Geomicrobiology Journal, 12: 239-251.

Pentecost, A., 1995. Geochemistry of carbon dioxide in six travertine-depositing waters of Italy. Journal of Hydrology, 167: 263-278.

Rimstidt, D.J., 1997. Gangue mineral transport and Deposition. In: H.L. Barnes (Editor), Geochemistry of hydrothermal ore deposits. John Wiley & Sons, New York, pp. 488-515.

Saratovkin, D.D., 1959. Dendritic Crystallization. Consultants Bureau, New York, 126 pp.

van Everdingen, R.O., 1972. Thermal and mineral springs in the southern Rocky Mountains of Canada. Water Management Service, Department of the Environment, Environment Canada.

Chapter 5

Comparative Analysis of Soft-Tissue Preservation in the Hot Creek Carbonate Spring Deposit, British Columbia, Canada

Introduction

Due to decay resistance, organisms containing biomineralized parts (e.g. bone, shell, or teeth) are more likely to be preserved in the rock record than organisms formed solely of soft tissues (Briggs 2003). Excellent preservation of soft-bodied organisms is generally thought to be reserved for event deposits related to anoxia or rapid burial, such as Burgess Shale-type deposits (e.g. Allison and Briggs 1993). Soft tissue preservation is possible however, in other depositional environments like mineral springs, where precipitation is faster than or contemporaneous with decay. Regular and continual mineral precipitation at springs causes nearly instantaneous mineralization of biota, whereas preservation in most other geological environments is a diagenetic event mediated by mineralizing fluids after death and burial (Schopf 1975; Briggs 2003).

Rapid mineral precipitation facilitates exceptional preservation of soft-tissue flora growing in and around spring systems, which in turn, controls the fabrics and textures of mineral spring deposits, and in the case of relict deposits, provides valuable insights into the nature of the original depositional system (e.g. water temperature, pH). The processes responsible for the preservation of microbes in mineral spring deposits have been intensely studied for over a century (e.g. Weed 1888; Allen and Day 1935; Irion and Müller 1968; Pentecost 1978, 2003; Chafetz and Folk 1984; Koban and Schweigert 1993; Renaut and Jones 2000; Pedley 2000; Bonny and Jones 2003a; Pentecost and Coletta 2007), and several investigations have examined bryophyte mineralization (e.g. Weijermars et al. 1986; Pentecost 1996; Rainey and Jones 2007). Nevertheless, a comprehensive comparison of microbe, bryophyte (moss), macrophyte (plants), and wood mineralization in a spring system has yet to be completed.

The relict carbonate spring deposit at Hot Creek in British Columbia (Figs. 5-1 and 5-2) is composed almost entirely of filamentous microbial deposits that were preserved by calcite precipitated from spring water, with lesser amounts of preserved wood, macrophytes, bryophytes, and diatoms. Among these organisms however, greater tissue durability and hardness unexpectedly decreased, rather than increased, the likelihood of preservation. Preservation potential was influenced by taxonomic, taphonomic, structural, and compositional differences between organisms, and by the effects of spring water physicochemical properties on biotic decay and calcite precipitation. These factors controlled the balance between calcite precipitation rates and biotic decay rates, which ultimately determined if photosynthesizing organisms that lived in and adjacent to the Hot Creek spring water were preserved.

Materials and Methods

In the summer of 2003, 10 samples of tufa were collected from a road cut and a quarry test pit. Subsequently in 2004, the areal extent of the deposit was mapped (Fig. 5-1B), and 32 carbonate samples, two embedded charcoal and two wood samples for ^{14}C dating were collected (Figs. 5-2A to D). Water temperature and pH were measured in the field in March 2007. Unfiltered water samples were collected in 100 ml Nalgene plastic bottles. Filtered samples, for isotope analysis, were collected using a syringe and a 0.22 μm filter, and stored in Teflon-capped 5 dram vials.

Of the 42 samples collected, large (5 X 7 cm) thin sections were produced from 18 samples containing preserved cyanobacteria, bryophytes, macrophytes, and woody material. Petrographic investigations were made using transmitted light microscopy. Fractured carbonate samples, sputter coated with a thin layer of gold, were examined on a JEOL 6301F field emission scanning electron microscope (SEM) at accelerating voltages of 5 to 20 kV. Carbonate samples were confirmed to be calcite by powdering and analyzing them using X-ray

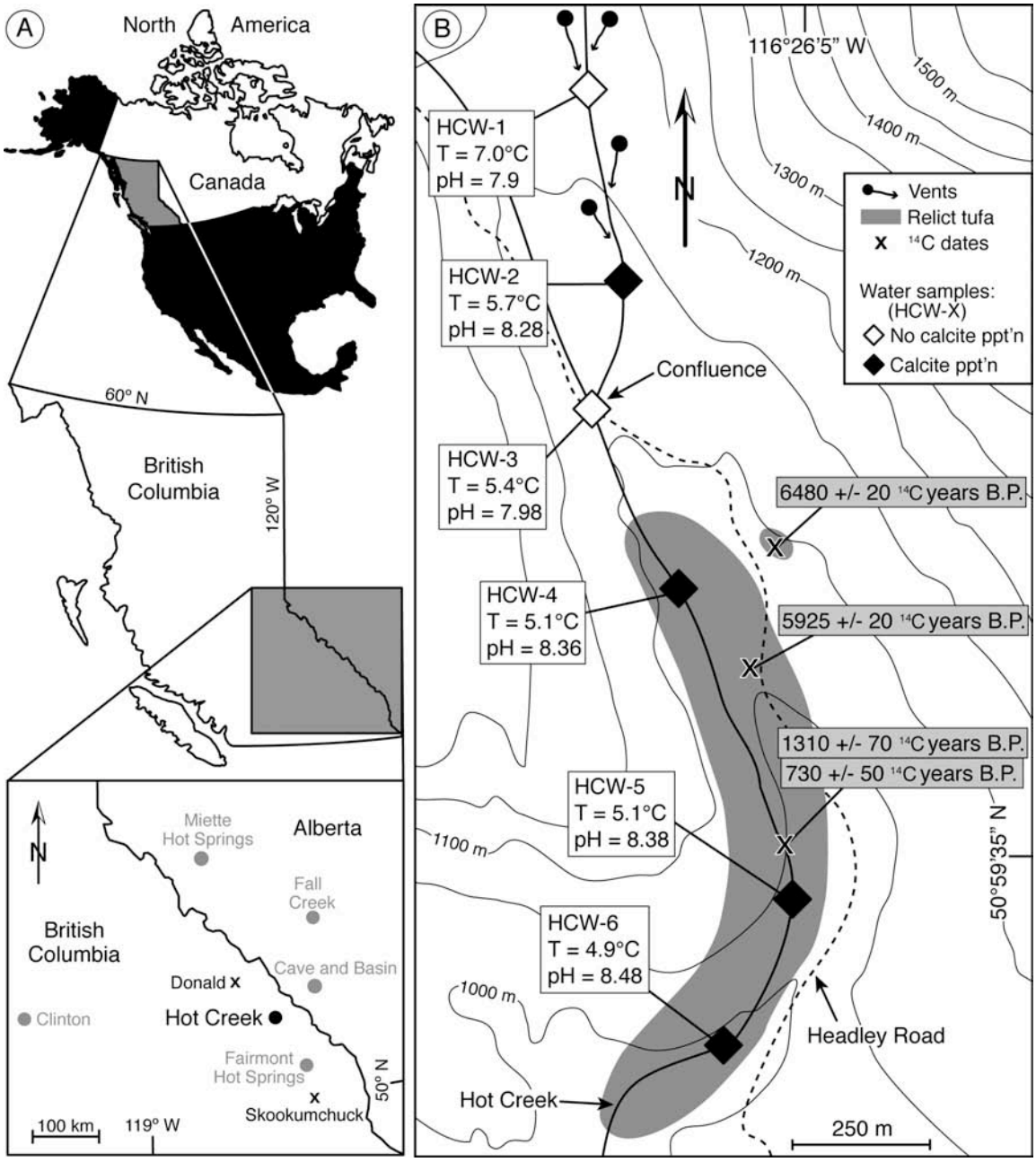

Fig. 5-1 Location and overview of relict Holocene Hot Creek carbonate spring deposit. A) Hot Creek, southern British Columbia and Alberta deposits that have been dated. Hot Creek was ice-free and exposed in late Pleistocene, as inferred from radiocarbon dates obtained at Donald and Skookumchuck. B) Locations of Hot Creek relict carbonate spring deposit, water samples, and radiocarbon dated material.

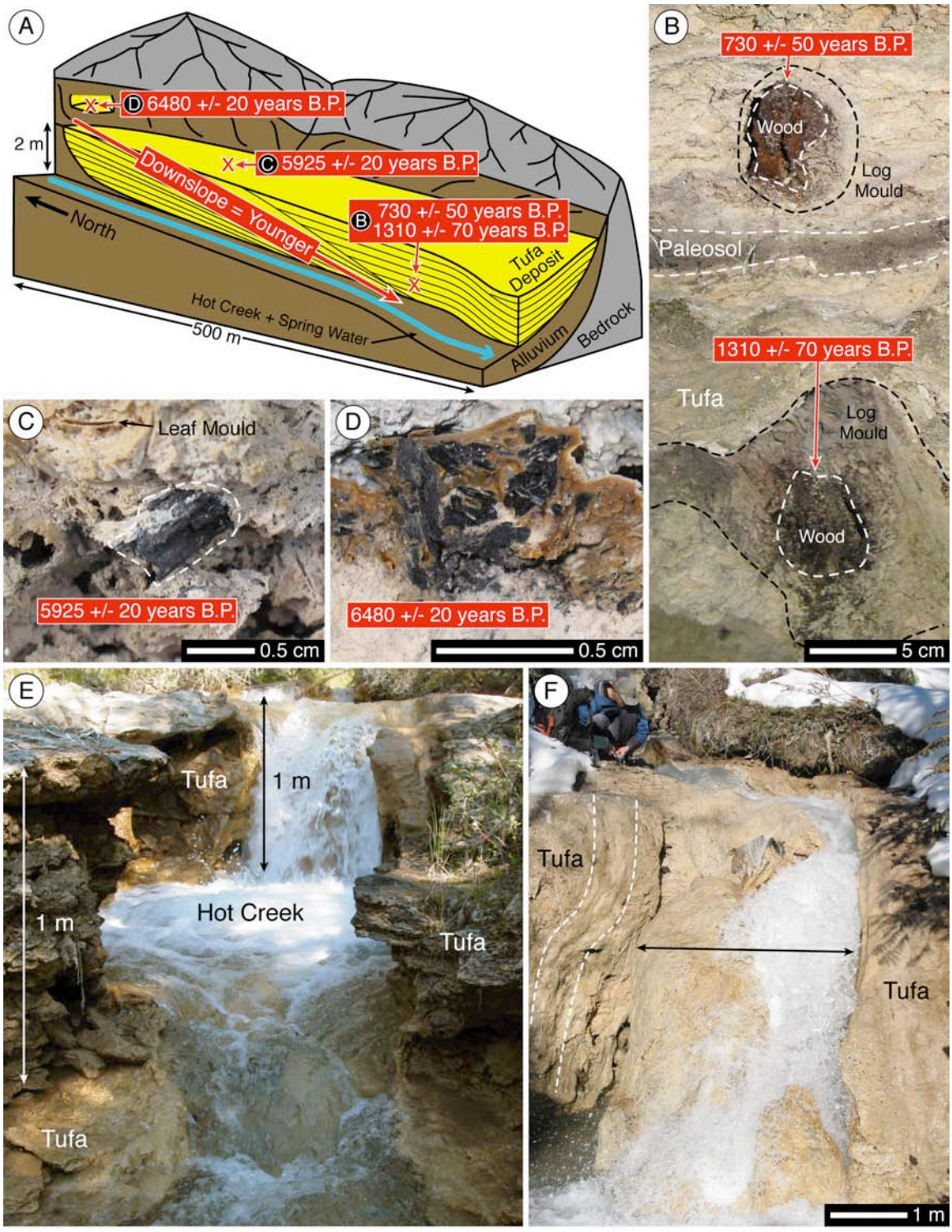

Fig. 5-2 Morphology of Hot Creek carbonate spring deposit and locations of material recovered for radiocarbon dating. A) Stratigraphic relationships between radiocarbon dates. B) Wood recovered for radiocarbon dating. C) Charcoal fragment recovered from tufa exposed in quarry test pit. D) Oldest charcoal recovered from minor deposit at upper end of main deposit. E) Horizontally bedded tufa incised by Hot Creek. F) Modern cascade incising sub-recent, steeply dipping tufa beds while simultaneously precipitating calcite in flow path (black arrow).

diffraction with a Rigaku Geigerflex Powder Diffractometer. Standard water analyses were completed within four weeks of being collected. The oxygen isotopic compositions of the spring water were determined by the Environmental Isotope Laboratory at the University of Waterloo.

Wood samples were sent to Beta Analytic Inc., Miami, Florida for pre-treatment and conventional ^{14}C dating. Charcoal sample pre-treatment was completed at the University of Alberta. Samples were washed with 10% HCl for 1 hour to remove calcium carbonate, then washed with 1M NaOH hourly until the wash was colourless. This was followed by a final 10% HCl wash and rinsing with ultra-pure H_2O until neutral. Accelerator mass spectrometry dating of the washed samples was completed at the Keck Carbon Cycle AMS facility, Earth System Science Department, University of California, Irvine. Conventional radiocarbon ages were converted to calendar years using the CALIB radiocarbon calibration program and the IntCal04 terrestrial radiocarbon age calibration for 26 to 0 ka BP, and calibrated ages are reported as 2 sigma ranges (Stuiver and Reimer 1993; Reimer et al. 2004).

The contrast and brightness of the digital field images and SEM photomicrographs used in this paper were adjusted using Adobe Photoshop©. For some SEM photomicrographs, black backgrounds were introduced in order to highlight the features being shown.

Terminology

Most of the Hot Creek deposit is cyanobacterial tufa, with *tufa* being freshwater carbonate deposits whereby preserved biota controlled deposit fabrics and textures (cf. Rainey and Jones 2009). Cyanobacteria filaments at Hot Creek are structures formed of an extracellular sheath surrounding a *trichome*, which is a row of cyanobacterial cells joined together (cf. Merz 1992). Most of the calcite crystals in the Hot Creek deposit are *composite crystals* (cf. Given and Wilkinson 1985; Sandberg 1985) that are formed of numerous subcrystals (cf. Sandberg 1985; Jones 1989; Rainey and Jones 2007). It is common for a composite crystal to be formed of subcrystals that are two different sizes. In such cases, the smaller

subcrystals are called primary subcrystals, whereas the larger subcrystals are called secondary subcrystals.

Despite important differences between the terms *permineralization* and *petrifaction*, they are commonly used interchangeably to characterize the processes that lithify biota (e.g. Schopf 1975; Weibel 1996; Nowak et al. 2005). For the purpose of this paper, *permineralization* is used to denote the infiltration of cells and interstices by mineral-precipitating fluids, and the subsequent precipitation of calcite in those empty cells without organic matter replacement (cf. Oehler and Schopf 1971; Briggs 2003). In contrast, *petrifaction* involves the replacement of organic matter by a mineral (cf. Scurfield and Segnit 1984; Briggs 2003). *Sheath impregnation* refers to the precipitation of minerals within the mucilaginous sheath (cf. Riding 1977), and is treated as a different process than *petrifaction* because it is not known if the calcite crystals replace or merely grow among the molecules that form the sheath. *Encrustation* occurs where minerals nucleate on and grow away from the outer surface of an organism (cf. Irion and Müller 1968). The term *encapsulation* is introduced here to refer to the process whereby an organism becomes encased in minerals that nucleated on a surface adjacent to it, rather than on its own outer surface. *Filament casts* formed from calcite that precipitated inside of encrustation moulds after the trichomes and sheaths decayed. *Sheath casts* formed by precipitation of calcite inside of the hollow tubes created when the trichomes decayed and the sheaths remained intact.

Study Site

Hot Creek is located on the east side of the Rocky Mountain Trench at the base of the Rocky Mountains at their western limit (Fig. 5-1A). Its location was revealed by the operator of the Wolfenden tufa quarry ~ 20 km southeast of Hot Creek, and prior literature references to the Hot Creek deposit could not be located. It is accessible by Headley Road on the east side of Highway 95 near the town of Harrogate in southeast British Columbia. In should be noted that Hot Creek and the adjacent springs are two separate systems, and despite its moniker,

neither the creek nor the spring water registered temperatures above 7°C (Fig. 5-1B; Table 5-1).

Hot Creek, 1 to 3 m wide and several cm to 1 m deep, runs through a 100 to 250 m wide, north-south trending flat-bottomed valley. The creek flows north to south and joins the Columbia River west of Harrogate. The Hot Creek springs are a collection of large and small vents that emerge across a forested hillside on the east side of Hot Creek (Fig. 5-1B). At least a dozen vents were encountered while tracing the origin of the springs; however, the branching nature of the flow and the thick forest made it difficult to determine the locations of all vents. The spring water flows in narrow and shallow (< 1 m wide, 2 to 30 cm deep) channels that converge and diverge in an anastomosing pattern until their confluence with Hot Creek at a small bridge where Headley Road crosses over Hot Creek at the upper end of the deposit. The volume of spring water entering Hot Creek at the confluence is approximately one quarter to one half of the creek volume.

Tufa Deposits

This paper focuses on photosynthesizing organisms preserved by calcite in the relict tufa deposit. The spatial associations of Hot Creek, the springs, the relict deposits, and the modern deposits are best described by using the location of the confluence of Hot Creek and the spring water flow path as a reference point (Fig. 5-1B). No relict or modern tufa deposits exist along Hot Creek upstream of the confluence. Upstream of the confluence along the spring water flow path, there are no relict deposits, and modern calcite precipitation is limited to < 1 cm thick, discontinuous crusts at the bottom of spring water channels. All relict deposits are present downstream of the confluence. Modern deposits downstream of the confluence are restricted to < 1 mm thick calcite crusts on gravel and detrital and *in situ* vegetation along the margins of the creek, and rollovers and cascades at the distal terminus of the deposit.

Relict deposits

The main relict Hot Creek tufa deposit is < 150 m wide, up to 3 m thick, and extends along the valley for ~ 1 km (Fig. 5-1B). The best and most

Table 5-1 Hot Creek unfiltered spring water chemistry and stable oxygen isotope compositions.

Sample	T (°C)	pH	Ca^{2+}	Mg^{2+}	Na^{+}	K^{+}	HCO_3^{-}	SO_4^{2-}	Cl^{-}	Total Dissolved Solids (TDS)	Langelier Saturation Index (LSI)	$\delta^{18}O$ VSMOW (‰)
HCW-1	7.0	7.9	153	28	0.5	0.6	217	300	2	676	0.33	-16.9
HCW-2	5.7	8.3	147	28	0.4	0.5	184	310	1	662	0.61	-15.9
HCW-3	5.4	8.0	164	30	0.5	0.5	221	330	<1	920	0.42	-17.0
HCW-4	5.1	8.4	153	29	0.5	1.4	198	320	<1	882	0.74	-16.0
HCW-5	5.1	8.4	153	31	0.5	0.6	187	330	<1	869	0.72	-16.5
HCW-6	4.9	8.5	148	30	0.5	0.5	183	320	<1	865	0.79	-16.6

Notes: All temperature and pH measurements were taken in the field. Unless stated, all units are in $mg \cdot L^{-1}$, with the exception of pH, which is the negative log of [H+], and LSI, which is unitless. LSI was calculated using $[Ca^{2+}]$, $[HCO_3^{-}]$, T, pH and TDS.

continuous exposure through the tufa is along a 1 to 5 m wide channel that was incised by Hot Creek (Fig. 5-2E). The road cut and a small quarry test pit (20 m long, 5 m wide, 1.5 m deep) provide additional, but limited, outcrop access.

The tufa is formed of cyanobacteria preserved in massive to well-bedded laterally continuous deposits. Calcite has also preserved minor amounts of wood, bryophytes, and macrophytes that are randomly dispersed through the deposit. The living vegetation that covers most of the deposit makes it difficult to ascertain if the spatial distribution of the mineralized biota is stratigraphically controlled. Most bedding is parallel with a shallow (0 to 10°) dip down valley, which corresponds to gradual elevation loss along the length of the deposit. Near the distal terminus of the deposit, however, there is a 100 m long section where steeper gradients coincide with several 0.5 to 2 m high rollovers with beds that dip at 30 to 70° (Fig. 5-2F).

A separate, smaller deposit (5 m wide, 1 m thick) is exposed on the east side of the road near the upper end of the main deposit (Fig. 5-1B). This deposit is a rollover structure that is not associated with any modern water flow. It is distinctly different from the main deposit in that half of it displays cyanobacterial textures and half is formed of well-cemented, fine (< 1mm thick) laminations that are abiotic. It is probably a minor paleo-vent that acted as a small seep and never precipitated enough calcite to connect to the main deposit. It is an important deposit because it contains charcoal fragments (1 to 5 mm long) that were collected for radiocarbon dating.

Modern deposits

Modern calcite precipitation is minimal, especially when compared to the large volume of relict calcite found in the area. Other spring systems in western Canada (e.g. Fairmont Hot Springs, Miette Hot Springs, Big Hill Springs, Fall Creek) have a similar association whereby extensive relict deposits are present, yet modern calcite precipitation is sparse (see locations in Fig. 5-1A; Bonny 2002; Bonny and Jones 2003b; Grasby et al. 2003; Turner and Jones 2005; Rainey and Jones 2007; Rainey and Jones 2009).

Modern deposits upstream of the confluence are unlike the other modern or relict deposits in that they contain large amounts of clay. Modern deposits downstream of the confluence are morphologically similar to the relict deposits in that they are formed of crystalline calcite with mineralized cyanobacteria, wood, macrophyte leaves, and bryophytes.

Hemispherical microstromatolites (< 1 cm wide and < 5 mm high) and biofilms commonly grow at the edges of the creek where flow is slow, and some streamer fabrics are growing on distal rollover structures and cascades (Fig. 5-3). Microstromatolites are formed mainly of tapering *Rivularia* filaments that are 10 to 15 μm in diameter and have trichomes that are 4 to 5 μm in diameter extending from the ends of the sheaths (Figs. 5-3A to D). Biofilms and streamers are formed largely of *Lyngbya* filaments that are 10 to 15 μm in diameter (Fig. 5-3E). A wide variety of diatoms grow in association with the modern cyanobacteria, but their identification was deemed unnecessary as none are found in the relict deposit (Figs. 5-3F to I). Modern calcite precipitation associated with cyanobacteria is limited to 0.5 to 2 μm long calcite rhombs (Figs. 5-3J,K).

Modern Spring Activity and Water Chemistry

At 7°C, the Hot Creek Springs have some of the coldest measured spring water temperatures from southern British Columbia (Table 5-1; Grasby and Hutcheon 2001, their table 1). Low spring water temperatures and lack of H_2S suggest appreciable atmospheric contact or shallow subsurface circulation of the spring water. In comparison with other southern British Columbian springs, springs that emerged with vent temperatures of 24°C required minimum circulation depths of 0.9 km (Allen et al. 2006), and springs at 11°C had estimated circulation depths of 0.6 km (Grasby and Hutcheon 2001). The meteoric water that infiltrated the recharge area around Hot Creek probably circulated no deeper than ~ 0.5 km. The spring water has $\delta^{18}O$ VSMOW values from –15.9 to –17.0‰ (average –16.5‰; Table 5-1), is meteoric in origin, and is unlikely to have a large hydrothermal component (cf. Clark et al. 1982; Grasby et al. 2000; Grasby and Hutcheon 2001). All bedrock in the vicinity of the creek is covered, but the

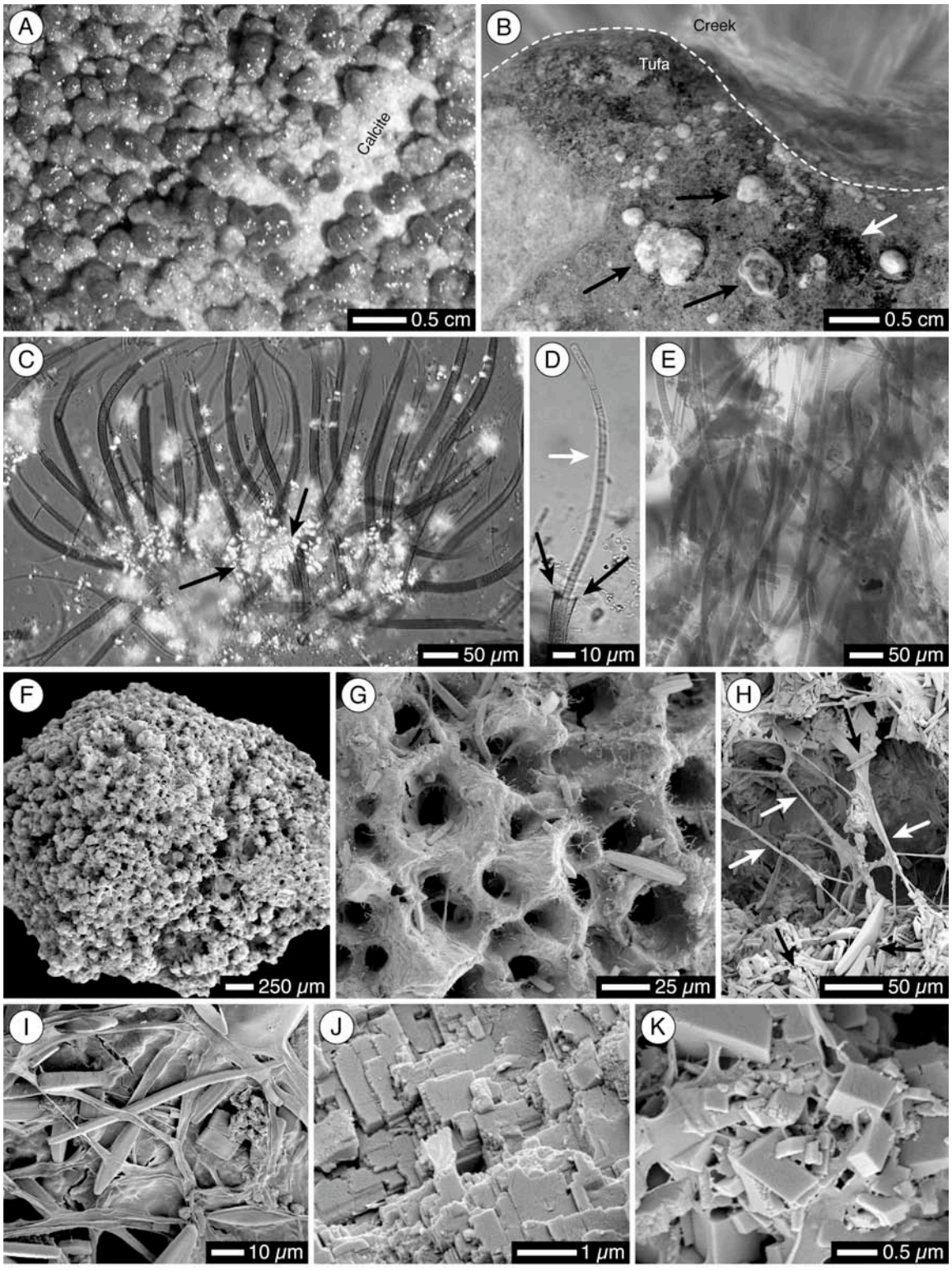
A
Calcite
0.5 cm
B
Creek
Tufa
0.5 cm
C
50 μm
D
10 μm
E
50 μm
F
250 μm
G
25 μm
H
50 μm
I
10 μm
J
1 μm
K
0.5 μm

Fig. 5-3 Modern cyanobacteria tufa formation. (A-B) Field photographs; (C-E) Thin section photomicrographs; (F-K) SEM photomicrographs. A) Hemispherical microstromatolites with minimal calcite precipitation. B) Microstromatolites with abundant calcite precipitation (black arrows) adjacent to unmineralized biofilm (white arrow). C) Colony of *Rivularia* in mass of calcite crystals (black arrow). D) Typical *Rivularia* filament with trichome (white arrow) extending from sheath (black arrow). E) *Lyngbya* filaments randomly arranged in mass of calcite. F) Partially mineralized hemispherical microstromatolite. G) Cyanobacterial moulds in calcite. H) Unmineralized cyanobacteria filaments (white arrow) and diatoms (black arrow) forming microstromatolite. I) Cyanobacteria, diatoms, and mucus in microstromatolite. J) Rhombohedral subcrystals aligned in modern composite crystal from microstromatolite. K) Randomly oriented calcite rhombs forming in mucus in modern microstromatolite.

springs are probably related to groundwater circulation associated with the southwest-dipping Purcell Thrust (Grasby and Hutcheon 2001).

Downstream changes in pH, water temperature, and dissolved ions provide insight into the chemical changes responsible for modern calcite precipitation, even though tufa formation is limited (Table 5-1; Fig. 5-1B). Of the ionic species analyzed (Ca^{2+}, Mg^{2+}, Na^{+}, K^{+}, HCO_3^{-}, SO_4^{2-}, Cl^{-}), only Ca^{2+} and HCO_3^{-} showed appreciable downstream concentration changes (Table 5-1; Fig. 5-1B). Of the two spring water samples collected above the confluence, HCW-1 (the uppermost sample) was not associated with calcite precipitation, whereas HCW-2 was associated with a 1 cm thick crust of calcite at the bottom of the spring water channel. From HCW-1 to HCW-2, there was a downstream increase in pH (7.9 to 8.3) and decrease in HCO_3^{-} (217 to 184 $mg \cdot L^{-1}$), but only a slight drop in Ca^{2+} (153 to 147 $mg \cdot L^{-1}$). At the confluence (sample HCW-3), there is a decrease in pH (8.3 to 8.0), increases in Ca^{2+} (147 to 164 $mg \cdot L^{-1}$) and HCO_3^{-} (184 to 221 $mg \cdot L^{-1}$) and no calcite precipitation. From HCW-3 to HCW-4, precipitation of < 1 mm thick calcite crusts at the margins of the creek is accompanied by an increase in pH (8.0 to 8.4) and decreases in Ca^{2+} (164 to 153 $mg \cdot L^{-1}$) and HCO_3^{-} (221 to 198 $mg \cdot L^{-1}$). Minor calcite precipitation continues between HCW-4 to HCW-6, but only HCO_3^{-} exhibits a marked decrease (198 to 183 $mg \cdot L^{-1}$), whereas pH and Ca^{2+} change only slightly (8.4 to 8.5 and 153 to 148 $mg \cdot L^{-1}$, respectively).

The likelihood of the water samples to precipitate calcite can be determined by calculating their Langelier Saturation Indices (LSI). Water samples with positive LSI values are saturated with respect to $CaCO_3$, with higher values representing greater saturation (Langelier 1936). All samples have positive

LSI values, but samples HCW-2, HCW-4, HCW-5 and HCW-6 have LSI values > 0.5 and were collected where modern calcite is precipitating, whereas samples HCW-1 and HCW-3 have LSI values < 0.5 and did not have associated calcite precipitation. Progressive downstream increase in pH coupled with decreasing Ca^{2+} and HCO_3^- indicate that $CaCO_3$ saturation was driven by removal of CO_2 from solution. Water turbulence and a lack of photosynthesizing organisms along the flow path indicate that inorganic CO_2 degassing facilitated calcite precipitation. Slight downstream cooling from HCW-1 to HCW-6 (7°C to 4.9°C) probably resulted from heat loss to the atmosphere as a result of the near freezing ambient temperature. Although $CaCO_3$ solubility increases with decreasing temperature, most modern calcite precipitation occurs where the water temperature is the lowest, indicating that CO_2 degassing was able to overcome the effects of cold water on carbonate solubility. Flow paths and topography have not changed from the time of relict tufa deposition to present, suggesting that modern and past downstream increases in calcite saturation were probably similar.

Deposit Age

Like other western Canadian carbonate spring deposits, the Hot Creek deposit is post-glacial in age. The Rocky Mountain Trench was filled with a large valley glacier until the end of the Pleistocene, when it retreated northwards. Skookumchuk, ~ 120 km south of Hot Creek, was ice-free by 11,500 years B.P (Fig. 5-1A), and Donald, ~ 80 km northwest of Hot Creek was probably ice-free by 10,000 years B.P. (Fulton 1971). Thus, Hot Creek was ice-free no later than 10,000 years B.P.. It is unknown how much time elapsed between deglaciation and initiation of spring deposit formation, but four samples of dateable material (two charcoal and two wood samples) recovered from the Hot Creek deposit provided some constraints on periods of spring activity and deposit development (Figs. 5-1B and 5-2A to D).

The charcoal samples, which were present as small angular fragments (< 5 mm long) embedded in the tufa, yielded dates of 6480 +/- 20 ^{14}C years B.P. (7327 to 7432 years BP) and 5925 +/- 20 ^{14}C years B.P. (6677 to 6790 years BP). The

oldest charcoal was recovered from the middle of the 1 m thick, small rollover deposit near the upper end of the main deposit. The younger charcoal was collected from the quarry test pit ~ 200 m south (down-slope) of the older charcoal. This sample was collected ~ 0.5 m from the surface of the 1.5 m deep exposure. The pit had not been excavated to the base of the deposit, so it could not be determined exactly how much tufa had formed prior to the charcoal being incorporated into the deposit. The charcoal was underlain by at least 1 m of tufa, however, indicating that significant deposit formation had occurred prior to charcoal deposition.

Most coarse sediment produced by forest fires is transported to streams by rain and snowmelt within 5 years (Reneau et al. 2007). The Hot Creek charcoal may have been transported onto the deposit soon after formation, in which case the charcoal dates approximate the age of the surrounding tufa. It is possible however, that the charcoal remained buried elsewhere prior to being incorporated into the deposit. The charcoal dates must therefore be treated as maximum deposit ages.

The wood samples yielded dates of 1310 +/- 70 ^{14}C years B.P. (1070 to 1340 years BP) and 730 +/- 50 ^{14}C years B.P. (570 to 730 years BP). The two wood samples were recovered from the lower third of a 3 m thick exposure along Hot Creek, about halfway down the length of the deposit (Figs. 5-1B and 5-2A). Stratigraphically, the samples were ~ 20 cm apart and were separated by a small unconformity represented by a thin (1 to 2 cm thick) paleosol (Fig. 5-2B). Each of the 5 to 10 cm wide log moulds yielded approximately 10 g of wood. The outer surfaces of the logs had been encrusted by calcite, and most of the wood had decayed. Inside of the mostly empty moulds was a < 1 cm thick layer of permineralized wood, which probably protected the logs from complete decay. The logs probably underwent little to no transport after death, suggesting that their ages closely approximate the age of the beds in which they were located. The presence of the wood near the base of the deposit and significant tufa formation above the samples indicates that at this locality, most of the tufa is likely no older than 1500 years and could be as young as a couple of hundred years.

Paleoenvironmental Implications of Spring Deposits

The ages and distribution of the wood and charcoal in the Hot Creek deposit provide a temporal framework for the development of the deposit. The charcoal samples (6677 to 7327 years B.P.) were embedded in the deposit further upslope than the wood, proximal to the paleo-vents and near the top of the deposit. The wood samples (570 to 1340 years B.P.) were embedded in the deposit further downslope, distal to the paleo-vents, and near the base of the deposit. This indicates that the distal parts of the deposit (or some of them) formed much later than the proximal parts. The deposit is < 3 m thick but over 1 km long, so the spatial distribution of the dates suggests that the deposit formed as a result of down-valley progradation with limited vertical aggradation. Extensive vegetation cover and limited exposure however, made it difficult to corroborate the distribution of the dates with morphological features that may have formed by progradation such as multiple lobes, rimstone dams, and rollovers.

The radiocarbon dates from the two wood samples emphasize the importance of hiatuses in the development of the deposit. Although only 20 cm apart vertically, stratigraphically they differ in age by 540 to 770 years. Without the wood to date, it was not apparent that over 500 years had elapsed between the incorporation of the two logs into the deposit. During this period, there was paleosol development where no calcite was being precipitated at that location. It could not be determined, however, if lobe switching caused calcite to be precipitated elsewhere at that time, or if the spring stopped precipitating calcite altogether.

The Hot Creek deposit and other western Canadian carbonate spring deposits did not form continuously throughout the Holocene, but limited numbers of dates from these deposits make it difficult to correlate their development with specific climatic intervals. Dating of other deposits suggest that their development was most pronounced during the latter half of the Holocene in response to cooler, wetter climatic conditions associated with the Neoglacial and the Little Ice Age (Fig. 5-1A; Renaut and Long 1986; Bonny 2002; Bonny and Jones 2003b; Grasby et al. 2003; Rainey and Jones 2007; Jones and Renaut 2008).

Charcoal recovered from the Hot Creek and Fairmont Hot Springs deposits revealed that significant deposit formation took place 6600 to 8800 years B.P., during the early Holocene (Rainey and Jones 2009). Such extensive spring activity seems anomalous considering that the first half of the Holocene was characterized by warm, dry conditions (e.g. Porter and Denton 1967; Kearney and Luckman 1983a, b; Ritchie et al. 1983; Luckman and Kearney 1986; MacDonald 1989; Beaudoin and King 1990; Luckman et al. 1993). This apparent contradiction between spring activity and climatic conditions highlights the need for high resolution dating of carbonate spring deposits in western Canada, which would allow for comparisons to other climatic proxies.

Calcite Crystal Morphologies

The relict Hot Creek deposit is formed largely of crystalline calcite that precipitated in association with filamentous cyanobacteria. Composite calcite crystals are most abundant, with lesser amounts of nano-scale calcite (Figs. 5-4 and 5-5). The composite crystals, classified as compact, porous, or elongate, are formed of subcrystals that have their *a* and *c* axes aligned parallel to one another. All of these crystals have rhombohedral crystal terminations with variable morphological expression and/or arrangement of trigonal subcrystals. Most of the crystals are pristine and unaffected by early diagenesis.

Fig. 5-4 SEM photomicrographs of composite calcite crystals from relict deposit. A) Fractured cyanobacteria tufa showing compact composite crystals lining pore with *c* axes perpendicular to substrate. B) Rhombohedral terminations of compact composite crystals. C) Compact composite crystal showing rhombohedral arrangement of subcrystals (white dashed line). D) Rhombohedral subcrystals (white arrow) visible on outer surface of composite crystal, yet no crystal habit discernible on fractured surface. E) Microporous composite crystals formed of subcrystals with perfect euhedral crystal terminations. Each crystal magnified in corresponding lettered image. F) Triangular microporous composite crystal with triangular subcrystals. G) Euhedral termination of composite crystal. Bright face has joined with adjacent subcrystals that have same crystallographic orientation (white arrow). H) Euhedral termination with triangular gap in crystal face. I) Three separate microporous composite crystals each with aligned subcrystals. Crytals 1 and 2 have *c* axes coming out of the page but *a* axes have different orientations. Crystal 3 has *c* axis oriented towards top of page. J) Top crystal has *c* axis aligned to right of image (white arrow). Bottom crystals have *c* axes directed out of the page. K) Composite crystals exhibiting features of compact and elongate composite crystals. L) Composite crystals whereby each subcrystal is elongate. M) Five separate elongate composite crystals as determined by subcrystal alignment. N) Elongate subcrystals with zig-zagging centerline along *c* axes. O) Elongate subcrystals with irregular, sinuous stems and well developed terminal crystal faces (white arrows). P) Imperfect, elongate subcrystals lacking well developed terminal crystal faces.

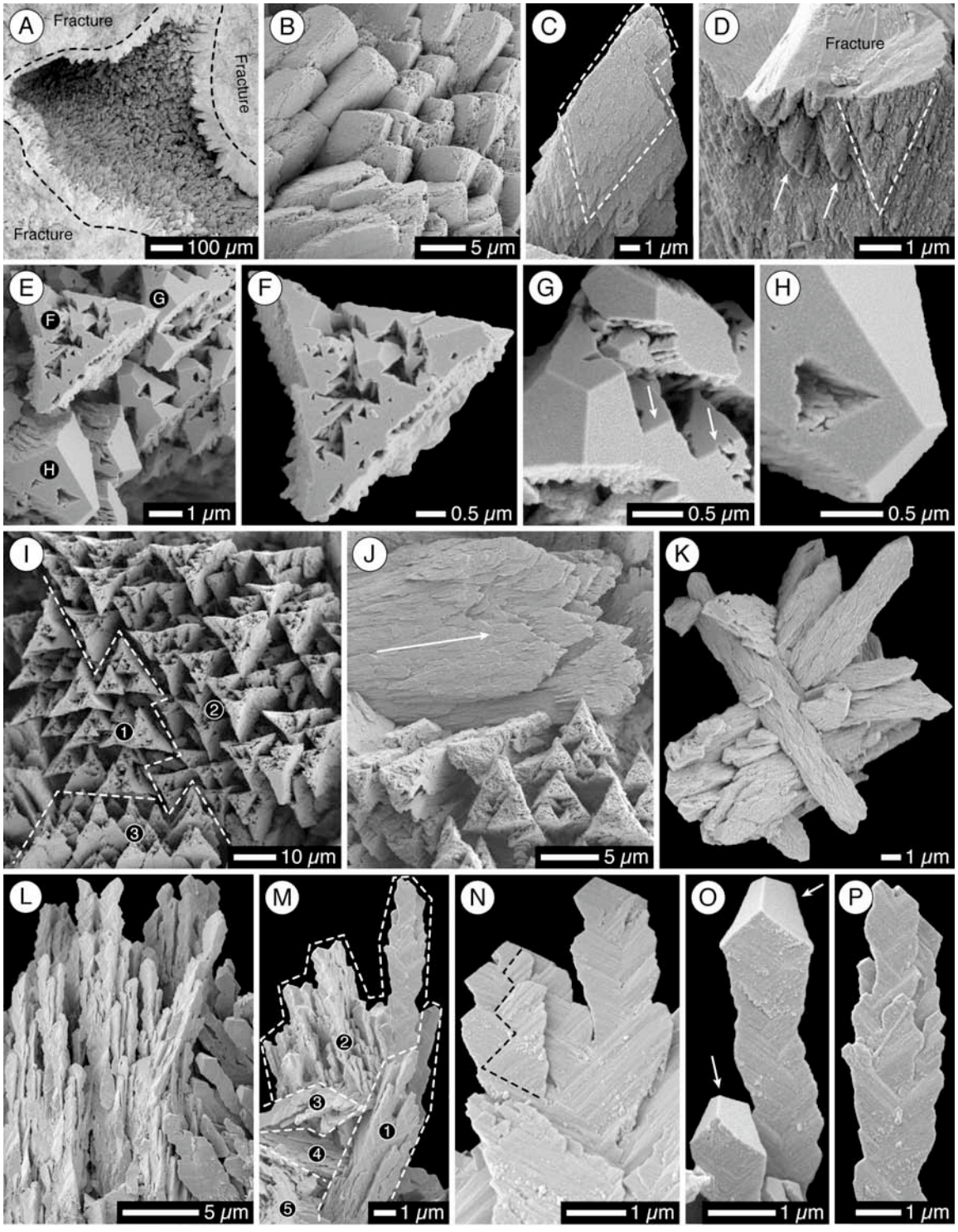
A
Fracture
Fracture
Fracture
100 μm
B
5 μm
C
1 μm
D
Fracture
1 μm
E
F
G
H
1 μm
F
0.5 μm
G
0.5 μm
H
0.5 μm
I
1
2
3
10 μm
J
5 μm
K
1 μm
L
5 μm
M
1
2
3
4
5
1 μm
N
1 μm
O
1 μm
P
1 μm

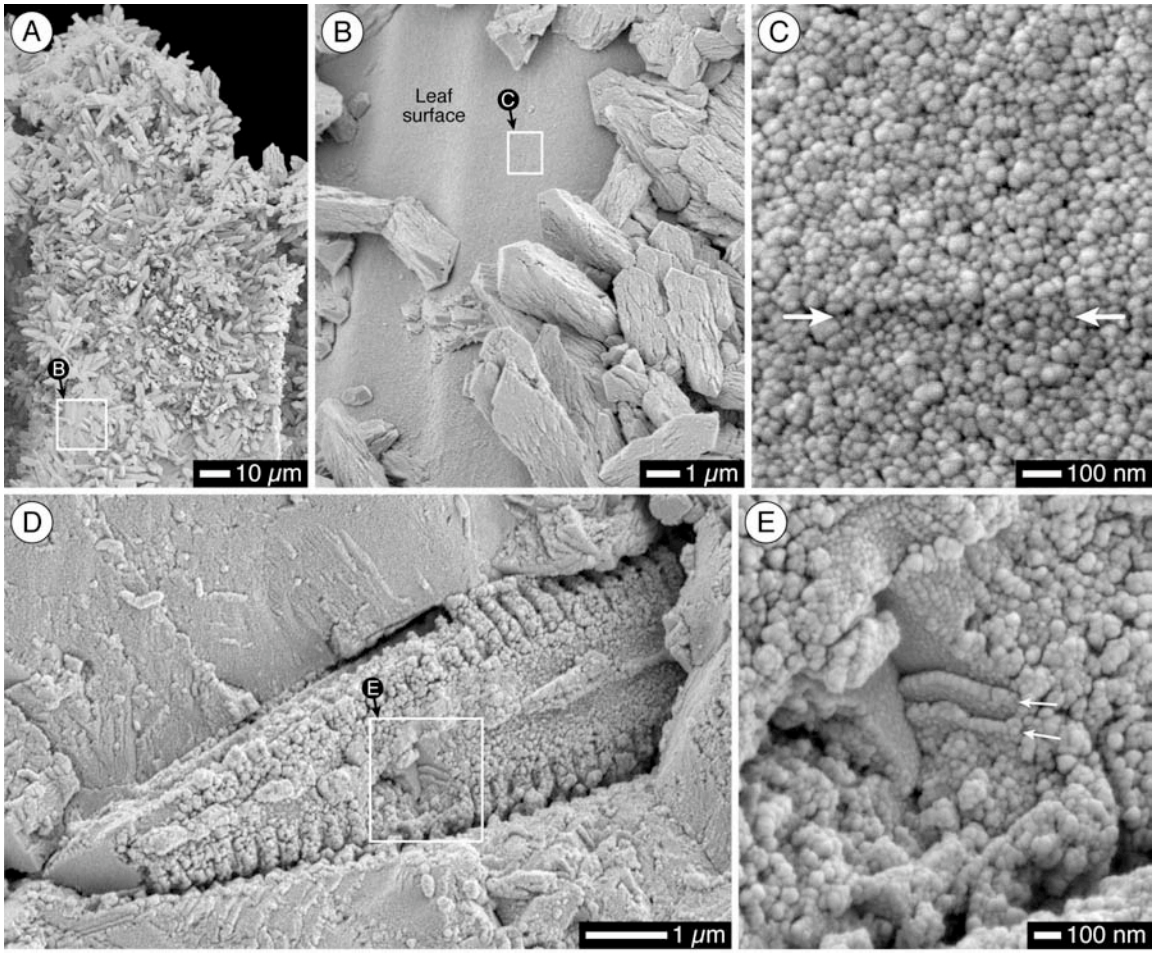

Fig. 5-5 SEM photomicrographs of nano-scale calcite on bryophyte leaf and in diatom mould. A) Bryophyte leaf almost entirely encrusted with composite calcite crystals with exception of region with white box. White box enlarged in B) shows nano-scale calcite. B) Area devoid of crystals enlarged in C) reveals a coating of nano-scale calcite on leaf surface. C) Spherical calcite bodies on leaf surface. White arrows highlight distortion caused by electron beam heating organic matter beneath nano-scale calcite coating. D) Internal mould of diatom frustule. Nano-scale calcite that preserved appearance of pore structure enlarged in E). E) Most nano-scale calcite lacks ordered arrangement with exception of few layered crystal faces developing (white arrows).

Compact composite crystals

Compact composite crystals are trigonal-shaped crystals with three main edges and faces that are convexly curved and meet in a single point at the tip of the crystal (Figs. 5-4A to D). Compact crystals lack microporosity and have tightly packed subcrystals with pointed euhedral crystal terminations. Compact composite crystals are longer than they are wide, and subcrystals have variably elongated *c* axes which caused them to stack on top of one another (offset by 1 to 3 μm wide steps). The composite crystals have a bimodal size distribution that reflects their formation as primary subcrystals, or primary and secondary subcrystals. Crystals with only primary subcrystals are 1 to 3 μm wide and 3 to 15 μm long, whereas crystals with primary and secondary subcrystals are 20 to 40 μm wide and 30 to 80 μm long. Primary subcrystals are the smallest, being 0.5 to 2 μm wide. Secondary subcrystals are larger, being 5 to 15 μm wide, and are formed of primary subcrystals. Few subcrystals exist that are 2 to 5 μm wide because crystals > 2 μm wide join adjacent subcrystals to form composite subcrystals > 5 μm wide.

Porous composite crystals

Porous composite crystals (20 to 40 μm wide and 30 to 80 μm long) have primary and secondary subcrystals (Figs. 5-4E to J). The secondary subcrystals, 5 to 15 μm wide, are formed of primary subcrystals, 0.5 to 2 μm wide. Adjacent subcrystals merged to form a composite crystal, but the subcrystals did not overlap and develop stepped faces like the compact crystals. As with the compact crystals, there are few subcrystals that are 2 to 5 μm wide because subcrystals > 2 μm wide joined adjacent subcrystals to form secondary subcrystals > 5 μm wide. Porous composite crystals contain numerous 2 to 5 μm wide triangular gaps systematically arranged between the secondary subcrystals. The gaps do not appear to have been filled by later cements. The secondary subcrystals may lack pointed euhedral crystal terminations, or have well-developed euhedral terminations. Porous composite crystals tend to be wider than they are long with all subcrystals exhibiting uniform *c* axis elongation.

Elongate composite crystals

Elongate composite crystals, 20 to 40 μm wide and 30 to 80 μm long, are formed solely of primary subcrystals (Figs. 5-4K to P). The subcrystals, 0.5 to 3 μm wide and 2 to 15 μm long, have a zig-zagging center-line with growth bands oriented ~ 45° to the *c* axis (Fig. 5-4N). Some subcrystals are straight, whereas others have a weakly sinuous habit (Fig. 5-4O). Likewise, some subcrystals have perfect euhedral rhombohedral terminations at the top of the elongate, irregular stem (Fig. 5-4O), whereas others have irregularly tapered terminations similar in appearance to the stem (Fig. 5-4P).

Nano-scale carbonate

Nano-scale carbonate, 20 to 80 nm in diameter, is subspherical and lacks a well-developed crystal habit (Fig. 5-5). Individual subspherical precipitates may form framboidal aggregates that are 50 to 150 nm in diameter. Little nano-scale carbonate was found in the Hot Creek deposit, being present only on a bryophyte leaf and forming an internal mould of a diatom frustule. The small amounts of nano-scale carbonate in the deposit may be a result of limited formation, or from being buried by subsequent composite calcite crystal formation. In the diatom mould, some nano-scale carbonate was arranged to form a crystalline edge (Fig. 5-5E). This suggests that $CaCO_3$ may have a critical size below which precipitates are non-crystalline and are unable to develop a crystalline form.

Biota

The Hot Creek deposit contains cyanobacteria, bryophytes, macrophytes, wood, and diatoms preserved by calcite, in addition to primary charcoal and wood. These organisms were preserved in different ways and each had different susceptibility for being preserved (Table 5-2).

Cyanobacteria

Filamentous microbes are the most abundant organisms preserved in the Hot Creek deposit and exhibit the most diverse modes of preservation (Figs. 5-6 to 5-8). External moulds are most common, followed by sheath casts, and rare

Table 5-2 Modes of preservation of biota contained in the Hot Creek carbonate spring deposit.

Organism	Mode of Preservation					
	Encrustation	Encapsulation	Permineralization	Sheath impregnation	Casts	Primary
Cyanobacteria	Yes	Yes		Rare	Yes	
Wood	Yes		Rare			Rare
Charcoal	Yes					Yes
Diatoms	Rare					
Macrophytes (plants)	Yes					
Bryophytes (mosses)	Yes					

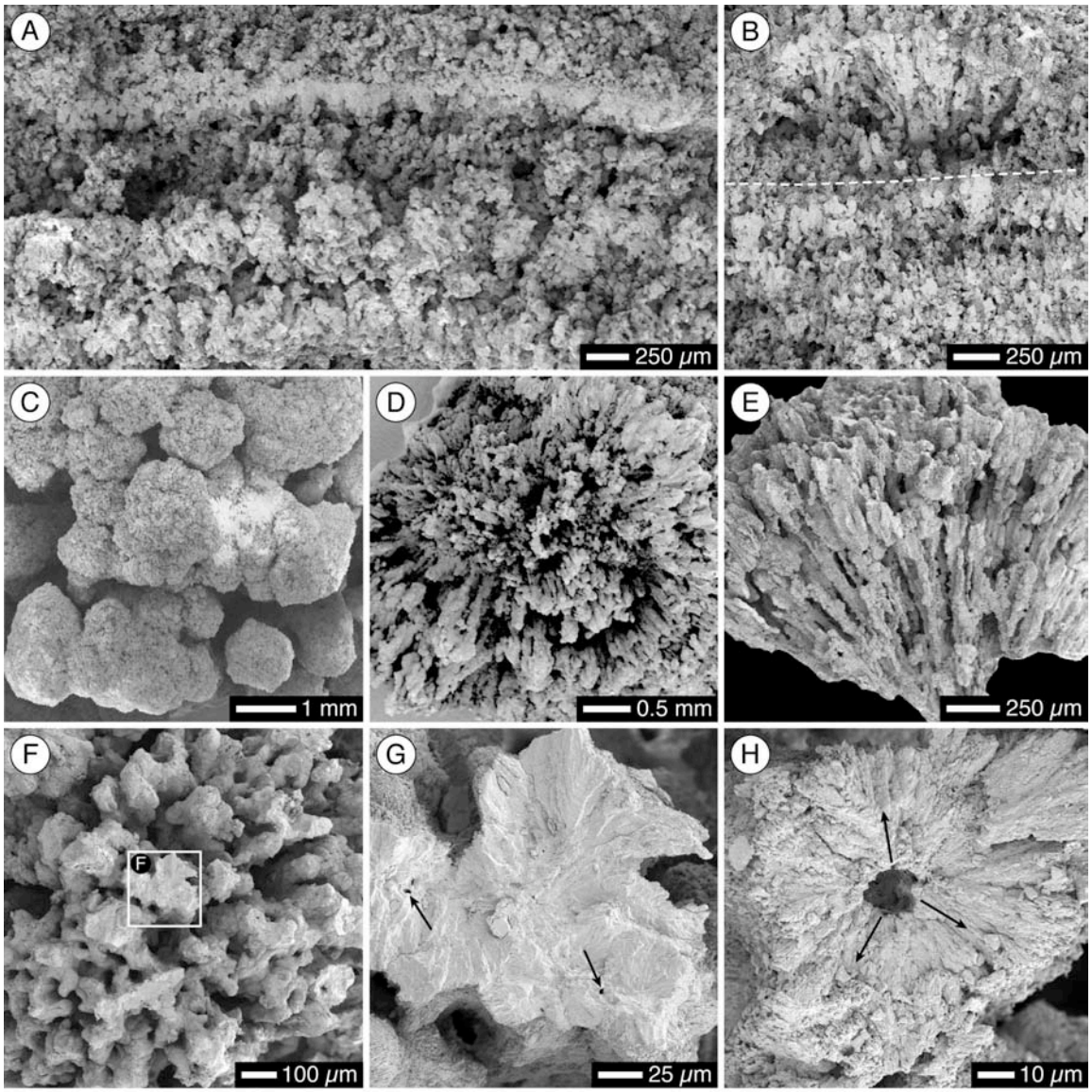

Fig. 5-6 SEM photomicrographs of cyanobacteria tufa. A) Laminations of preserved cyanobacateria visible due to porosity differences between layers. B) Mineralized hemispherical colony developed above laminations. C) Top view of hemispherical colonies. D) Magnified view of hemispherical colony showing radiating nature of filaments. E) Fractured hemispherical colony reveals radiating structure. F, G) Cyanobacteria encrustation moulds. H) Filament mould formed by encrustation. Black arrows show direction of crystal growth.

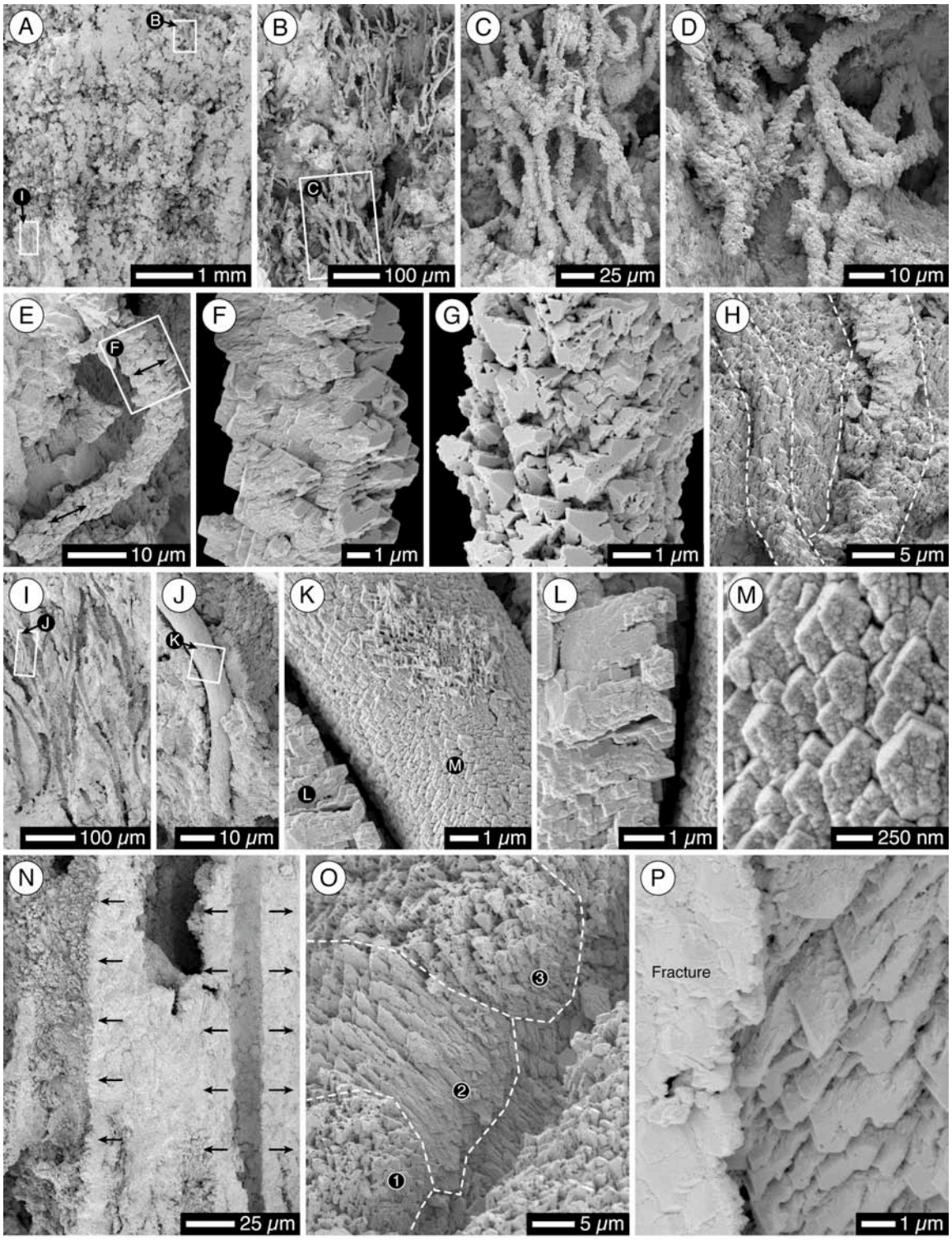
A
B
I
1 mm
B
C
100 μm
C
25 μm
D
10 μm
E
F
10 μm
F
1 μm
G
1 μm
H
5 μm
I
J
100 μm
J
K
10 μm
K
M
L
1 μm
L
1 μm
M
250 nm
N
25 μm
O
3
2
1
5 μm
P
Fracture
1 μm

Fig. 5-7 SEM photomicrographs of filamentous microbes preserved by calcite. A) Weak laminations visible due to slight porosity differences in cyanobacteria tufa. Upper white box indicates image magnified in B). Lower white box indicates image magnified in I). B) Sheath casts oriented perpendicular to bedding plane. White box indicates image magnified in C). C) Sheath casts are the same width as cyanobacteria trichomes and inner sheath diameters. D) Sheath casts randomly oriented along bedding plane. E) Curved sheath cast formed of a single composite crystal. Black arrows indicate orientation of subcrystal *c* axes. White box indicates image magnified in F). F) Sheath cast formed of subcrystals with *c* axes aligned from left to right. Note lack of septae preservation by calcite. G) Sheath cast lacking preserved septae. Subcrystals are aligned perpendicular to filament length and have *c* axes directed out of plane of page. H) Sheath casts (between white dashed lines) difficult to discern because filament subcrystals and substrate subcrystals are aligned. I) Crystalline lamination containing abundant filamentous microbe moulds, few of which contain sheath casts. Sheath cast in white box magnified in J). J) Sheath cast in mould. White box indicates image magnified in K). K) Sheath cast composed of finely crystalline subcrystals aligned parallel to filament length. Subcrystals magnified in M). Calcite crystals forming mould are larger than and have different orientation than filament subcrystals. Crystals forming mould magnified in L). L) Close-up of subcrystals forming mould. M) Close-up of subcrystals forming sheath cast. N) Encrustation mould on right and encapsulation mould on left. Encrustation mould formed by nucleation of calcite on outer sheath surface and crystal growth away from filament as indicated by black arrows. Encapsulation mould formed by growth of calcite crystals toward filament as indicated by black arrows. O) Encapsulation mould. White dashed lines outline three of the composite crystals that grew around a filament that has decayed, leaving mould. P) Magnified view of inner encapsulation mould surface. Direction of crystal growth was into mould (out of plane of page) indicating that crystals grew towards filament and did not nucleate on the sheath.

impregnated sheaths and filament casts. Preserved microbes are present as isolated erect or prostrate filaments in flat-lying laminations that are 100 μm to 1 mm thick (Figs. 5-6A,B), or as radiating masses of filaments arranged into hemispherical colonies that are 250 μm to 5 mm wide and 0.5 to 5 mm high (Figs. 5-6C to H). Comparisons to modern cyanobacteria from Hot Creek suggest that the filaments are *Lyngbya* and *Rivularia* (Figs. 5-3A to E).

The mode of cyanobacterial preservation was controlled by the location of calcite crystal nucleation in relation to the filament and the direction of crystal growth. Most filaments were preserved as external moulds, but two different processes produced these moulds. Calcite crystals that precipitated on a filament and grew away from it in a radiating manner formed encrustation moulds. Filament decay subsequent to encrustation left calcite crusts 20 to 100 μm in diameter with 5 to 15 μm diameter moulds at their centers (Figs. 5-6F,G and 5-8). Moulds that are < 10 μm in diameter probably formed by the encrustation of *Rivularia* trichomes, which regularly extend from the ends of the sheaths (Fig. 5-3D). Encapsulation moulds, 10 to 25 μm in diameter, are 5 to 15 μm larger than

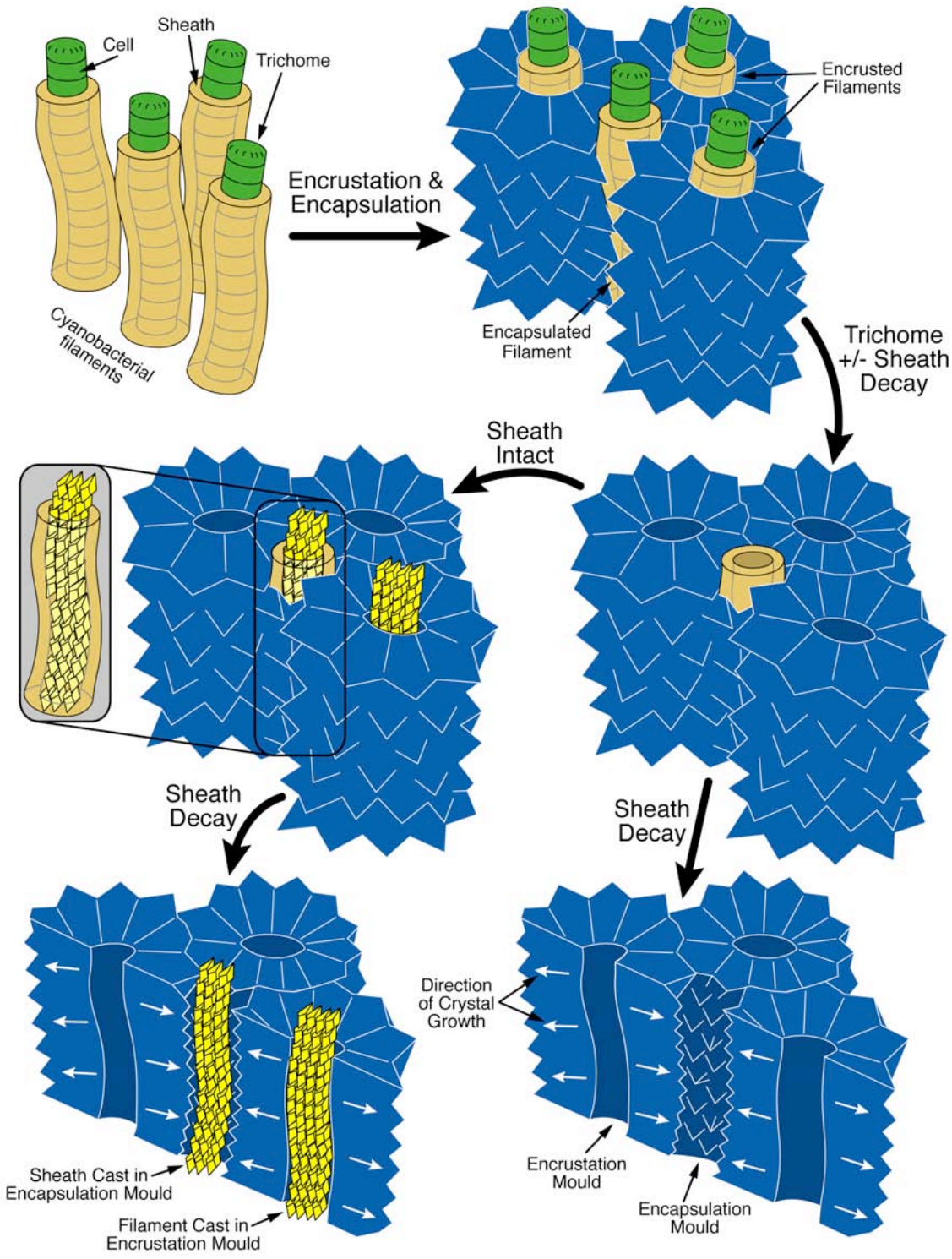

Fig. 5-8 Development of cyanobacteria tufa formed of encrustation moulds, encapsulation moulds, sheath casts, and filament casts.

the largest modern filaments and the largest encrustation moulds. They formed when a filament without encrusting calcite was trapped by calcite crystals that nucleated on, and grew from adjacent filaments (Figs. 5-7I to L, N to P). Encrustation moulds thus formed when calcite crystal growth was directed away from the filament, whereas encapsulation moulds formed from calcite crystal growth that was directed toward the filament (Fig. 5-8). Differences between encapsulation and encrustation moulds may be due to taxonomic differences between filaments, or could have resulted from changing the direction of calcite crystal growth in relation to the filament.

Sheath casts (4 to 10 μm wide) are present in encapsulation moulds and as free-standing structures in pores along laminations and in hemispherical colonies (Figs. 5-7A to M). The sheath casts may be formed of one or several composite crystals. Single crystal casts are formed of composite crystals with subcrystals 200 nm to 1 μm wide. The *c* axes of single crystal casts are generally, but not always, parallel to the length of the filament. Casts formed of several composite crystals have subcrystals with *c* axes that are oriented at variable angles to the filament length. Sheath casts in encapsulation moulds are formed of smaller crystals than those forming the mould, and the mould crystals have a different orientation than the cast crystals. Free-standing sheath casts are commonly formed of calcite crystals that are the same size and same orientation as the calcite crystals forming the lamination.

Filament casts have irregular margins, varying diameters along the length of the cast, and little to no space exists between the cast and the mould. Although rare, some cyanobacteria were preserved by sheath impregnation. The impregnated sheaths have external diameters of 10 to 15 μm and internal diameters of 5 to 10 μm.

None of the preserved cyanobacteria display septae or individual cells. This is probably due to calcite crystals utilizing external and internal sheath surfaces as nucleation sites, rather than trichomes. In effect, the inability of the calcite crystals to use individual cells and trichomes as templates prevented the preservation of cyanobacteria morphology at the cellular level.

Wood and charcoal

Preserved wood in the Hot Creek deposit is present mainly as moulds formed by its decay after being encrusted with calcite 50 μm to 1 cm thick. Most of the wood moulds are empty, but two contained small amounts of primary and permineralized wood (Figs. 5-2B and 5-9). Most of the permineralized wood cells are 20 to 30 μm wide, but some are up to 70 μm wide. The permineralized cells are much longer than they are wide, being 100 μm to 5 mm long. Permineralizing calcite nucleated on the interior of the cell wall and grew into the lumen at variable angles. Calcite commonly precipitated around the periphery of the lumen, but also variably filled the cells. Later decay of the cell wall left behind a rigid framework of permineralized cells. Calcite did not replace the cell wall, nor did it precipitate in or across the cell wall. Some calcite however, appears to have precipitated in place of the cell wall after decay of the organic matter. Charcoal fragments (< 5 mm long) are rare in the Hot Creek deposit, but were preserved by encrustation of the outer surface by calcite, with no subsequent decay or permineralization.

Macrophytes and bryophytes

All macrophytes (plants) and bryophytes (mosses) were preserved by encrustation by composite calcite crystals, with the exception of a single bryophyte leaf with a coating of nano-scale calcite (Figs. 5-5A to C and 5-10). The calcite crystals grew with their *c* axes (sub)perpendicular to the substrate and formed crusts 50 μm to 1 cm thick around the vegetable matter. As the crystals enlarged, they merged with adjacent crystals until the plants were completely encrusted. Calcite precipitated only on the external cell surfaces of leaves and stems, creating external moulds after the plants decayed. The inner surfaces of the moulds preserve excellent surface detail and macroscopic features such as leaf veins and micron-scale ribbing on stems. Discontinuous growth of large calcite crystals on the plant surface left gaps between the crystals, which generated incomplete imprints of the plant surface.

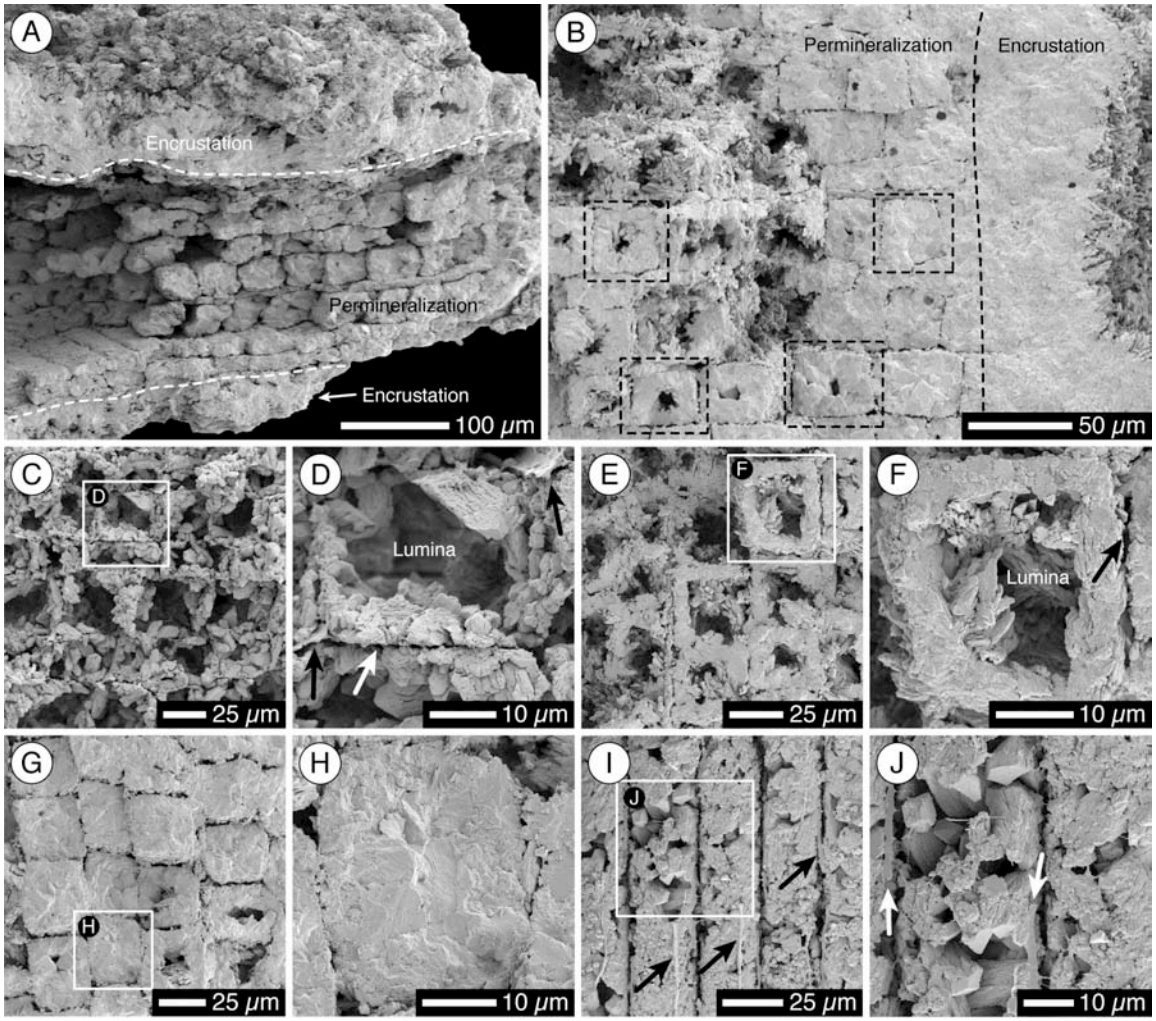

Fig. 5-9 SEM photomicrographs of preserved wood. A) Fragment of permineralized wood encrusted by calcite. B) Calcite encrusting permineralized wood cells that have been filled to varying degrees by calcite. Black dashed boxes outline examples of individual permineralized cells. C) Porous network of calcite crystals formed by few calcite crystals precipitating in cell lumen. White box indicates image magnified in D). D) Close up of cell showing calcite around periphery of inner cell wall. Most cell walls (black arrow) have decayed leaving thin mould (white arrow). E) Calcite crystals coating inner cell wall surfaces. White box indicates image magnified in F). F) Calcite crystals formed at various angles to the inner cell wall surface. G) Cells completely filled by calcite and all cell wall material decayed. White box indicates image magnified in H). H) Cell completely filled with calcite and no crystal habit discernible. I) Parallel alignment of elongate permineralized wood cells. Black arrows highlight ribs of cell wall not yet decayed. White box indicates image magnified in J). J) White arrows indicate cell wall material remaining between permineralized cells.

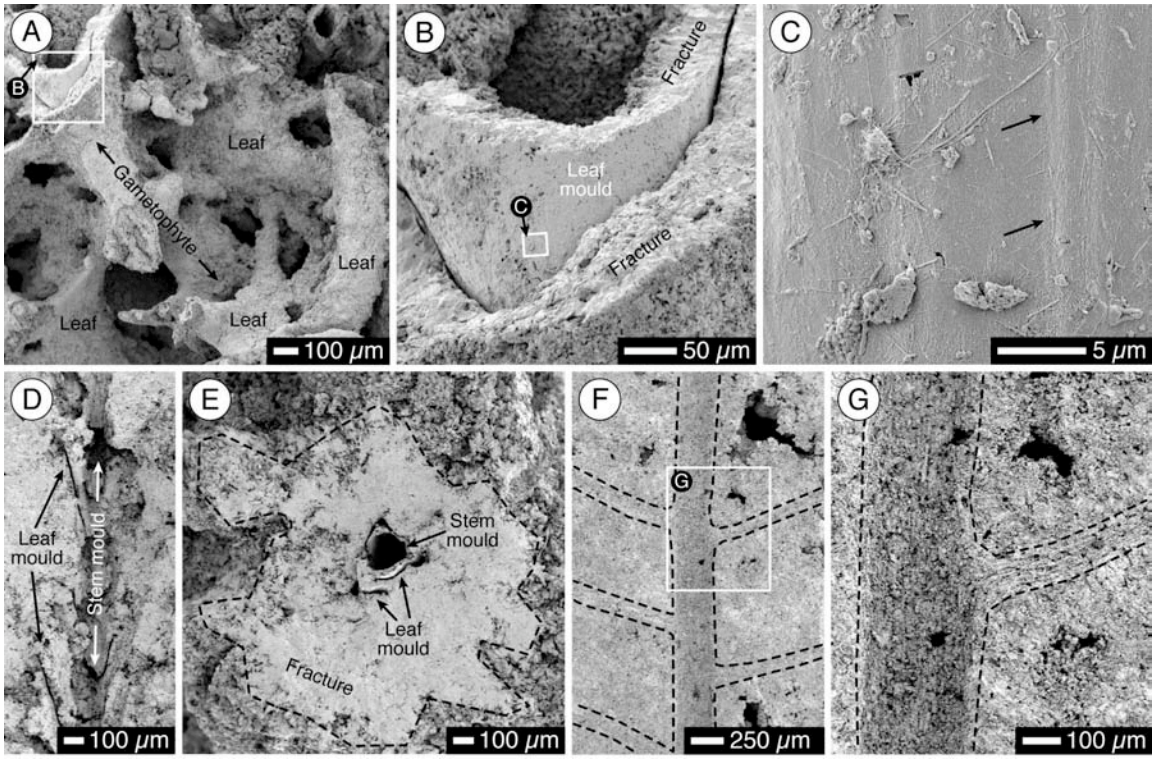

Fig. 5-10 SEM photomicrographs of bryophyte (moss) and macrophyte (plant) moulds. A) Encrusted bryophyte gametophytes (analogous to plant stems) and leaves. White box indicates fractured leaf mould encrustation magnified in B). B) Bryophyte leaf mould showing thickness of calcite encrustation. White box indicates Basal surface of calcite encrustation magnified in C). C) No calcite crystal habit visible on surface of mould, but textural ridges from bryophyte leaf still preserved (black arrow). D) Longitudinal view through bryophyte mould preserved in massive calcite. E) Transverse view looking down on bryophyte mould showing thickness of calcite encrustation. F) Macrophyte (plant) leaf mould with morphology of vein system preserved. White box indicates image magnified in G). G) Magnified view showing branching nature of vein system.

Diatoms

Diatoms are abundant in modern microstromatolites, but preserved diatoms are rare in the relict tufa. Only a single diatom mould was discovered, and no siliceous diatom tests were found (Figs. 5-5D,E). The external mould is preserved in solid, nearly featureless crystalline calcite with scattered rhombohedral crystal faces being visible. An internal mould of the diatom formed of nano-scale calcite preserved pores and ornamentation of the diatom frustule.

Discussion

Normally, biomineralized parts (e.g. shell, bone, teeth) are readily preserved because they are hard and durable, whereas easily degradable, delicate soft tissues are not. In the relict Hot Creek carbonate deposit, the opposite is true – organisms composed of hard or supposedly durable compounds were not as well preserved as soft-tissue organisms. Diatoms, for example, are virtually nonexistent in the relict Hot Creek deposit, despite having hard, siliceous frustules, whereas cyanobacterial filaments with mucilaginous extracellular sheaths were readily preserved, and are the most abundant organisms in the deposit. Preferential preservation of soft-tissue organisms in the relict Hot Creek deposit shows that hardness does not equate to durability, because given the appropriate environment, delicate structures may express exceptional decay resistance and be preserved (Schopf 1975).

Calcite precipitating in or on an organism creates a "mineral replica," whose resolution is dependent upon the amount of detail preserved. The level of detail preservation is largely controlled by crystal size relative to the size of the tissues or cells being mineralized. Crystals or precipitates that are smaller than the cells or their organelles are capable of preserving greater internal cellular detail than crystals that are larger than the cells (e.g. Jones and Renaut 2007). The inverse relationship between smaller crystal size and increased resolution is "…analogous to the impact of pixel number on the clarity of computer images" (Briggs 2003). Despite the finely crystalline nature of calcite forming the Hot Creek deposit, much cellular detail was lost during mineralization, suggesting that

nucleation site location is more important than crystal size for controlling the quality of preservation (cf. Carson 1991).

In the Hot Creek deposit, organisms that facilitated rapid mineral precipitation, like the non-obligate calcifying cyanobacteria *Lyngbya* and *Rivularia* (Pentecost and Riding 1986), had greater structural detail preserved during deposit formation than other organisms that grew in and around the spring water. Filamentous microbes lack hard features such as shells, woody cell walls or waxy cuticles, which suggests that at Hot Creek, hardness was an impediment to mineralization. The differences in preservation potential of the Hot Creek flora can largely be attributed to the various organisms having different nucleation sites upon which calcite could precipitate. Factors that directly controlled where calcite could nucleate include cell structure, composition, and the balance between biotic decay rates and calcite precipitation rates.

All organisms in the relict Hot Creek deposit were preserved by precipitation of calcite on the outermost surface of the organism (encrustation), around the organism but not on it (encapsulation), within spaces once occupied by decayed organisms (casts), or within empty cells and interstices (permineralization). Although rare in the Hot Creek deposit, sheath impregnation is a common mode of microbial preservation in other calcite, iron and silica precipitating systems (e.g. Ferris et al. 1988; Merz 1992; Renaut et al. 1998; Walter et al. 1998; Jones et al. 2001). Each mode of preservation at Hot Creek carried a different capacity for preserving detail. Encrustation and encapsulation made imprints of the exterior surface morphology of the organism, but did not preserve any interior detail. Encrusting calcite used the outer surfaces of organisms as templates upon which crystals nucleated and grew, which allowed for the formation of moulds with exquisite surface detail preservation (e.g. macrophyte leaves and bryophytes). In contrast, encapsulating calcite crystals did not nucleate on organisms' outer surfaces, and were thus only able to roughly mimic their form. Filament casts copied encrustation moulds and sheath casts copied the interior of intact sheaths that lacked a trichome, whereas permineralization copied the interior of dead wood cells.

Diatoms are the only organisms living at Hot Creek that contain biomineralized parts, yet siliceous tests or calcite copies of diatoms are virtually nonexistent in the relict deposit. High levels of alkalinity and basic pH levels promote calcite precipitation, but readily cause dissolution of diatom silica (Flower 1993; Barker et al. 1994; Ryves et al. 2006). The presence of Ca^{2+} and Mg^{2+} as the major ionic species in the spring water further drive diatom frustule dissolution (Barker et al. 1994), whereas many other metals in solution (e.g. Al, Be, Fe) are capable of binding with SiO_2 and retarding diatom dissolution (Lewin 1961). In other calcite-precipitating springs, low concentrations of non-Ca^{2+} and Mg^{2+} metals can facilitate diatom preservation by minerals such as barite (Bonny and Jones 2007). In the relict Hot Creek deposit, high pH, strong alkalinity and a lack of dissolved elements besides Ca^{2+} and Mg^{2+} promoted rapid dissolution of diatom frustules and prevented their preservation.

Despite being the hardest and most durable of the soft-tissue organisms in the Hot Creek deposit, wood had low preservation potential, and only rarely was any internal cellular detail maintained. Permineralized wood is rare in carbonate spring deposits, and has never before been reported from any western Canadian spring deposits. Wood is formed of several cell types with varying forms, functions and compositions, with most being characterized as either vascular or supportive. The cell walls of vascular tissues are formed of cellulose and are relatively soft, whereas supportive fibers have lignified cells walls that are hard and tough (Leo and Barghoorn 1976; Raven et al. 1999). The size and morphology of the permineralized wood cells in the Hot Creek deposit suggests that they are support fibers that had lignified cell walls. Most of the wood in the Hot Creek deposit decayed without being preserved because the cellulose-rich cell walls rapidly decayed, whereas the lignin in the fiber cell walls resisted decay long enough to allow calcite to precipitate in the lumen. Preferential permineralization of supportive wood cells over vascular cells is the only example of more durable, decay-resistant cells being favoured over less durable cells during preservation at Hot Creek.

The main factor that contributed to the poor preservation of wood, macrophytes, and bryophytes was the inability of mineral-precipitating fluids to penetrate durable cell walls. Calcite readily precipitated on the outer surface of the plants, but could not penetrate the waxy cuticle until a certain amount of decay occurred to increase permeability (cf. Leo and Barghoorn 1976). By the time mineralizing fluids were able to penetrate the waxy cuticle, the inner cells had already decayed. Most preservation of wood, macrophytes and bryophytes occurred post-mortem and was restricted to outer cell surfaces, making it a simpler process than cyanobacterial preservation.

Cyanobacterial preservation was a complex process because cyanobacteria could be mineralized while dead or alive, and mineralization was commonly associated with the sheath, rather than the cells. The affinity of extracellular substances for binding divalent metal cations has been well established (e.g. Lowenstam 1981; Beveridge 1989; Ferris et al. 1988; Schultze-Lam et al. 1995; Phoenix et al. 2000), and extracellular mineral precipitation was by far the most common mode of cyanobacterial preservation in the Hot Creek deposit. Cast formation was less common and presumably occurred after cell death.

The commonality of species-specific cyanobacteria preservation shows that taxonomy can exert a strong influence on their modes of preservation (e.g. Riding 1977; Jones and Kahle 1986; Pentecost and Riding 1986; Freytet and Plet 1996). In the Hot Creek deposit, however, filaments adjacent to each other (microns apart) in colonies of apparently similar cyanobacteria show different modes of preservation. Thus, it cannot be assumed that differing modes of cyanobacterial preservation automatically imply taxonomic differences. This is perhaps best illustrated by work on mineralization of living cyanobacteria by Merz-Preiß and Riding (1999), who showed that physicochemical calcite precipitation under high supersaturation conditions caused sheath encrustation, whereas photosynthetic bicarbonate uptake under low supersaturation conditions caused sheath impregnation. The ubiquitous nature of encrusted and encapsulated filaments and the deficiency of impregnated sheaths in the relict Hot Creek deposit suggests that the cyanobacteria did not induce microenvironmental

changes in their surroundings that facilitated preservation (cf. Merz 1992; Merz-Preiß and Riding 1999; Bissett et al. 2008).

Hot Creek cyanobacteria were encrusted and encapsulated while alive, whereas post-mortem preservation was restricted to formation of sheath casts and filament casts. Calcite precipitation readily occurs on and within the sheaths of many cyanobacteria species, yet seems to be inhibited from forming on the cells of the trichome (Merz 1992). After trichomes of the Hot Creek cyanobacteria decayed, the hollow sheaths remained intact long enough for calcite to be precipitated inside (cf. Gerdes et al. 1994; Freytet and Plet 1996; Arp et al. 2001). Dessicated filaments rapidly collapse, so in order for the Hot Creek sheaths to have remained intact long enough for calcite to precipitate inside, they must have remained in a subaqueous environment throughout mineralization, or were very rapidly mineralized. Maintaining an open sheath while simultaneously destroying the trichome was likely facilitated by encapsulation of the filament while it was living. Moulds formed by filament encrustation never housed sheath casts, suggesting that encrustation was an impediment to sheath preservation. Encapsulation moulds commonly contain sheath casts, indicating that moulds formed without calcite nucleating on the outer surface of the sheath provided support for the filaments and aided sheath preservation for later filling with calcite.

The excellent preservation of sheath morphology by sheath casts in the Hot Creek deposit suggests that heterotrophic decay bacteria were not abundant and did not significantly contribute to microenvironmental changes around cyanobacteria being preserved by calcite (cf. Bartley 1996). Briggs (2003) specifically implicated heterotrophic decay bacteria as being important for increasing porosity and permeability during biotic preservation, and for setting geochemical conditions that are favourable to mineral precipitation during diagenesis. It is difficult to establish the importance of decay bacteria on preservation processes in the Hot Creek deposit because of the lack of non-filamentous microbes preserved with the calcite crystals. Mucous coatings are common in the modern hemispherical microstromatolites, yet are rare in the relict

tufa. This could mean that most soft-tissue decay was attributable to abiotic processes, or that no evidence of decay bacteria was preserved. Arp et al. (2001) found, however, that decay bacteria consuming cyanobacterial cells and sheaths decreased $CaCO_3$ saturation. Although sheath casts are approximately the same width as filament trichomes, they lack any evidence of having conformed to the septate structure of the cells forming the trichome. This suggests that calcite precipitated in the hollow sheaths after death and decay of the trichome. It has also been established that sheaths can remain intact well after trichome decay (Golubic and Hofmann 1976; Bartley 1996). Leo and Barghoorn (1976) go so far as to suggest that sheath material may be as chemically and morphologically resistant to decay as lignin and cellulose in wood. All of this evidence suggests that cyanobacterial sheaths, despite not being biomineralized hard parts, were the most durable tissues present in the Hot Creek spring system, which allowed their delicate structure to be preserved by calcite.

Although their sizes and orientations may differ, the calcite crystals that precipitated in empty sheaths have similar habits to the calcite crystals that encrusted and encapsulated all biota. This indicates a similar fluid chemistry for all calcite precipitation in the Hot Creek deposit and that localized microenvironmental changes in the vicinity of the filaments were not important for driving their calcification. Variable forms of composite calcite crystals and the existence of some impregnated sheaths suggest that spring water chemistry did occasionally change, and may have caused minor changes in the modes of preservation through time.

Conclusions

- Preservation styles at Hot Creek were controlled by morphologic differences in the floral organisms that grew in and adjacent to the spring, however, taxonomic differences between related organisms (e.g. *Rivularia* and *Lyngbya*) did not influence calcite precipitation.
- The variable modes of preservation displayed in the Hot Creek deposit resulted from the competition between calcite precipitation rates and biotic

decay processes, and in the case of cyanobacteria, whether calcite precipitation occurred pre- or post-mortem.

- The hardest organisms (diatoms, wood, macrophytes, bryophytes) were the least durable organisms and were the least likely to exhibit exceptional preservation during deposit formation because of the extensive decay required for the mineral-bearing fluids to permeate the tissues.
- The lack of sheath impregnation indicates that cyanobacterial photosynthesis and other metabolic processes did not contribute to calcite precipitation.
- The preservation of a delicate sheath after trichome decay suggests that decay bacteria had little effect on taphonomic processes.

References

Allen, D.M., Grasby, S.E., Voormeij, D.A., 2006. Determining the circulation depth of thermal springs in the southern Rocky Mountain Trench, south-eastern British Columbia, Canada using geothermometry and borehole temperature logs. Hydrogeology Journal, 14: 159-172.

Allen, E.T., Day, A.L., 1935. Hot Springs of the Yellowstone National Park, Publication No. 466. Carnegie Institution of Washington, Washington, 525 pp.

Allison, P.A., Briggs, D.E.G., 1993. Exceptional fossil record; distribution of soft-tissue preservation through the Phanerozoic. Geology, 21(6): 527-530.

Arp, G., Wedemeyer, N., Reitner, J., 2001. Fluvial tufa formation in a hard-water creek (Deinschwanger Bach, Franconian Alb, Germany). Facies, 44: 1-22.

Barker, P., Fontes, J.-C., Gasse, F., Druart, J.-C., 1994. Experimental dissolution of diatom silica in concentrated salt solutions and implications for paleoenvironmental reconstruction. Limnology and Oceanography, 39(1): 99-110.

Bartley, J.K., 1996. Actualistic taphonomy of cyanobacteria: implications for the Precambrian fossil record. Palaios, 11: 571-586.

Beaudoin, A.B., King, R.H., 1990. Late Quaternary vegetation history of Wilcox Pass, Jasper National Park, Alberta. Palaeogeography, Palaeoclimatology, Palaeoecology, 80: 129-144.

Beveridge, T.J., 1989. Role of cellular design in bacterial metal accumulation and mineralization. Annual Review of Microbiology, 43: 147-171.

Bissett, A., Reimer, A., de Beer, D., Shiraishi, F., Arp, G., 2008. Metabolic microenvironmental control by photosynthetic biofilms under changing macroenvironmental temperature and pH conditions. Applied and Environmental Microbiology, 74(20): 6306-6312.

Bonny, S., 2002. Relic tufa at Miette Hot Springs, Jasper National Park, Alberta. M.Sc. Thesis, University of Alberta, Edmonton.

Bonny, S., Jones, B., 2003a. Microbes and mineral precipitation, Miette Hot Springs, Jasper National Park, Alberta, Canada. Canadian Journal of Earth Sciences, 40: 1483-1500.

Bonny, S., Jones, B., 2003b. Relict tufa at Miette Hot Springs, Jasper National Park, Alberta, Canada. Canadian Journal of Earth Sciences, 40: 1459-1481.

Bonny, S.M., Jones, B., 2007. *Diatom*-mediated barite precipitation in microbial mats calcifying at Stinking Springs, a warm sulphur spring system in northwestern Utah, USA. Sedimentary Geology, 194(3-4): 223-244.

Briggs, D.E.G., 2003. The role of decay and mineralization in the preservation of soft-bodied fossils. Annual Review of Earth & Planetary Sciences, 31: 275-301.

Carson, G.A., 1991. Silicification of fossils. In: P.A. Allison and D.E.G. Briggs (Editors), Taphonomy: releasing the data locked in the fossil record. Plenum Press, New York, pp. 455-499.

Chafetz, H.S., Folk, R.L., 1984. Travertines: depositional morphology and the bacterially constructed constituents. Journal of Sedimentary Petrology, 54(1): 289-316.

Clark, I., Fritz, P., Michel, F., Souther, J.G., 1982. Isotope hydrology and geothermometry of the Mt. Meager geothermal area. Canadian Journal of Earth Sciences, 19: 1454-1473.

Ferris, F.G., Fyfe, W.S., Beveridge, T.J., 1988. Metallic ion binding by *Bacillus subtilis*: implications for the fossilization of microorganisms. Geology, 16: 149-152.

Flower, R.J., 1993. Diatom preservation: experiments and observations on dissolution and breakage in modern and fossil material. Hydrobiologia, 269/270: 473-484.

Freytet, P., Plet, A., 1996. Modern freshwater microbial carbonates: the *Phormidium* stromatolites (tufa-travertine) of southeastern Burgundy (Paris Basin, France). Facies, 34: 219-238.

Fulton, R.J., 1971. Radiocarbon geochronology of southern British Columbia. Geological Survey of Canada Paper 71-37: 28.

Gerdes, G., Dunajtschik-Piewak, K., Riege, H., Taher, A.G., Krumbein, W.E., Reineck, H.-E., 1994. Structural diversity of biogenic carbonate particles in microbial mats. Sedimentology, 41: 1273-1294.

Given, R.K., Wilkinson, B.H., 1985. Kinetic control of morphology, composition, and mineralogy of abiotic sedimentary carbonates. Journal of Sedimentary Petrology, 55(1): 109-119.

Golubic, S., Seong-Joo, L., Browne, K.M., 2000. Cyanobacteria: architects of sedimentary structures. In: R.E. Riding and S.M. Awramik (Editors), Microbial Sediments. Springer-Verlag, Berlin, pp. 57-67.

Grasby, S.E., Hutcheon, I., 2001. Controls on the distribution of thermal springs in the southern Canadian Cordillera. Canadian Journal of Earth Sciences, 38: 427-440.

Grasby, S.E., Hutcheon, I., Krouse, H.R., 2000. The influence of water-rock interaction on the chemistry of thermal springs in western Canada. Applied Geochemistry, 15: 439-454.

Grasby, S.E., van Everdingen, R.O., Bednarski, J., Lepitzki, D.A.W., 2003. Travertine mounds of the Cave and Basin National Historic Site, Banff National Park. Canadian Journal of Earth Sciences, 40: 1501-1513.

Irion, G., Müller, G., 1968. Mineralogy, petrology and chemical composition of some calcareous tufa from the Schwäbische Alb, Germany. In: G. Müller and G.M. Friedman (Editors), Recent Developments in Carbonate Sedimentology in Central Europe. Springer Verlag, New York, pp. 157-171.

Jones, B., 1989. Calcite rafts, peloids and micrite in cave deposits from Cayman Brac, British West Indies. Canadian Journal of Earth Sciences, 26(4): 654-664.

Jones, B., Kahle, C.F., 1986. Dendritic calcite crystals formed by calcification of algal filaments in a vadose environment. Journal of Sedimentary Petrology, 56(2): 217-227.

Jones, B., Renaut, R.W., 2007. Selective mineralization of microbes in Fe-rich precipitates (jarosite, hydrous ferric oxides) from acid hot springs in the Waiotapu geothermal area, North Island, New Zealand. Sedimentary Geology, 194: 77-98.

Jones, B., Renaut, R.W., 2008. Cyclic development of large, complex, calcite dendrite crystals in the Clinton travertine, Interior British Columbia, Canada. Sedimentary Geology, 203: 17-35.

Jones, B., Renaut, R.W., Rosen, M.R., 2001. Microbial construction of siliceous stalactites at geysers and hot springs: examples from the Whakarewarewa geothermal area, North Island, New Zealand. Palaios, 16: 73-94.

Kearney, M.S., Luckman, B.H., 1983a. Holocene timberline fluctuations in Jasper National Park, Alberta. Science, 221(4607): 261-263.

Kearney, M.S., Luckman, B.H., 1983b. Postglacial vegetational history of Tonquin Pass, British Columbia. Canadian Journal of Earth Sciences, 20: 776-786.

Koban, C.G., Schweigert, G., 1993. Microbial origin of travertine fabrics -- two examples from southern Germany (Pleistocene Stuttgart travertines and Miocene Riedöschingen travertine). Facies, 29: 251-264.

Langelier, W.F., 1936. The analytical control of anticorrosion water treatment. Journal of the American Water Works Association, 28: 1500-1521.

Leo, R.F., Barghoorn, E.S., 1976. Silicification of wood. Harvard University Botanical Museum Leaflets, 25: 1-47.

Lewin, J.C., 1961. The dissolution of silica from diatom walls. Geochimica et Cosmochimica Acta, 21: 182-198.

Lowenstam, H.A., 1981. Minerals formed by organisms. Science, 211(4487): 1126-1131.

Luckman, B.H., Kearney, M.S., 1986. Reconstruction of Holocene changes in alpine vegetation and climate in the Maligne Range, Jasper National Park, Alberta. Quaternary Research, 26: 244-261.

Luckman, B.H., Holdsworth, G., Osborn, G.D., 1993. Neoglacial glacier fluctuations in the Canadian Rockies. Quaternary Research, 39: 144-153.

MacDonald, G.M., 1989. Postglacial palaeoecology of the subalpine forest - grassland ecotone of southwestern Alberta: new insights on vegetation and climate change in the Canadian Rocky Mountains and adjacent foothills. Palaeogeography, Palaeoclimatology, Palaeoecology, 73: 155-173.

Merz, M.U.E., 1992. The biology of carbonate precipitation by cyanobacteria. Facies, 26: 81-102.

Merz-Preiß, M., Riding, R., 1999. Cyanobacterial tufa calcification in two freshwater streams: ambient environment, chemical thresholds and biological processes. Sedimentary Geology, 126: 103-124.

Nowak, J., Florek, M., Kwiatek, W., Lekki, J., Chevallier, P., Zieba, E., Mestres, N., Dutkiewicz, E.M., Kuczumow, A., 2005. Composite structure of wood cells in petrified wood. Materials Science and Engineering, C 25: 119-130.

Oehler, J.H., Schopf, J.W., 1971. Artificial microfossils: experimental studies of permineralization of blue-green algae in silica. Science, 174(4015): 1229-1231.

Pedley, H.M., 2000. Ambient temperature freshwater microbial tufas. In: R.E. Riding and S.M. Awramik (Editors), Microbial Sediments. Springer-Verlag, Berlin, pp. 179-186.

Pentecost, A., 1978. Blue-green algae and freshwater carbonate deposits. Proceedings of the Royal Society of London, Series B: Biological Sciences, 200(1138): 43-61.

Pentecost, A., 1996. Moss Growth and Travertine Deposition: The Significance of Photosynthesis, Evaporation and Degassing of Carbon Dioxide. Journal of Bryology, 19: 229-234.

Pentecost, A., 2003. Cyanobacteria associated with hot spring travertines. Canadian Journal of Earth Sciences, 40: 1447-1457.

Pentecost, A., Riding, R., 1986. Calcification in cyanobacteria. In: B.S.C. Leadbeater and R. Riding (Editors), Biomineralization in lower plants and animals: proceedings of an international symposium held at the University of Birmingham, April 1985. Oxford University Press, New York, pp. 73-90.

Pentecost, A., Coletta, P., 2007. The role of photosynthesis and CO_2 evasion in travertine formation: a quantitative investigation at an important travertine-depositing hot spring, Le Zitelle, Italy. Journal of the Geological Society, London, 164: 843-853.

Phoenix, V.R., Adams, D.G., Konhauser, K.O., 2000. Cyanobacterial viability during hydrothermal biomineralisation. Chemical Geology, 169: 329-338.

Porter, S.C., Denton, G.H., 1967. Chronology of the Neoglaciation in the North American Cordillera. American Journal of Science, 265: 177-210.

Rainey, D.K., Jones, B., 2007. Rapid cold water formation and recrystallization of relict bryophyte tufa at the Fall Creek cold springs, Alberta, Canada. Canadian Journal of Earth Sciences, 44: 889-909.

Rainey, D.K., Jones, B., 2009. Abiotic versus biotic controls on the development of the Fairmont Hot Springs carbonate spring deposit, British Columbia, Canada. Sedimentology, doi: 10.1111/j.1365-3091.2009.01059.x.

Raven, P.H., Evert, R.F., Eichhorm, S.E., 1999. Biology of Plants, Sixth Edition. W.H. Freeman and Company, New York.

Reimer, P., Baillie, M., Bard, E., Bayliss, A., Beck, J., Bertrand, C., Blackwell, P., Buck, C., Burr, G., Cutler, K., Damon, P., Edwards, R., Fairbanks, R., Friedrich, M., Guilderson, T., Hughen, K., Southon, J., Stuiver, M., Talamo, S., Taylor, F., van der Plicht, J., Weyhenmeyer, C., 2004. IntCal04 Terrestrial radiocarbon age calibration, 26-0 ka BP. Radiocarbon, 46: 1029-1058.

Renaut, R.W., Long, P.R., 1986. Post-glacial travertine deposits of the Clinton area, interior British Columbia, GAC, MAC, CGU Joint Annual Meeting Program With Abstracts. Carleton University, Ottawa, Canada, pp. 117.

Renaut, R.W., Jones, B., 2000. Microbial precipitates around continental hot springs and geysers. In: R.E. Riding and S.M. Awramik (Editors), Microbial Sediments. Springer-Verlag, Berlin, pp. 187-195.

Renaut, R.W., Jones, B., Tiercelin, J.-J., 1998. Rapid *in situ* silicification of microbes at Loburu hot springs, Lake Bogoria, Kenya Rift Valley. Sedimentology, 45: 1083-1103.

Reneau, S.L., Katzman, D., Kuyumjian, G.A., Lavine, A., Malmon, D.V., 2007. Sediment delivery after a wildfire. Geology, 35(2): 151-154.

Riding, R., 1977. Calcified *Plectonema* (blue-green algae), a recent example of *Girvanella* from Aldabra Atoll. Palaeontology, 20: 33-46.

Ritchie, J.C., Cwynar, L.C., Spear, R.W., 1983. Evidence from north-west Canada for an early Holocene Milankovitch thermal maximum. Nature, 305: 126-128.

Ryves, D.B., Battarbee, R.W., Juggins, S., Fritz, S.C., Anderson, N.J., 2006. Physical and chemical predictors of diatom dissolution in freshwater and saline lake sediments in North America and West Greenland. Limnology and Oceanography, 51(3): 1355-1368.

Sandberg, P., 1985. Aragonite cements and their occurrence in ancient limestones. In: N. Schneidermann and P.M. Harris (Editors), Carbonate Cements: SEPM, Special Publication 36, pp. 33-57.

Schopf, J.M., 1975. Modes of fossil preservation. Review of Palaeobotany and Palynology, 20: 27-53.

Schultze-Lam, S., Ferris, F.G., Konhauser, K.O., Wiese, R.G., 1995. In situ silicification of an Icelandic hot spring microbial mat: implications for microfossil formation. Canadian Journal of Earth Sciences, 32: 2021-2026.

Scurfield, G., Segnit, E.R., 1984. Petrification of wood by silica minerals. Sedimentary Geology, 39: 149-167.

Stuiver, M., Reimer, P., 1993. Extended 14C database and revised CALIB radiocarbon calibration program. Radiocarbon, 35: 215-230.

Turner, E.C., Jones, B., 2005. Microscopic calcite dendrites in cold-water tufa; implications for nucleation of micrite and cement. Sedimentology, 52(5): 1043-1066.

Walter, M.R., McLoughlin, S., Drinnan, S., Farmer, J.D., 1998. Palaeontology of Devonian thermal spring deposits, Drummond Basin, Australia. Alcheringa, 22: 285-314.

Weed, W.H., 1888. Formation of travertine and siliceous sinter by the vegetation of Hot Springs. United States Geological Survey Annual Report, 9, 613-676 pp.

Weibel, R., 1996. Petrified wood from an unconsolidated sediment, Voervadsbro, Denmark. Sedimentary Geology, 101: 31-41.

Weijermars, R., Mulder-Blanken, C.W., Wiegers, J., 1986. Growth rate observation from the moss-built Checa travertine terrace, central Spain. Geological Magazine, 123(3): 279-286.

Chapter 6

Summary of Factors Controlling Carbonate Spring Deposit Development in the Canadian Rocky Mountains

Calcium carbonate is one of the most abundant and reactive substances near Earth's surface, precipitating from tap water as readily from ocean water and freshwater (Morse 1983). Its modern uses range from manufacturing cement to relieving acid reflux, whereas secretion of protective $CaCO_3$ exoskeletons by marine organisms over 535 million years ago facilitated preservation of organisms associated with the Cambrian explosion of life. Calcium carbonate exhibits a plethora of crystal habits, and among the 2,544 calcite crystal forms drawn by Goldschmidt (1913), the array of bizarre calcite crystals from spring deposits and the effect of biological activity on crystal habits and macro-textures were not considered (Fig. 6-1; Folk et al. 1985).

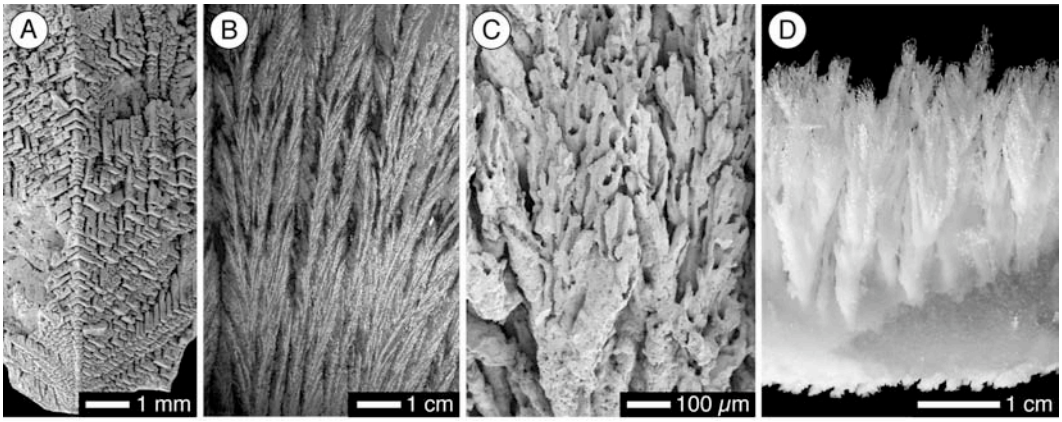

Fig. 6-1 Dendrite crystals from various spring systems. A) Abiogenic crystallographic calcite dendrite from Mammoth Hot Springs, Yellowstone, USA. B) Abiogenic noncrystallographic calcite feather dendrites from Fairmont Hot Springs, British Columbia. C) Biogenic noncrystallographic calcite dendrites formed by encrustation of filamentous microbes at Wolfenden, British Columbia. D) Abiogenic water ice feather dendrites formed from steam at Liard Hot Springs, British Columbia are morphologically similar to calcite dendrites from carbonate spring deposits.

Springs are complex natural systems characterized by continued spatial and temporal changes in physicochemical and biological interactions that drive carbonate spring deposit development. This thesis includes four investigations of the nature of these interactions at three carbonate depositing spring systems in the

Canadian Rocky Mountains: Fall Creek cold sulphur springs, Alberta, Fairmont Hot Springs, British Columbia (BC), and Hot Creek cold springs, BC (Fig. 6-2). These springs are currently active, however, it is clear that the modern water is not responsible for the relict deposits. For example, modern spring waters from Hot Creek and Fairmont are undersaturated or only slightly saturated with respect to $CaCO_3$, and Fall Creek spring water is only precipitating native sulphur (Allen et al. 2006, their table 3; Rainey and Jones 2007; this thesis Chapter 5). Current calcite accumulation rates (Table 6-1) are thus too low to be responsible for the abundance of calcite and the variety of depositional fabrics contained in the relict deposits. The relict deposits have also been subjected to extensive diagenesis (e.g. Fall Creek bryophyte tufa recrystallization), indicating that past developmental processes are no longer occurring. Additionally, the areal extents of the modern deposits are much smaller than the relict deposits (Fig. 6-3), and modern spring water inundates only 1% of the surface area that was required to form the relict deposits (Table 6-1). Thus, the magnitude of calcite precipitation that is currently taking place is insufficient to have formed the relict deposits. Nevertheless, analyses of modern spring water chemistry do provide a framework for understanding the physicochemical conditions that may have been in place when the calcite of these deposits was originally formed.

The Fall Creek, Fairmont and Hot Creek relict carbonate spring deposits are formed mostly of calcite that precipitated from spring water according to the CO_2-H_2O-$CaCO_3$ system (equation 1).

[1] $$Ca^{2+}(aq) + 2HCO_3^-(aq) \leftrightarrow CaCO_3(s) + \uparrow CO_2(g) + H_2O(l)$$

Although equation 1 is simple in appearance, calcite precipitation is governed by complex interactions among solid, gaseous and aqueous phases. Accordingly, many factors influence the forward reaction (calcite precipitation) and the reverse reaction (calcite dissolution), often simultaneously. For example, CO_2 degassing from hot spring water flowing down-slope forces equation 1 to the right and decreases calcite solubility, however, progressive cooling of the water increases CO_2 solubility and forces equation 1 to the left. Furthermore,

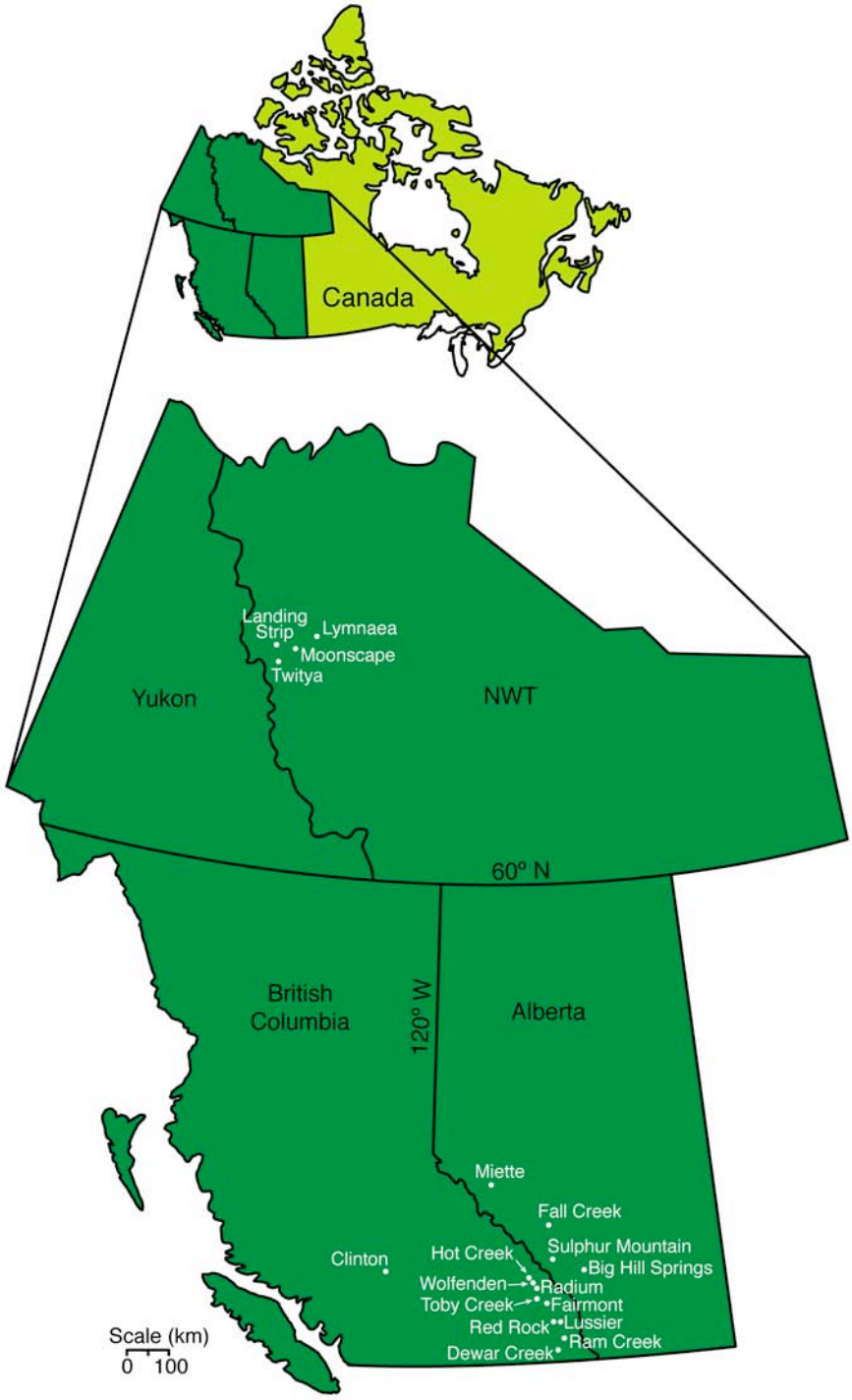

Fig. 6-2 Locations of all Canadian springs and deposits referenced in text, tables and figures.

Table 6-1 "Back of the envelope" calculations for carbonate spring deposit development.

Deposit	Surface Area of Deposit Covered by Modern Spring Water (m^2)	Relict Deposit Surface Area (m^2)	% of Relict Deposit Surface Area Covered by Modern Flow	Maximum Modern Carbonate Deposit Thickness	Maximum Relict Deposit Thickness	Relict Growth Rate ($cm \cdot yr^{-1}$)		Relict Deposit Formation Duration (years)	
						Min	Max	Min	Max
Fairmont Hot Springs	5×10^2	2.5×10^5	< 1%	~ 1 m	16 m	0.5	5	320	3200
Fall Creek	5×10^1	5×10^3	1%	none	5 m	0.2	2	250	2500
Hot Creek	1×10^3	1×10^5	1%	< 1 cm	3 m	0.1	1	300	3000

Note: Maximum and minimum yearly growth rates were estimated using bedding and lamination thicknesses from each deposit.

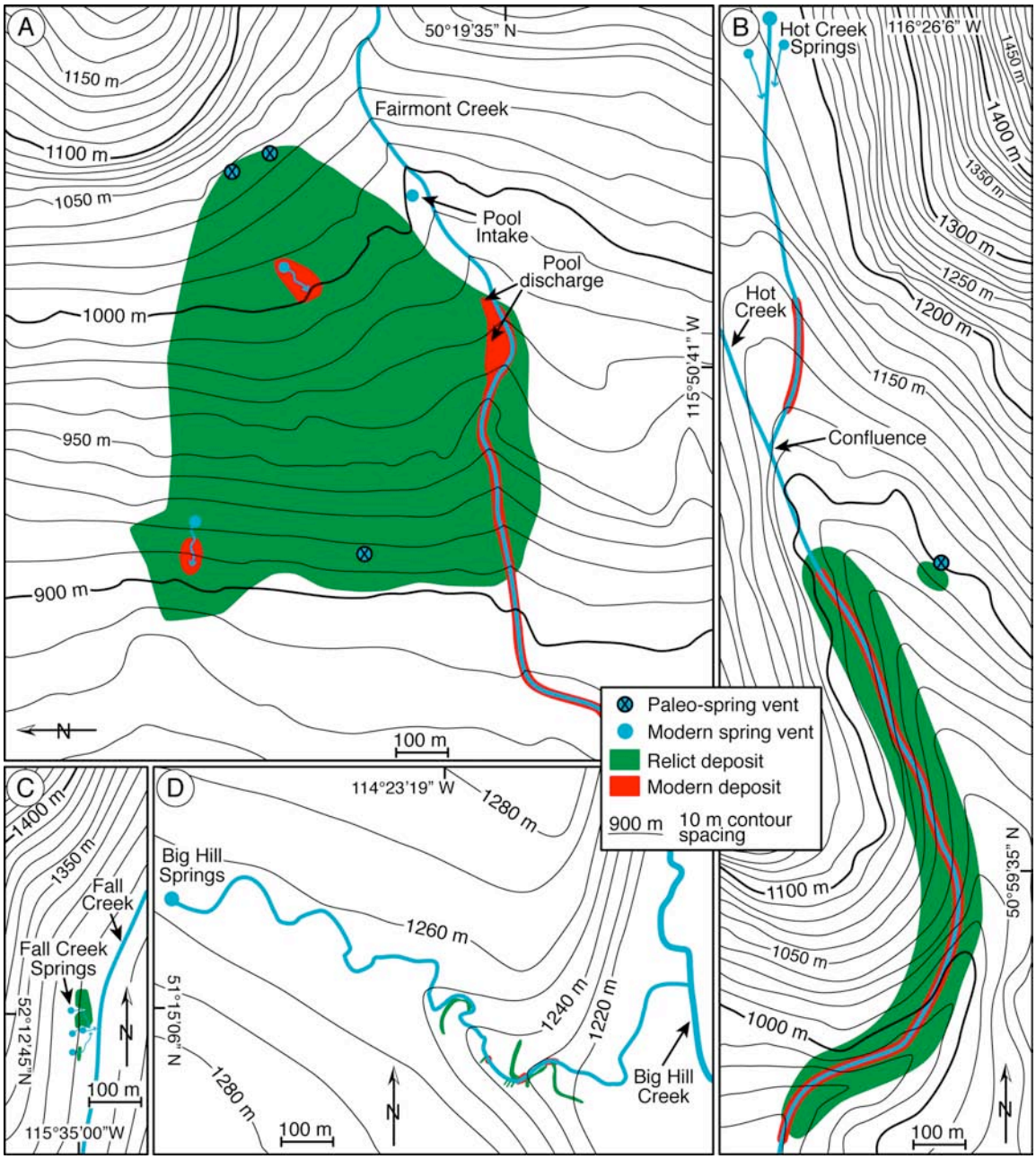

Fig. 6-3 Relationship between vent location, topography and carbonate spring deposits at Fairmont Hot Springs, Hot Creek, Fall Creek and Big Hill Springs. All maps share the same scale and contour spacing. Note limited extent of modern deposits compared to relict deposits. A) Fairmont Hot Springs emit water with high [Ca^{2+}] and [HCO_3^-]. Spring water precipitates calcite immediately upon emerging from the vent. B) Hot Creek springs emit water with moderate [Ca^{2+}] and low [HCO_3^-]. Currently, spring water flows ~ 300 m before calcite precipitates, then dilution by Hot Creek stops calcite precipitation until further downstream CO_2 degassing increases $CaCO_3$ supersaturation. Relict deposit formed ~ 1 km downstream of vent. C) Fall Creek water has high [Ca^{2+}], but deposit is much smaller than Fairmont and Hot Creek deposits because of much shorter flow path. D) Big Hill Springs emit water with low [Ca^{2+}] and moderate [HCO_3^-]. Water emerges from vent and flows ~ 0.5 km before topographic relief drives CO_2 degassing and causes $CaCO_3$ supersaturation. Calcite precipitation ceased after topographic leveling at 1220 m elevation.

evaporation promotes $CaCO_3$ precipitation by increasing ionic concentrations, yet evaporative cooling increases $CaCO_3$ solubility.

For calcite to precipitate from spring water, it must be supersaturated with respect to $CaCO_3$. Supersaturation state is a measure of disequilibrium, which is a primary factor controlling reaction rate (Morse 1983). If a solution is weakly to moderately supersaturated, crystal growth will be near equilibrium and relatively slow, resulting in polyhedral crystals with well-formed faces (Kuroda et al. 1987; Rimstidt 1997). Calcite precipitation may even be inhibited by water that is only mildly supersaturated with respect to $CaCO_3$ (Suarez 1983). High levels of supersaturation cause fast crystal growth rates under disequilibrium conditions that generate complex, branching crystal habits (Given and Wilkinson 1985; Kuroda et al. 1987; Gonzalez et al. 1992; Rimstidt 1997). Except for the dendrites in the Fairmont deposit, most of the crystals contained in the deposits from this study formed from low to moderately supersaturated solutions (Rainey and Jones 2007, 2009; this thesis Chapter 5). Thus, modern spring waters from Fall Creek, Fairmont and Hot Creek are insufficiently supersaturated with respect to $CaCO_3$ to have formed the complex calcite crystal habits contained in the relict deposits.

The primary determinants for $CaCO_3$ supersaturation are the temperature and chemistry of the water upon emerging from the vent. Calcite solubility decreases with increasing spring water temperature, meaning that hot spring water can achieve elevated supersaturation states more readily than cold spring water. The principal ionic species that influence equation 1 are Ca^{2+} and HCO_3^-. With the exception of Fairmont Hot Springs, which contains nearly as much dissolved CO_2 as HCO_3^-, western Canadian springs contain negligible amounts of CO_2 (Mazor et al. 1983). Magnesium is present in spring water, but does not exert a common ion effect because the Mg:Ca ratios are < 1 (Table 6-2; Herman and Lorah 1988).

Calcium carbonate supersaturation is achieved by forcing equation 1 to the right by way of CO_2 removal and/or evaporation. Excluding the radiating calcite

Table 6-2 Water chemistry and properties of select spring systems in the Rocky Mountains.

Spring Name	$[Ca^{2+}]$ ($mg \cdot L^{-1}$)	$[Mg^{2+}]$ ($mg \cdot L^{-1}$)	$[HCO_3^-]$ ($mg \cdot L^{-1}$)	Temp. (°C)	pH	$CaCO_3$ Deposit	References
Big Hill Springs	57 - 68	32 - 33	329 - 371	4.7 - 8.8	8.1 - 8.6	Small relict, little to no modern	Turner & Jones 2005
Dewar Creek	27.9	0.3	149	82.8	6.4	Some relict and modern	Grasby et al. 2000
Fairmont Hot Springs	314 - 485	107 - 112	559 - 770	27.8 - 49	6.1 - 7	Large relict, medium modern	Grasby et al. 2000; This thesis
Fall Creek	457 - 471	104 - 107		13 - 13.4	7.4 - 8.0	Large relict, no modern	This thesis
Hot Creek	147 - 164	28 - 31	183 - 221	4.9 - 7	7.9 - 8.5	Large relict, small modern	This thesis
Lussier Hot Springs	115 - 145	24.8 - 25	218 - 222	43	7.1	None	Grasby et al. 2000
Miette Hot Springs	330 - 408	56 - 73	117 - 148	51.2 (mean)	6.9 (mean)	Large relict, small modern	Bonny & Jones 2003b

Radium Hot Springs	142 - 150	28.3 - 33.2	212 - 217	43 - 44	6.7	None	Grasby et al. 2000
Ram Creek	49.2 - 50	14.5 - 15	148 - 155	35 - 37	7.7	Small relict and modern	Grasby et al. 2000
Red Rock	220	59	511	18.3	6.3	Large relict, no modern	Allen et al. 2006
Sulphur Mountain (Banff)	126 - 414	26.8 - 75.6	96 - 193	26.8 - 47.3	6.7 - 7.8	Large relict, small modern	van Everdingen 1972; Grasby & Lepitzki 2002; Grasby et al. 2003
Toby Creek	509	124	1307	8.9	6.3	Unknown	Grasby et al. 2000
Wolfenden	120	84.7	531	27.7	6.8	Large relict, small modern	Grasby et al. 2000

dendrites contained in the Fairmont deposit, whose formation was facilitated mainly by evaporation, calcite comprising carbonate spring deposits in the southern Rocky Mountains formed by CO_2 degassing from flowing water (Rainey and Jones 2005, 2007, 2009; this thesis Chapter 5). Though difficult to quantify, evaporation probably has a greater influence on $CaCO_3$ precipitation as flow rates decrease, and as temperature differentials between spring water and the atmosphere increase. Evaporation, however, is a much slower process than CO_2 removal, so its effect is diminished in environments where CO_2 degassing is enhanced.

The rate of CO_2 degassing increases with partial pressure of CO_2 in solution (pCO_2), agitation, temperature, pH, spring water surface area, and photosynthesis. Not all of these factors are equally important in western Canadian spring systems. Most western Canadian spring water is subjected to downstream pH increases because of CO_2 degassing, despite contemporaneous cooling promoting CO_2 solubility (cf. Chafetz et al. 1991). Hot Creek was the only active spring system studied that could be analyzed for downstream physicochemical changes, and it also exhibited downstream cooling and pH increases (Fig. 5-1B, Table 5-1). This indicates that changing water temperature is not a dominant control on CO_2 solubility, and pH changes do not control, but are caused by CO_2 degassing. There is also no textural or stable carbon isotopic evidence to suggest that calcite precipitation at Fairmont, Hot Creek and Fall Creek was facilitated by photosynthesis (Rainey and Jones 2007, 2009, in review). Initial pCO_2, agitation and surface area thus controlled CO_2 degassing and had important implications for where carbonate spring deposits formed in relation to the vents. Once discharged from the vent, agitation and CO_2 degassing rate are controlled by the flow regime (sheeted versus channeled flow), the topography encountered along the flow path, and the distance flowed before confluence with surficial water.

Continued CO_2 degassing along spring water flow paths is facilitated mainly by agitation driven by topographic relief, and increased surface area of the spring water associated with sheet flow. A comparison of spring water chemistry,

flow path and deposit size and location at Fairmont Hot Springs, Hot Creek, Fall Creek and Big Hill Springs shows how these concepts apply to relict and modern deposits in the Rocky Mountains (Tables 6-1, 6-2; Fig. 6-3). Of these spring systems, Fairmont has the highest [Ca^{2+}] and [HCO_3^-], and also has CO_2(g) in solution. Big Hill Springs has the lowest [Ca^{2+}] and moderate [HCO_3^-], whereas Hot Creek has the lowest [HCO_3^-] and moderate [Ca^{2+}]. Fall Creek has elevated [Ca^{2+}], but HCO_3^- analyses of water samples are not available. Big Hill Springs, despite having relatively high [HCO_3^-], has very low [Ca^{2+}] and consequently developed much smaller deposits than Hot Creek and Fairmont. Spring water from Big Hill Springs and Hot Creek however, required flow paths of 0.5 to 1.0 km in order to attain elevated $CaCO_3$ supersaturation states. The location of deposit development at both of these sites coincides with the steepest topographic gradients along the flow paths. Steep gradients increased flow rates and caused turbulence leading to increased CO_2 degassing. Fairmont spring water, conversely, was highly supersaturated with respect to $CaCO_3$ immediately upon being emitted from the vents and deposited large amounts of calcite at the vent and extending for 700 m along the steepest part of the flow path. Fall Creek spring water contains high [Ca^{2+}] and turbulently flows down-slope immediately upon emerging from the vents, but does not currently precipitate calcite along the 50 m long channeled flow path before flowing into Fall Creek. With a longer flow path, greater topographic relief, elevated [HCO_3^-] and increased spring water surface area, Fall Creek spring water would probably degas enough CO_2 to precipitate calcite.

A major focus of this thesis was determining causes for the difference between the large volume of calcite forming the relict deposits and the small volume of calcite presently being precipitated. That relationship however, is not so simple as just being volume discrepancies between spring water discharge and calcite in the deposits (Table 6-1, Fig. 6-3). For instance, at Fall Creek, there are numerous vents discharging volumes of water that are probably capable of having formed the relict deposit, yet modern bedding surfaces have mineral coatings rich in native sulphur and devoid of calcite. At present, Hot Creek also contains

significant volumes of water but low supersaturation and very little modern calcite precipitation. At Fairmont, spring water discharge volume is too small to have formed the relict deposit, but there is modern calcite precipitation. Most of the modern precipitation, however, occurs along Fairmont Creek for several kilometers downstream of the relict deposit. The different characteristics observed at each of these sites have similar explanations rooted in spatial and temporal changes in spring water discharge, flow regime and $CaCO_3$ supersaturation state.

One difference common to all of these spring systems is that their current flow patterns are incapable of having created the gross morphologies of the relict deposits. All of the relict deposits are formed of laterally and longitudinally continuous strata that could only have developed from extensive sheet flow over the active discharge aprons, whereas modern flow is contained within discrete channels. The relict Fairmont and Fall Creek deposits are fan-shaped accumulations, as opposed to the elongate valley-filling Hot Creek deposit. Fairmont and Fall Creek deposit formation probably involved lateral migration of sheet flow across the discharge apron so that only a portion of the apron was actively forming at any one time. In contrast, the Hot Creek deposit formed by continued down-valley progradation (Fig. 5-2A). The modern channeled flow is not conducive to calcite precipitation because it promotes deposit incision rather than aggradation, and thicker water columns hinder calcite precipitation at the bedding surface (Rogerson et al. 2008). Sheet flow promotes calcite precipitation and deposit aggradation by maximizing the surface area of spring water exposed to the atmosphere, thus promoting more rapid CO_2 degassing, elevated $CaCO_3$ supersaturation states and faster calcite precipitation. Sheet flow also maximizes the surface area of the bedding plane that is in contact with $CaCO_3$ supersaturated spring water, and decreases the distance between the air-water interface (where CO_2 degassing occurs) and the bedding surface-spring water interface (where calcite nucleates).

Though all of the modern Rocky Mountain spring systems are characterized by channeled flow, the cause and timing of the shift from sheeted to

channeled flow at each deposit could not be determined. It is apparent that the shift to channeled flow was accompanied, and probably caused by, an erosional event that incised the paleo-discharge aprons. Channeled flow regimes established by the spring systems have not undergone reversions to sheeted flow. A possible chronology of deposit aggradation and incision at Fairmont Hot Springs is presented in figure 6-4, and similar events with alternate timing probably occurred at Fall Creek and Hot Creek.

All carbonate spring deposits in western Canada formed during the Holocene after deglaciation (Table 6-3). It could not be determined, however, how much time elapsed from deglaciation to the start of deposit formation. Accurate dating of western Canadian carbonate spring deposit development has proven difficult because of a low rate of incorporation of dateable material into deposits, rapid decay of incorporated dateable material (e.g. wood, plants), and poor development of annual depositional cycles. Deposit growth rate calculations indicate that the deposits required not more than 3000 years to form (Table 6-1), further limiting the time available for dateable material to be incorporated into the deposits. Prior research suggested that western Canadian carbonate spring deposits formed during the Neoglacial in response to a mid Holocene climatic shift from warm and dry conditions to cool and wet conditions (Bonny 2002; Bonny and Jones 2003; Grasby et al. 2003; Rainey and Jones 2007). Decay resistant charcoal recovered from the Fairmont and Hot Creek deposits indicates that deposit development was very active during the deduced warm and dry climate of the early Holocene. The misconception that springs were inactive during early Holocene probably relates to a sampling bias whereby dateable material was more likely to be preserved in younger parts of deposits than older ones, thus obscuring their true antiquity.

Spring water discharge volume is probably one of the most important factors controlling carbonate spring deposit development, yet is one of the most difficult factors to resolve in the relict deposits. The lack of well-defined annual cycles in the deposits attests to continually fluctuating discharge volumes being a significant control on facies development, as portrayed by the complex facies

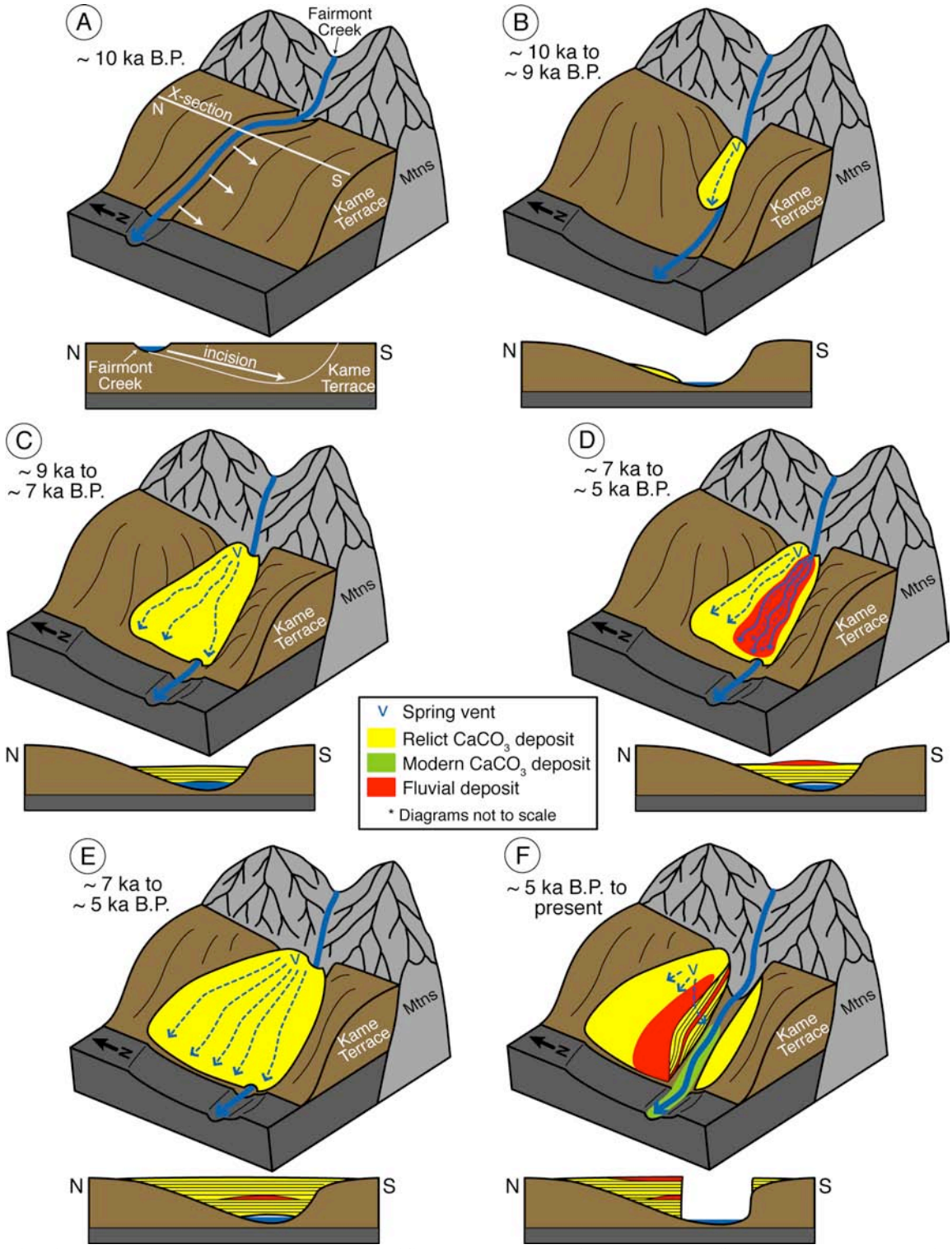

Fig. 6-4 Approximate chronology and simplified development of Fairmont Hot Springs carbonate deposit. A) Post-deglaciation incision of kame terrace by Fairmont Creek. B) Fairmont Hot Springs become active and precipitate calcite. C) Deposition of Lower Carbonate Sequence. D) Deposition of Middle Clastic Sequence. E) Deposition of Upper Carbonte Sequence. F) Deposit incision, development of Fairmont Creek valley and establishment of current depositional patterns that are controlled by channeled, rather than sheeted flow.

Table 6-3 Dates obtained from western Canadian carbonate spring deposits

Deposit	^{14}C Years B.P.	Calendar Years B.P.	Material
[1]Clinton	2400	2400	Bridge River Tephra
Fairmont	7905 +/- 25	8690 +/- 90	Charcoal
Hot Springs	7455 +/- 20	8270 +/- 70	Charcoal
Fall Creek	585 +/- 20	590 +/- 50	Wood
	310 +/- 50	390 +/- 105	Wood
Hot Creek	6480 +/- 20	7380 +/- 55	Wood
	5925 +/- 20	6735 +/- 55	Wood
	1310 +/- 70	1200 +/- 135	Charcoal
	730 +/- 50	650 +/- 90	Charcoal
[2]Miette	3770 +/- 60	4140 +/- 165	Bone
Wolfenden	2165 +/- 15	2210 +/- 90	Charcoal

Note: Conventional radiocarbon ages were converted to calendar years using the CALIB radiocarbon calibration program and the IntCal04 terrestrial radiocarbon age calibration for 26 to 0 ka BP, and calibrated ages are reported as 2 sigma ranges (Stuiver and Reimer 1993; Reimer et al. 2004)

[1]Jones and Renaut 2008

[2]Bonny 2002; Bonny and Jones 2003

associations contained in the Fairmont deposit (Rainey and Jones 2009). Discharge volumes are strongly linked to seasonality and meteoric precipitation, and are greatest from May to July due to melting snow pack and spring rains (van Everdingen 1972; Grasby and Lepitzki 2002). During peak discharge, spring water temperatures and ionic concentrations are at their lowest because cold, near-surface meteoric water mixes with hotter, deeply derived spring water. Water temperatures and ionic concentrations are at their peak at the end of summer and beginning of autumn when discharged water is not diluted by surficial water. Ironically, during this period of favourable water chemistry, discharge is typically reduced or has stopped completely at some vents, such as Emanation Hill at Fairmont.

Meteoric precipitation in western Canada has fluctuated between drier and wetter intervals on seasonal, decadal, centennial and millennial scales throughout the Holocene (MacDonald and Case 2000; Cumming et al. 2002). Spring water discharge volumes have therefore fluctuated in a similar manner and on similar time scales. Radiocarbon evidence indicates that carbonate spring deposit development has occurred throughout the Holocene, but unconformities present in the deposits and deposit growth rate estimates of 250 to 3200 years (Table 6-1) indicate that development has been episodic rather than continuous and protracted during the Holocene. Reduced modern spring water discharges from western Canadian springs are probably caused by modern climates that are drier than the climatic intervals responsible for past increases in spring discharge volumes. Unfortunately, accurate timing and duration of increased spring discharge episodes could not be resolved from the Rocky Mountain carbonate spring deposits.

The Fairmont, Fall Creek and Hot Creek deposits contain fabrics that formed by precipitation of calcite in association with biota such as microbes and plants (Rainey and Jones 2005, 2007, 2009; this thesis Chapter 5). The most common mode of preservation for all biota was encrustation by calcite crystals. Hot Creek displayed rare calcite precipitation inside cyanobacterial sheaths and wood cells. The calcite crystals that precipitated in biotic facies formed from low

to moderately $CaCO_3$ supersaturated spring water. The prevalence of calcite being precipitated from flowing as opposed to stagnant spring water in these spring systems, as well as a lack of isotopic or textural evidence for active calcite precipitation by photosynthesizers indicates that chemical evolution of spring water was caused mainly by inorganic CO_2 degassing. Physicochemical CO_2 degassing predominates in flowing systems, whereas microbial influences become more important in sluggish or static waters such as those at some Italian and Yellowstone springs (Pedley et al. 1996; Chafetz and Guidry 2003). The lack of lacustrine or paludal facies development at Fairmont, Hot Creek and Fall Creek is probably the primary indication that microbial metabolism had little effect on calcite precipitation.

Though photosynthesis did not likely contribute to elevated $CaCO_3$ supersaturation states in the western Canadian spring systems, several experiments and studies at other spring systems have revealed that microbial biofilms and extracellular polymeric substances (EPS) provide nucleation sites and facilitate $CaCO_3$ precipitation in environments that otherwise would not be sufficiently supersaturated to drive abiotic calcite precipitation (Bissett et al. 2008; Kandianis et al. 2008; Rogerson et al. 2008; Shiraishi et al. 2008; Pedley et al. 2009). Biofilms and EPS may have facilitated calcite precipitation at Fairmont, Hot Creek and Fall Creek by acting as catalysts to lower the activation energy required for $CaCO_3$ nucleation. Not only would this have aided calcite precipitation under low saturation conditions, but could also have prevented spring water from attaining high supersaturation levels, which are required for generating complex, branching calcite crystals.

Calcite crystals with dendritic morphologies ranging from irregular shrubs to crystallographic forms are common constituents of many carbonate spring deposits. The most irregular forms are microbial shrubs formed by concurrent calcite crystal formation and microbial growth, whereas the most ordered forms are abiotic crystallographic dendrites formed rapidly from supersaturated solutions (Chafetz and Folk 1984; Folk et al. 1985; Guo and Riding 1992, 1994; Chafetz and Guidry 1999; Jones et al. 2000). The origin of noncrystallographic

dendrites is less obvious. Chafetz and Guidry (1999) interpreted etch pits in noncrystallographic calcite dendrites to be bacterial moulds, then inferred a biologic origin for the crystals. Etch pits, however, could be abiotic, or could have resulted from microbial crystal degradation during diagenesis (cf. Guo and Riding 1994). Furthermore, the presence of bacteria during calcite crystal growth does not imply that they influence rapid abiotic crystal growth. For example, Jones and Renaut (1995) outlined physicochemical mechanisms for formation of noncrystallographic calcite denrites from a very hot spring (> 90°C) in Kenya. Based on analysis of 1,586 scanning electron photomicrographs of calcite samples from the Fairmont deposit (some of which were etched by dilute HCl), it was determined that the noncrystallographic calcite feather dendrites in the Fairmont deposit formed abiotically, and that diagenetic micritization masked the dendrites' crystalline nature. Such micritization could easily be considered a primary precipitate rather than a product of diagenetic breakdown.

At western Canadian springs, biota acted as passive nucleation sites upon which calcite precipitated. Detrital and *in situ* biota, however, further enhanced inorganic CO_2 degassing by creating surface roughness on the discharge apron, which increased agitation. Rimstone dams preserved in the Fairmont deposit commonly formed in this manner because of increased calcite precipitation rates localized on turbulence-generating leaves, twigs or logs. Alternately, biota may have hampered abiotic calcite precipitation by impeding flow and reducing turbulence. This may have been the case at Fall Creek, where the paleo-discharge apron was covered by moss hummocks. Calcite crystal growth rates also strongly impact biotic growth and distribution, as exemplified by the Fairmont deposit. High levels of $CaCO_3$ supersaturation caused rapid calcite crystal growth, and faster crystal growth rates prevented slow growing organisms (e.g. trees, plants, mosses) from becoming incorporated into the deposit. If crystal growth rates are fast enough, microbes can even be prevented from colonizing bedding surfaces and crystal faces (Rainey and Jones 2009).

In much the same way that topography, flow regime and discharge volumes control the physicochemical parameters responsible for calcite

precipitation, these factors also control the growth and distribution of biota on the discharge aprons. Microbes survive in faster flowing and more turbulent water than higher plants such as mosses and grasses. Microbial colony morphologies however, change in response to turbulence and flow intensity. For example, at Fairmont, filamentous microbes commonly exist as solitary organisms in weakly flowing water, but form mats as turbulence and flow rates increase . Bryophytes and macrophytes prefer environments associated with sluggish flow. Bryophytes grow directly in spring water and are partially submerged, whereas macrophytes grow at the margins of the flow path where they receive moisture but are not immersed in the water. An additional factor that controlled biotic growth at the springs is the presence of H_2S. Fall Creek spring water has elevated H_2S levels, which promotes growth of sulphur-oxidizing microbes and inhibits growth of cyanobacteria, whereas the H_2S free spring water at Fairmont and Fall Creek is conducive to abundant cyanobacterial growth.

The aspect and exposure of the Fairmont, Fall Creek and Hot Creek deposits may also have contributed to the types and abundance of vegetation that inhabited the discharge aprons. Hot Creek and Fall Creek are both present in valley bottoms and are surrounded by trees, which limits the amount of direct solar radiation they receive. Shaded discharge aprons, coupled with wet spring environments made the Fall Creek and Hot Creek discharge aprons conducive to bryophyte growth. Fairmont is present on an exposed terrace and receives abundant solar radiation, which prevented bryophytes from being established as an important part of the biotic assemblage. It could be argued that elevated Fairmont spring water temperatures prevented bryophyte growth, however, bryophytes are common in the Miette Hot Springs deposit, which emits hotter water than Fairmont (Bonny and Jones 2003). The Miette deposit is present in a narrow, shaded valley and exhibits biotic depositional fabrics that resemble the cold water deposits of Fall Creek and Hot Creek, rather than the warmer water Fairmont deposit.

In the Fairmont, Fall Creek and Hot Creek deposits, biota may not have metabolically contributed to calcite precipitation, however non-photosynthetic

microbes actively caused crystalline calcite degradation. These deposits are formed mainly of crystalline calcite with lesser amounts of micrite (calcite grains < 4 μm long), but most of the micrite contained in these deposits formed by the microbial breakdown of crystalline calcite. This breakdown was not restricted to diagenesis, but was an integral part of deposit development. Cyclic calcite crystal formation and degradation generated the isopachous banded cements common in the Fall Creek deposit, and many of the dendrite crystals in the Fairmont deposit lost their crystalline appearance because of bacterial degradation (Rainey and Jones 2007, 2009). The tangential fabrics preserved in oncoid cortices from Fairmont were also the direct result of bacterial calcite degradation during the developmental process (Rainey and Jones 2005). This highlights how microbial activities affected deposit fabrics by disrupting, rather than promoting, crystalline calcite formation.

Application to Other Spring Systems and Deposits

The validity of observations and conclusions drawn from the Fairmont, Fall Creek and Hot Creek studies can be tested by making comparisons to other spring systems and deposits. What is most apparent from field observations at other spring systems is that their current discharge volumes and $CaCO_3$ precipitation rates are also too low to have created the sizeable relict deposits. For example, at the Clinton deposit in south-central BC, there is no active spring water discharge and the only evidence of past spring activity is the presence of a large deposit containing intricate depositional fabrics (Fig. 6-5A,B; Jones and Renaut 2008). Other relict carbonate spring deposits in the Rocky Mountains are present next to active vents (Table 6-2), but the spring water flows in channels incised through the deposits, just like at Fairmont, Hot Creek and Fall Creek. This shift in hydrologic conditions is well portrayed at Big Hill Springs, Alberta, where relict arcuate barrage tufa dams that formed pools up to 3 m deep have been incised, allowing spring water to flow around them (Fig. 6-5C). At Red Rock Springs, BC, and Miette Hot Springs, Alberta, the modern vents discharge

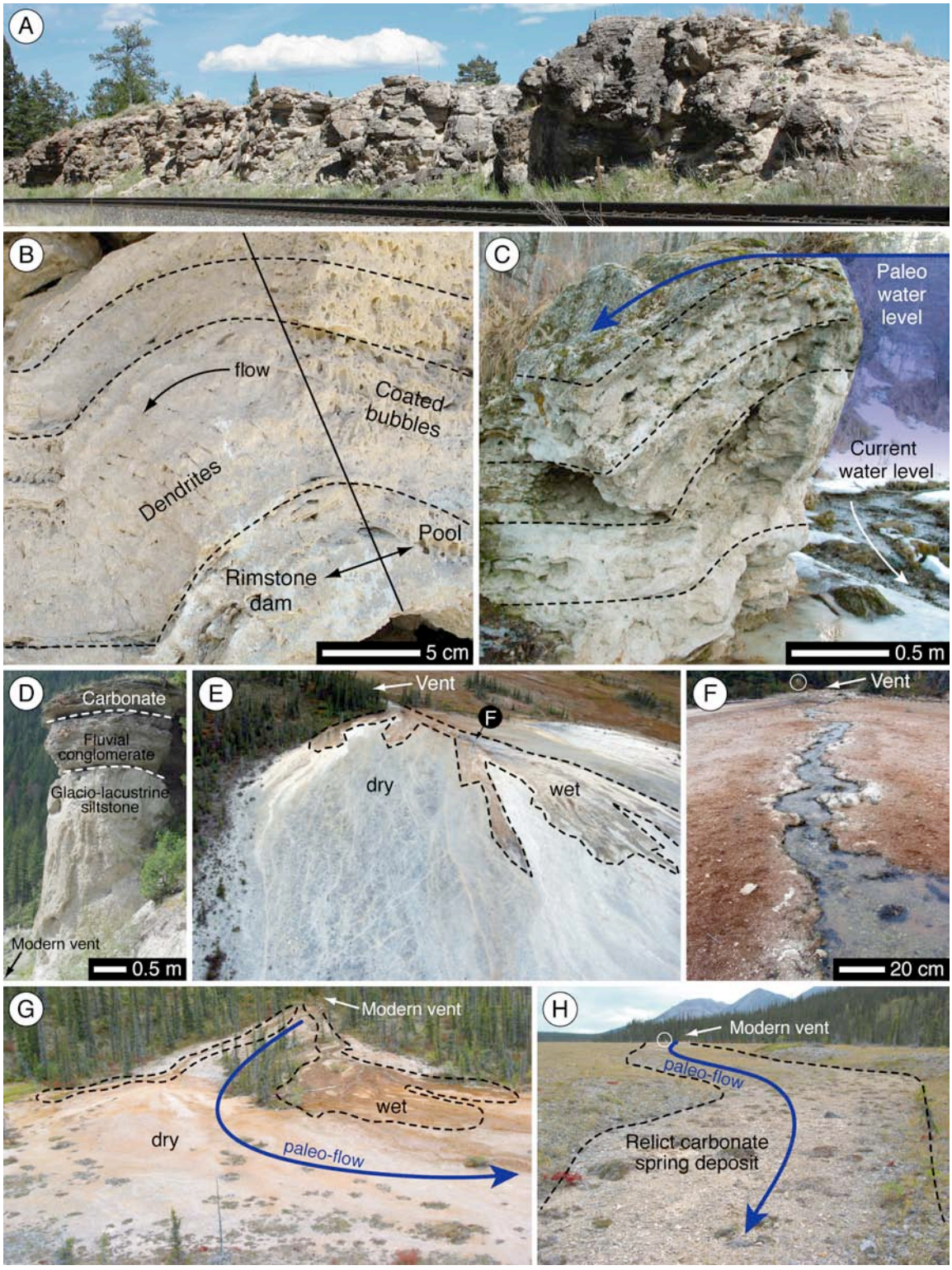
A
B
flow
Coated bubbles
Dendrites
Pool
Rimstone dam
5 cm
C
Paleo water level
Current water level
0.5 m
D
Carbonate
Fluvial conglomerate
Glacio-lacustrine siltstone
Modern vent
0.5 m
E
Vent
F
dry
wet
F
Vent
20 cm
G
Modern vent
wet
dry
paleo-flow
H
Modern vent
paleo-flow
Relict carbonate spring deposit

Fig. 6-5 Current flow conditions are incapable of having formed relict western Canadian carbonate spring deposits. A) Relict deposit at Clinton, British Columbia, has no active springs. Train tracks in foreground. B) Complex facies association in Clinton deposit. Calcite coated bubbles formed in rimstone pool on right grade laterally into calcite dendrites that formed the rimstone dam. Dashed lines highlight bedding. C) Incised relict barrage tufa dam at Big Hill Springs, Alberta. Dashed lines highlight bedding. D) Relict carbonate deposit at Red Rock, British Columbia. Modern vent is not visible in image, but CO_2–rich water emerges from the bottom of the Kootenay River 5 m below road level in lower left. E) Lymnaea springs, Mackenzie Mountains, Northwest Territories. Spring water is rapidly absorbed by relict deposit. F) Spring water flows in narrow channel on surface of relict deposit before being absorbed. Scale bar applies to foreground. Person circled near vent for background scale. G) Landing Strip springs, Mackenzie Mountains, Northwest Territories. Modern spring water absorbed within 100 m of vent as it flows over relict deposit. H) Landing Strip springs. Relict deposit extends over ~ 1 km further from vent than modern flow. Dashed lines mark margins of deposit. Helicopter near vent circled for scale.

spring water at lower elevations than the relict deposits and are incapable of depositing calcite in formerly active environments (Fig. 6-5D).

The discrepancy between modern discharge volumes and relict deposit size is also illustrated by several carbonate-depositing springs in the Mackenzie Mountains, North-West Territories (NWT). Unlike the incised Rocky Mountain deposits, the Mackenzie deposits still have modern discharge flowing over the relict deposits. The spring water, however, only flows over a fraction of the discharge apron and the porous deposits rapidly absorb most of the water (Fig. 6-5E to H). The shift from sheeted to channeled flow also occurred at some of the Mackenzie Mountain deposits (Figs. 6-5E to H), but these deposits lack the deep incision that affected the Rocky Mountain deposits. One of the biggest differences between the relict Mackenzie deposits and the relict Rocky Mountain deposits is that the Rocky Mountain deposits are adjacent to creeks that were capable of eroding or undercutting the relict deposits. Some hydrologic changes at Rocky Mountain springs are less easily explained, such as the existence of modern vents at Miette and Red Rock being present at elevations below the incised relict deposits. Possible explanations include isostatic rebound following deglaciation, local lowering of the water table or recent (late Holocene) tectonic uplift/faulting.

Depositional processes that facilitated calcite precipitation at Fairmont, Fall Creek and Hot Creek were based mainly on features of the relict deposits, and not on modern depositional processes. Twitya springs, NWT, provide an excellent modern example of spring water evolution leading to calcite

precipitation (Fig. 6-6A). Upon being discharged from the vent, the spring water is not sufficiently supersaturated with respect to $CaCO_3$ to drive calcite precipitation, but within 10 m of flowing down-slope, agitation-driven CO_2 degassing causes high supersaturation levels and dendrite formation (Bonny and Jones 2008a). If the Twitya Springs emerged at a lower elevation and did not flow down-slope, or flowed in channels rather than in sheets, then the spring water probably would have flowed into the Twitya River without achieving high enough $CaCO_3$ supersaturation to drive calcite precipitation. Such is the case at Fall Creek and Lussier Hot Springs, BC. Lussier spring water has $[Ca^{2+}]$ and $[HCO_3^-]$ similar to other calcite precipitating springs and is weakly supersaturated with respect to $CaCO_3$ (Table 6-2; van Everdingen 1972). The Lussier spring water however, flows into the Lussier River without precipitating calcite (Fig. 6-6B). With a longer flow path, greater topographic relief, and increased spring water surface area, Lussier spring water would probably degas enough CO_2 to increase $CaCO_3$ supersaturation sufficiently to precipitate calcite. These examples illustrate that if spring water emitted from a vent is not adequately supersaturated with respect to $CaCO_3$, it may achieve supersaturation further along its flow path if there is ample CO_2 degassing before the spring water flows into and is diluted by surficial water.

A test of understanding the dynamics of $CaCO_3$ supersaturation in spring systems is the ability to predict the initial spring water chemistry for carbonate deposits lacking modern discharge. For instance, El Santo Madero carbonate deposit in Parras, Mexico, is a domed mound that sits atop a hill with no down-slope deposits (Fig. 6-6C). This indicates that the spring water precipitated calcite immediately upon leaving the vent without requiring downstream degassing to elevate supersaturation levels. The relatively small size of the domed deposit and its proximity to the paleo-vent suggests that the paleo-spring water had very high concentrations of bicarbonate and/or CO_2, and low to moderate $[Ca^{2+}]$.

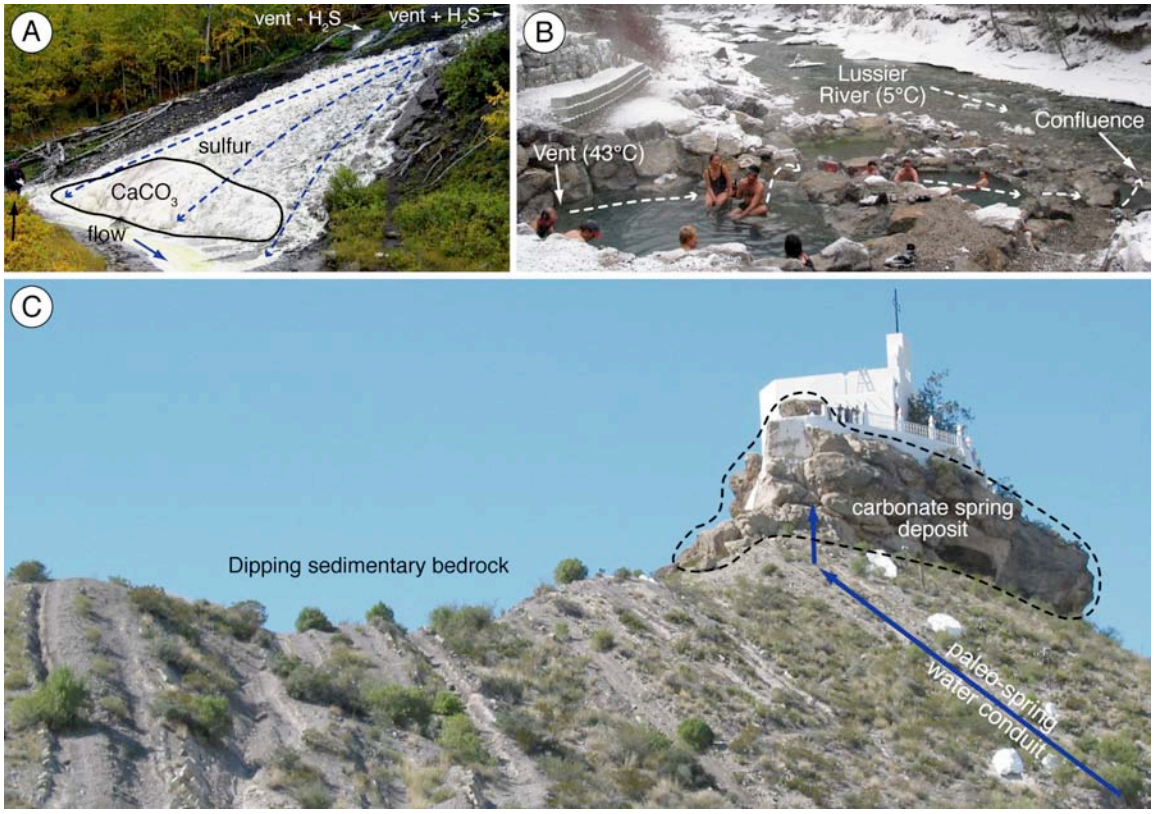

Fig. 6-6 Spring water chemistry and evolution. A) Twitya sulphur spring, Mackenzie Mountains, Northwest Territories. Spring water precipitates native sulfur immediately upon emerging from the vent, but only precipitates calcite at the toe of the discharge apron after down-slope CO_2 degassing caused a critical level of $CaCO_3$ supersaturation to be attained. Person at left of image for scale. B) Lussier Hot Springs, British Columbia. The spring water, despite having a chemical composition suitable for $CaCO_3$ precipitation, lacks precipitates. This is likely due to minor agitation (from little topographic relief) and a short flow distance before the confluence with the Lussier River. C) The church, El Santo Madero, was built upon a relict carbonate spring deposit in Parras, Mexico. There is no active vent at the deposit, but the excellent stratigraphic exposure allows one to visualize the conduit utilized while the spring was active. The domed mound and lack of down-slope deposits indicate that the calcite precipitated immediately upon the spring water being discharged from the vent and did not flow a great distance to achieve $CaCO_3$ supersaturation. This is probably because of rapid CO_2 degassing caused by very high [HCO_3^-] in solution.

Future Research Directions and Global Implications of Carbonate Spring Deposit Studies

This thesis involved detailed study of three carbonate spring deposits in the Rocky Mountains of Alberta and British Columbia. It is not an exhaustive study of carbonate spring deposit development in western Canada and much work remains to be done on local and regional scales. In Alberta alone, Borneuf (1983) lists 568 springs, ~ 60 of which have carbonate spring deposits that vary in size from being thin veneers of limited extent to large carbonate accumulations that are meters thick and cover tens to hundreds of square meters.

The current body of knowledge pertaining to carbonate spring deposit development in western Canada would benefit greatly from future investigations of carbonate depositing spring systems with characteristics that differ from previously studied deposits. Three intriguing candidates are Dewar Creek springs and Toby Creek springs in southeast BC, and Moonscape springs in the Mackenzie Mountains, NWT. At 82.2°C, the Dewar Creek springs are the hottest known carbonate-depositing springs in Canada (Woodsworth 1999), and the deposits are formed in association with thermophilic (or thermo-tolerant) microbes from water with low [Ca^{2+}] and moderate [HCO_3^-] (Table 6-2). The Toby Creek springs have not been personally visited, thus it is unknown if the springs are associated with a carbonate deposit, but the water contains the highest concentrations of Ca^{2+} and HCO_3^- of any western Canadian spring (Table 6-2). Such elevated concentrations have the capability of causing extremely rapid crystal growth and generating crystal fabrics not possible at other western Canadian springs. The Moonscape cold springs are presently active in a diminished capacity compared to its large, well-exposed deposit (Fig. 6-7). This is an intriguing spring system because it presents an opportunity to compare modern spring activity and a relict carbonate deposit that formed in a cold, northern climate. Furthermore, biota commonly flourish in cold spring environments, but the relict deposit does not appear to contain fabrics that were biotically influenced.

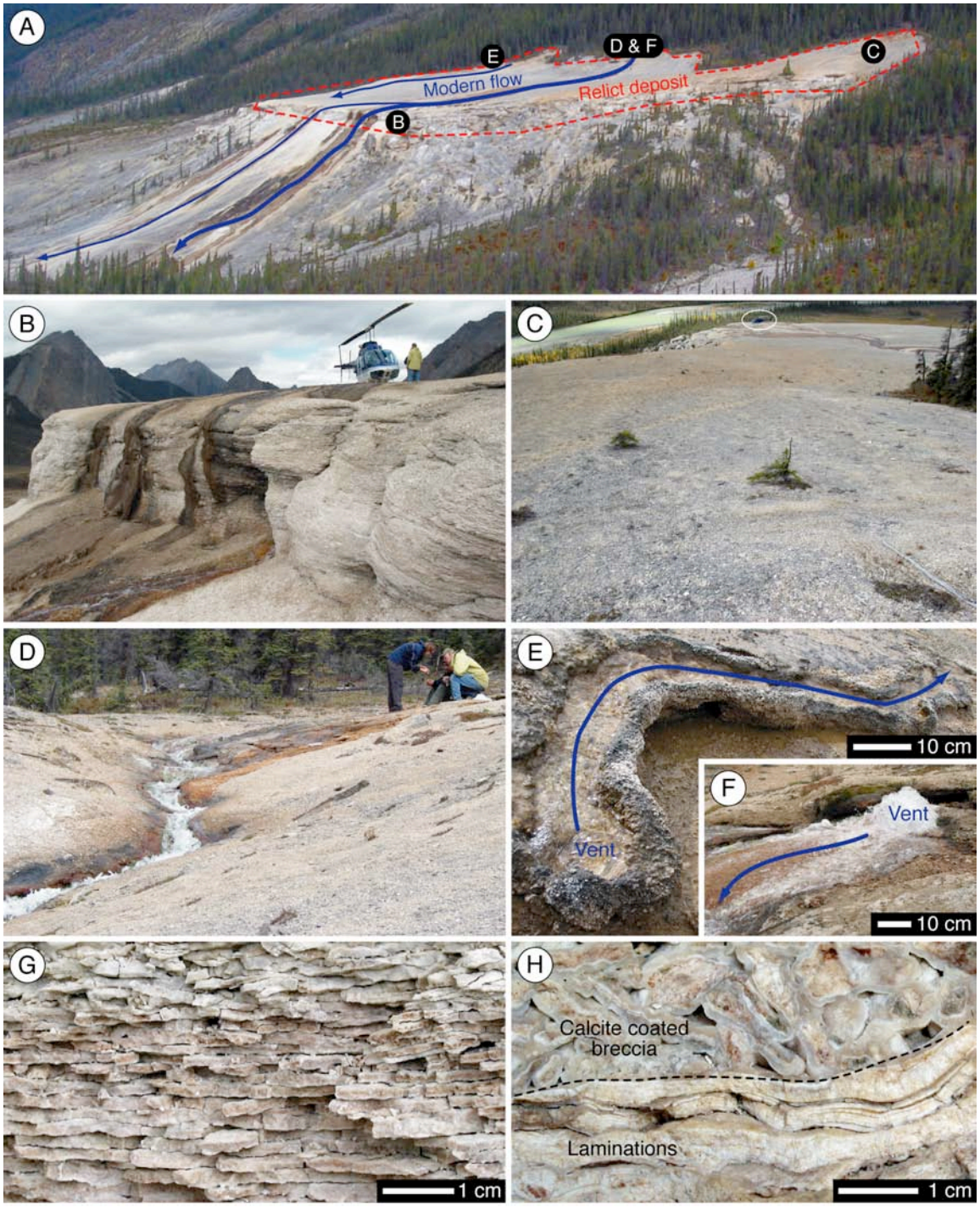

Fig. 6-7 Moonscape cold springs, Mackenzie Mountains, Northwest Territories. A) Relict carbonate spring deposit outlined in red formed mostly on terrace rather than steep slopes flanking deposit. Letters indicate photograph locations. B) Fractured terminus of deposit with minimal spring water coverage of bedding surfaces. C) View of sparsely vegetated relict deposit looking down-slope toward helicopter (white circle). D) Main vent near people discharges spring water into incised channel. E) Minor vent created an elevated, self-built channel. F) Close-up of gushing vent from D). G) Most of the deposit is formed of horizontal laminations with little macroscopic evidence of biotic influence. H) Calcite-encrusted breccia clasts possibly formed from freeze-thaw action.

Stable carbon and oxygen isotope analyses of calcite from spring deposits in the Rocky Mountains were completed with the intention of determining if photosynthesizing organisms (mainly cyanobacteria and bryophytes) actively contributed to calcite precipitation by removing CO_2 from solution. Results indicated that inorganic CO_2 degassing caused most of the calcite precipitation (Rainey and Jones 2007, 2009). A comparison of the stable carbon and oxygen isotope results from several spring deposits however, revealed trends that provide insight into the regional controls on carbonate spring deposit development in western Canada (Fig. 6-8). Calcite from Miette and Fairmont (the hottest springs of the group) displayed the most negative but greatest range in $\delta^{18}O$ values, and the highest $\delta^{13}C$ values. Calcite from the cooler springs at Fall Creek, Hot Creek and Wolfenden displayed the highest and most tightly clustered $\delta^{18}O$ values, and the lowest $\delta^{13}C$ values. These emerging trends show distributions that appear to be related to spring water temperature. Incorporating results from more spring deposits would probably provide insight into depth of penetration of spring water, and the Ca^{2+} and CO_2 sources for the calcite precipitated from the spring water.

Understanding the physicochemical factors responsible for generating the crystal morphologies found in modern and relict carbonate spring deposits has the potential to help earth scientists understand global changes going back to the Precambrian. For example, feathery crystal carbonate dendrites are common components of Neoproterozoic marine cap carbonates that formed after intervals of widespread global glaciation (e.g. Peryt et al. 1990; James et al. 2001; Hoffman and Schrag 2002; Fraiser and Corsetti 2003; Lorentz et al. 2004). By analogy with carbonate spring deposits, for extensive beds of dendritic carbonate crystals to have formed on the ocean floor, rapid and massive releases of CO_2 from shallow seawater were likely necessary. These CO_2 releases were apparently related to cap carbonates that formed after Neoproterozoic warming, suggesting that warming had occurred prior to the CO_2 releases, and may have actually caused the releases. This suggests that further warming could have happened because of carbonate precipitation, or that during that time period, CO_2 was not a significant contributor to atmospheric warming.

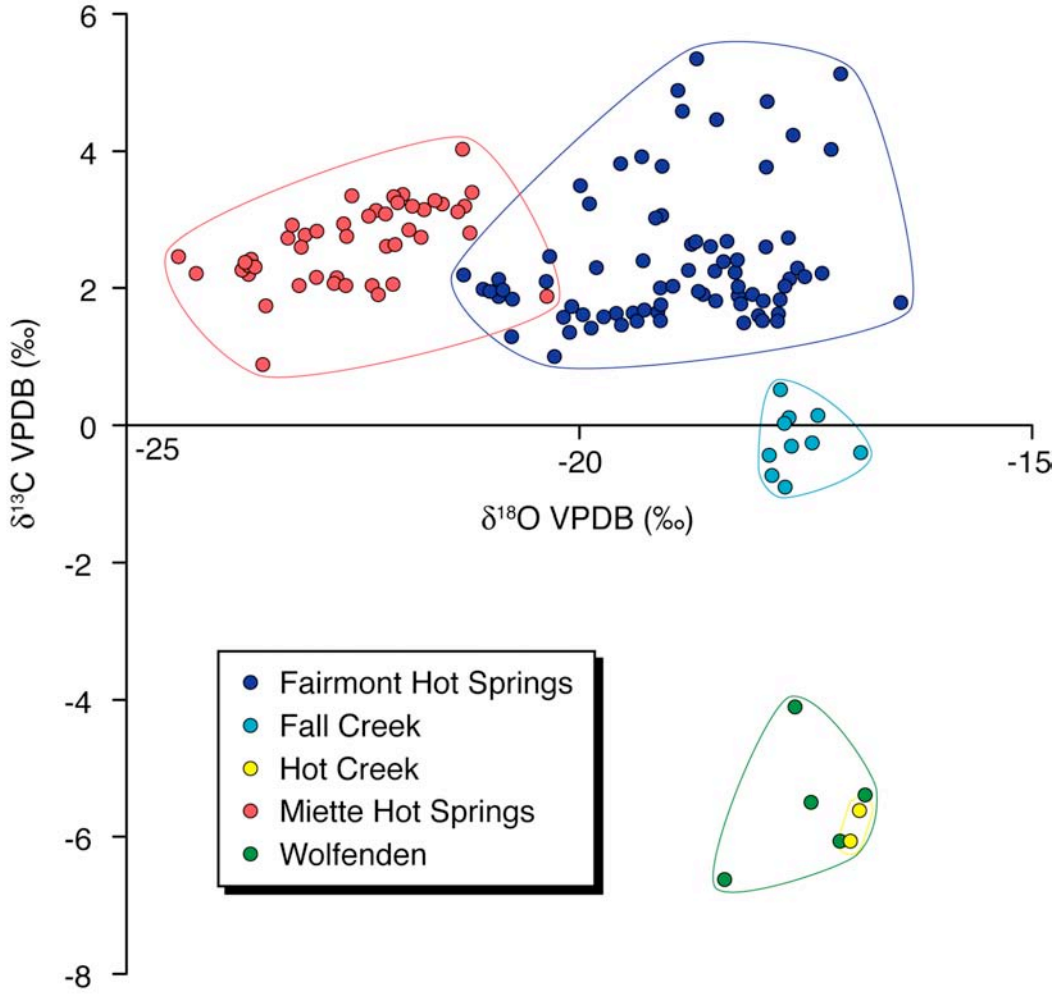

Fig. 6-8 Stable carbon and oxygen isotope plot for calcite from Rocky Mountain carbonate spring deposits. Miette data from Bonny (2002).

Conclusions

Comparison of modern spring systems to the relict carbonate deposits in the Canadian Rocky Mountains have yielded the following conclusions:

- Modern discharge volumes and flow regimes are incapable of having produced the large, texturally diverse relict deposits that are common in western Canada.
- Modern flow regimes are characterized by channeled flow that reduces the ability of spring water to rapidly degas CO_2 and attain high levels of $CaCO_3$ supersaturation, whereas relict flow regimes were characterized by extensive sheeted flow that facilitated rapid precipitation of calcite and development of laterally continuous strata.
- With few exceptions, calcite forming western Canadian carbonate spring deposits formed from flowing spring water that rapidly degassed CO_2. As a result, most of the deposits are formed of crystalline calcite with only minor amounts of detrital, mechanically deposited or biogenic carbonate.
- Biota did not contribute greatly to crystalline calcite precipitation beyond acting as passive nucleation sites, but did actively degrade the crystalline calcite after precipitation.
- Water with high temperatures and elevated $[Ca^{2+}]$ and $[HCO_3^-]$ enhanced deposition of calcite immediately upon being discharged from the vent.
- Water that was incapable of precipitating calcite immediately upon being discharged from the vent could attain elevated $CaCO_3$ supersaturation states by way of agitation-induced CO_2 degassing along the flow path.
- Facies distribution on the spring water discharge aprons was controlled by spring water discharge volumes and flow rate changes induced by steeper gradients caused by underlying topography.
- Discharge volume fluctuations that acted on seasonal to millennial scales were probably the most influential controls on deposit development, yet are the most difficult to quantify.
- Carbonate spring deposit development occurred episodically throughout the Holocene.

References

Allen, D.M., Grasby, S.E., Voormeij, D.A., 2006. Determining the circulation depth of thermal springs in the southern Rocky Mountain Trench, south-eastern British Columbia, Canada using geothermometry and borehole temperature logs. Hydrogeology Journal, 14: 159-172.

Bissett, A., Reimer, A., de Beer, D., Shiraishi, F., Arp, G., 2008. Metabolic microenvironmental control by photosynthetic biofilms under changing macroenvironmental temperature and pH conditions. Applied and Environmental Microbiology, 74(20): 6306-6312.

Bonny, S., 2002. Relic tufa at Miette Hot Springs, Jasper National Park, Alberta. M.Sc. Thesis, University of Alberta, Edmonton.

Bonny, S., Jones, B., 2003. Relict tufa at Miette Hot Springs, Jasper National Park, Alberta, Canada. Canadian Journal of Earth Sciences, 40: 1459-1481.

Bonny, S.M., Jones, B., 2008a. Controls on the precipitation of barite ($BaSO_4$) crystals in calcite travertine at Twitya Spring, a warm sulphur spring in Canada's Northwest Territories. Sedimentary Geology, 203: 36-53.

Bonny, S.M., Jones, B., 2008b. Petrography and textural development of inorganic and biogenic lithotypes in a relict barite tufa deposit at Flybye Springs, NT, Canada. Sedimentology, 55: 275-303.

Borneuf, D., 1983. Springs of Alberta. Earth Sciences Report 82-3. Alberta Research Council, Calgary, 95 pp.

Chafetz, H.S., Folk, R.L., 1984. Travertines: depositional morphology and the bacterially constructed constituents. Journal of Sedimentary Petrology, 54(1): 289-316.

Chafetz, H.S., Guidry, S.A., 1999. Bacterial shrubs, crystals shrubs, and ray-crystal shrubs: bacterial vs. abiotic precipitation. Sedimentary Geology, 126: 57-74.

Chafetz, H.S., Guidry, S.A., 2003. Deposition and diagenesis of Mammoth Hot Springs travertine, Yellowstone National Park, Wyoming, U.S.A. Canadian Journal of Earth Sciences, 40: 1515-1529.

Chafetz, H.S., Rush, P.F., Utech, N.M., 1991. Microenvironmental controls on mineralogy and habit of $CaCO_3$ precipitates: an example from an active travertine system. Sedimentology, 38: 107-126.

Cumming, B.F., Laird, K.R., Bennett, J.R., Smol, J.P., Salomon, A.K., 2002. Persistent millennial-scale shifts in moisture regimes in western Canada during the past six millennia. PNAS, 99(25): 16117-16121.

Folk, R.L., Chafetz, H.S., Tiezzi, P., 1985. Bizarre forms of depositional and diagenetic calcite in hot-spring travertines, central Italy. In: N. Schneidermann and P.M. Harris (Editors), The SEPM Special Publication no. 36, pp. 349-369.

Fraiser, M.L., Corsetti, F.A., 2003. Neoproterozoic carbonate shrubs: interplay of microbial activity and unusual environmental conditions in Post-Snowball Earth oceans. Palaios, 18: 378-387.

Given, R.K., Wilkinson, B.H., 1985. Kinetic control of morphology, composition, and mineralogy of abiotic sedimentary carbonates. Journal of Sedimentary Petrology, 55(1): 109-119.

Goldschmidt, V., 1913. Atlas Der Krystallformen. Carl Winters Universitätsbuchhandlung, Heidelberg.

Gonzalez, L.A., Carpenter, S.J., Lohmann, K.C., 1992. Inorganic calcite morphology: roles of fluid chemistry and fluid flow. Journal of Sedimentary Petrology, 62(3): 382-399.

Grasby, S.E., Lepitzki, D.A.W., 2002. Physical and chemical properties of the Sulphur Mountain thermal springs, Banff National Park, and implications for endangered snails. Canadian Journal of Earth Sciences, 39: 1349-1361.

Grasby, S.E., Hutcheon, I., Krouse, H.R., 2000. The influence of water-rock interaction on the chemistry of thermal springs in western Canada. Applied Geochemistry, 15: 439-454.

Grasby, S.E., van Everdingen, R.O., Bednarski, J., Lepitzki, D.A.W., 2003. Travertine mounds of the Cave and Basin National Historic Site, Banff National Park. Canadian Journal of Earth Sciences, 40: 1501-1513.

Guo, L., Riding, R.E., 1992. Aragonite laminae in hot water travertine crusts, Rapolano Terme, Italy. Sedimentology, 39: 1067-1079.

Guo, L., Riding, R., 1994. Origin and diagenesis of Quaternary travertine shrub fabrics, Rapolano Terme, central Italy. Sedimentology, 41: 499-520.

Herman, J.S., Lorah, M.M., 1988. The chemical evolution of a travertine-depositing stream: geochemical processes and mass transfer reactions. Water Resources Research, 24(9): 1541-1552.

Hoffman, P.F., Schrag, D.P., 2002. The snowball Earth hypothesis: testing the limits of global change. Terra Nova, 14: 129-155.

James, N.P., Narbonne, G.M., Kyser, T.K., 2001. Late Neoproterozoic cap carbonates: Mackenzie Mountains, northwestern Canada: precipitation and global glacial meltdown. Canadian Journal of Earth Sciences, 38: 1229-1262.

Jones, B., Renaut, R.W., 1995. Noncrystallographic calcite dendrites from hot-spring deposits at Lake Bogoria, Kenya. Journal of Sedimentary Research, A65(1): 154-169.

Jones, B., Renaut, R.W., 2008. Cyclic development of large, complex, calcite dendrite crystals in the Clinton travertine, Interior British Columbia, Canada. Sedimentary Geology, 203: 17-35.

Jones, B., Renaut, R.W., Rosen, M.R., 2000. Trigonal dendritic calcite crystals forming from hot spring waters at Waikite, North Island, New Zealand. Journal of Sedimentary Research, 70(3): 586-603.

Kandianis, M.T., Fouke, B.W., Johnson, R.W., Veysey, J., Inskeep, W.P., 2008. Microbial biomass; a catalyst for $CaCO_3$ precipitation in advection-dominated transport regimes. Geological Society of America Bulletin, 120(3-4): 442-450.

Lorentz, N.J., Corsetti, F.A., Link, P.K., 2004. Seafloor precipitates and C-isotope stratigraphy from the Neoproterozoic Scout Mountain Member of the Pocatello Formation, southeast Idaho: implications for Neoproterozoic earth system behavior. Precambrian Research, 130: 57-70.

MacDonald, G.M., Case, R.A., 2000. Biological evidence of multiple temporal and spatial scales of hydrological variation in the western interior of Canada. Quaternary International, 67: 133-142.

Mazor, E., van Everdingen, R.O., Krouse, H.R., 1983. Noble-gas evidence for geothermal activity in a karstic terrain: Rocky Mountains, Canada. Geochimica et Cosmochimica Acta, 47: 1111-1115.

Morse, J.W., 1983. The kinetics of calcium carbonate dissolution and precipitation. In: R.J. Reeder (Editor), Carbonates: Mineralogy and Chemistry. Mineralogical Society of America, pp. 227-264.

Pedley, H.M., Andrews, J.E., Ordonez, S., Garcia del Cura, M.A., Gonzales Martin, J.-A., Taylor, D., 1996. Does climate control the morphological fabric of freshwater carbonates? A comparative study of Holocene barrage tufas from Spain and Britain. Palaeogeography, Palaeoclimatology, Palaeoecology, 121: 239-257.

Pedley, M., Rogerson, M., Middleton, R., 2009. Freshwater calcite precipitates from *in vitro* mesocosm flume experiments: a case for biomediation of tufas. Sedimentology, 56: 511-527.

Peryt, T.M., Hoppe, A., Bechstädt, T., Köster, J., Pierre, C., Richter, D.K., 1990. Late Proterozoic aragonitic cement crusts, Bambui Group, Minas Gerais, Brazil. Sedimentology, 37: 279-286.

Rainey, D.K., Jones, B., 2005. Radiating calcite dendrites -- precursors for coated grain formation in the Fairmont Hot Springs Travertine, Canada. In: M. Özkul, S. Yagiz and B. Jones (Editors), Proceedings of1st International Symposium on Travertine, Denizli, Turkey, pp. 25-32.

Rainey, D.K., Jones, B., 2007. Rapid cold water formation and recrystallization of relict bryophyte tufa at the Fall Creek cold springs, Alberta, Canada. Canadian Journal of Earth Sciences, 44: 889-909.

Rainey, D.K., Jones, B., 2009. Abiotic versus biotic controls on the development of the Fairmont Hot Springs carbonate spring deposit, British Columbia, Canada. Sedimentology, doi: 10.1111/j.1365-3091.2009.01059.x.

Rainey, D.K., Jones, B., 2009. Comparative Analysis of Soft-Tissue Preservation in the Hot Creek Carbonate Spring Deposit, British Columbia, Canada. Sedimentary Geology, in review.

Reimer, P., Baillie, M., Bard, E., Bayliss, A., Beck, J., Bertrand, C., Blackwell, P., Buck, C., Burr, G., Cutler, K., Damon, P., Edwards, R., Fairbanks, R., Friedrich, M., Guilderson, T., Hughen, K., Southon, J., Stuiver, M., Talamo, S., Taylor, F., van der Plicht, J., Weyhenmeyer, C., 2004. IntCal04 Terrestrial radiocarbon age calibration, 26-0 ka BP. Radiocarbon, 46: 1029-1058.

Rimstidt, D.J., 1997. Gangue mineral transport and Deposition. In: H.L. Barnes (Editor), Geochemistry of hydrothermal ore deposits. John Wiley & Sons, New York, pp. 488-515.

Rogerson, M., Pedley, H.M., Wadhawan, J.D., Middleton, R., 2008. New insights into biological influence on the geochemistry of freshwater carbonate deposits. Geochimica et Cosmochimica Acta, 72: 4976-4987.

Shiraishi, F., Reimer, A., Bissett, A., de Beer, D., Arp, G., 2008. Microbial effects on biofilm calcification, ambient water chemistry and stable isotope records in a highly supersaturated setting (Westerhöfer Bach, Germany). Palaeogeography, Palaeoclimatology, Palaeoecology, 262: 91-106.

Stuiver, M., Reimer, P., 1993. Extended ^{14}C database and revised CALIB radiocarbon calibration program. Radiocarbon, 35: 215-230.

Suarez, D.L., 1983. Calcite supersaturation and precipitation kinetics in the lower Colorado River, All American Canal and east High-land Canal. Water Resources Research, 19: 653-661.

Turner, E.C., Jones, B., 2005. Microscopic calcite dendrites in cold-water tufa; implications for nucleation of micrite and cement. Sedimentology, 52(5): 1043-1066.

van Everdingen, R.O., 1972. Thermal and mineral springs in the southern Rocky Mountains of Canada. Water Management Service, Department of the Environment, Environment Canada.

Woodsworth, G., 1999. Hot Springs of Western Canada. Gordon Soules Book Publisher's Ltd., West Vancouver, 288 pp.

Appendix A

Stable Isotope Data

Fall Creek Stable Isotope Data

SAMPLE # (see Fig. 2-1C for sample locations)	DESCRIPTION	DELTA 18O (VSMOW)	DELTA 18O (VPDB)	DELTA 13C (VPDB)	1000 ln alpha	T (°C)	ISOTOPE GROUP
Bryo1	Yellow calcite encrusting bryophytes	12.2	-18.1	0.5	31.5	13.0	Recent, <350 years B.P.
Bryo2	Partly cemented, highly porous bryophyte tufa	12.6	-17.7	0.1	31.9	11.2	Relict, >350 years B.P.
FC21i	Highly cemented bryophyte tufa, white to brown calcite	12.6	-17.8	-0.3	31.9	11.5	Relict, >350 years B.P.
FC24b	Highly cemented bryophyte tufa, white to brown calcite	12.3	-18.1	0.1	31.6	12.7	Relict, >350 years B.P.
FC28	Very dense bryophyte tufa, homogeneous brown calcite	12.3	-18.0	-0.3	31.7	12.5	Relict, >350 years B.P.
FC32i	Isopachous banded cements, porous charophyte tufa	12.1	-18.2	-0.7	31.4	13.4	Relict, >350 years B.P.
FC32ii	Isopachous banded cements, porous charophyte tufa	12.3	-18.1	-0.9	31.6	12.7	Relict, >350 years B.P.
FC33	Partly cemented, highly porous bryophyte tufa	12.1	-18.3	-0.5	31.4	13.6	Relict, >350 years B.P.
FC40i	Partly cemented, highly porous bryophyte tufa	12.3	-18.1	0.0	31.6	12.7	Relict, >350 years B.P.
FC40ii	Dark brown soil carbonate	13.1	-17.3	-0.4	32.4	9.1	Soil carbonate
FC NM1	Yellow calcite encrusting bryophytes	12.1	-18.3	0.5	31.4	13.7	Recent, <350 years B.P.
FC NM2	Yellow calcite encrusting bryophytes	12.0	-18.4	0.0	31.3	14.2	Recent, <350 years B.P.
FC MM1	Calcite actively formed on modern moss drapes	12.1	-18.3	-0.1	31.4	13.6	Modern

SAMPLE #	DESCRIPTION	DELTA 18O (VSMOW)	DELTA 18O (VPDB)	DELTA 13C (VPDB)	1000 ln alpha	T (°C)	ISOTOPE GROUP
FC MM2	Calcite actively formed on modern moss drapes	12.5	-17.8	-0.3	31.8	11.6	Modern
FC CMT	Porous bryophyte tufa containing C14 wood sample	12.5	-17.9	-0.2	31.8	11.8	Relict, >350 years B.P.
FC CMB	Porous bryophyte tufa containing C14 wood sample	12.2	-18.2	0.2	31.5	13.3	Relict, >350 years B.P.
FC Wood	Calcite encrusted bryophytes, homogenous brown	12.2	-18.1	-1.2	31.5	13.0	Relict, >350 years B.P.
FC 40a	Porous network of "wormy" textured bryophyte tufa	11.9	-18.4	-1.2	31.2	14.4	Relict, >350 years B.P.
FC 40b	Porous network of "wormy" textured bryophyte tufa	12.0	-18.4	-0.6	31.3	14.1	Relict, >350 years B.P.
FC 16a	Highly cemented bryophyte tufa, white to brown calcite	12.2	-18.2	-0.2	31.5	13.1	Relict, >350 years B.P.
FC 16b	Highly cemented bryophyte tufa, white to brown calcite	11.9	-18.4	-0.9	31.2	14.4	Relict, >350 years B.P.
FC 16c	Highly cemented bryophyte tufa, white to brown calcite	12.0	-18.4	-0.8	31.3	14.1	Relict, >350 years B.P.

Fairmont Hot Springs Stable Isotope Data

SAMPLE #	FACIES	DELTA 18O (VSMOW)	DELTA 18O (VPDB)	DELTA 13C (VPDB)	DISTANCE EAST OF MEASURED SECTION A (m) (see Fig. 3-1B)	DEPTH FROM SURFACE (m)	HEIGHT FROM BASE (m)	1000 ln alpha	T (°C)
RMRap1-1i	Radiating dendrite travertine	10.4	-19.9	1.6	0	-7.9	2.1	28.5	27.4
RMRap1-1ii	Stromatolite tufa	10.3	-20.0	1.5	0	-7.9	2.1	28.5	27.5
RMRap1-1iii	Stromatolite tufa	10.1	-20.2	1.3	0	-7.9	2.1	28.2	28.7
RMRap1-1iv	Stromatolite tufa	10.2	-20.1	1.5	0	-7.9	2.1	28.3	28.4
RMRap1-1v	Stromatolite tufa	9.7	-20.5	1.5	0	-7.9	2.1	27.9	30.4
FMRap1-1top	Stromatolite tufa	10.4	-19.9	1.6	0	-7.9	2.1	28.5	27.2
FMRap1-1bot	Radiating dendrite travertine	11.0	-19.3	2.0	0	-7.9	2.1	29.1	24.2
FMRap1-2	Stromatolite tufa	10.5	-19.8	1.5	0	-5.4	4.6	28.6	26.9
FMRap1-3	Radiating dendrite travertine	10.9	-19.4	1.6	0	-5.4	4.6	29.0	24.9
FMRap1-4	Stromatolite tufa	11.4	-19.0	1.9	0	-4.7	5.3	29.5	22.6
FMRap1-5i	Radiating dendrite travertine	9.8	-20.5	1.6	0	-2.9	7.1	27.9	30.0
FMRap1-5ii	Radiating dendrite travertine	10.6	-19.7	1.6	0	-2.9	7.1	28.7	26.2
FMRap1-5iii	Radiating dendrite travertine	10.7	-19.6	1.7	0	-2.9	7.1	28.8	25.7
FMRap1-5iv	Radiating dendrite travertine	10.6	-19.7	1.5	0	-2.9	7.1	28.7	26.1
FMRap1-6	Microbe tufa	9.7	-20.5	1.0	0	-1.5	8.5	27.8	30.5
FMRap2-1	Feather dendrite travertine	11.8	-18.6	1.9	34	-12.7	2.3	29.9	20.7
FMRap2-2	Bubble tufa	11.7	-18.6	2.2	34	-12	3	29.8	20.9
FMRap2-3	Feather dendrite travertine	12.2	-18.1	1.8	34	-11.7	3.3	30.3	18.6
FMRap2-4a	Microbe tufa	10.9	-19.4	1.6	34	-4.5	10.5	29.0	24.8
FMRap2-4b	Radiating dendrite travertine	12.0	-18.3	1.6	34	-3.8	11.2	30.1	19.6
FMRap2-5	Microbe tufa	9.9	-20.4	1.4	34	-0.6	14.4	28.0	29.7
FMRap3-1	Bubble tufa	11.8	-18.5	1.5	54	-10.8	1.2	29.9	20.4
FMRap3-2	Feather dendrite travertine	12.0	-18.3	1.6	54	-7.9	4.1	30.1	19.5
FMRap3-3	Bubble tufa	10.1	-20.2	1.4	54	-4.6	7.4	28.2	28.5
FMRap3-4i	Feather dendrite travertine	12.7	-17.7	2.2	54	-3.7	8.3	30.8	16.4
FMRap3-4ii	Stromatolite tufa	12.3	-18.1	2.0	54	-3.7	8.3	30.4	18.3
FMRap3-5	Feather dendrite travertine	12.0	-18.3	1.8	54	-1.5	10.5	30.1	19.5

SAMPLE #	FACIES	DELTA 18O (VSMOW)	DELTA 18O (VPDB)	DELTA 13C (VPDB)	DISTANCE EAST OF SECTION A (m) (see Fig. 3-1B)	DEPTH FROM SURFACE (m)	HEIGHT FROM BASE (m)	1000 ln alpha	T (°C)
FMRap4-1	Feather dendrite travertine	11.8	-18.6	1.8	109	-9	1	29.9	20.6
FMRap4-2	Feather dendrite travertine	11.9	-18.4	1.9	109	-7.8	2.2	30.0	20.0
FMRap4-3i	Stromatolite tufa	10.9	-19.4	1.7	109	-7.5	2.5	29.0	24.8
FMRap4-3ii	Feather dendrite travertine	11.3	-19.0	1.9	109	-7.5	2.5	29.4	22.6
FMRap4-4	Feather dendrite travertine	10.2	-20.1	2.3	109	-4.9	5.1	28.3	28.2
FMRap4-5i	Feather dendrite travertine	11.7	-18.6	2.4	109	-4.5	5.5	29.8	20.8
FMRap4-5ii	Radiating dendrite travertine	11.2	-19.1	2.3	109	-4.5	5.5	29.3	23.3
FMRap4-6	Feather dendrite travertine	10.7	-19.6	2.4	109	-4.1	5.9	28.8	25.7
FMRap4-7	Feather dendrite travertine	10.9	-19.4	3.0	109	-3	7	29.0	24.8
FMRap4-8i	Radiating dendrite travertine	11.3	-19.0	2.6	109	-1	9	29.4	23.0
FMRap4-8ii	Feather dendrite travertine	10.3	-20.0	1.6	109	-1	9	28.4	27.8
FMRap5-1	Feather dendrite travertine	12.3	-18.0	2.7	147	-12.4	2.6	30.4	18.2
FMRap5-1a	Radiating dendrite travertine	12.3	-18.0	2.1	147	-12.7	2.3	30.4	18.1
FMRap5-2	Feather dendrite travertine	13.5	-16.8	1.8	147	-7.2	7.8	31.6	12.6
FMRap5-3	Feather dendrite travertine	9.9	-20.4	1.7	147	-5.4	9.6	28.0	29.5
FMRap5-5	Feather dendrite travertine	11.8	-18.6	2.0	147	-3.7	11.3	29.9	20.7
FMRap5-6i	Feather dendrite travertine	9.7	-20.6	2.5	147	-2	13	27.8	30.8
FMRap5-6ii	Feather dendrite travertine	12.4	-18.0	4.2	147	-2	13	30.5	17.9
FMRap5-6iii	Feather dendrite travertine	11.6	-18.7	2.4	147	-2	13	29.7	21.4
FMRap5-7	Feather dendrite travertine	9.1	-21.1	1.9	147	-1	14	27.2	33.5
FMRap6-1	Feather dendrite travertine	12.5	-17.9	2.2	177	-6.5	1.5	30.6	17.3
FMRap6-2	Feather dendrite travertine	11.6	-18.7	2.7	177	-4.2	3.8	29.7	21.3
FMRap6-3i	Feather dendrite travertine	9.1	-21.1	2.1	177	-4	4	27.2	33.6
FMRap6-3ii	Feather dendrite travertine	9.2	-21.0	1.8	177	-4	4	27.4	32.9
FMRap6-5	Feather dendrite travertine	9.0	-21.3	2.0	177	-1.9	6.1	27.1	34.2
FMRap6-6	Microbe tufa	10.0	-20.3	1.6	177	-0.5	7.5	28.1	29.0
FMRap7-1i	Feather dendrite travertine	10.0	-20.3	3.5	197	-7	1	28.1	29.1
FMRap7-1ii	Feather dendrite travertine	9.2	-21.1	1.9	197	-7	1	27.3	33.4
FMRap7-2	Feather dendrite travertine	10.9	-19.4	2.0	197	-4	4	29.0	24.8
FMRap7-3i	Feather dendrite travertine	8.7	-21.5	2.2	197	-1	7	26.9	35.6
FMRap7-3ii	Feather dendrite travertine	9.6	-20.6	2.1	197	-1	7	27.7	31.0

SAMPLE #	FACIES	DELTA 18O (VSMOW)	DELTA 18O (VPDB)	DELTA 13C (VPDB)	DISTANCE EAST OF SECTION A (m) (see Fig. 3-1B)	DEPTH FROM SURFACE (m)	HEIGHT FROM BASE (m)	1000 ln alpha	T (°C)
FMRap8-1	Feather dendrite travertine	10.8	-19.5	3.0	227	-4.5	3.5	28.9	25.1
FMRap8-2i	Feather dendrite travertine	12.1	-18.3	3.8	227	-2.4	5.6	30.2	19.3
FMRap8-2ii	Feather dendrite travertine	10.5	-19.8	3.8	227	-2.4	5.6	28.6	26.9
FMRap8-3	Feather dendrite travertine	8.9	-21.3	2.0	227	-1.4	6.6	27.1	34.5
FMRap8-4	Feather dendrite travertine	11.3	-19.0	5.3	227	-0.7	7.3	29.4	22.9
FMRap8-5	Feather dendrite travertine	11.1	-19.2	4.9	227	-0.2	7.8	29.2	23.8
FMRap9-1	Feather dendrite travertine	11.5	-18.8	2.2	272	-6.2	1.8	29.6	21.9
FMRap9-2	Stromatolite tufa	12.1	-18.3	2.6	272	-5.8	2.2	30.2	19.3
FMRap9-3	Feather dendrite travertine	9.3	-21.0	1.3	272	-5.4	2.6	27.4	32.9
FMRap9-4	Radiating dendrite travertine	11.5	-18.8	1.8	272	-5.1	2.9	29.6	21.9
FMRap9-5	Radiating dendrite travertine	11.3	-19.0	2.7	272	-5	3	29.4	22.9
FMRap9-6i	Microbe tufa	11.2	-19.2	4.6	272	-3	5	29.3	23.6
FMRap9-6ii	Microbe tufa	12.8	-17.6	4.0	272	-3	5	30.9	16.0
FMRap9-7i	Microbe tufa	12.1	-18.3	4.7	272	-3	5	30.2	19.2
FMRap9-7ii	Microbe tufa	12.9	-17.5	5.1	272	-3	5	31.0	15.5
FMRap9-8	Feather dendrite travertine	10.1	-20.2	3.2	272	-1.2	6.8	28.2	28.6
FMRap10-1i	Feather dendrite travertine	12.2	-18.2	1.6	310	-5	0.5	30.3	18.7
FMRap10-1ii	Radiating dendrite travertine	12.4	-18.0	2.3	310	-5	0.5	30.5	17.8
FMRap10-2	Feather dendrite travertine	11.5	-18.9	2.6	310	-4	1.5	29.6	22.1
FMRap10-3	Feather dendrite travertine	10.7	-19.6	3.9	310	-1.5	4	28.8	25.8
FMRap10-4	Microbe tufa	11.5	-18.8	4.4	310	-0.5	5	29.6	21.8
FMRap10-5	Microbe tufa	10.9	-19.4	3.8	310	-0.1	5.4	29.0	24.7

Wolfenden Stable Isotope Data

SAMPLE #	DELTA 18O (VSMOW)	DELTA 18O (VPDB)	DELTA 13C (VPDB)
Wolf1	12.9	-17.5	-6.1
Wolf2	12.6	-17.8	-5.5
Wolf3	11.6	-18.7	-6.6
Wolf4	12.4	-18.0	-4.1
Wolf5	13.2	-17.2	-5.4

Hot Creek Stable Isotope Data

SAMPLE #	DELTA 18O (VSMOW)	DELTA 18O (VPDB)	DELTA 13C (VPDB)
Head1	13.1	-17.3	-5.6
Head2	12.9	-17.5	-6.1

"The person who says it cannot be done should not interrupt the person doing it."
Chinese Proverb